ENVIRONMENTAL CONTROLS ON BIOTURBATION PROCESSES IN MARINE BENTHIC HABITATS

by

© Lina Marie Stolze

A Dissertation submitted to the

School of Graduate Studies

in partial fulfillment of the requirements for the degree of

Doctor of Philosophy

Department of Earth Sciences

Memorial University of Newfoundland

May 2016

St. John's Newfoundland

ABSTRACT

Through bioturbation, the macrofauna mediate chemical, physical and biological processes in marine benthic ecosystems. Because of the importance of bioturbation as ecosystem mediator, various studies have been conducted on bioturbation intensity and depth, and the relation of bioturbation processes to environmental condition and ecosystem state. This thesis builds on those previous studies, using a standard field and analytical protocol and by expanding the geographical scale to three climatic regions along Canada's East Coast and Arctic margins, the Arctic Archipelago, the coastal Subarctic (Labrador Fjords), and the temperate continental climate zone (Gulf of Maine and adjacent Scotian shelf/slope). This Ph.D. study provides a comprehensive assessment of environmental influences on bioturbation along gradients in latitude and ocean depth. Bioturbation intensity, mixing depth, and bioturbation structures were studied in relation to the quantity and quality of potential food sources (organic matter) and substrate characteristics to gain an understanding of the environmental controls on bioturbation in these regions. The three main research chapters of this thesis are divided based on the contrasting climatic and geographical regions studied.

The analytical approach included seabed sampling with a boxcorer, describing the sedimentary fabric and bioturbation structures by X-radiography, estimating bioturbation intensity and depth applying a biodiffusion model to particle tracer profiles of $^{210}Pb_{xs}$, $^{228}Th_{xs}$, $^{234}Th_{xs}$, and chlorophyll-a, and analyzing benthic organic matter and substrate characteristics. Strong regional and cross-climatic relations of bioturbation processes with combinations of environmental factors were observed. In particular, bioturbation depth and the vertical extent of bioturbation structures responded to the environmental patterns observed and, therefore, represented potentially applicable predictors of

environmental conditions and ecosystem state. The results of this Ph.D. study may be further extended to other geographical regions with similar environmental characteristics to predict the effects of benthic habitat alterations through environmental stresses on a global scale. Integrated with biological data produced by fellow CHONe scientists the presented data may provide valuable information about functional roles of macrofaunal species and community traits in marine benthic ecosystems along Canada's extensive East Coast and Arctic margins.

ACKNOWLEDGEMENTS

First, I would like to thank my thesis supervisor Dr. Samuel J. Bentley, for the guidance and mentorship he provided throughout my Ph.D. thesis. I am grateful to my thesis committee members, Dr. Suzanne Dufuor, Dr. Paul Snelgrove and Dr. Sue Ziegler, for their support and the many helpful suggestions. My special thanks goes to Dr. John M. Hanchar for assuming the supervisory duties in my second year of study.

I am grateful to the staff of the CHONe and the Earth Science Main offices, and especially Kerry Hiscock, for much appreciated administrative and logistic support. I also wish to thank Helen Gillespie and Wanda Aylward, who assisted with handling laboratory instruments and analyses at MUN.

This work would not have been possible without the support from ArcticNet and CHONe. Through their funding I had the opportunity to participate in sampling expeditions, conferences, courses, and scientific meetings. My appreciation extends to the captains, crew and sampling expedition teams of the *CCGS Amundsen* and *CCGS Hudson* cruises in 2008, 2009 and 2010. The teamwork and atmosphere onboard was exceptional, which made all sampling expeditions a wonderful and rewarding experience. I especially thank Heike Link and the "boxcoring team" for collecting several sediment cores for me that significantly contributed to my work.

My thanks are also extended to Dr. Kanchan Maiti, LSU, USA for his help with some analytical approaches to my radioisotope work.

I am truly indebted to my family for their continued love and support in all my pursuits. Thank you for always believing in me.

I am also very grateful to my friends and their continued moral support throughout the years. To my Rock Lobster friends, there is nothing that cheered me up more than

playing a good game of Ultimate with you fine people. You made my time in Newfoundland a really good one. To Eli, thank you for endless talks and discussions about thesis matters, and for always being there in times of thesis crisis and freak-outs. You are awesome. Finally, I want to thank my partner Flo for his patience and encouragement throughout my studies, and through all the dark and rainy thesis storms. It really “ain’t all buttons and charts”, and I am lucky to have a co-pilot who knows what the first rule of flying is.

Table of Contents

List of Tables

List of Figures

CHAPTER 3

CHAPTER 4

CO-AUTHORSHIP STATEMENT

The doctoral thesis and the research papers presented here (Chapter 2-4) have been prepared predominantly by the thesis author, with guidance from the thesis supervisor S.J. Bentley (Department of Geology and Geophysics, Louisiana State University, USA). The sediment cores collected in 2008 used in chapter 2 were provided by H. Link and *CCGS Amundsen* boxcoring team. Some of the chlorophyll-a and phaeopigment data presented in chapter 2 and 4, and chapter 3 were provide by H. Link and P. Archambault (ISMER-UQAR, Rimouski, CA) and by A. Robar and P. Snelgrove (Department of Ocean Sciences, Memorial University of Newfoundland, CA), respectively. Near bottom temperature and salinity data in chapter 2 and 4 were provided by Y. Gratton and D. Boisvert (INRS-Eeau, terre et environment) and P. Guillot (Institut des Sciences de la Mer de Rimouski (ISMER), and bathymetry data in chapter 4 were provided by the Ocean Mapping Group (OMG) (University of New Brunswick, Fredericton, New Brunswick, CA). K. Maiti (Department of Oceanography and Coastal Sciences, Louisiana State University, USA) generously offered his assistance with some of the radioisotope data processing and interpretation and therefore was offered co-authorship for the publication of chapter 2. Beside these contributions, the design of the research proposal, sample collection and processing, analytical work, data processing and interpretation, and preparation of the manuscripts were conducted exclusively by the thesis author.

Funding for this thesis was provided by CHONe (Canadian Healthy Oceans Network), Memorial University, Newfoundland, Canada, and ArcticNet, with facilities and additional resources provided by the Canada Foundation for Innovation and the Canada Research

Chairs Secretariat in grants to S.J. Bentley. And also by the Memorial University Earth Sciences Department.

CHAPTER 1 - Introduction

This Ph.D. thesis comprises five chapters, including three manuscripts (chapter 2, 3 and 4) written as research papers. Chapter 1 gives an overview of the project background and rationale, as well as the research objectives and analytical approaches. Chapters 2 to 4 are divided based on contrasting climatic and geographical regions, and present the research conducted within the framework of this Ph.D. study. Descriptions of geographical study regions, analytical approaches and discussions of the results are provided in each of these chapters. Chapter 5 provides a summary of the findings of chapters 2 to 4, as well as potential objectives for future studies to which the findings of this research may contribute.

1.1 Project background and rationale

1.1.1 General background

The ocean floor, which is mostly covered with unconsolidated sediment, represents the largest habitat on Earth (Snelgrove, 1997; Gray and Elliott, 2009), and the sediment-water interface is a gateway to sedimentary carbon storage, and a large repository of ecosystem nutrients. Bioturbation, the locomotion, digging, tube irrigation, feeding, and fecal pellet egestion activities of the species-rich marine macorofauna causes particle and solute transport and thus, constantly alters and mediates chemical, physical and biological characteristics and processes of this important ecosystem (e.g. Aller, 1982; Rhoads and Boyer, 1982; Meadows et al., 1990; Aller, 1994; Mayer et al., 1995; Aller and Aller, 1998; Snelgrove, 1998; Sun et al., 2002; Needham et al., 2005; Bentley et al.,

2006; Meysman et al., 2006). Depending on the life habits, feeding modes and mobility of the animal, the magnitude of particle transport and mixing is realized to different extents (Aller, 1982). Some influences of bioturbation on sedimentary structures and processes include the alteration of algal pigment composition (Abele-Oeschger and Theede, 1991), biodegradation of clay minerals (McIlroy et al., 2003; Needham et al., 2005), sediment stability and particle size distribution (Meadows et al., 1990; de Deckere et al., 2001; Shull and Yasuda, 2001), and remobilization of contaminants (Breadshaw et al., 2006). Most infauna ventilate their burrows with oxygen-rich overlying water which transports oxygen and other oxidized compounds into the unconsolidated sediment and removes metabolites from burrows (Kristensen, 1988, Aller and Aller, 1998). These processes greatly influence microbial populations, which are primarily responsible for processes such as the decomposition of organic material and nutrient cycling, and thus bioturbation affects not only the immediate benthic environment, but also provides nutrients that fuel primary production in the water column (Gilbert et al., 1995; Biles et al., 2002; Sun et al. 2002; Lohrer et al., 2004; Nizzoli et al., 2007).

The rate of bioturbation-associated mixing of marine sediments further depends greatly on factors such as macrobenthic species composition and infaunal activity, which in turn are driven by various physical and biological environmental factors (e.g. Gerino et al., 1998; Sandnes et al., 2000). Previous studies demonstrated that bioturbation processes vary as functions of multiple environmental factors such as temperature (Middelburg et al., 1997), water depth (Smith and Rabouille, 2002), sediment accumulation rates (Boudreau, 1994), particulate organic carbon (POC) flux (Smith and Rabouille, 2002), organic matter concentration at the sediment surface (Boudreau, 1998), particle size (Wheatcroft, 1992), and seasonality (Teal et al., 2008). For example, by using a multi-

tracer approach, Legeleux et al. (1994) found higher bioturbation intensities at eutrophic study sites compared to oligo- and mesotrophic study sites where mixing intensities were generally lower. Thus, the degree of bioturbation in marine sediments seems to link to benthic faunal abundance, organic carbon flux, and primary production in the water column. Because of these linkages between bioturbation and the marine environment, bioturbation surrogates, such as bioturbation intensity, depth and trace morphology, represent potential indicators of ecosystem state and predictors of environmental change on ecosystem functions and services (e.g., Snelgrove et al., 2014).

In recent decades, stress on marine benthic ecosystems has intensified, especially because of anthropogenic disturbances that include expanding economic activities and living resource extraction (Naeem et al., 1994). Along with these disturbances, the impact on bioturbation and ecosystem processes may have unforeseen cascading consequences for ocean ecosystems on a much broader scale. Describing and quantifying bioturbation, and unraveling links to physical and biological environmental parameters and processes as controlling factors, is therefore of primary importance. Because of the importance of bioturbators in mediating ecosystem processes, various studies on quantifying bioturbation intensity and mixing depth have been conducted to date (Teal et al., 2008 and references therein). Most studies, however, were conducted at limited regional scales, and variation in methodological approaches among studies reduce the comparability of data on interregional and across climatic scales. This Ph.D. project builds upon those studies, using a standard field and analytical protocol and by expanding the geographical scale of study to three climatic regions: The Canadian Arctic Archipelago (Amundsen Gulf, Northwest Passage, northern Baffin Bay), the Canadian coastal Subarctic (Labrador Fjords: Nachvak, Saglek, Okak, and Anaktalak) and the

Canadian temperate continental climate zone (Gulf of Maine and adjacent Scotian shelf/slope) (Fig. 1.1). These regions are located along a latitudinal/climatic gradient and vary in benthic environmental conditions that are driven, for example, by differences in glacial influence and seasonality.

1.1.2 Objectives and research questions

This Ph.D. thesis provides a comprehensive assessment of environmental controls on bioturbation intensity, depth in sediment, and structures along gradients in latitude and ocean depth, in three contrasting climatic regions. In particular, the current study focuses on:

1) Analyzing bioturbation intensity, structures, and depth in seafloor sediments collected from 77 °N to 41 °N and from water depths between 50 and 2500 meters along Canada's East Coast and Arctic margins.
2) Understanding the environmental controls on bioturbation processes by studying potential environmental factors and how they relate to bioturbation on regional scale and along a climatic gradient. This analysis includes the determination of the quality and amount of potential food sources available to the benthic macrofauna, and substrate characteristics of the benthic habitat.

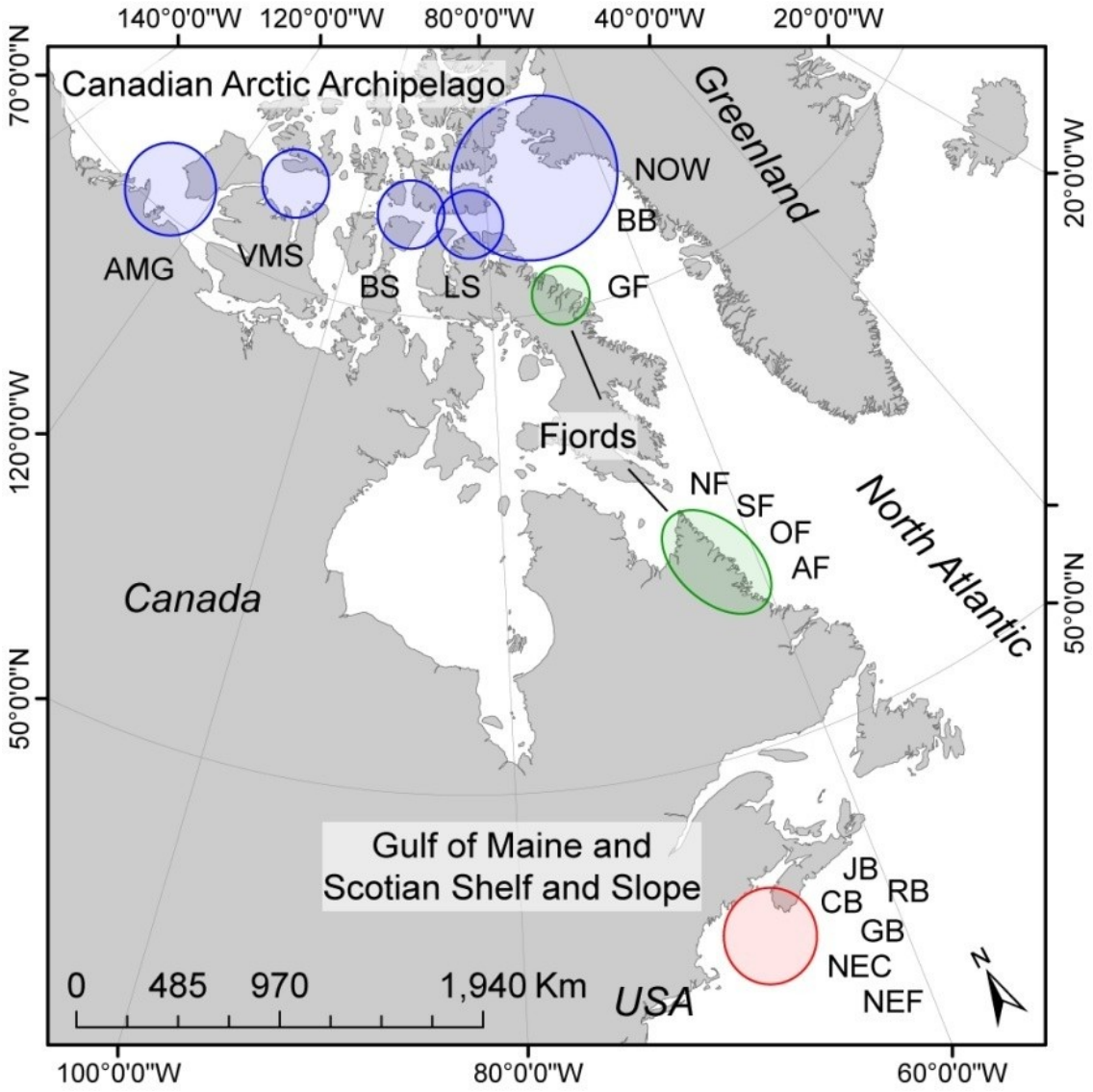

Figure 1.1: Overview of study regions. Blue: Canadian Arctic Archipelago study sites as discussed in chapter 2 (AMG: Amundsen Gulf, VMS: Viscount Melville Sound, BS: Barrow Strait, LS: Lancaster Sound, NOW: Northwater Polynya, and BB: Baffin Bay). Green: Labrador and Baffin Island Fjords studied in chapter 4 (GF: Gibbs Fjord, NF: Nachvak Fjord, SF: Saglek Fjord, OF: Okak Fjord, and AF: Anaktalak Fjord). Red: Gulf of Maine and Scotian Shelf and Slope study sites discussed in chapter 3 (JB: Jordan Basin, RB: Roseway Basin, CB: Crowell Basin, GB: Georges Basin, NEC: Northeast Channel, and NEF: Northeast Fan).

Because of the environmental differences among the three study regions and the linkages between environmental conditions and bioturbation, the three main research questions of this Ph.D. study are:

1) Can the environmental differences among the three study regions be treated as an environmental gradient following a latitudinal trend, or does each climatic region represent its own distinctive environmental pattern?
2) Are bioturbation surrogates, including bioturbation intensity, depth and trace structure, linked to these environmental patterns or gradient, and can they potentially be used as indicators of ecosystem state?
3) If bioturbation-environmental pattern/gradient linkages are discovered, are they similar for each region and on an across-climatic scale, or do they vary between regions and with the geographical extent?

1.1.3 Methods and potential limitations

To address these objectives and research questions the following approaches were used:

1) Seabed sediment sampling using a boxcorer during the ArcticNet and CHONe (Snelgrove et al., 2012) cruises in 2008 and 2009 onboard the Canadian Coast Guard vessel *CCGS Amundsen*, and a multicorer during the CHONe cruises in 2009 and 2010 onboard the Canadian Coast Guard vessel *CCGS Hudson*.
2) Describing the sedimentary fabric and bioturbation structures as visualized by X-radiography of sediment cores.

3) Estimating bioturbation intensities and depth by applying a biodiffusion model to sedimentary profiles of the naturally occurring particle tracers $^{210}Pb_{xs}$, $^{228}Th_{xs}$, $^{234}Th_{xs}$, and chlorophyll-a.
4) Estimating sedimentation rates from $^{210}Pb_{xs}$ and ^{137}Cs sedimentary profiles.
5) Analyzing the total organic carbon (TOC), total nitrogen (TN), chlorophyll-a and phaeopigments, $\delta^{13}C$ of the organic carbon, sediment particle size, as well as water percentage and sediment porosity.

This study applied a multi-tracer approach using the radioisotopes $^{210}Pb_{xs}$, $^{228}Th_{xs}$ and $^{234}Th_{xs}$, as well as the photopigment chlorophyll-a to study bioturbation processes in surface sediments. The application of these tracers in concert provides insight into bioturbation processes on short (seasonal)- to long-temporal scales, which equate to a few half-lives of the respective tracer.

The use of natural occurring particle-reactive radioisotopes is a common method to estimate sedimentation and sediment mixing rates in freshwater and coastal settings (Hancock and Hunter, 1999, and references therein). Whereas ^{210}Pb is derived from ^{222}Rn decay in the atmosphere and from ^{226}Ra decay in the water column, ^{234}Th is produced through the decay of ^{238}U in the water column (Stephens et al., 1997). Both radioisotopes are steady-state particle tracers with half-lives of 22 years and 24 days, respectively, which are continuously supplied to the sediment from the overlying water column (Gerino et al., 1998). ^{228}Th has a half-life of 1.9 years and is produced in the water column by the decay of its parent nuclide ^{228}Ra, which has effused from bottom sediments due to its solubility in saline water and by diffusion and bioirrigation processes

(Hancock et al., 1997). In the water column, ^{210}Pb, ^{234}Th and ^{228}Th are scavenged by suspended fine-grained particles and transported to the seafloor where they are buried as excess (indicated as lower case “xs” after the radioisotope name) activity by sediment accumulation and bioturbation. Within the sediment, radioisotope activities decrease with depth due to radioactive decay. Resulting activity-depth profiles in surface sediments are therefore functions of the tracer’s half-life, sedimentation rate and biogenic and/or physical downward mixing of sediment particles (Guinasso and Schink, 1975).

In addition to the above described radioisotopes, the most widely occurring phytoplankton photopigment chlorophyll-a was used as a tracer to track the mixing of fresh organic matter into the seabed and describe bioturbation processes on short-term, seasonal scales. In sediments the initial mass of chlorophyll-a decreases over time through chemical degradation processes (Sun et al., 1991; Gerino et al., 1998), and sedimentary chlorophyll-a concentration-depth profiles are functions of degradation rate, sedimentation rate and biogenic and/or physical mixing of the tracer into the sediment (Sun et al., 1991; Green et al., 2002).

In order to estimate bioturbation intensities in surface sediments a diffusion model, which assumes a spatially random and relatively frequent displacement of particles over small spatial scales (Boudreau, 1986a), was fitted to $^{210}Pb_{xs}$, $^{228}Th_{xs}$ and $^{234}Th_{xs}$ activity-depth, and chlorophyll-a concentration-depth distributions. The biodiffusion model was first introduced by Goldberg and Koide (1962) and has been applied extensively throughout the literature and in radiotracer studies since then (Meysman et al., 2010). However, the current knowledge on the ecology of sediment burying benthic organisms shows that the assumptions for diffusion-like bioturbation processes are often not met and sediment reworking modes may meet the conditions for a particle transport where particles are

displaced directionally between relatively distant points in the sediment (Boudreau, 1986b; Meysman et al., 2003, 2010). Nevertheless, the biodiffusion model is still most widely used because it is relatively user friendly and easy to apply. Furthermore, the biodiffusion model is still a valuable tool and proven to be an accurate empirical model in this field of research under many circumstances (Meysman et al., 2010). As discussed by Meysman et al. (2010), the latter is especially true for the application of long-term particle tracers such as ^{210}Pb, unless head-down deposit feeders or large-bodied burrow excavators such as some crustaceans dominate sediments, in which case the diffusion model would fail, and other models should be used (Bentley and Nittrouer, 2012; Bentley et al., 2014). For relatively short-lived particle tracers, tracer depth profiles may differ from classical diffusive profiles and the biodiffusion model would not be applicable in that case. The present study reviewed bioturbation traces visible in X-radiographs as well as particle tracer profiles in an attempt to identify if the conditions for biodiffusion are given before applying the biodiffusion model to particle tracer profiles.

1.2 Funding and context

This Ph.D. study was funded through CHONe (NSERC Canadian Healthy Oceans Network), Memorial University, Newfoundland, Canada, and ArcticNet, with facilities and additional resources provided by the Canada Foundation for Innovation and the Canada Research Chairs Secretariat in grants to Dr. Samuel J. Bentley. Memorial University Earth Sciences Department also provided funding.

CHONe was a large marine biodiversity study funded by NSERC (Natural Sciences and Engineering Research Council of Canada) and headquartered at Memorial University. CHONe aligned Canadian marine science capacities from 14 Canadian universities, the

DFO (Department of Fisheries and Oceans in Canada), as well as other governmental laboratories, to address a need for scientific criteria for conservation and sustainable use of Canada's marine biodiversity resources (Snelgrove et al., 2012, Canadian Healthy Oceans Network (CHONe), 2015). This Ph.D. project is part of one of CHONe's three research themes, *Ecosystem Function* that focused on studying how species influence marine ecosystem function, in connection with ocean health and anthropogenic and natural disturbances. Within CHONe, which was particularly focused on biological aspects, my work emphasizes a sedimentological/geochemical background and contributes data and insights that provide a uniquely geological approach to these important studies of ecosystem diversity and sustainability.

Sample collection in Baffin Bay and Labrador onboard the Canadian research icebreaker *CCGS Amundsen* was funded by ArcticNet, through the Canadian government funded Network of Centres of Excellence. Within this Network scientists and managers of the natural, human health, and social sciences, and their partners from Inuit organizations, northern communities, federal and provincial agencies and the private sector, work together to study the impact of climate change on societies, and on terrestrial and marine coastal ecosystems in the Canadian Arctic (ArcticNet, 2015).

Part of the stable isotope and organic carbon analyses were funded through a grant received from the International Association of Sedimentologists (IAS) (Postgraduate Grant Scheme), Ghent University, Belgium.

1.3 References

Abele-Oeschger, D. and Theede, H. (1991). Digestion of algal pigments by the common periwinkle Littorina littorea L. (Gastropoda). Journal of Experimental Marine Biology and Ecology 147, 177-184.

Aller, R.C. (1982). The effects of macrobenthos on chemical properties of marine sediment and overlying water. In: McCall, P.L., Tevesz, M.J.S. (Eds.). Animal-sediment relations - The biogenic alteration of sediments. Plenum Press, New York, 53-102.

Aller, R.C. (1994). Bioturbation and remineralization of sedimentary organic matter: Effects of redox oscillation. Chemical Geology 114, 331-345.

Aller, R.C. and Aller, J.Y. (1998). The effect of biogenic irrigation intensity and solute exchange on diagenetic reaction rates in marine sediments. Journal of Marine Research 56, 905-936.

ArcticNet (2015). Rationale, http://www.arcticnet.ulaval.ca/about us/rationale.php.

Bentley, S.J., Sheremet, A., Jaeger, J.M. (2006). Event sedimentation, bioturbation, and preserved sedimentary fabric: Field and model comparisons in three contrasting marine settings. Continental Shelf Research 26, 2108-2124.

Bentley, S.J. and Nittrouer, C.A. (2012). Accumulation and intense bioturbation of bioclastic muds along a carbonate-platform margin: Dry Tortugas, Florida. Marine Geology 315-318, 44-57.

Bentley, S.J., Swales, A., Pyenson, B., Dawe, J. (2014). Sedimentation, bioturbation, and sedimentary fabric evolution on a modern mesotidal mudflat: A multi-tracer study of processes, rates, and scales. Estuarine, Coastal and Shelf Science 141, 58-68.

Biles, C.L., Paterson, D.M., Ford, R.B., Solan, M., Raffaeli, D.G. (2002). Bioturbation, ecosystem functioning and community structure. Hydrology and Earth System Sciences 6, 999-1005.

Boudreau, B.P. (1986a). Mathematics of tracer mixing in sediments: I. Spatially-dependent, diffusive mixing. The American Journal of Science 286, 161-198.

Boudreau, B.P. (1986b). Mathematics of tracer mixing in sediments: II. Nonlocal mixing and biological conveyor-belt phenomena. American Journal of Science 286, 199-238.

Boudreau, B.P. (1994). Is burial velocity a master parameter for bioturbation? Geochimica et Cosmochimica Acta 58, 1243-1249.

Boudreau, B.P. (1998). Mean mixed depth of sediments: The wherefore and why. American Society of Limnology and Oceanography 43, 524-526.

Breadshaw, C., Kumblad, L., Fagrell, A. (2006). The use of tracers to evaluate the importance of bioturbation in remobilizing contaminants in Baltic sediments. Estuarine, Coastal and Shelf Science 66, 123-134.

Canadian Healthy Oceans Network (CHONe) (2015). Home, http://chone.marinebiodiversity.ca/.

de Deckere, E.M.G.T, Tolhurst, T.J., de Brouwer, J.F.C. (2001). Destabilization of cohesive intertidal sediments by infauna. Estuarine, Coastal and Shelf Science 53, 665-669.

Gerino, M., Aller, R.C., Lee, C., Cochran, J.K., Aller, J.Y., Green, M.A., Hirschberg, D. (1998). Comparison of different tracers and methods used to quantify bioturbation during a spring bloom: 234-Thorium, luminophores and chlorophyll a. Estuarine, Coastal and Shelf Science 46, 531-547.

Gilbert, F., Bonin, P., Stora, G. (1995). Effect of bioturbation on nitrification in a marine sediment from the West Mediterranean littoral. Hydrobiologia 304, 49-58.

Goldberg, E.D. and Koide, M. (1962). Geochronological studies of deep sea sediments by the ionium/thorium method. Geochimica et Cosmochimica Acta 26, 417-450.

Gray, J.S. and Elliot, M. (2009). Ecology of marine sediments: From science to management, second edition. Oxford University Press.

Green, M.A., Aller, R.C., Cochran, J.K., Lee, C., Aller, J.Y. (2002). Bioturbation in shelf/slope sediments off Cape Hatteras, North Carolina: the use of ^{234}Th, Chl-a, and Br^- to evaluate rates of particle and solute transport. Deep-Sea Research II 49, 4627-4644.

Guinasso, N.L and Schink, D.R. (1975). Quantitative estimates of biological mixing rates in abyssal sediments. Journal of Geophysical Research-Oceans and Atmosphere 80, 3032-3043.

Hancock, G.J., Webster, I.T., Murray, A.S. (1997). Estimation of rates of sedimentation, water column mixing and porewater exchange in Port Phillip Bay using fallout and lithogenic radionuclides. Consultancy Report 97-55 (October 1997) for the Port Phillip Bay Environmental Study, 41 pp.

Hancock, G.J. and Hunter, J.R. (1999). Use of excess ^{210}Pb and ^{228}Th to estimate rates of sediment accumulation and bioturbation in Port Phillip Bay, Australia. Marine Freshwater Research 50, 533-545.

Kristensen, E. (1988). Benthic fauna and biogeochemical processes in marine sediments: microbial activities and fluxes. In: Blackburn, T.H., Sørensen, J. (Eds.). Nitrogen cycling in coastal marine environments. John Wiley & Sons Ltd., Chichester, 275-299.

Legeleux, F., Reyss, J.-L., Schmidt, S. (1994). Particle mixing rates in sediments of the northeast tropical Atlantic: Evidence from $^{210}Pb_{xs}$, ^{137}Cs, $^{228}Th_{xs}$ and $^{234}Th_{xs}$ downcore distributions. Earth and Planetary Science Letters 128, 545-562.

Lohrer, A.M., Thrush, S., Gibbs, M.M. (2004). Bioturbators enhance ecosystem function through complex biogeochemical interactions. Nature 431, 1092-1095.

Mayer, M.S., Schaffner, L., Kemp, W.M. (1995). Nitrification potentials of benthic macrofaunal tubes and burrow walls: effects of sediment NH4 + and animal irrigation behavior. Marine Ecology Progress Series 121, 157-169.

McIlroy, D., Worden, R.H., Needham, S.J. (2003). Faeces, clay minerals and reservoir potential. Journal of the Geological Society 160, 489-493.

Meadows, P.S., Tait, J., Hussain, S.A. (1990). Effects of estuarine infauna on sediment stability and particle sedimentation. Hydrobiologia 190, 263-266.

Meysman, F.J.R., Boudreau, B.P., Middleburg, J.J. (2003). Relations between local, nonlocal, discrete and continuous models of bioturbation. Journal of Marine Research 61, 391-410.

Meysman, F.J.R., Galaktionov, O.S., Gribsholt, B., Middelburg, J.J. (2006). Bioirrigation in permeable sediments: Advective pore-water transport induced by burrow ventilation. American Society of Limnology and Oceanography 51, 142-156.

Meysman, J.R., Boudreau, B.P., Middleburg, J.J. (2010). When and why does bioturbation lead to diffusive mixing? Journal of Marine Research 68, 881-920.

Middelburg, J.J., Soetaert, K., Herman, P.M. (1997). Empirical relationships for use in global diagenetic models. Deep-Sea Research 44, 327-344.

Naeem, S., Thompson, L.J., Lawer, S. P., Lawton, J.H., Woodfin, R.M. (1994). Declining biodiversity can alter the performance of ecosystems. Nature 368, 734-737.

Needham, S.J., Worden, R.H., McIlroy, D. (2005). Experimental production of clay rims by macrobenthic sediment ingestion and excretion processes. Journal of Sedimentary Research 75, 1028-1037.

Nizzoli, D., Bartoli, M., Cooper, M., Welsh, D.T., Underwood, G.J.C., Viaroli, P. (2007). Implications for oxygen, nutrient fluxes and denitrification rates during the early stage of sediment colonization by the polychaete *Nereis* spp. in four estuaries. Estuarine, Coastal and Shelf Science 75, 125-134.

Rhoads, D.C. and Boyer, L.F. (1982). The effects of marine benthos on physical properties of sediments - A successional perspective. In: McCall, P.L., Tevesz, M.J.S. (Eds.). Animal-sediment relations - The biogenic alteration of sediments. Plenum Press-New York and London. 3-52.

Sandnes, J., Forbes, T., Hansen, R., Sandnes, B., Rygg, B. (2000). Bioturbation and irrigation in natural sediments, described by animal-community parameters. Marine Ecology Progress Series 197, 169-179.

Shull, D.H. and Yasuda, M. (2001). Size-selective downward particle transport by cirratulid polychaetes. Journal of Marine Research 59, 453-473.

Smith, C.R. and Rabouille, C. (2002). What controls the mixed-layer depth in deep-sea sediments? The importance of POC flux. Limnology and Oceanography 47, 418-426.

Snelgrove, P.V.R (1997). The importance of marine sediment biodiversity in ecosystem processes. Ambio 26, 578-583. Published by Allen Press on behalf of Royal Swedish Academy of Sciences.

Snelgrove, P.V.R. (1998). The biodiversity of macrofaunal organisms in marine sediments. Biodiversity and Conservation 7, 1123-1132.

Snelgrove P.V.R., Archambault, P., Juniper, K., Lawton, P., and others (2012). Canadian Healthy Oceans Network (CHONe): An academic–government partnership to develop scientific guidelines for conservation and sustainable usage of marine biodiversity. Fisheries 37, 296-304.

Snelgrove, P.V.R., Thrush, S.F., Wall, D.H., Norkko, A. (2014). Real world biodiversity-ecosystem functioning: a seafloor perspective. Trends in Ecology & Evolution 29, 398-405.

Stephens, M.P., Kadko, D.C., Smith, C.R., Latasa, M. (1997). Chlorophyll-a and phaeopigments as tracers of labile organic carbon at the central equatorial Pacific seafloor. Geochimica et Cosmochimica Acta 61, 4605-4619.

Sun, M., Aller, R.C., Lee, C. (1991). Early diagenesis of chlorophyll-a in Long Island Sound sediments: A measure of carbon flux and particle reworking. Journal of Marine Research 49, 379-401.

Sun, M.-Y., Cai, W.-J., Joye, S.B., Ding, H. Dai, J., Hollibaugh, J.T. (2002). Degradation of algal lipids in microcosm sediment with different mixing regimes. Organic Geochemistry 33, 445-459.

Teal, L.R., Bulling, M.T., Parker, E.R., Solan, M. (2008). Global patterns of bioturbation intensity and mixed depth of marine soft sediments. Aquatic Biology 2, 207-218.

Wheatcroft, R.A. (1992). Experimental tests for particle size-dependent bioturbation in the deep ocean. American Society of Limnology and Oceanography 37, 90-104.

CHAPTER 2 – Environmental Controls on Bioturbation Intensity in Sediments of the Canadian Arctic Archipelago

Lina M. Stolze[1]* and Samuel J. Bentley, Sr.[2]

*Corresponding author: Email: lmstolze@mun.ca

[1]Department of Earth Sciences, Memorial University of Newfoundland, St John's, Canada NL A1B 3X5

[2]Samuel J. Bentley, Sr., Department of Geology and Geophysics, Louisiana State University, Baton Rouge, Louisiana, USA 70803

In preparation for submission to: Estuarine, Coastal and Shelf Science.

Abstract

Through bioturbation, the benthic fauna in marine habitats plays an important role in mediating numerous benthic ecosystem processes. In Arctic marine ecosystems, however, bioturbation processes are still poorly understood. Due to climate change and the economic use of Arctic seaways the marine Arctic ecosystem is increasingly affected by environmental changes such as varying ice-coverage. To gain a better understanding of the consequences of environmental change on marine ecosystems in these regions it is important to understand the environmental factors that influence marine organisms and their activities. The activity of macrofauna was characterized by determining the rates of sediment mixing calculated from down-core depth distributions of excess ^{210}Pb and ^{228}Th, and chlorophyll-a within sediment cores from the Canadian Arctic Archipelago. Sediments were collected with a boxcorer on two cruises in fall 2008 and 2009. Specifically, sediment cores were obtained along the Canadian coastline between 70˚N and 77˚N and in water depths between 151 m and 795 m. Radioisotope activities were measured by non-destructive gamma spectrometry, whereas chlorophyll-a concentrations of surface sediments were determined by fluorometry. Particle tracer distributions of $^{210}Pb_{xs}$, $^{228}Th_{xs}$ and chlorophyll-a show that endobenthic macrofauna rework surface sediments. Additional evidence for sediment mixing was obtained from X-radiographs. Assuming sediment-mixing events to be random diffusion-like processes, bioturbation rates were calculated by fitting solutions of the diagenetic model to excess activity profiles of ^{210}Pb, ^{228}Th and chlorophyll-a within sediment cores. In addition, biotic and abiotic environmental parameters, including total organic carbon, total nitrogen and chlorophyll-a concentrations, δ^{13}C of organic carbon, as well as sediment texture, were analyzed to describe the benthic environmental conditions of each sampling site.

Highest bioturbation rates in surface sediments were found in Lancaster Sound and the North Water region responding to relatively high organic matter input and quality. Compared to other stations, higher inputs of clay and terrigenous or low quality organic matter, and episodic sediment deposition events in the Amundsen Gulf and Viscount Melville Sound regions, appear to inhibit bioturbation. In the Arctic sediments studied, organic matter input and quality were the main drivers of biological activities with respect to sediment mixing.

Keywords: Particle tracer, $^{210}Pb_{xs}$, $^{228}Th_{xs}$, chlorophyll-a, biodiffusion, bioturbation depth, bioturbation structures, organic matter

2.1 Introduction

The benthic fauna in marine habitats plays an important role in mediating numerous benthic ecosystem processes through their bioturbation activities. Particularly in Arctic regions, where human activities and climate shifts have already substantially altered marine ecosystems, benthic processes remain poorly understood. To date, extensive sea-ice coverage and high concentrations of pack-ice have limited scientific studies in Arctic regions (Michel et al., 2006), and thus only few scientific data sets exist from these regions (Teal et al., 2008).

The marine environment of the Canadian Arctic is characterized by a topographically and hydrographically complex environment and represents an important region in which to advance the study of environmental-benthic community relationships on various spatial scales (Roy et al., 2014). The Canadian Arctic Archipelago is a network of shallow channels and passages that connect the central Arctic with the Baffin Bay (Archambault et al., 2010). To the west of the Archipelago, the Beaufort Sea and Amundsen Gulf are strongly influenced by freshwater and sediment discharges from the Mackenzie River system (Darby et al., 2009). The Archipelago is ice-covered in winter, but sea ice can also be found throughout the summer, particularly in the central part of the region (Roy et al., 2014). In the northeastern part of the Archipelago, large polynya systems exhibit intense marine biological productivity and tight pelagic-benthic coupling (Link et al., 2013). The Canadian Arctic, which has been a pristine natural environment until recently, is now confronted with the consequences of increasing anthropogenic impact associated with global climate change and the resulting decrease of sea ice coverage over the past 30 years (Michel et al., 2006; Archambault et al., 2010). The anthropogenic impact not only affects ocean circulation and water mass characteristics

and significantly influences primary production and carbon transfer to higher trophic levels (Michel et al., 2006; Darnis et al., 2012; Tremblay et al., 2012), but also potentially creates newly accessible shipping routes through the Canadian Arctic Archipelago (Lasserre and Pelletier, 2011; Smith and Stephenson, 2013). In order to evaluate the impact of environmental change on Arctic ecosystems, reliable baseline information from which changes can be identified is needed (Wassmann et al., 2011). The comprehensive baseline data presented here elucidates bioturbation-environmental relationships in Arctic environments, and may also help to evaluate future impacts of environmental change on bioturbation in this region. The specific objectives of this study were: 1) to conduct a baseline assessment of bioturbation intensity and type, and 2) to evaluate the relationships of bioturbation processes and environmental factors along a longitudinal transect across the topographically and hydrographically complex marine environment of the Canadian Arctic Archipelago from the Amundsen Gulf to the Baffin Bay.

To assess these objectives the current study, which is part of a large biodiversity program entitled CHONe (Canadian Healthy Oceans Network) (Snelgrove et al., 2012), aims to evaluate relationships of biogenic sediment mixing (bioturbation) and environmental factors in sediments of the Canadian Arctic Archipelago. In particular, bioturbation intensities and mixing depths were estimated by applying a multi-tracer approach using excess ^{210}Pb and ^{228}Th, and chlorophyll-a. Biogenic sedimentary structures produced by endobenthic macrofauna were described by X-ray imaging of sediment cores. Additionally, abiotic and biotic environmental conditions of the benthic habitats were studied through the analyses of organic matter concentration, organic matter source and the quality and texture of sediments. Finally, potential linkages

between environmental conditions and bioturbation intensities, mixing depths and biogenic structures were assessed using correlation and multivariate analyses.

2.2 Methods

2.2.1 Regional setting and sediment sample collection

This current study was conducted in the Canadian Arctic Archipelago between 70°N and 78°N and 127°W and 65°W during the collaborative ArcticNet (http://www.arcticnet.ulaval.ca) and Canadian Healthy Oceans Network (Snelgrove et al., 2012) expedition in September 2008 (leg 11a) and October 2009 (leg 4a) (Fig. 2.1). The Canadian Arctic Archipelago covers approximately 50 % of the total Arctic continental shelf area (Michel et al., 2006; Archambault et al., 2010) and represents one of the largest shallow-water Arctic marine habitats (Hunt and Corliss, 1992). Narrow channels and interconnected basins formed through glacial action comprise the large and complex Arctic Ocean shelf, which adjoins the Arctic Ocean to the West and the Baffin Bay to the East (Michel et al., 2006). Sea ice occurs in the Canadian Arctic Archipelago for most of the year (Hunt and Corliss, 1992; Michel et al., 2006) and exhibits substantial seasonal and interannual variation in distribution and ice type (Grant et al., 2002). Several polynyas, regions of open water isolated within pack-ice representing important components of physical and biological systems in ice-covered seas, occur in waters of the Canadian Arctic Archipelago (Hannah et al., 2009). The North Water Polynya in northern Baffin Bay is considered to be the most productive region in the Arctic as a result of high phytoplankton production (Michel et al., 2006),

high annual fluxes of particulate matter (Hargrave et al., 2002), and, hence, efficient organic carbon transfer to higher trophic levels (Link et al., 2013; Roy et al., 2015).

Sediment samples were collected in the Amundsen Gulf (AMG), Viscount Melville Sound (VMS), Barrow Strait (BS), Lancaster Sound (LS), the North Water region (NOW), and northern Baffin Bay (BB), in depths of 151 to 795 m (Table 2.1), on board the *CCGS Amundsen* by using a 0.25 m^2 boxcorer. Boxcores were then sub-sampled with PVC-core tubes (10 cm diameter) for geochemical analyses and with Plexiglas trays (57 cm x 20 cm x 2 cm) for X-ray imaging. On board, Plexiglas trays were sealed for water tightness and PVC-cores collected in 2008 were extruded and sliced into 1 cm intervals, whereas PVC-cores collected in 2009 were extruded and sliced into 1 cm intervals in surface layers (0-10 cm) and in 2 cm intervals below surface layers. Sediment samples for elemental, stable isotope and chlorophyll-a analyses were stored at -18 °C and kept frozen and in the dark until analysis. Sediment samples for radioisotope analysis were stored in watertight Whirl-PAK bags at 4 °C along with the Plexiglas trays.

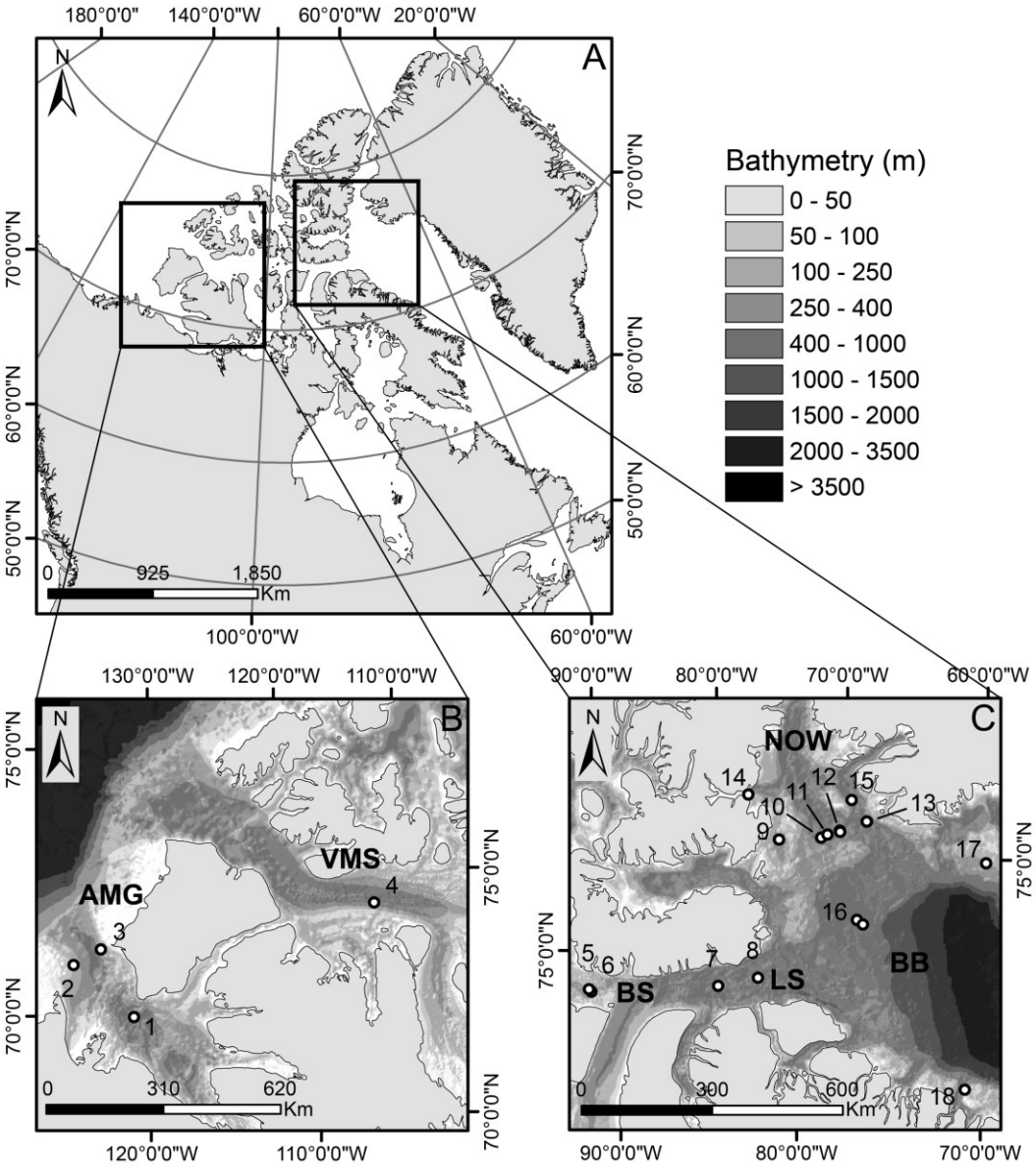

Figure 2.1: Location of the study area. A) Map of the Canadian Arctic Archipelago. Rectangles display main sampling regions. For sub-regions and sampling stations: B) Amundsen Gulf (AMG) and Viscount Melville Sound (VMS) with sampling stations 1) 405, 2) 408, 3) 437, and 4) 308. C) Barrow Strait (BS), Lancaster Sound (LS), North Water (NOW), and Baffin Bay (BB) with sampling stations 5) 304, 6) BS, 7) 301, 8) 323, 9) 101, 10) 108, 11) 109, 12) 111 and 111b, 13) 115 and 115b, 14) 205, 15) 233, 16) 136 and 136b, 17) 140, and 18) 141.

Table 2.1: Sediment sampling regions and stations, water depths, near seafloor salinity and temperature. Region abbreviations: AMG (Amundsen Gulf), VMS (Viscount Melville Sound), BS (Barrow Strait), LS (Lancaster Sound), NOW (North Water), and BB (Baffin Bay).

Region	Number on Map	Station	Year of collection	Latitude	Longitude	Depth (m)	At Seafloor Salinity (psu)[a]	At Seafloor Temperature (°C)[a]
AMG	**1**	**405**	**2009**	70° 39.85	122° 59.77	558	35	0.33
AMG	**2**	**408**	**2009**	71° 17.21	127° 47.89	151	35	-0.02
AMG	**3**	**437**	**2009**	71° 46.90	126° 28.31	320	35	0.34
VMS	**4**	**308**	**2009**	74° 06.07	108° 50.19	574	35	0.42
BS	**5**	**BS**	**2008**	74° 16.28	91° 14.85	353	34	-0.25
BS	**6**	**304**	**2009**	74° 19.02	91° 24.15	333	34	-0.13
LS	**7**	**301**	**2008**	74° 09.18	83° 12.525	707	34	1.44
LS	**8**	**323**	**2009**	74° 11.01	80° 37.95	781	34	1.14
NoW	**9**	**101**	**2008**	76° 24.04	77° 29.53	402	34	-0.05
NoW	**10**	**108**	**2008**	76° 16.18	74° 35.63	444	34	-0.30
NoW	**11**	**109**	**2009**	76° 17.51	74° 07.34	455	34	-0.17
NoW	**12**	**111**	**2008**	76° 18.34	73° 13.18	611	34	-0.27
NoW	**12**	**111b**	**2009**	76° 17.08	73° 13.02	567	34	-0.14
NoW	**13**	**115**	**2008**	76° 19.53	71° 12.92	668	34	0.35
NoW	**13**	**115b**	**2009**	76° 20.03	71° 14.34	674	34	-0.15
NoW	**14**	**205**	**2008**	77° 13.14	78° 58.88	623	34	-0.23
NoW	**15**	**233**	**2008**	76° 44.34	71° 50.63	696	34	1.02
BB	**16**	**136**	**2008**	74° 47.15	73° 37.96	795	34	0.93
BB	**16**	**136b**	**2009**	74° 41.11	73° 20.32	784	34	1.00
BB	**17**	**140**	**2008**	75° 01.67	64° 28.64	286	34	1.83
BB	**18**	**141**	**2009**	71° 22.97	70° 09.27	413	34	1.10

[a]Near bottom salinity and temperatures were provided by Y. Gratton and D. Boisvert (INRS-Eau, terre et environnement) and P. Guillot (Institut des Sciences de la Mer de Rimouski (ISMER)).

2.2.2 Radiochemistry

Sediments were dried for 24 h at 70 °C and finely ground. The dried sample aliquots of 5-15 g were then transferred to 0.7 x 5 cm counting dishes and sealed to allow the ingrowth of the ^{210}Pb grandparent ^{222}Rn and the ^{228}Th and ^{228}Ra daughter nuclides (^{224}Ra and ^{228}Ac respectively). Sediment sample aliquots were subsequently measured for 24 h using three Canberra low energy germanium detectors (model GL-3825R). Gamma-ray

spectra were analyzed with the gamma acquisition and analysis software Genie 2000. The activities of radionuclides are reported in dpm g^{-1} (decays per minute per gram dry sediment, with 1 dpm = 60 Becquerel), and were corrected for decay from sample collection to counting. Total activities of ^{210}Pb were measured by its gamma emission at 46.5 keV and activities of supported ^{210}Pb were determined by analyzing ^{226}Ra via its daughter isotopes ^{214}Pb (295 keV and 352 keV) and ^{214}Bi (609 keV). ^{228}Th and ^{228}Ra activities were obtained by measuring the gamma emissions of their daughter isotopes ^{212}Pb (238.6 keV) and ^{208}Tl (583.1 keV), and ^{228}Ac (338.4 keV, 911.1 keV and 968.9 keV) respectively. Activities of ^{137}Cs were directly determined by measuring its gamma emission at 661 keV. The detector efficiencies for these radioisotopes were estimated by counting the International Atomic Energy Agency standards IAEA-135, IAEA-RGTh-1 and IAEA-RGU-1 (for gamma energies >200 keV), and the National Institute of Standards and Technology standards NIST-4337 and NIST-4321c and by correcting for self-absorption of low gamma energy peaks (for gamma energies <200 keV). Finally, excess activities of ^{210}Pb and ^{228}Th were calculated by subtracting supported activities of ^{210}Pb from total activities of ^{210}Pb, and by subtracting the activities of total ^{228}Ra from total ^{228}Th activities.

2.2.3 Granulometry and X-radiography

Sediment subsamples were disaggregated in a $NaPO_3$ (0.05 %) solution and sonicated for 1 h using an ultrasonic bath. After leaving them in the solution overnight, samples were analyzed with a HORIBA Partica LA-950 laser diffraction particle size analysis system. Relative percentages of clay (<3.9 µm), silt (3.9 - <62.5 µm) and sand (62.5 - <2000 µm), as well as the mean grain size M_z, standard deviation σ_I (sorting), and

skewness SK_I of grain size distributions within the upper 10 cm of the sediment (Folk and Ward, 1957) were then calculated from the particle size distribution report.

Sedimentary structures and biogenic structure morphologies in sediment cores were analyzed by X-ray imaging of sediment slabs preserved in Plexiglas trays using a Thales Flashscan 35 X-ray detector illuminated with an Acoma PX15HF X-ray generator. All images were stored as 14-bit TIFF data files and analyzed with ImageJ (Schneider et al., 2012). Burrow morphologies imaged in X-radiographs were described with respect to burrow diameter (in cm), orientation and shape.

Biogenic structures were grouped based on structure geometry, fill, and boundary with the surrounding sediment. The number of tiers, or the vertical partitioning of the benthic habitat, was identified using depth distributions of biogenic structure groups and structure group associations, which potentially represent different types of sediment processing.

The concentration of ice-rafted debris clasts was also estimated from X-radiographs using a counting method established by Grobe (1987). For this purpose, the number of particles with a diameter of 2 mm and larger was determined within the upper 10 cm of sediment cores. The results were then converted to obtain the number of ice-rafted debris per 1 cm^3 of sediment.

2.2.4 Chlorophyll-a analysis

Sample aliquots of ~1 g thawed, wet sediment were transferred to high density polyethylene 15 ml centrifuge tubes and extracted in 10 ml 90 % acetone. Samples were sonicated for 5 minutes using an ultrasonic bath and stored horizontally and overnight at -18 °C to ensure complete extraction. Acetone extracts were separated from sediments

by centrifugation for 10 min at 3000 rpm and the fluorescence of extracts measured with a Turner Design 10 Fluorometer before and after acidification with ~2 drops 5 % HCl. Chlorophyll-a concentrations were calculated after Riaux-Gobin and Klein (1993) and expressed in units of μg g^{-1} dry sediment. Chlorophyll-a samples from 2008 were collected and analyzed by H. Link and P. Archambault (ISMER-UQAR, Rimouski, CA) using the same analytical approach. Standard deviations (1 σ) of chlorophyll-a concentrations were calculated from triplicate measurements of ~40 % of the sediment samples collected in 2009 and all sediment samples provided by H. Link and P. Archambault. Triplicate measurements of the samples collected in 2009 were done on sample aliquots, whereas triplicate measurements provided by H. Link and P. Archambault were done on three individual samples taken from the same location. Therefore, standard deviations for samples collected in 2009 represent the degree of measurement error, whereas standard deviations for samples provided by H. Link and P. Archambault represent a measure of environmental variability.

2.2.5 Elemental and stable isotope analysis

Thawed, wet sediment samples (~1-2 mg) were transferred to high density polyethylene 45 ml centrifuge tubes, acidified overnight with 5 M HCl, washed and centrifuged, and dried in a box oven at 40 °C until dry. Dried sediments were then finely powdered with mortar and pestle and transferred and stored in glass vials until analysis.

Organic carbon (C_{org}) and total nitrogen (N_{total}) contents were measured on the acid extracted and washed residues with a Carlo Erba NA1500 Series II Elemental Analyser, and stable carbon isotopes $\delta^{13}C$ were measured by interfacing the elemental analyser through a ConfloII interface with a ThermoElectronDeltaVPlus Gas Source Isotope Ratio

Mass Spectrometer. The data were normalized using the standards IAEA-N-1, IAEA-N-2, IAEA-CH-6, B2153 (low organic content soil standards), and two Memorial University laboratory standards (MUN-CO-2 ($CaCO_3$) and MUN Sulfanilamide). The average precision on these reference materials was ± 0.5 ‰ for $\delta^{13}C$, ± 2 % for wt.% C_{org} and ± 3 % for wt.% N_{total}. The carbon isotopic ratios were reported in ‰ relative to VPDB, and elemental data of C_{org} and N_{total} are reported in wt. %. Standard deviations (1 σ) of C_{org}, N_{total} and $\delta^{13}C$ values were calculated from duplicate measurements of sample aliquots of ~19 % of the analyzed samples.

Elemental carbon/nitrogen ratios (C/N) and isotopic carbon analysis ($\delta^{13}C$) have been widely used to distinguish between various organic matter sources (e.g. Schubert and Calvert, 2001; Ogrinc et al., 2005; Goñi et al., 2005; Magen et al., 2010). In general, $\delta^{13}C$ values of terrigenous organic matter, which is mainly produced by freshwater plankton and vascular plants, ranges from -25 ‰ to -33 ‰ in C_3-dominated environments. C/N ratios of vascular plant material are around 12 and higher. Marine organic matter, mostly of autotrophic and heterotrophic origin, has $\delta^{13}C$ values from -16 ‰ to -23 ‰ (Lamb et al., 2006). C/N ratios of marine organic matter such as phytoplankton and particulate organic carbon generally range from 4 to 10 (Lamb et al., 2006). For the end-member modeling, -19.5 ‰ as marine $\delta^{13}C$ end-member and -29 ‰ as terrigenous $\delta^{13}C$ end-member were therefore chosen, which are the middle points of $\delta^{13}C$ ranges of marine algae and marine particulate organic matter and freshwater algae and freshwater particulate organic matter as pointed out by Lamb et al. (2006). C_{org}, N_{total} and $\delta^{13}C$ data are only available for sediment cores collected in 2009.

To calculate the relative proportions of marine and terrestrial organic carbon a two-component mixing model (Schultz and Calder, 1976; Addison et al., 2012) (Eq. 1 and 2) was used.

$$m_{\text{terr}} = \left(\frac{\delta^{13}C_{\text{sample}} - \delta^{13}C_{\text{marine}}}{\delta^{13}C_{\text{terr}} - \delta^{13}C_{\text{marine}}}\right) \quad (1)$$

$$C_{\text{org marine}} = C_{\text{org sample}} - (m_{\text{terr}} \times C_{\text{org sample}}) \quad (2)$$

where m_{terr} is the terrestrial fraction of the organic carbon, $\delta^{13}C_{sample}$ is the isotopic carbon composition of the sediment sample [‰], $\delta^{13}C_{marine}$ is the marine $\delta^{13}C$ end-member [‰], $\delta^{13}C_{terr}$ is the terrestrial $\delta^{13}C$ end-member [‰], $C_{org\ marine}$ is the marine organic carbon fraction [wt. %] of the sediment sample, and $C_{org\ sample}$ is the organic carbon concentration of the sediment sample [wt. %]. A minor correction of the C_{org}/N_{total} ratios to C_{org}/N_{org} as described by Schubert and Calvert (2001) was made by using the linear regression of N_{total} versus C_{org} ($r^2 = 0.93$, $N_{total} = 0.12 \times C_{org} + 0.01$).

The ratio of chlorophyll-a to C_{org} of surface sediments was calculated as an indicator of fresh and highly reactive organic matter and food quality (e.g. Grebmeier and Barry, 1991; Sun et al., 1991 and 1994; Boon and Duineveld, 1996 and 1998; Stephens et al., 1997; Morata et al., 2008; Gutiérrez et al., 2000; Link et al., 2011).

2.2.6 Modeling of bioturbation and sedimentation rates

The approach used to measure particle mixing rates in the current study is based on the assumption that a diffusion-like process redistributes sediment particles, and the

application of a biodiffusion model to vertical tracer distributions (e.g. Goldberg and Koide, 1962; Guinasso and Schink, 1975; Berner, 1980; Aller, 1982; Cochran, 1985; Boudreau, 1986). Biodiffusion coefficients D_b [$cm^2\ y^{-1}$] of bioturbated surface sediments were calculated from regressions against downcore distributions of excess ^{210}Pb and excess ^{228}Th with Eq. 3 (Bentley and Nittrouer, 2003):

$$A = A_0 \exp\left(-z\left(\sqrt{\frac{\lambda}{D_b}}\right)\right) \quad (3)$$

where A is the activity of the tracer [dpm g^{-1}], A_0 is the tracer activity at the sediment-water interface [dpm g^{-1}], λ is the decay constant of the tracer ($\lambda^{228}Th$ = 0.362 y^{-1}, $\lambda^{210}Pb$ = 0.031 y^{-1}) and z is the depth in sediment [cm] (e.g. Green et al., 2002); and from vertical distributions of chlorophyll-a and Eq. 4

$$C = (C_0 - C_\infty)\exp\left(-z\sqrt{\frac{k_d}{D_b}}\right) + C_\infty \quad (4)$$

where C is the concentration of chlorophyll-a [µg g^{-1} dry sediment] at a certain depth, C_0 is the chlorophyll-a concentration at the sediment-water interface [µg g^{-1} dry sediment], C_∞ is the background concentration of chlorophyll that is unreactive over the timescale of interest, k_d is the degradation rate constant for chlorophyll-a [d^{-1}], and z is the depth in sediment [cm] (Sun et al., 1991; Green et al., 2002; Josefson et al., 2002). The degradation constant k_d was estimated using Eq. 5 based on laboratory incubation data by Sun et al. (1993)

$$\ln k_d = 18.3 - 6160\ T^{-1} \quad (5)$$

where T is temperature [K]. Temperature data in the current study were obtained from near bottom CTD measurements provided by Y. Gratton and D. Boisvert (INRS-Eau, terre et environnement, CA) and P. Guillot (Institut des Sciences de la Mer de Rimouski (ISMER), CA). Values of k_d [d^{-1}] were converted to units of y^{-1} and used in Eq. 4 to obtain biodiffusion coefficients (D_b) in units of $cm^2\ y^{-1}$.

Below the sediment zone where particle mixing by bioturbation dominates (L_b), sediment accumulation rates (ω) were calculated from regressions against depth distributions of excess ^{210}Pb with Eq. 6, assuming negligible sediment mixing below L_b (Bentley and Nittrouer, 2003):

$$A = A_0 \exp\left(-\frac{\lambda z}{\omega}\right) \quad (6)$$

where A is the $^{210}Pb_{xs}$ activity [dpm g^{-1}], A_0 is the $^{210}Pb_{xs}$ activity at the sediment-water interface, λ denotes the decay constant of ^{210}Pb (λ = 0.031 y^{-1}), z is the depth in sediment [cm], and ω represents the sediment accumulation rate [cm y^{-1}]. Sediment accumulation rates from $^{210}Pb_{xs}$ down core distributions were further validated by sediment accumulation rates calculated from activity profiles of the anthropogenic radionuclide ^{137}Cs, which was first introduced to the atmosphere in 1954 by nuclear weapon tests, as well as Eq. 7

$$\omega\,(^{137}\mathrm{Cs}) = \frac{(z_p - L_b)}{(T - 1954)} \qquad (7)$$

where $\omega(^{137}Cs)$ is the sediment accumulation rate obtained from ^{137}Cs depth distribution [cm y^{-1}], z_p is the maximum penetration depth of ^{137}Cs in sediment cores [cm], $L_b(^{210}Pb_{xs})$ is the mixing layer depth [cm] obtained from excess ^{210}Pb profiles, and T is the year of sample collection [y] (Krishnaswami et al., 1980).

Equations 3, 4 and 6 were then fitted to tracer distributions with a least square method and the Marquard-Levenberg algorithm using SigmaPlot 11.0 (Systat Software, San Jose, CA, USA).

2.2.7 Statistics

Correlation strengths of bioturbation proxies with environmental variables, analyzed to describe environmental processes, were evaluated by calculating the Pearson product-moment (r_p) and Spearman's rank-order (r_s) correlation coefficients using R 3.0.1 (R Development Core Team, 2013). Both correlation methods were used in tandem to estimate linear and/or monotonic relationships between bioturbation proxies and environmental variables. To further explore relationships among environmental variables a principal component analysis (PCA) was conducted with R 3.0.1 and the CRAN package FactoMineR (Husson et al., 2013).

2.3 Results

2.3.1 Tracer profiles and biodiffusion coefficients (D_b), mixing depths, and sedimentation rates (ω)

$^{210}Pb_{xs}$ activity-depth distributions

Type I $^{210}Pb_{xs}$ profiles dominated collected sediments and were characterized by a distinct inflection point above which activities are nearly constant, as indicated by close to vertical profile segments between the surface of sediment cores and a depth of 1.5-6.5 cm. Below inflection points, $^{210}Pb_{xs}$ activities decreased exponentially with depth (Fig. 2.2 A, Table 2.2). Similar to *Type I* profiles, nearly vertical profile segments in the top centimeters of the cores (4.5-5.5 cm) characterized *Type Ia $^{210}Pb_{xs}$* profiles (Fig. 2.2 B, Table 2.2). Below this surface zone, $^{210}Pb_{xs}$ activities decreased exponentially with depth over a short range of 2-3 cm and then increased again to form a subsurface activity peak in depths of 8.5 and 12.5 cm. Only two sediment cores collected at stations 109 and 233 exhibit *Type Ia* profiles. *Type II $^{210}Pb_{xs}$ profiles* showed exponentially decreasing surface profile segments to steep and nearly vertical activity-depth distributions that characterized three sediment cores collected at stations 136, 140 and 308 (Fig. 2.2 C, Table 2.2). Surface segments ranged from 2.5 to 5.5 cm depth, below which no $^{210}Pb_{xs}$ activities were detected.

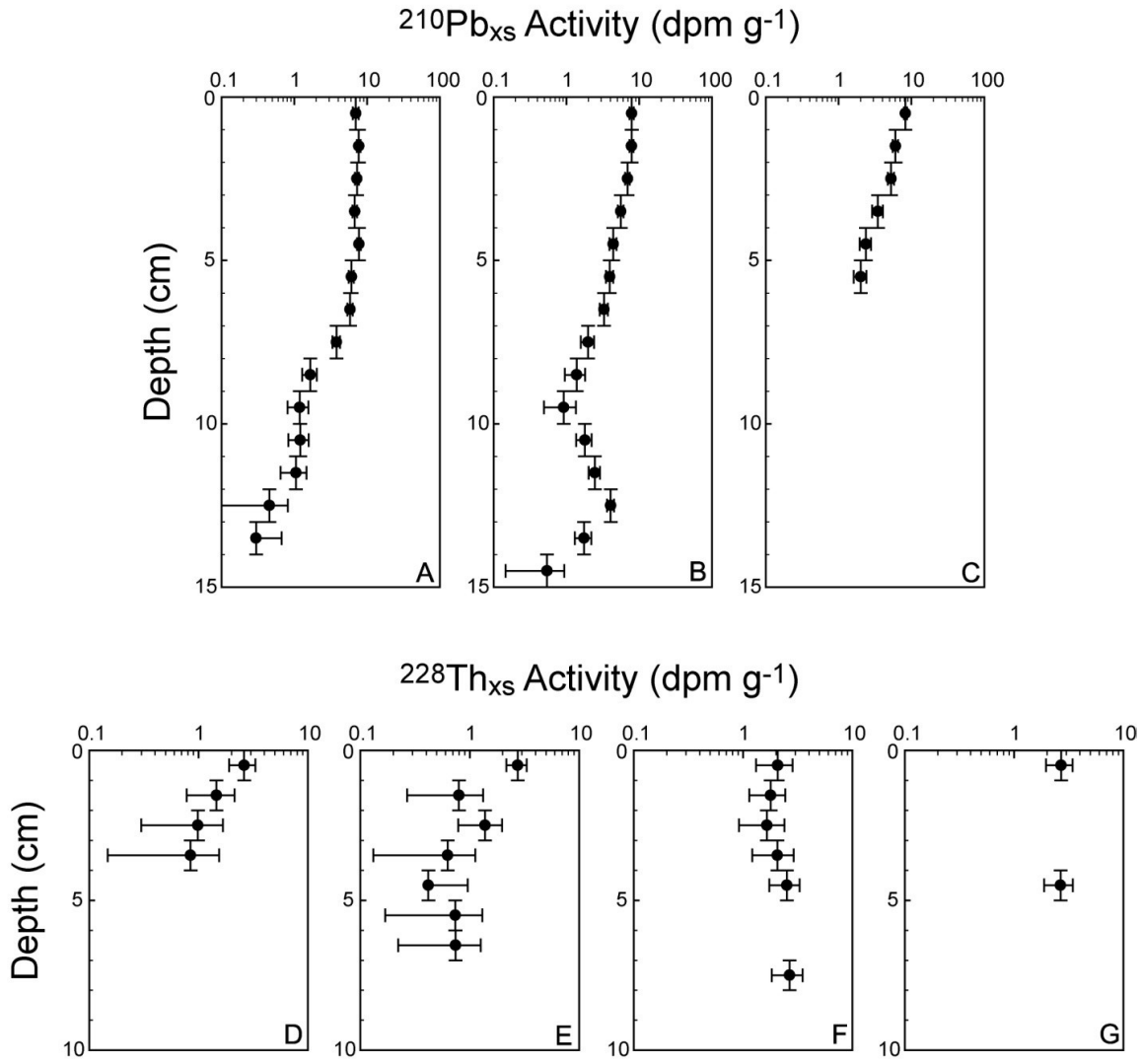

Figure 2.2: $^{210}Pb_{xs}$ and $^{228}Th_{xs}$ activity-depth distributions. Horizontal error bars represent standard deviations of net peak areas (1 σ) from gamma counting of radionuclides. Vertical error bars represent the thickness of analyzed sediment sections. Examples for $^{210}Pb_{xs}$ profile A) Type I (108), B) Type Ia (233) and C) Type II (136). Examples for $^{228}Th_{xs}$ profile D) Type I (233), E) Type Ia (101), F) Type II (111b), and G) Type III (115b).

Biodiffusion coefficients ($D_b(^{210}Pb_{xs})$) were calculated from surface $^{210}Pb_{xs}$ profile segments ($L_b(Pb)$) in which bioturbation influences are assumed to be dominant. The

occurrence of bioturbation structures found in corresponding depth intervals of X-radiographs (see chapter 2.3.2) support this assumption. $^{210}Pb_{xs}$ biodiffusion coefficients varied between 0.1 and 20.1 $cm^2\ yr^{-1}$. On average, the North Water region exhibited higher biodiffusion coefficients than any other sampled region, with highest values of $D_b(^{210}Pb_{xs})$ at stations 101 and 111b (Table 2.2).

Table 2.2: Particle tracer derived biodiffusion coefficients D_b, bioturbation depths L_b, tracer penetration depths z_p, tracer profile types, and $^{210}Pb_{xs}$ and ^{137}Cs derived sedimentation rates ω.

		$^{210}Pb_{xs}$			$^{228}Th_{xs}$			Chl-a			ω (cm yr^{-1})	
Region	Station	L_b (cm)	Profile	D_b ($cm^2\ yr^{-1}$)[a]	z_p (cm)	Profile	D_b ($cm^2\ yr^{-1}$)[a]	z_p (cm)	Profile	D_b ($cm^2\ yr^{-1}$)[a]	$^{210}Pb_{xs}$[a]	^{137}Cs
AMG	**405**	1.5	I		4.5	I	8.78 ± 6.21	3.5	III	6.74 ± 4.23	0.03 ± 0.00	0.07
AMG	**408**	2.5	I	3.64 ± 1.80	2.5	II	* 530.51 ± 2685.60		IV	* 84.58 ± 464.59	0.09 ± 0.01	0.09
AMG	**437**	2.5	I	3.82 ± 0.82	2.5	Ia	0.89 ± 0.67		III	* 31.48 ± 38.27	0.03 ±	0.07
VMS	**308**	2.5	II	0.11 ± 0.09	0.5	III		2.5	I	3.05 ± 0.47		0.06
BS	**BS**	6.5	I	4.50 ± 2.01	5.5	Ia	* 4.48 ± 4.90	4.5	I	9.23 ± 0.09	0.09 ± 0.03	0.13
BS	**304**	3.5	I	* 6.72 ± 6.79	2.5	Ia	* 0.93 ± 1.58	1.5	I	* 0.03 ± 349.07	0.10 ± 0.01	0.07
LS	**301**	3.5	I	0.63 ± 0.04	5.5	I	0.80 ± 0.23	5.5	I	12.60 ± 2.93	0.12 ± 0.05	0.07
LS	**323**	1.5	I	3.21	3.5	I	0.70 ± 0.05	3.5	III	* 28.95 ± 35.88	0.07 ± 0.01	0.05
NoW	**101**	4.5	I	11.79 ± 11.32	6.5	Ia	2.80 ± 2.00	9.5	II	* 126.06 ± 183.18	0.13 ± 0.01	0.13
NoW	**108**	5.5	I	* 85.67 ± 191.94	8.5	I	10.95 ± 3.05	7.5	I	37.88 ± 27.55	0.07 ± 0.01	0.06
NoW	**109**	4.5	Ia	0.82 ± 0.23	3.5	I	6.32 ± 5.60		IV		0.05 ± 0.01	0.07
NoW	**111**	4.5	I	5.12 ± 1.20	5.5	I	7.55 ± 2.88	n.m.		n.m. n.m.	0.12 ± 0.01	0.11
NoW	**111b**	5.5	I	20.10 ± 12.40	7.5	II	26.85 ± 9.66	9.5	II		0.10 ± 0.01	0.07
NoW	**115**	4.5	I	1.82 ± 1.12	4.5	I	17.85 ± 12.92	4.5	I	26.06 ± 15.82	0.09 ± 0.03	0.09
NoW	**115b**	4.5	I	0.45 ± 0.05	4.5	III		3.5	I	* 16.33 ± 18.14	0.06 ± 0.03	0.04
NoW	**205**	3.5	I		6.5	I	5.11 ± 1.24	4.5	III	* 1945.94 ± 10581.33	0.15 ± 0.01	0.19
NoW	**233**	5.5	Ia	1.53 ± 0.46	3.5	I	1.80 ± 0.55	3.5	I	15.83 ± 9.03	0.07 ± 0.00	0.04
BB	**136**	5.5	II	0.38 ± 0.05	0.5	III			IV			
BB	**136b**	n.m.	n.m.	n.m. n.m.	n.m.	n.m.	n.m. n.m.	n.m.	IV			
BB	**140**	5.5	II	0.19 ± 0.10	0.5	III			IV			
BB	**141**	0.5	I		2.5	III		2.5	III	5.28 ± 3.62	0.07 ± 0.01	0.04
	mean	3.9		3.87	4.1		7.30	4.7		14.58	0.08	0.08
	st.dev.	1.6		5.41	2.3		7.64	2.5		11.89	0.03	0.04

[a]Uncertainties are standard errors of the estimate resulting from least square regression analyses with SigmaPlot 11.0. Values of D_b with standard errors that exceed the actual estimated value of D_b and values that seem unrealistically high (marked with a star) were excluded from the discussion.

From profile segments below surface layers, calculated sedimentation rates ($\omega(^{210}Pb_{xs})$) ranged from 0.03 cm yr^{-1} at station 405 and 437 in the Amundsen Gulf to 0.15 cm yr^{-1} in the North Water region (Table 2.2). $^{210}Pb_{xs}$ sedimentation rates were validated with sedimentation rates obtained from ^{137}Cs profiles (significant correlation of $\omega(^{210}Pb_{xs})$ with

$\omega(^{137}Cs)$, $r_p = 0.69$ and $r_s = 0.63$, $p < 0.01$). The North Water region yielded the highest sedimentation rates for both tracers, in contrast to the relatively low sedimentation rates in the Amundsen Gulf.

$^{228}Th_{xs}$ activity-depth distributions

Penetration depths of $^{228}Th_{xs}$ ($z_p(^{228}Th_{xs})$) ranged from 0.5 to 8.5 cm throughout the study area (Table 2.2). Most sediment cores exhibited *Type I $^{228}Th_{xs}$ profiles* defined by near exponential activity decreases with depth (Fig. 2.2 D). *Type Ia $^{228}Th_{xs}$ profiles* mirrored *Type I profiles* showing a decrease of $^{228}Th_{xs}$ activities with depth (Fig. 2.2 E, Table 2.2), but were more variable then *Type I $^{228}Th_{xs}$ profiles*. Only two sediment cores from stations 111b and 408 exhibited activity-depth distributions of a *Type II $^{228}Th_{xs}$ profile* (Fig. 2.2 F, Table 2.2), which displayed nearly constant $^{228}Th_{xs}$ activities with depth. Finally, *Type III $^{228}Th_{xs}$* profiles consisted of only one and two data points and showed no apparent trends over corresponding depth intervals (Fig. 2.2 G, Table 2.2).

Biodiffusion coefficients calculated from $^{228}Th_{xs}$ profiles varied between 0.70 $cm^2\ yr^{-1}$ at station 323 in Lancaster Sound and 26.85 $cm^2\ yr^{-1}$ at station 111b in the North Water region (Table 2.2). Subsurface activity peaks were not used in calculations and D_b values were estimated from $^{228}Th_{xs}$ surface profile segments that decreased with depth (e.g. Fig. 2.2 F).

Chlorophyll-a concentration-depth distributions

Sampled sediment cores produced four types of chlorophyll-a profiles (Fig. 2.3, Table 2.2). *Type I and II profiles* both showed decreasing concentrations with depth (Fig. 2.3 A

and B). Chlorophyll-a concentrations in *Type I profiles* approach a constant value. In *Type II* profiles the background chlorophyll-a concentration (C_∞) in deeper sediment layers gradually decreased to a depth of 10 cm. Most sediment cores exhibited *Type I profiles*, whereas *Type II profile*s characterized only cores collected at stations 101 and 111b in the North Water region (Table 2.2). *Type III profiles* were characterized by depth-decreasing chlorophyll-a concentrations with subsurface concentration spikes (Fig. 2.3 C). *Type IV* profiles (stations 136 and 136b in Baffin Bay) showed a nearly vertical distribution of constant chlorophyll-a concentrations within the upper four centimeters of the core and a sudden increase with depth between 5 and 10 cm (Fig. 2.3 D).

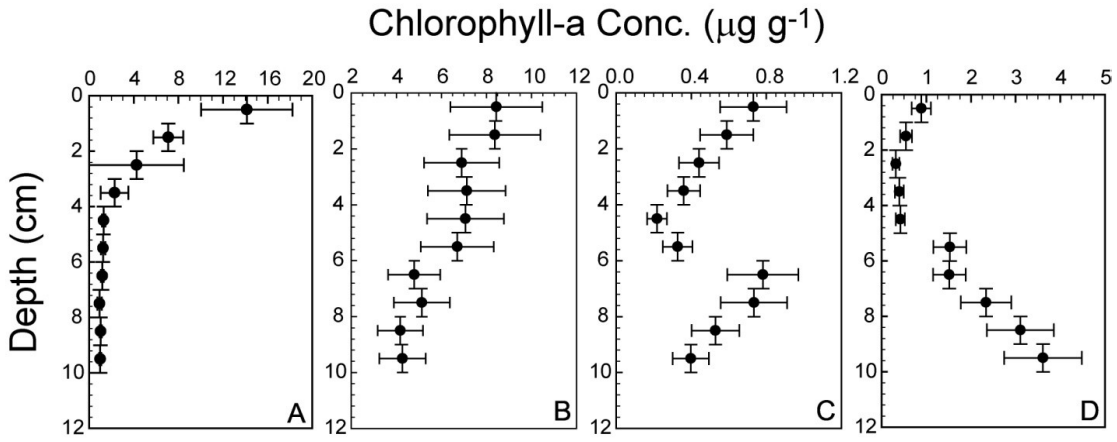

Figure 2.3: Chlorophyll-a concentration-depth distributions. Horizontal error bars represent standard deviations (1 σ) of triplicate measurements of all sediment samples provided by H. Link and P. Archambault (ISMER-UQAR, Rimouski, CA) and approximately 40 % of the sediment samples collected in 2009. Vertical error bars represent the thickness of analyzed sediment sections. Examples for chlorophyll-a profile A) Type I (BS), B) Type II (111b), C) Type III (437), and D) Type IV (136b).

The depth where chlorophyll-a concentrations reach C_∞ was estimated from the individual profiles and used to define the penetration depth of reactive chlorophyll-a (z_p(chl-a)) (Table 2.2). Values of z_p(chl-a) ranged from 1.5 to 9.5 cm across the study area with highest values at station 101 and 111b in the North Water region. Biodiffusion coefficients calculated from chlorophyll-a profiles (D_b(chl-a) were highest in Lancaster Sound and the North Water region, with values varying between 3.05 and 37.88 $cm^2\ yr^{-1}$ throughout the Canadian Arctic Archipelago.

2.3.2 Bioturbation traces and sedimentary fabric revealed by X-radiography

Figure 2.4 shows selected X-radiographs representing each sub-region of the study area (for an overview of all X-radiographs see Appendix 2.1). Fine-grained muddy matrices with scattered ice-rafted debris clasts (> 2 mm) consistently dominated sediment cores. Sediments were not stratified except for station 308 in Viscount Melville Sound and, to a lesser extent, station 141 in Baffin Bay (Fig. 2.4 F and H). Incorporated ice-rafted debris clast (IRD) had size ranges from ~2 mm to several centimeters in diameter (e.g. Fig. 2.4 G).

From 21 sediment cores, all X-radiographs showed evidence of bioturbation in the form of biomottled sediment and/or the occurrence of burrow tracks and tubes created by benthic macrofauna. Even though bioturbation traces were well preserved in sediments throughout the cores (Figure 2.4 A, D, E, and G; Table 2.3), the fabric of some sediment cores appeared biomottled and nearly homogeneous, with few or no distinct bioturbation structures (Fig. 2.4 B and C; Table 2.3).

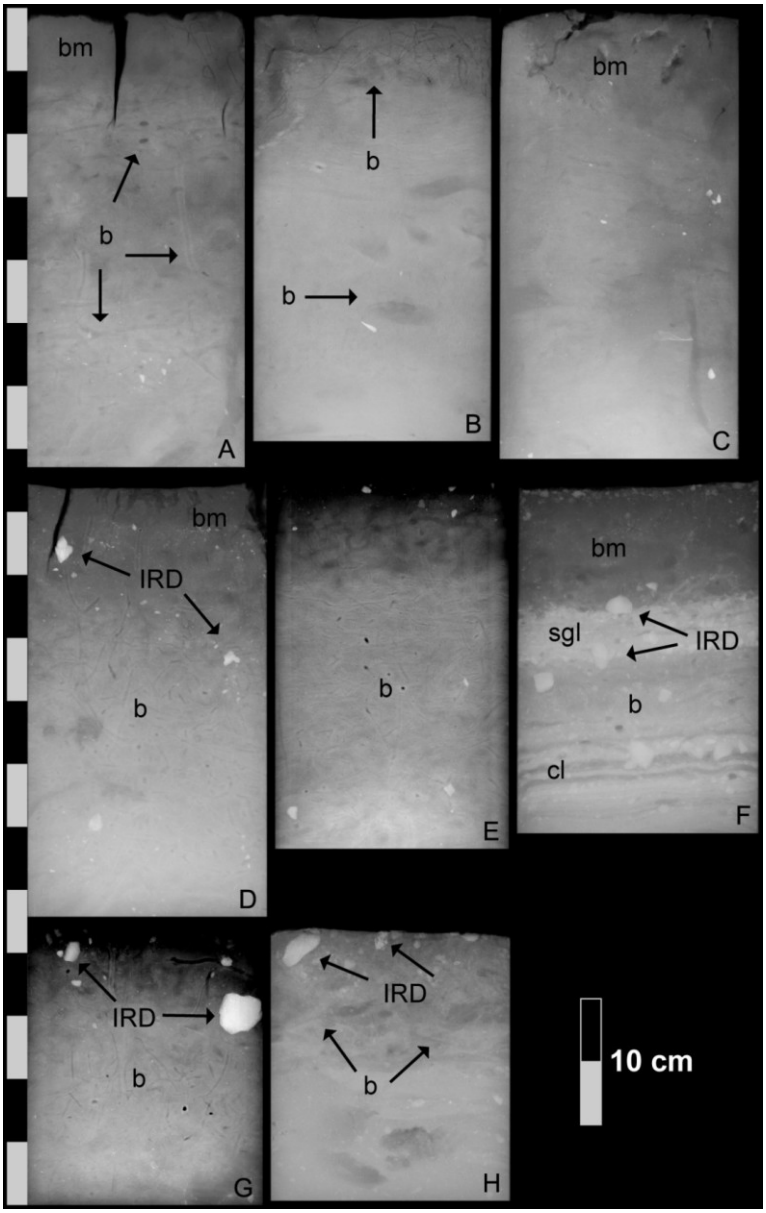

Figure 2.4: Examples of bioturbation traces and sedimentary fabric in sediment cores collected throughout the Canadian Arctic Archipelago (X-radiograph negatives: high density=light, low density=dark) and at the sampling stations A) 111b (North Water), B) 408 (Amundsen Gulf), C) 304 (Barrow Strait), D) 323 (Lancaster Sound), E) 136 (Baffin Bay), F) 308 (Viscount Melville Sound), G) 233 (North Water), and H) 141 (Baffin Bay). IRD=ice-rafted debris clast, b=burrow, bm=biomottled, sgl=sand gravel layer, cl=clay layer.

Table 2.3: Burrow diameter, number of tiers, and number of bioturbation structure types and sediment fabric description of sediment cores.

Region	Station	Mean Diameter (cm) 0-10 cm	Mean Diameter (cm) Full core	Number of Bioturbation Structures 0-10 cm	Number of Bioturbation Structures Full core	Number of Tiers	Sediment Fabric
AMG	**405**	0.89	0.89	1	1	1	bioturbated, nearly homogeneous mud
AMG	**408**	0.10	0.34	2	4	3	bioturbated, nearly homogeneous mud, few distinct bioturbation traces
AMG	**437**	0.24	0.15	2	4	3	bioturbated, nearly homogeneous mud, few distinct bioturbation traces
VMS	**308**	0.36	0.30	1	2	2	interlaminated sands and muds, partially bioturbated, few distinct bioturbation traces
BS	**BS**	0.11	0.48	1	2	2	bioturbated, nearly homogeneous mud, few distinct bioturbation traces
BS	**304**	0.06	0.06	1	1	1	bioturbated, nearly homogeneous mud
LS	**301**	0.20	0.14	1	2	2	bioturbated mud, distinct bioturbation traces
LS	**323**	0.23	0.18	1	2	2	bioturbated mud, distinct bioturbation traces
NOW	**101**	0.65	0.35	1	2	2	bioturbated mud, distinct bioturbation traces
NOW	**108**	0.33	0.33	2	2	2	bioturbated mud, distinct bioturbation traces
NOW	**109**	0.17	0.25	2	2	2	gravelly mud, very few distinct bioturbation traces
NOW	**111**	0.99	0.17	3	4	4	bioturbated mud, distinct bioturbation traces
NOW	**111b**	0.15	0.20	2	4	4	bioturbated mud, distinct bioturbation traces
NOW	**115**	0.22	0.18	1	2	2	bioturbated mud, distinct bioturbation traces
NOW	**115b**	0.52	0.45	2	4	4	bioturbated mud, distinct bioturbation traces
NOW	**205**	0.13	0.61	2	3	3	bioturbated, nearly homogeneous mud, few distinct bioturbation traces
NOW	**233**	0.11	0.11	2	3	2	bioturbated mud, distinct bioturbation traces
BB	**136**	0.23	0.16	2	4	2	bioturbated mud, distinct bioturbation traces
BB	**136b**	0.23	0.16	2	4	2	bioturbated mud, distinct bioturbation traces
BB	**140**	0.06	0.29	1	2	2	bioturbated, nearly homogeneous mud, few distinct bioturbation traces
BB	**141**	0.11	0.11	1	1	1	gravelly mud (core top) and slightly interlaminated muds, few distinct bioturbation traces

Faintly visible traces and biomottling were observed in X-radiographs of sediment cores from station 308 in Viscount Melville Sound and station 141 in Baffin Bay (Fig. 2.4 F and H). The number of different burrow types, based on general burrow morphology and orientation, ranged from 1 to 3 within the upper 10 cm of sediment cores and from 1 to 4 within full cores. Mean burrow diameters ranged between 0.06 and 0.99 cm in the upper 10 cm of cores and 0.06 and 0.89 cm in full cores. Tiering could be identified on X-radiographs by the cross-cutting relationship of open burrow systems. The number of tiers and tiering depths varied between 1 and 4 tiers per core, respectively (Table 2.3).

2.3.3 Substrate characteristics of the surface sediment (0-10 cm)

Surface sediments across the study area consisted mainly of silt (61-97 %) with lesser fractions of sand (0-32 %) and clay (0-23 %). Comparatively high percentages of sand occurred at stations 109 (31.5 %) in the North Water region and 141 (31.9 %) in Baffin Bay (Fig. 2.5 A).

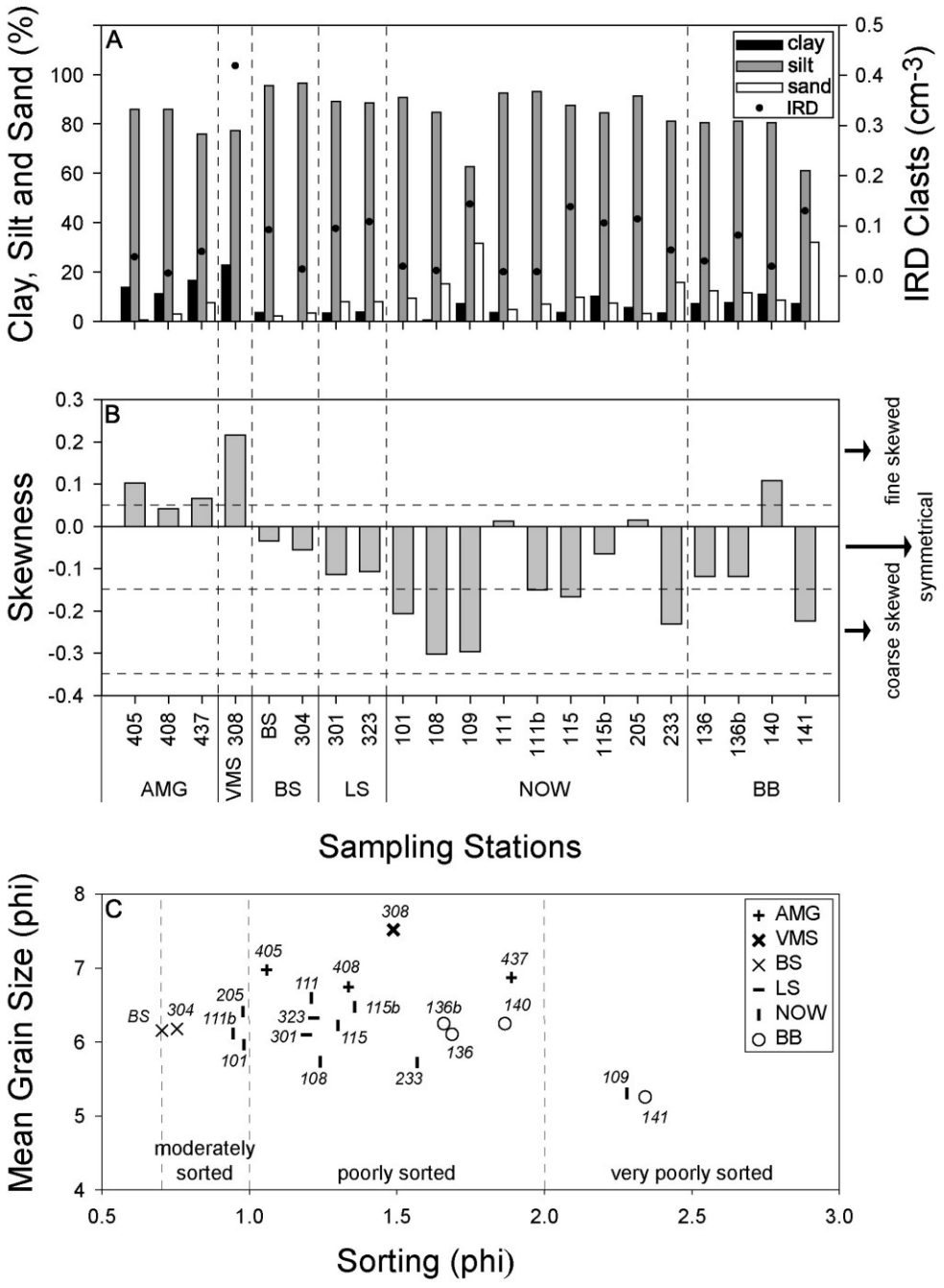

Figure 2.5: Substrate characteristics of surface sediments (0-10 cm) collected in Amundsen Gulf (AMG), Viscount Melville Sound (VMS), Barrow Strait (BS), Lancaster Sound (LS), North Water (NOW), and Baffin Bay (BB). A) Percentages of clay, silt and sand, and number of ice-rafted debris clasts (IRD) per cm^3 sediment, B) Skewness of particle size distributions (within the measured range of 11 to -1.6 phi) and C) Mean grain size (phi) and sorting of particle size distributions (within the measured range of 11 to -1.6 phi).

Concentrations of IRD clasts varied between 0.005 clasts/cm^3 at station 408 and 0.4 clasts/cm^3 at station 308 in sampled surface sediments. Although higher clay content and positive skewness characterized sediment cores collected from the Amundsen Gulf and Viscount Melville Sound, higher sand proportions and symmetric to coarsely skewed particle frequency distributions characterized sediment cores from the North Water region and Baffin Bay (Fig. 2.5 B). An exception was station 140 in Baffin Bay, which showed a positively, fine skewed particle distribution.

Sorting of the particle size class 11 to -1.6 phi varied from moderately to very poorly sorted (Fig. 2.5 C). The majority of cores collected throughout the study region contained moderately to poorly sorted, medium to fine silt sediments (stations: 405, 408, 437 (AMG), 301, 323 (LS), 101, 108, 111, 111b, 115, 115b, 205, 233 (NOW), 136, 136b, 140 (BB)). Both stations in Barrow Strait (BS and 304), station 308 in Viscount Melville Sound, and stations 141 (Baffin Bay) and 109 (North Water) exhibited slightly different characteristics with moderately sorted fine silt sediments, poorly sorted very fine sediments, and very poorly sorted medium silt sediments, respectively.

2.3.4 C_{org}, N_{total}, $\delta^{13}C$, and chl-a

The organic carbon analyzed in surface sediments collected across the Canadian Arctic Archipelago derived mainly from marine organic matter sources (Fig. 2.6). In fact, C_{org} and the marine derived C_{org} correlated significantly with chlorophyll-a concentrations (r_p = 0.7 with $p \leq 0.05$, r_p = 0.8 with $p \leq 0.01$, Appendix 2.9) suggesting that most organic matter in surface sediments originated primarily from marine phytoplankton sources.

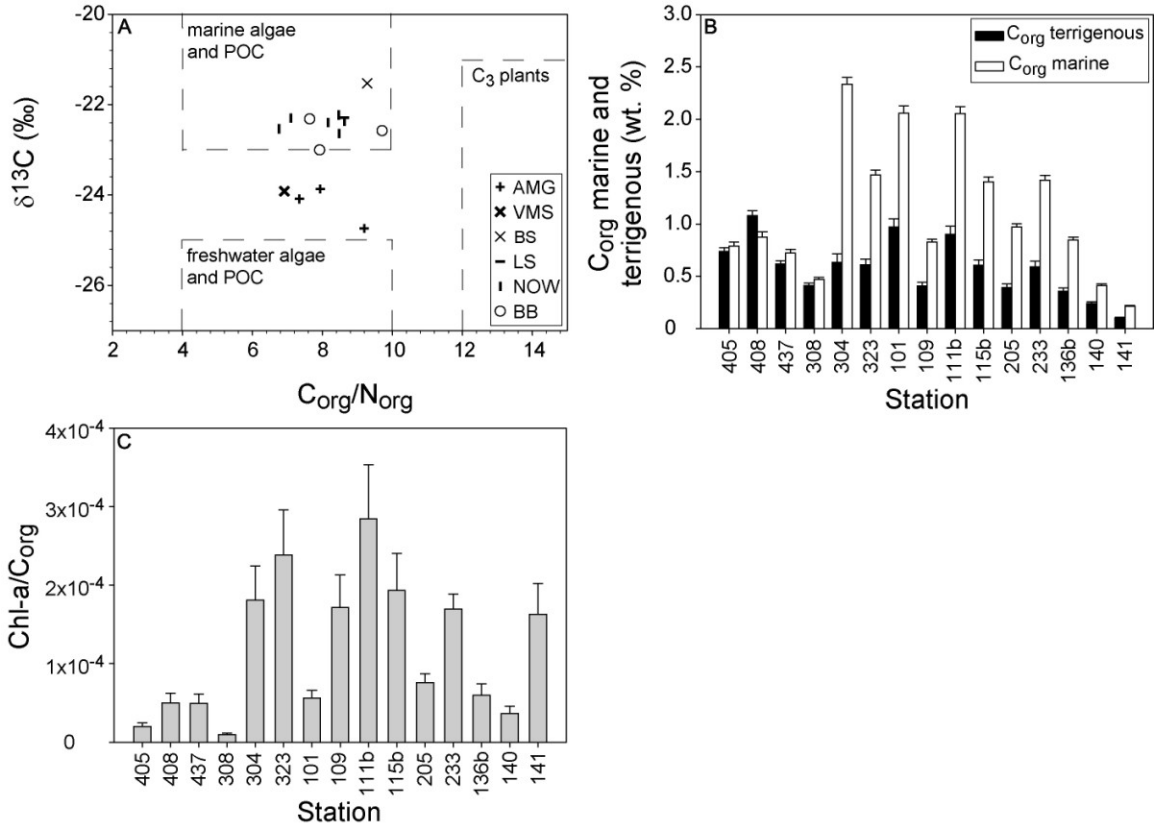

Figure 2.6: Organic matter characteristics of surface sediments (0-2 cm) collected in the Amundsen Gulf (AMG), Viscount Melville Sound (VMS), Barrow Strait (BS), Lancaster Sound (LS), North Water (NOW), and Baffin Bay (BB). A) Organic matter sources as revealed by $\delta^{13}C$ and C_{org}/N_{org} data, B) Portions of marine and terrigenous organic carbon as calculated from $\delta^{13}C$ data, error bars represent standard deviations (1 σ) of duplicate measurements of approximately 19 % of all sediment samples analyzed, and C) chlorophyll-a to organic carbon ratios representing organic matter quality, error bars represent standard deviations (1 σ) calculated from C_{org} and chlorophyll-a standard deviations of duplicate and triplicate sample measurements.

Total organic carbon concentrations (C_{org}) of surface sediments ranged from 0.32 to 3.03 wt. % and were highest in Barrow Strait and at stations 101 and 111b in the eastern and central parts of the North Water region, with values of 2.97, 3.03 and 2.96 wt. %. C_{org}

concentrations were lowest in sediments from Viscount Melville Sound and station 140 and 141 in northern Baffin Bay (0.88, 0.65, 0.32 wt. %) (Table 2.4).

Table 2.4: Total organic carbon (C_{org}), total nitrogen (N_{total}), $\delta^{13}C$, organic carbon to nitrogen ratio (C_{org}/N_{org}), and chlorophyll-a concentration of surface sediments (0-2 cm).

Region	Station	C_{org} (wt. %)[a]	$\delta^{13}C$ (‰)[a]	N_{total} (wt. %)[a]	C_{org}/N_{org}[a]	chl-a (µg g^{-1})[b]
AMG	**405**	1.53 ± 0.04	-24.09 ± -0.20	0.22 ± 0.03	7.34 ± 0.86	0.30 ± 0.07
AMG	**408**	1.95 ± 0.05	-24.75 ± -0.21	0.22 ± 0.03	9.20 ± 1.08	0.98 ± 0.24
AMG	**437**	1.34 ± 0.03	-23.87 ± -0.20	0.18 ± 0.02	7.94 ± 0.93	0.66 ± 0.16
VMS	**308**	0.88 ± 0.02	-23.95 ± -0.20	0.14 ± 0.02	6.91 ± 0.81	0.08 ± 0.02
BS	**BS**					10.62 2.72
BS	**304**	2.97 ± 0.07	-21.53 ± -0.18	0.33 ± 0.04	9.28 ± 1.09	5.36 ± 1.30
LS	**301**					3.01 0.79
LS	**323**	2.08 ± 0.05	-22.29 ± -0.19	0.25 ± 0.03	8.62 ± 1.01	4.95 ± 1.20
NoW	**101**	3.03 ± 0.07	-22.54 ± -0.19	0.46 ± 0.05	6.76 ± 0.80	1.71 ± 0.28
NoW	**108**					1.95 0.73
NoW	**109**	1.24 ± 0.03	-22.64 ± -0.19	0.16 ± 0.02	8.48 ± 1.00	2.12 ± 0.51
NoW	**111**					
NoW	**111b**	2.96 ± 0.07	-22.40 ± -0.19	0.37 ± 0.04	8.17 ± 0.96	8.41 ± 2.03
NoW	**115**					2.34 0.29
NoW	**115b**	2.01 ± 0.05	-22.37 ± -0.19	0.24 ± 0.03	8.63 ± 1.02	3.89 ± 0.94
NoW	**205**	1.36 ± 0.03	-22.23 ± -0.18	0.17 ± 0.02	8.47 ± 1.00	1.03 ± 0.15
NoW	**233**	2.01 ± 0.05	-22.30 ± -0.19	0.29 ± 0.03	7.11 ± 0.84	3.41 ± 0.38
BB	**136**					0.13 0.04
BB	**136b**	1.20 ± 0.03	-22.32 ± -0.19	0.17 ± 0.02	7.50 ± 0.88	0.72 ± 0.17
BB	**140**	0.65 ± 0.02	-23.00 ± -0.19	0.09 ± 0.01	7.79 ± 0.92	0.24 ± 0.06
BB	**141**	0.32 ± 0.01	-22.58 ± -0.19	0.04 ± 0.00	9.58 ± 1.13	0.51 ± 0.12

[a]standard deviations (1 σ) were calculated from duplicate measurements of approximately 19 % of all sediment samples analyzed.

[b]standard deviations (1 σ) were calculated from triplicate measurements of all sediment samples provided by H. Link and P. Archambault, ISMER-UQAR, Rimouski, CA and approximately 40 % of the sediment samples collected in 2009.

Barrow Strait, Lancaster Sound, the North Water region, and northern Baffin Bay exhibited highest $\delta^{13}C$ values of surface sediments (0-2 cm), ranging from -21.5 ‰ to -23.0 ‰. Surface sediment $\delta^{13}C$ values in the Amundsen Gulf and Viscount Melville Sound were slightly lower with values between -23.9 ‰ and -24.7 ‰ (Table 2.4). The C/N ratios calculated from organic carbon and nitrogen data ranged from 6.8 to 9.6 in surface sediments (Table 2.4).

As suggested by $\delta^{13}C$ values and C/N ratios, organic matter in sediments from stations in Barrow Strait, Lancaster Sound, the North Water region, and Baffin Bay was mainly of marine origin, whereas terrigenous organic matter sources contributed in part to the organic matter from the Amundsen Gulf and Viscount Melville Sound ($\delta^{13}C$: -23.9 - -24.8 ‰, C/N: 6.9-9.2) (Fig. 2.6 A, Table 2.4). Figure 2.6 B shows the relative portions of marine and terrigenous organic carbon (wt. %) obtained from end-member calculations.

Chlorophyll-a concentrations of surface sediments varied throughout the sampling sites from 0.08 to 10.62 µg g^{-1} dry sediment (Table 2.4). The highest chlorophyll-a concentrations occurred in surface sediments from both stations in Barrow Strait, station 323 in Lancaster Sound and stations in the western and central area of the North Water region (111b, 115, 115b, and 233). This is in contrast to relatively low surface sediment chlorophyll-a concentrations in the Amundsen Gulf, Viscount Melville Sound, northern Baffin Bay, and the eastern part of the North Water region. The lowest values occurred in Amundsen Gulf, Viscount Melville Sound and northern Baffin Bay.

Sediments from Barrow Strait, Lancaster Sound, the central and eastern areas of the North Water region, and from station 141 in Baffin Bay contained relatively high quality organic matter (Fig. 2.6 C). Lower chlorophyll-a/C_{org} ratios, and therefore lower quality organic matter, predominantly characterized sediment cores collected from the

Amundsen Gulf, Viscount Melville Sound, stations 101 and 205 in the western part of the North Water region, and station 140 and 136b in northern Baffin Bay.

2.3.5 Correlation analysis and principal component analysis (PCA)

Correlations among environmental variables and bioturbation proxies

Pearson Product Moment and Spearman's Rank Correlation analyses revealed several significant correlations among environmental variables and bioturbation proxies (Fig. 2.7 A-K, and scatter plots visualizing the relationships among bioturbation proxies and environmental variables in Appendix 2.2). Particularly strong linear (Pearson, r_p) and/or monotonic (Spearman, r_s) relationships ($p \leq 0.01$) were found between 1) biodiffusion coefficients D_b estimated from $^{210}Pb_{xs}$ profiles and the organic carbon concentration, the amount of terrigenous organic carbon and the percentage of silt in surface sediments (Fig. 2.7 A), 2) $^{228}Th_{xs}$ penetration depths z_p and each of sea bottom temperature, percentages of clay and silt, and sorting of surface sediments (Fig. 2.7 E) and 3) biodiffusion coefficients D_b estimated from chlorophyll-a profiles and the clay content of surface sediments (Fig. 2.7 C).

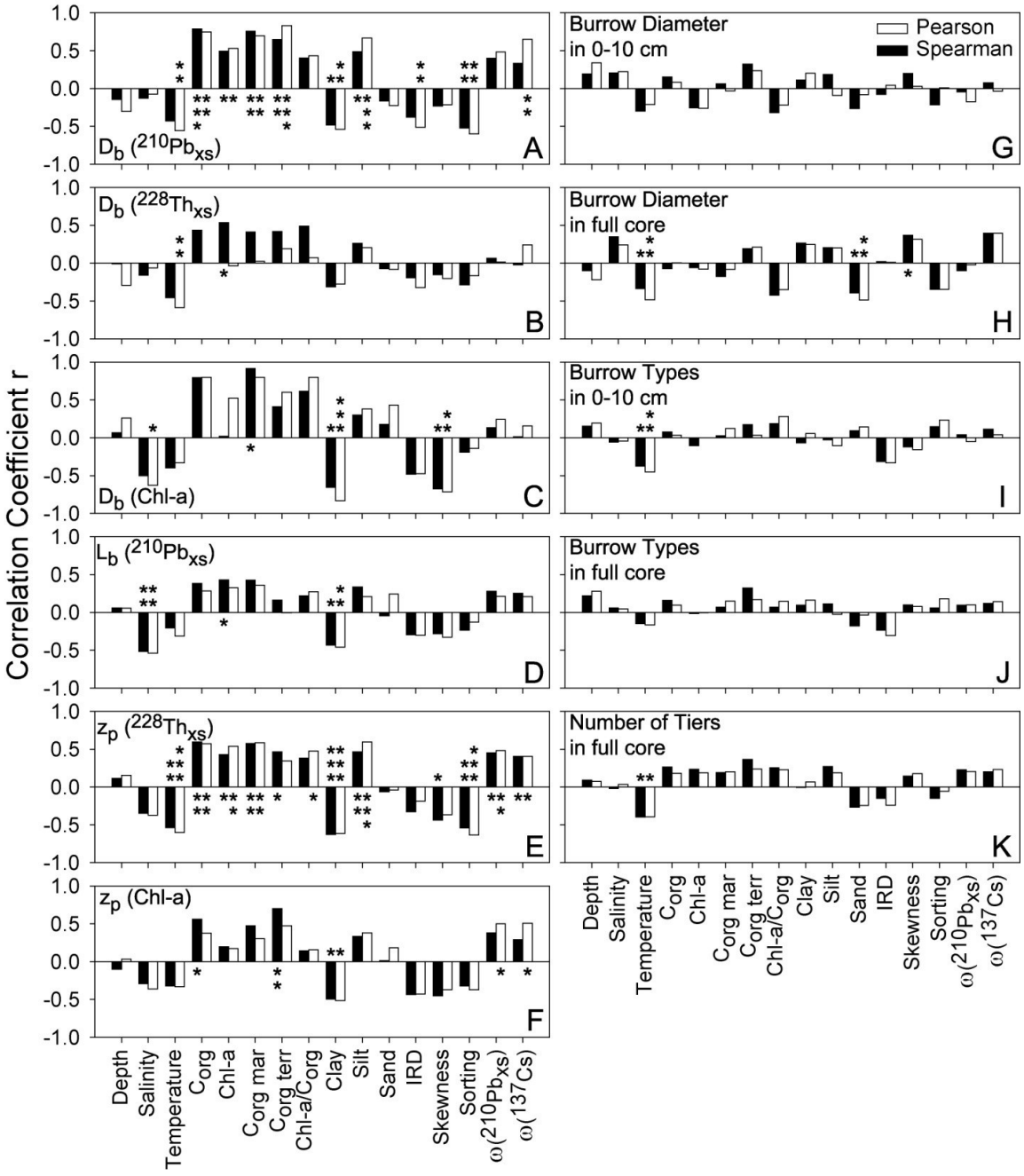

Figure 2.7: Pearson and Spearman correlations between bioturbation proxies (A-K) and environmental variables with significance levels $p \leq 0.1$ (*), $p \leq 0.05$ (**) and $p \leq 0.01$ (***). Each figure box shows the correlation strengths (bars) and significances (stars) of a bioturbation proxy with the environmental variables on the bottom axis.

Principal component analysis (PCA)

Two principal components captured much of the variability in relationships among environmental variables collected in the current study, explaining a total of 60.24 % of the data variability (Fig. 2.8 A and B, Appendix 2.3). Salinity was excluded from the principal components analysis because it varied little throughout the region. With correlation coefficients ≥ l0.8l, the concentrations of total organic carbon and marine organic carbon, the percentage of silt, and the sorting of sediments primarily defined component 1 (Fig. 2.8 B). Chlorophyll-a, terrigenous organic carbon, $^{210}Pb_{xs}$ derived sedimentation rate, chl-a/C_{org} ratio, temperature, the percentages of sand and clay, and the number of IRD in sediments were less influential but also correlated significantly with principal component 1. Skewness of particle distributions, the percentage of sand as well as the ratio of chlorophyll-a to total organic carbon (correlation coefficient ≥ l0.8l), and to a lesser extent the percentage of clay and the ^{137}Cs derived sedimentation rate correlated most strongly with principal component 2.

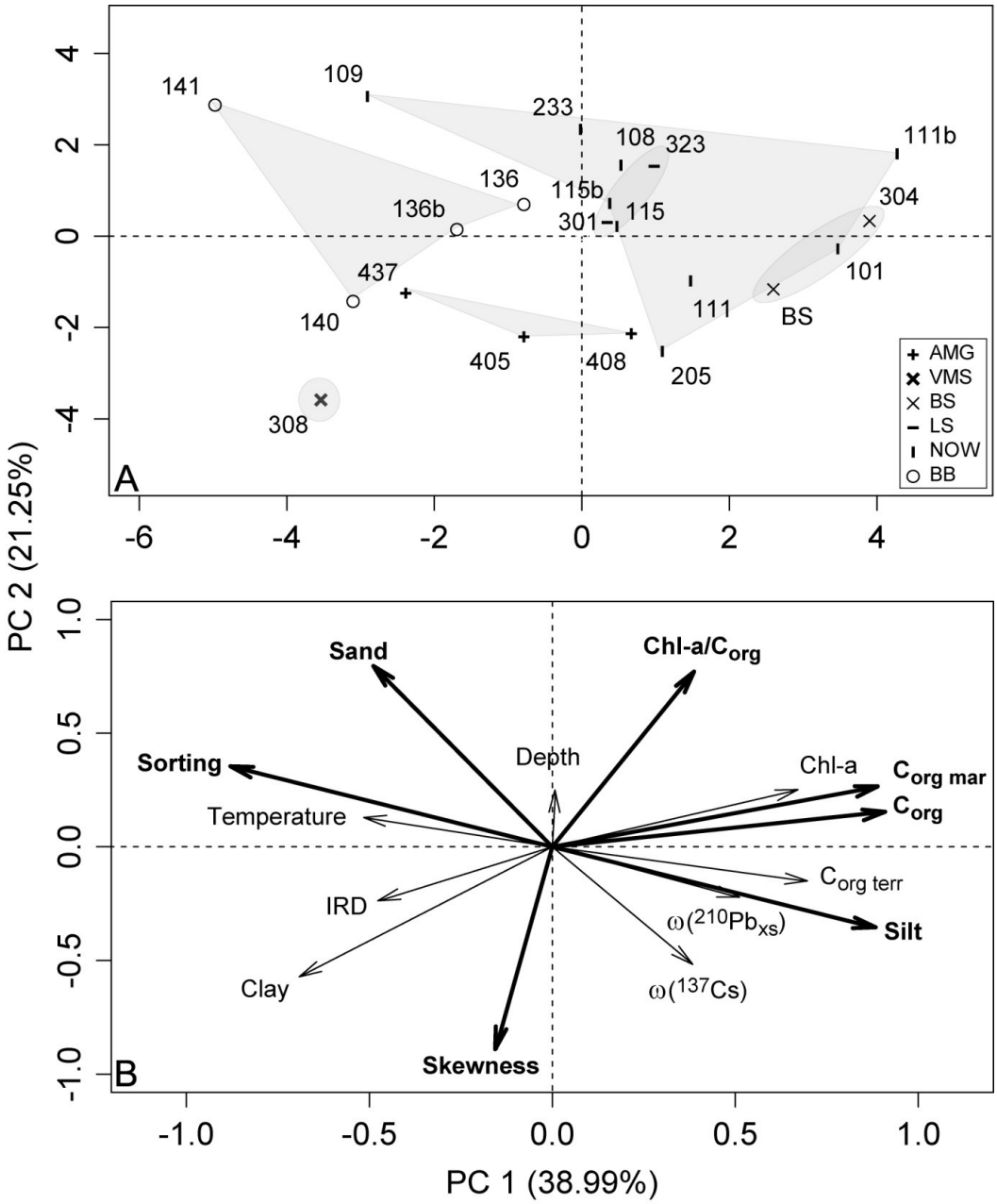

Figure 2.8: Results of principal component analysis with environmental variables analyzed in sediment cores collected from Amundsen Gulf (AMG), Viscount Melville Sound (VMS), Barrow Strait (BS), Lancaster Sound (LS), North Water (NOW), and Baffin Bay (BB). Principal components explain a total of 60.24 % of the variability in environmental data collected across the study region. A) Scatter plot of principal components 1 (PC 1) and 2 (PC 2). B) Vector plot of principal component loadings (PC1 and PC 2). Heavily weighted loadings (≥ l0.8l) are indicated in bold.

PCA results indicated similarities in environmental characteristics between sampling locations. Generally, regions in the north-eastern part of the study area (Barrow Strait, Lancaster Sound and North Water) were characterized by high organic matter (C_{org}, chl-a) input and quality, and symmetrical to coarse-skewed substrates with higher percentages of sand. Low organic matter input and quality, and relatively high clay percentages characterized the western part of the study region (Amundsen Gulf and Viscount Melville Sound), and low organic matter input and quality, and relatively high sand percentages were typical for most Baffin Bay sediments. Figure 2.9 illustrates the relationships between bioturbation proxies and environmental patterns uncovered by PCA. Bioturbation intensity and depth (Fig. 2.9 A-F), as well as bioturbation structure diameter (Fig. 2.9 G) responded well to environmental patterns and significantly correlated with PC1 and PC2, respectively. The number of burrow types and tiers, however, did not respond to the spatial distribution of identified benthic environmental conditions (Fig. 2.9 H and I).

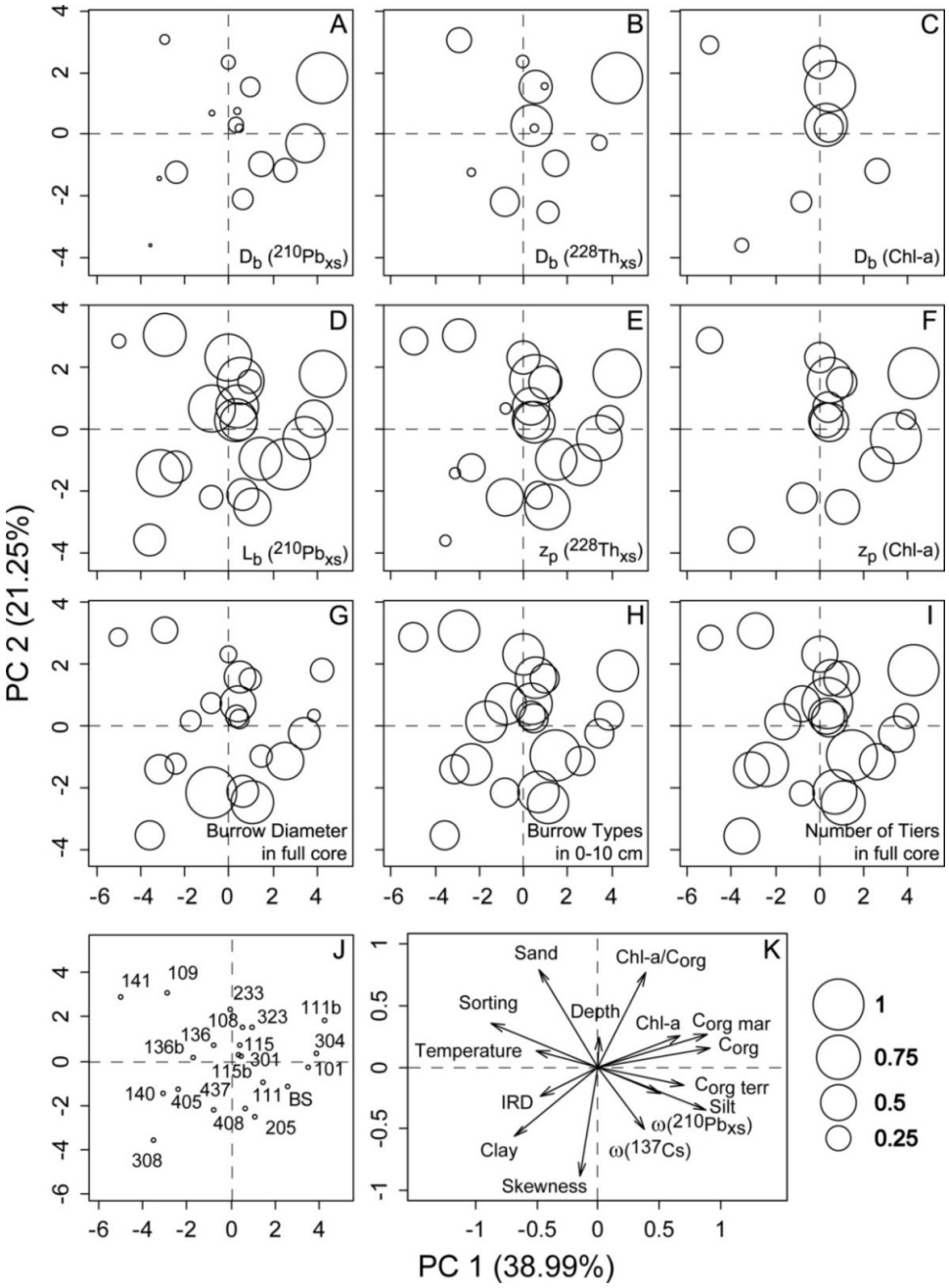

Figure 2.9: Relation of bioturbation proxies (A-I) to principal component analysis results. Bubble sizes represent bioturbation proxy magnitudes normalized to 1. J) Scatter plot of principal components 1 (PC 1) and 2 (PC 2). K) Vector plot of principal component loadings (PC1 and PC 2). Significant regressions were found between PC 1 and $D_b(^{210}Pb_{xs})$ (r^2 = 0.55, p = 0.002), PC 1 and $z_p(^{228}Th_{xs})$ (r2 = 0.37, p = 0.004), and between PC 2 and burrow diameters in full cores (r^2 = 0.26, p = 0.018).

2.4 Discussion

2.4.1 The utility of a multi-tracer approach in analyzing bioturbation rates in the Canadian Arctic Archipelago

The simultaneous application of short- and long-lived particle tracers allows the detection of mixing processes over short- (seasonal) to long-term (perennial) scales. Short-lived radiotracers such as ^{234}Th ($t_{1/2}$ = 24.1 d) and ^{7}Be ($t_{1/2}$ = 53.3 d) are more sensitive to seasonal biological mixing whereas long-lived radiotracers such as $^{210}Pb_{xs}$ ($t_{1/2}$ = 22.3 y) can detect biological mixing at a longer time scale (Lecroart et al., 2007, 2010).

Most of the particle tracer profiles in the current study indicated bioturbated surface sediments. In particular, the nearly constant activity-depth distributions of $^{210}Pb_{xs}$ profile types *I* and *Ia* suggested that mixing processes over long-term scales occurred in most samples. The X-radiographs of sediment cores that contained bioturbation traces and lack sedimentary structures (e.g. sediment layering) in sediment surface layers, strongly support this interpretation. On average, $^{210}Pb_{xs}$ derived biodiffusion coefficients were smaller than those calculated from $^{228}Th_{xs}$ and chlorophyll-a profiles, and chlorophyll-a derived biodiffusion coefficients yielded the greatest overall values throughout the Canadian Arctic Archipelago. These variations may have resulted from a process termed age-dependent mixing, which is associated with the tracer half-life. The inverse relationship between the estimated biodiffusion coefficients and the half-life of the radiotracers shows smaller bioturbation intensities if the period of mixing is relatively long, with the characteristic radiotracer time-scale of approximately 5 times that of its half-life (Smith et al., 1993; Teal et al., 2008; Lecroart et al., 2010). Lecroart et al. (2010) discussed further that the concept of age-dependent mixing and the associated tracer-

dependent mixing, which characterizes environments with low mixing intensities, can result from particle-selective feeding of deposit-feeders that prefer recently deposited organic-rich sediments associated with high activities of short-lived radiotracers. Alternatively, short-lived radiotracers may violate the basic assumptions required for the application of the biodiffusion model because they experience an insufficient number of mixing events before decaying, which eventually leads to positively biased biodiffusion coefficients. The current study used chlorophyll-a as a short-lived tracer with an estimated average chlorophyll-a degradation constant of ~5.3 y^{-1} that equates to an approximate half-life of 48 days. Because chlorophyll-a and most $^{228}Th_{xs}$-derived biodiffusion coefficients exhibited values greater than 2 cm^2 y^{-1}, sediments throughout the Canadian Arctic Archipelago experience sufficiently intense mixing. Thus, the application of the biodiffusion model to the depth distributions of short-lived chlorophyll-a remains appropriate (Lecroart et al., 2010).

The biodiffusion model, which was first introduced by Goldberg and Koide (1962), is the most widely used model to describe particle mixing in marine sediments numerically (Guinasso and Schink, 1975; Wheatcroft et al., 1990; Bentley and Nittrouer, 2003; Lecroart et al., 2010). However, if benthic organisms influence particle transport over a relatively long distance (e.g. several centimeters) in less time than required for the tracer to decay substantially (Boudreau, 1986), then the diffusion model does not apply. In the current study, the observed subsurface tracer activity/concentration peaks within sediment cores from stations 437, 109, 233, 136, and 136b (also see Appendix 2.4, 2.5 and 2.6) may indicate non-local transport of sediment particles and associated tracers from the surface to deeper parts of the sediment; application of a model that accounts for this particle transport mode might offer a reasonable estimate of bioturbation rates.

Food-caching, an adaption to episodic food supply to the benthos, may promote non-local particle transport (Jumars et al., 1990) in which benthic macrofauna bury organic material at depth to reduce availability to competitors and periodically “mine” the cached food (Wheatcroft et al., 1994). Many studies have documented pronounced seasonality of biological processes in Arctic ecosystems, driven largely by changes in sea ice cover (Carmack and Wassmann, 2006). Melting sea-ice in spring causes pulsed inputs of organic carbon to the Arctic Ocean through associated increases in primary production (Brown and Belt, 2012). This organic matter provides an important food source to the benthic fauna, generally enhancing benthic activity (e.g. Gerino et al., 1998; Rysgaard et al., 1998; Renaud et al., 2007). Sediment samples from the current study were collected in the fall during the months of September, October and early November. Subsurface concentration increases of short-lived chlorophyll-a in collected sediment cores were observed at stations 437, 136 and 136b (*profile types III* and *IV*, Appendix 2.6), with a less distinct concentration increase in core 109 (*profile type IV*, Appendix 2.6). These observations may have therefore resulted from pulsed input of organic matter following the sea-ice melt in the spring and seasonal food-caching by benthic organisms. The subsurface activity peaks of the longer-lived radioisotope ^{210}Pb in sediments from stations 109 and 233, however, suggested persistence of buried particles for several years within the sediment, which is inconsistent with the assumption of temporary food-caching (Crusius et al., 2004).

2.4.2 Response of bioturbation to environmental patterns

Organic matter input and quality, and especially the marine derived organic matter, varied substantially across the study region forming strong environmental patterns.

Similarly, sand, silt and clay percentages, and substrate sorting and skewness varied greatly throughout the study region, reflecting differences in depositional settings and processes. The current study discovered strong relationships of bioturbation intensity and depths, and burrow diameter with these environmental patterns.

Bioturbation intensity and depth in regions with high organic matter input and quality

Highest bioturbation intensities and mixing depths were observed in the north-eastern part of the study region, in Barrow Strait, Lancaster Sound, and the North Water region. The sampling locations were characterized by high marine organic matter quality and concentrations, exceeding those of terrigenous organic carbon, and were located near polynyas (see Michel et al., 2006 and Hannah et al., 2009 for polynya locations in the Canadian Arctic Archipelago). Because enhanced biological and primary productivity characterizes polynyas (Hannah et al., 2009), a greater amount of fresh and reactive organic matter likely reaches the seafloor beneath polynyas than in other Arctic regions covered with sea-ice most of the time (Carmack and Wassmann, 2006). The observed high organic matter input in the Barrow Strait, Lancaster Sound and North Water region, therefore, dominantly controlled bioturbation. This interpretation is consistent with Boudreau's (1994) argument that the intensity of bioturbation correlate positively with the flux of organic carbon to the seafloor given that the latter correlates well with macrofaunal abundance, biomass, mean body size, and feeding rates which, in turn, potentially relate to the bioturbation intensity as discussed by Smith (1992). The relatively high concentrations of chlorophyll-a in Barrow Strait may have resulted from an abrupt release and rapid transport of ice-algae to the seafloor in the spring. For example,

the early removal of snow from sea-ice in Barrow Strait in 1994 and 1995 caused strong under-ice phytoplankton blooms and downward exports of organic carbon and chlorophyll-a to the seafloor (Fortier et al., 2002). The relatively high chlorophyll-a/C_{org} ratios of sediments in Barrow Strait found in the current study support the assumption of rapid transport of high quality and less degraded organic matter to the seafloor. Further, the generally higher $\delta^{13}C$ values in Barrow Strait sediments compared to other regions of the Arctic Archipelago, also suggest a significant carbon contribution from ice-algae to the regional phytoplankton pool and emphasize the importance of ice-algae as carbon source for benthic communities in this region (Tamelander et al., 2008; Roy et al., 2015). However, carbon isotopic signatures may not always clearly distinguish sea-ice algae from phytoplankton (Brown and Belt, 2012).

Bioturbation intensity and depth in regions characterized through low organic matter input and quality, and high clay and sand percentage

Low organic matter qualities and/or low chlorophyll-a concentrations characterized the Amundsen Gulf and Viscount Melville Sound in the western part, as well as the Baffin Bay in the eastern part of the study region. Compared to the northeastern part of the studied region, which was characterized through relatively intense bioturbation driven by high organic matter input and quality, the Amundsen Gulf, Viscount Melville Sound and Baffin Bay exhibited low bioturbation intensities and depths. In particular the Amundsen Gulf region is strongly influenced by the input of terrestrial organic carbon and freshwater influxes from the Mackenzie River exerting stress on the local marine benthic fauna (Roy et al., 2015b). Other than extensive ice cover throughout most of the year, low organic matter input, in particular chlorophyll-a, and low organic matter quality in

these regions may have resulted from degradation of labile organic matter in the water column by pelagic grazers. For example, through pigment analyses of sediments in the Amundsen Gulf region, Morata et al. (2008) reported heavily degraded organic material, probably as a result of pelagic microbial degradation, reaching the seafloor. The low bioturbation intensities and depths discovered in the current study may have therefore resulted from strong competition for the general low input of high quality organic matter. As discussed earlier, the increased subsurface chlorophyll-a concentrations in Baffin Bay (stations 136 and 136b) and Amundsen Gulf (station 437) indicated seasonal food-caching by benthic organisms, which supports the argumentation of low organic matter input environments inhibiting bioturbation in these environments.

In addition to low organic matter input and quality, a fine-skewed substrate with abundant clay and symmetrical to coarse-skewed substrate with relatively high percentages of sand characterized the Amundsen Gulf and Viscount Melville Sound, and Baffin Bay region, respectively. The skewness of grain size distributions is sensitive to depositional processes and can be used to classify the depositional environment (Duane, 1964). Because of the poor sorting of sediments in Baffin Bay, it is unlikely that coarse-skewed sediments resulted from winnowing processes eliminating fine grains (e.g. Höppner and Heinrich, 1997 cited in Hüneke and Mulder, 2011, Duane, 1964), but most likely resulted from addition of sand-sized particles to the grain size pool (Martins, 1965). This would support the assumption of ice-rafting processes and deposition of relatively coarse grained debris to the benthos in these regions. Generally, sea ice in Arctic shelf and slope regions can transport significant volumes of sediments, influencing regional depositional processes (Darby et al., 2009). Even though the absence of large ice shelves in the modern North Atlantic largely precludes iceberg sedimentation,

iceberg sedimentation still occurs in the northern Baffin Bay between Ellesmere Island and North Greenland (Stein, 2008). Although glacial ice, or icebergs, can transport a wide range of sediment particle sizes (from fine-grained clay and silt to sometimes boulder size material), sea ice entrains predominantly fine-grained material by suspension-freezing (frazil ice) as well as potentially incorporating coarser material through freezing processes at the shelf bottom (anchor ice) (e.g. Clark and Hanson, 1983; Reimnitz et al., 1998; Hebbeln, 2000). The deposition of previously entrained sediment follows from the melting and break-up of the sea ice. In contrast, positively fine-skewed sediments in the Amundsen Gulf and Viscount Melville Sound, as well as at station 140 in Baffin Bay, indicate low-energy conditions that allowed fine particles to settle (Höppner and Heinrich, 1997 cited in Hüneke and Mulder, 2011; Duane, 1964). A finer-grained matrix with only few IRD clasts characterized sediment cores from the Amundsen Gulf compared to most other samples, which instead exhibited a muddy, often clast-bearing, bioturbated matrix. In the Amundsen Gulf region, the Mackenzie River contributes substantially to depositional processes. Its eastward transported plume dominates the supply of mostly fine-grained sediment to the shelf north of Alaska and Canada (Darby et al., 2009), and low-energy plume deposition may cause abundant clay-sized particles and fine-skewed particle distributions in the Amundsen Gulf.

Grain size data are important surrogates in interpreting depositional processes, and many previous studies used substrates in general as indicators of biological diversity because sediments significantly influence distributions of benthic species (e.g. Howell, 2010). For example, Sanders (1958) demonstrated a clear dependency of dominant feeding modes on sediment texture. Because substrate influences both feeding mode and biological diversity it also potentially influence bioturbation intensity and depth.

Whether the depositional processes or the limited input of high quality organic matter ultimately caused the observed low bioturbation intensities and depths in the Amundsen Gulf, Viscount Melville Sound and Baffin Bay, however, remains largely speculative. Because areas in the north-eastern part of the study region with environmental conditions favorable to bioturbation were influenced by similar depositional processes (e.g. sea-ice and iceberg sedimentation), as indicated by similar substrate characteristics to Baffin Bay sediments, it is likely that the organic matter was the crucial factor influencing bioturbation rates and intensity throughout the study region. However, regions that were particularly influenced by ice-rafting processes (stations 109 in North Water region and 141 in Baffin Bay) also showed low bioturbation intensities suggesting that strong ice-rafting conditions limit macrofaunal activities.

The sedimentary facies in Viscount Melville Sound was distinct since it showed interlaminated sands and muds at the base of the sediment core, which indicates either the past occurrences of turbidites (e.g. Forwick and Vorren, 2009) or other episodic mass-depositional events (e.g. Jaeger and Nittrouer, 2006). The large number of IRD clasts (> 2 mm) throughout the core collected in Viscount Melville Sound revealed an additional influence of iceberg and/or anchor ice sedimentation. By comparing actual records of preserved primary depositional sedimentary fabric from the Gulf of Alaska Shelf (Jaeger and Nittrouer, 2006) with model predictions of fabric, Bentley et al. (2006) showed that episodic or periodic variations in the sedimentation rate may preserve the primary sedimentary fabric, even if the thickness of the bioturbated zone far exceeds the thickness of the event layer. The partially laminated facies in Viscount Melville Sound therefore may have resulted from sediment deposition pulses causing sporadic preservation of event layer beds. The surface sedimentary facies in Viscount Melville

Sound, a bioturbated mud facies, exhibited similar characteristics than sediments in all other studied regions, and may be a result of bioturbation exceeding a continuously low sedimentation rate. It is therefore likely that environmental conditions in Viscount Melville Sound have transitioned from conditions that inhibited bioturbation or erase bioturbation traces (e.g. event deposition) to those that drive biological activities and sediment mixing in the recent past. However, bioturbation intensity and depth in this area were still low compared to other studied regions.

Relation of bioturbation structure diameter, number of burrow types, and number of tiers to environmental patterns

Numerous studies report that environmental variables such as salinity, temperature, food availability, sedimentation rate, and substrate consistency control the size, distribution and variety of bioturbation structures in sediments (e.g. Dashtgard et al., 2008; Belley et al., 2010). Wetzel (1991) surmises that the number of tiers (the vertical partitioning of the benthic habitat by the macrofauna) and their vertical extension in the sediment are a response to sedimentation rate, food content and oxygenation of sediments. Dashtgard et al. (2008) describe grain size as a sedimentary variable that affects oxygen content, permeability, and food availability of the benthos, and consequently influences organisms colonizing the sediment. In the current study, however, the number of different burrow types and the number of tiers varied little among sampling sites and did not respond to the environmental patterns discovered across the study region.

With few significant correlations between burrow diameters and temperature and substrate surrogates, larger burrow diameters were linked to fine skewed sediments with smaller sand fractions in Amundsen Gulf, Viscount Melville Sound and at station 140 in

Baffin Bay, and were largely independent of organic matter input and quality. Thus, the presented data indicate that abiotic environmental factors appeared to have influenced burrow sizes rather than the availability and quality of food. Furthermore, because biodiffusion coefficients varied more than the size and variety of burrows or number of tiers throughout the region, the actual rate of bioturbation apparently did not respond to macrofaunal body size. Nonetheless, this assessment of burrow diameter and number of burrow types probably underestimates traces of benthic organisms that move through the sediment without creating and maintaining distinct burrow systems. These traces could not be clearly identified and distinguished from biomottled sediments or were simply not well preserved.

2.5 Summary

All sediment cores collected in the Canadian Arctic Archipelago showed strong evidence of sediment mixing by bioturbation. High bioturbation intensities and depths occurred in environments with high inputs of high quality, mainly marine, organic matter. The benthos in these regions (Barrow Strait, Lancaster Sound and North Water) was strongly influenced by high seasonal water column primary production, particularly in or proximal to polynyas, and an increased export of, often high quality marine organic matter to the seafloor that fuels sediment mixing activities of benthic organisms. Ice-rafting through icebergs and/or anchor ice sedimentation processes further influenced the benthos in the eastern regions of the study area without inhibiting bioturbation. Stations with evidence of intense ice-rafting processes (109 in the North Water region and 141 in Baffin Bay) and low bioturbation activities are special cases, and further suggested little effect of ice-rafting on sediment mixing rates and depths on a regional scale. On

average, benthic regions that received comparatively high amounts of clay and larger proportions of terrigenous organic carbon, such as the Amundsen Gulf and Viscount Melville Sound regions, exhibited lower bioturbation intensities and depths. As compared to most sampling stations across the Canadian Arctic Archipelago, stations 136 and 136b represented a different type of sediment mixing as shown by chlorophyll-a concentrations markedly increasing with depth, potentially indicating food caching activities of benthic organisms in sediments. Overall, the burrow type variety and the number of tiers identified in the current study followed no particular spatial environmental pattern. The average burrow diameter of full cores, however, responded to spatial distributional patterns of sand and bottom temperature but was independent of organic matter input and quality.

The results obtained here, in particular the fact that organic matter input and quality in Arctic depositional environments, such as polynyas, were predominantly linked to sediment mixing intensity and depth, may be further extrapolated to other Arctic benthic regions to more effectively assess potential effects of environmental changes.

2.6 References

Addison, J.A., Finney, B.P., Dean, W.E., Davies, M.H., Mix, A.C., Stoner, J.S., Jaeger, J.M. (2012). Productivity and sedimentary $\delta^{15}N$ variability for the last 17,000 years along the northern Gulf of Alaska continental slope. Paleoceanography 27, PA1206.

Aller, R.C. (1982). The effects of macrobenthos on chemical properties of marine sediment and overlying water. In: McCall, P.L., Tevesz, M.J.S. (Eds.). Animal-sediment relations – The biogenic alteration of sediments. Plenum Press, New York, 53-102.

Archambault, P., Snelgrove, P.V.R., Fisher, J.A.D., Gagnon, J.-M., Garbary, D.J., Harvey, M., Kenchington, E.L., Lesage, V., Levesque, M., Lovejoy, C., Mackas, D.L., McKindsey, C.W., Nelson, J.R., Pepin, P., Piché, L., Poulin, M. (2010). From sea to sea: Canada's three oceans of biodiversity. PLoS ONE 5(8): e12182. doi: 10.1371/journal.pone.0012182.

ArcticNet (2015). Rationale, http://www.arcticnet.ulaval.ca/about us/rationale.php.

Belley, R., Archambault, P., Sundby, B., Gilbert, F., Gagnon, J.-M. (2010). Effects of hypoxia on benthic macrofauna and bioturbation in the Estuary and Gulf of St. Lawrence, Canada. Continental Shelf Research 30, 1302-1313.

Bentley, S.J. and Nittrouer, C.A. (2003). Emplacement, modification, and preservation of event strata on a flood-dominated continental shelf: Eel shelf, Northern California. Continental Shelf Research 23, 1465-1493.

Bentley, S.J., Sheremet, A., Jaeger, J.M. (2006). Event sedimentation, bioturbation, and preserved sedimentary fabric: Field and model comparisons in three contrasting marine settings. Continental Shelf research 26, 2108-2124.

Berner, R.A. (1980). Early diagenesis – A theoretical approach. Princeton University Press.

Boon, A.R. and Duineveld, G.C.A. (1996). Phytopigments and fatty acids as molecular markers for the quality of near-bottom particulate organic matter in the North Sea. Journal of Sea Research 35, 279-291.

Boon, A.R. and Duineveld, G.C.A. (1998). Chlorophyll a as a marker for bioturbation and carbon flux in southern and central North Sea sediments. Marine Ecology Progress Series 162, 33-43.

Boudreau, B.P. (1986). Mathematics of tracer mixing in sediments: I. Spatially-dependent, diffusive mixing. American Journal of Science 286, 161-198.

Boudreau, B.P. (1994). Is burial velocity a master parameter for bioturbation? Geochimica et Cosmochimica Acta 58, 1243-1249.

Brown, T.A. and Belt, S.T. (2012). Identification of the sea ice diatom biomarker IP_{25} in the Arctic benthic macrofauna: direct evidence for a sea ice diatom diet in Arctic heterotrophs. Polar Biology 34, 131-137.

Carmack, E. and Wassmann, P. (2006). Food webs and physical-biological coupling on pan-Arctic shelves: Unifying concepts and comprehensive perspectives. Progress in Oceanography 71, 446-477.

Clark, D.L. and Hanson, A. (1983). Central Arctic Ocean sediment texture: A key to ice transport mechanisms. In: Molnia, B.F. (Ed.). Glacial-marine sedimentation. Plenum Press, New York, pp. 301-330.

Cochran, J.K. (1985). Particle mixing rates in sediments of the eastern equatorial Pacific: Evidence from ^{210}Pb, $^{239,240}Pu$ and ^{137}Cs distributions at MANOP sites. Geochimica et Cosmochimica Acta 49, 1195-1210.

Crusius, J., Bothner, M.H., Sommerfield, C.K. (2004). Bioturbation depths, rates and processes in Massachusetts Bay sediments inferred from modeling of ^{210}Pb and $^{239+240}Pu$ profiles. Estuarine, Coastal and Shelf Science 61, 643-655.

Darby, D.A., Ortiz, J., Polyak, L., Lund, S., Jakobsson, M., Woodgate, R.A. (2009). The role of currents and sea ice in both slowly deposited central Arctic and rapidly deposited Chukchi-Alaskan margin sediments. Global and Planetary Change 68, 56-70.

Darnis, G., Robert, D., Pomerleau, C., Link, H., Archambault, P., Nelson, R.J., Geoffroy, M., Tremblay, J.-É., Lovejoy, C., Ferguson, S.H., Hunt, B.P.V., Fortier, L. (2012). Current state and trends in Canadian Arctic marine ecosystems: ll. Heterotrophic food web, pelagic-benthic coupling, and biodiversity. Climate Change 115, 161-178.

Dashtgard, S.E., Gingras, M.K., Pemberton, S.G. (2008). Grain -size controls on the occurrence of bioturbation. Palaeogeography, Palaeoclimatology, Palaeoecology 257, 224-243.

Duane, D.B. (1964). Significance of skewness in recent sediments, Western Pamlico Sound, North Carolina. Journal of Sedimentary Petrology 34, 864-874.

Fissel, D.B., de Saavedra Álvarez, M.M., Kulan, N., Mudge, T.D., Marko, J.R. (2011). Long-term trends for sea ice in the Western Arctic Ocean: Implications for shipping and offshore oil and gas activities. Proceedings International Society of Offshore and Polar Engineers (ISOPE).

Folk, R.L. and Ward, W.C. (1957). Brazos river bar: A study in the significance of grain size parameters. Journal of Sedimentary Petrology 27, 3-26.

Fortier, M., Fortier, L., Michel, C., Legendre, L. (2002). Climatic and biological forcing of the vertical flux of biogenic particles under seasonal Arctic sea ice. Marine Ecology Progress Series 225, 1-16.

Forwick, M. and Vorren, T.O. (2009). Late Weichselian and Holocene sedimentary environments and ice rafting in Isfjorden, Spitzbergen. Palaeogeography, Palaeoclimatology, Palaeoecology 280, 258-274.

Gerino, M., Aller, R.C., Lee, C., Cochran, J.K., Aller, J.Y., Green, M.A., Hirschberg, D. (1998). Comparison of different tracers and methods used to quantify bioturbation

during a spring bloom: 234-Thorium, luminophores and chlorophyll a. Estuarine, Coastal and Shelf Science 46, 531-547.

Goldberg, E.D. and Koide, M. (1962). Geochronological studies of deep sea sediments by the ionium/thorium method. Geochimica et Cosmochimica Acta 26, 417-450.

Goñi, M.A., Yunker, M.B., MacDonald, R.W., Eglinton, T.I. (2005). The supply and preservation of ancient and modern components of organic carbon in the Canadian Beaufort Shelf of the Arctic Ocean. Marine Chemistry 93, 53-73.

Grant, J., Hargrave, B., MacPherson, P. (2002). Sediment properties and benthic-pelagic coupling in the North Water. Deep-Sea Research II 49, 5259-5275.

Grebmeier, J.M. and Barry, J.P. (1991). The influence of oceanographic processes on pelagic-benthic coupling in polar regions: A benthic perspective. Journal of Marine Systems 2, 495-518.

Green, M.A., Aller, R.C., Cochran, J.K., Lee, C., Aller, J.Y. (2002). Bioturbation in shelf/slope sediments off Cape Hatteras, North Carolina: the use of ^{234}Th, Chl-a, and Br^- to evaluate rates of particle and solute transport. Deep-Sea Research II 49, 4627-4644.

Grobe, H. (1987). A simple method for the determination of ice-rafted debris in sediment cores. Polarforschung 57,123-126.

Guinasso, N.L and Schink, D.R. (1975). Quantitative estimates of biological mixing rates in abyssal sediments. Journal of Geophysical Research-Oceans and Atmosphere 80, 3032-3043.

Gutiérrez, D., Gallardo, V.A., Mayor, S., Neira, C., Vásquez, C., Sellanes, J., Rivas, M., Soto, A., Cerrasco, F., Baltazar, M. (2000). Effects of dissolved oxygen and fresh organic matter on the bioturbation potential of macrofauna in sublittoral sediments

off Central Chile during the 1997/1998 El Niño. Marine Ecology Progress Series 202, 81-99.

Hannah, C.G., Dupont, F., Dunphy, M. (2009). Polynyas and tidal currents in the Canadian Arctic Archipelago. Arctic 62, 83-95.

Hargrave, B.T., Walsh, I.D., Murray, D.W. (2002). Seasonal and spatial patterns in mass and organic matter sedimentation in the North Water. Deep-Sea Research II 49, 5227-5244.

Hebbeln, D. (2000). Flux of ice-rafted detritus from sea ice in the Fram Strait. Deep-Sea Research II 47, 1773-1790.

Höppner, R. and Heinrich, R. (1997). Kornsortierungsprozesse am Argentinschen Kontinentalhang anhand von Siltkorn-Analysen. Cited in: Hüneke, H., Mulder, T. (2011) (Eds.). Developments in sedimentology - Deep-Sea sediments. Elsevier, p. 372.

Howell, K.L. (2010). A benthic classification system to aid in the implementation of marine protected area networks in the deep/high seas of NE Atlantic. Biological Conservation 143, 1041-1056.

Hunt, A.S. and Corliss, B.H. (1992). Distribution and microhabitats of living (stained) benthic foraminifera from the Canadian Arctic Archipelago. Marine Micropaleontology 20, 321-345.

Husson, F., Josse, J., Le, S., Mazet, J. (2013). FactoMineR: Multivariate Exploratory Data Analysis and Data Mining with R. R package version 1.25. http://CRAN.R-project.org/package=FactoMineR.

Jaeger, J.M. and Nittrouer, C.A. (2006). A quantitative examination of modern sedimentary lithofacies formation on the glacially influenced Gulf of Alaska continental shelf. Continental Shelf Research 26, 2178-2204.

Josefson, A.B., Forbes, T., Rosenberg, R. (2002). Fate of phytodetritus in marine sediments: Functional importance of macrofaunal community. Marine Ecology Progress Series 230, 71-85.

Jumars, P.A., Mayer, L.M., Deming, J.W., Baross, J.A., Wheatcroft, R.A. (1990). Deep-Sea deposit feeding strategies suggested by environmental and feeding constraints. Philosophical Transactions of the Royal Society A - Mathematical, Physical and Engineering Sciences 331, 85-101.

Krishnaswami, S., Benninger, L.K., Aller, R.C., Von Damm, K.L. (1980). Atmospherically-derived radionuclides as tracers of sediment mixing and accumulation in near-shore marine and lake sediments: Evidence from ^{7}Be, ^{210}Pb, and ^{239,240}Pu. Earth and Planetary Science Letters 47, 307-318.

Lamb, A.L., Wilson, G.P., Leng, M.J. (2006). A review of coastal palaeoclimate and relative sea-level reconstructions using δ^{13}C and C/N ratios in organic material. Earth-Science Reviews 75, 29-57.

Lasserre, F. and Pelletier, S. (2011). Polar super seaways? Maritime transport in the Arctic: An analysis of shipowners' intentions. Journal of Transport Geography 19, 1465-1473.

Lecroart, P., Schmidt, S., Jouanneau, J.-M. (2007). Numerical estimation of the error of the biodiffusion coefficient in coastal sediments. Estuarine, Coastal and Shelf Science 72, 543-552.

Lecroart, P., Maire, O., Schmidt, S., Grémare, A., Anschutz, P., Meysman, F.J.R. (2010). Bioturbation, short-lived radioisotopes, and the tracer-dependence of biodiffusion coefficients. Geochimica et Cosmochimica Acta 74, 6049-6063.

Link, H., Archambault, P., Tamelander, T., Renaud, P.E., Piepenburg, D. (2011). Spring-to-summer changes and regional variability of benthic processes in the western Canadian Arctic. Polar Biology 34, 2025-2038.

Link, H., Piepenburg, D., Archambault, P. (2013). Are hotspots always hotspots? The relationship between diversity, resource and ecosystem functions in the Arctic. PLoS ONE 8(9): e74077. doi: 10.1371/journal.pone.0074077.

Magen, C., Chaillou, G., Crowe, S.A., Mucci, A., Sundby, B., Gao, A., Makabe, R., Sasaki, H. (2010). Origin and fate of particulate organic matter in the southern Beaufort Sea-Amundsen Gulf region, Canadian Arctic. Estuarine, Coastal and Shelf Science 86, 31-41.

Martins, L.R. (1965). Significance of skewness and kurtosis in environmental interpretation. Journal of Sedimentary Petrology 35, 768-770.

Michel, C., Ingram, R.G., Harris, L.R. (2006). Variability in oceanographic and ecological processes in the Canadian Arctic Archipelago. Progress in Oceanography 71, 379-401.

Morata, N., Renaud, P.E., Brugel, S., Hobson, K.A., Johnson, B.J. (2008). Spatial and seasonal variations in the pelagic-benthic coupling of the southeastern Beaufort Sea revealed by sedimentary biomarkers. Marine Ecology Progress Series 371, 47-63.

Ogrinc, N., Fontolan, G., Faganeli, J., Covelli, S. (2005). Carbon and nitrogen isotope compositions of organic matter in coastal marine sediments (the Gulf of Trieste, N

Adrianic Sea): indicators of sources and preservation. Marine Chemistry 95, 163-181.

Perovich, D.K. (2011). The changing Arctic sea ice cover. Oceanography 24, 162-173.

R Development Core Team (2013). R: A language and environment for statistical computing. R Foundation for Statistical Computing, Vienna, Austria. ISBN 3-900051-07-0. URL http://www.R-project.org.

Reimnitz, E., McCormick, M., Bischof, J., Darby, D.A. (1998). Comparing sea-ice sediment load with Beaufort Sea shelf deposits: Is entrainment selective? Journal of Sedimentary Research 68, 777-787.

Renaud, P.E., Morata, N., Ambrose Jr., W.G., Bowie, J.J., Chiuchiolo, A. (2007). Carbon cycling by seafloor communities on the eatsren Beaufort Sea shelf. Journal of Experimental Marine Biology and Ecology 349, 248-260.

Riaux-Gobin, C. and Klein, B. (1993). Microphytobenthic biomass measurements using HPLC and conventional pigment analysis. In: Kemp, P.F., Cole, J.J., Sherr, B.F., Sherr, E.B. (eds.). Handbook of methods in aquatic microbial ecology. Lewis Publishers, pp. 369-376.

Roy, V., Iken, K., Archambault, P. (2014). Environmental drivers of the Canadian Arctic megabenthic communities. PLoS ONE 9(7): e100900. doi: 10.1371/journal.pone.0100900.

Roy, V., Iken, K., Gosselin, M., Tremblay, J.-É., Bélanger, S., Archambault, P. (2015). Benthic faunal assimilation pathways and depth-related changes in food-web structure across the Canadian Arctic. Deep-Sea Research I 102, 55-71.

Roy, V., Iken, K., Archambault, P. (2015b). Regional variability of megabenthic community structure across the Canadian Arctic. Arctic 68, 180-192.

Rysgaard, S., Thamdrup, B., Risgaard-Petersen, N., Fossing, H., Berg, P., Christensen, P.B., Dalsgaard, T. (1998). Seasonal carbon and nutrient mineralization in a high-Arctic coastal marine sediment, Young Sound, Northeast Greenland. Marine Ecology Progress Series 175, 261-276.

Sanders, H.L. (1958). Benthic studies in Buzzards Bay. I. Animal-sediment relationships. Limnology and Oceanography 3, 245-258.

Schneider, C.A., Rasband, W.S., Eliceiri, K.W (2012). "NIH Image to ImageJ: 25 years of image analysis". Nature Methods 9, 671-675.

Schubert, C.J. and Calvert, S.E. (2001). Nitrogen and carbon isotopic composition of marine and terrestrial organic matter in Arctic Ocean sediments: Implications for nutrient utilization and organic matter composition. Deep-Sea Research I 48, 789-810.

Schultz, D.J. and Calder, J.A. (1976). Organic carbon $^{13}C/^{12}C$ variations in estuarine sediments. Geochimica et Cosmochimica Acta 40, 381-385.

Smith, C.R. (1992). Factors controlling bioturbation in deep-sea sediments and their relation to models of carbon digenesis. In: Rowe, G.T. and Pariente, V. (Eds.). Deep-sea food chains and the global carbon cycle. Kluwer Academic Publishers, pp. 375-393.

Smith, L.C. and Stephenson, S.R. (2013). New trans-Arctic shipping routes navigable by midcentury. Proceeding of the National Academy of Science of the United States of America 110, E1191-E1195.

Smith, C.R., Pope, R.H., DeMaster, D.J., Magaard, L. (1993). Age-dependent mixing of deep-sea sediments. Geochimica et Cosmochimica Acta 57, 1473-1488.

Snelgrove P.V.R., Archambault, P., Juniper, K., Lawton, P., and others (2012). Canadian Healthy Oceans Network (CHONe): An academic–government partnership to develop scientific guidelines for conservation and sustainable usage of marine biodiversity. Fisheries 37, 296-304.

Stein, R. (2008) (Ed.). Arctic Ocean Sediments: Processes, Proxies, and Paleoenvironment. Elsevier Science.

Stephens, M.P., Kadko, D.C., Smith, C.R., Latasa, M. (1997). Chlorophyll-a and phaeopigments as tracers of labile organic carbon at the central equatorial Pacific seafloor. Geochimica et Cosmochimica Acta 61, 4605-4619.

Stewart, E.J., Howell, S.E.L., Draper, D., Yackel,, J., Tivy, A. (2007). Sea ice in Canada's Arctic: Implications for cruise tourism. Arctic 60, 370-380.

Sun, M-Y.., Aller, R.C., Lee, C. (1991). Early diagenesis of chlorophyll-a in Long Island Sound sediments: A measure of carbon flux and particle reworking. Journal of Marine Research 49, 379-401.

Sun, M.-Y., Lee, C., Aller, R.C. (1993). Laboratory studies of oxic and anoxic degradation of chlorophyll-a in Long Island Sound sediments. Geochimica et Cosmochimica Acta 57, 147-157.

Sun, M.-Y., Aller, R.C., Lee, C. (1994). Spatial and temporal distributions of sedimentary chloropigments as indicators of benthic processes in Long Island Sound. Journal of Marine Research 52, 149-176.

Tamelander, T., Reigstad, M., Hop, H., Carroll, M.L., Wassmann, P. (2008). Pelagic and sympagic contribution of organic matter to zooplankton and vertical export in Barents Sea marginal ice zone. Deep-Sea Research 55, 2330-2339.

Teal, L.R., Bulling, M.T., Parker, E.R., Solan, M. (2008). Global patterns of bioturbation intensity and mixed depth of marine soft sediments. Aquatic Biology 2, 207-218.

Tremblay, J.-É., Robert, D., Varela, D. E., Lovejoy, C., Darnis, G., Nelson, R.J., Sastri, A.R. (2012). Current state and trends in Canadian Arctic marine ecosystems: I. Primary production. Climate Change 115, 161-178.

Wasmann, P., Duarte, C.M., Agust, S., Sejr, M.K. (2011). Footprints of climate change in the Arctic marine ecosystem. Global Change Biology 17, 1235-1249.

Wetzel, A. (1991). Ecologic interpretation of deep-sea trace fossil communities. Palaeogeography, Palaeoclimatology, Palaeoecology 85, 47-69.

Wheatcroft, R.A., Jumars, P.A., Smith, C.R., Nowell, A.R.M. (1990). A mechanistic view of the particulate biodiffusion coefficient: step-lengths, rest periods and transport directions. Journal of Marine Research 48, 177-207.

Wheatcroft, R.A., Olmez, I., Pink, F.X. (1994). Particle bioturbation in Massachusetts Bay: Preliminary results using a new deliberate tracer technique. Journal of Marine Research 52, 1129-1150.

CHAPTER 3 – Spatial Distribution of Bioturbation Structures and Bioturbation Processes in Basin to Slope and Rise Sediments of the Gulf of Maine and Scotian Shelf Region

Lina M. Stolze[1]* and Samuel J. Bentley, Sr.[2]

*Corresponding author: Email: lmstolze@mun.ca

[1]Department of Earth Sciences, Memorial University of Newfoundland, St John's, Canada NL A1B 3X5

[2]Samuel J. Bentley, Sr., Department of Geology and Geophysics, Louisiana State University, Baton Rouge, Louisiana, USA 70803

In preparation for submission to: Journal of Marine Systems.

Abstract

Environmental conditions of a benthic habitat strongly influence endobenthic animal life traits such as body size feeding mode and activity level and consequently, the resulting bioturbation structures. Studying these relationships may therefore improve our understanding of how benthic organisms respond to environmental change and disturbances, and determine their usefulness as indicators of ecosystem state. The Gulf of Maine, Scotian Shelf and adjacent slope and rise localities provide a wide range of benthic environments and an excellent opportunity to study these relationships in modern marine sediments. Here, the diversity, vertical extent, and diameter of bioturbation structures were analyzed in conjunction with biodiffusion rates and mixing depths, as well as substrate and organic matter related parameters to describe the benthic environmental conditions of each sampling site. Sediment samples were collected using a multicorer on two cruises onboard the CCGS Hudson in July/August 2009 and 2010. Bioturbation structure diversity and extent both responded to regional environmental trends characterized through variation in the quality and quantity of organic matter, the skewness of grain size distributions, and the amount of silt and sand in sediments across the study region. In general, benthic organisms intensely mixed basin sediments containing high concentrations of high quality organic matter, as reflected in X-radiographs collected throughout the study region. Feeding structures were more abundant in environments with low organic matter input and quality and could be linked to potential food caching behavior in the deep water settings of the Northeast Channel and Fan. Whereas bioturbation structure diversity and extent, and to some degree the $^{210}Pb_{xs}$- and $^{228}Th_{xs}$-derived bioturbation depth, were potentially good indicators of sediment mixing intensity, biodiffusion coefficients were apparently

unrelated to bioturbation structure characteristics and to spatial patterns of organic matter and substrate across the region.

Keywords: X-radiography, $^{210}Pb_{xs}$, $^{228}Th_{xs}$, $^{234}Th_{xs}$, Northeast Channel, Northeast Fan, biodiffusion, bioturbation depth, bioturbation structure diversity

3.1 Introduction

The Gulf of Maine is a 250,000 km^2 semi-enclosed, glacially carved continental shelf sea on the eastern North American continental slope that contains a series of basins separated by shallow sills and banks (Uchupi and Bolmer, 2008). With its heterogeneous sedimentology and geomorphology, the Gulf of Maine and adjacent Scotian shelf, slope, and rise further represent important study areas in which to advance the science of basin to deep-sea bioturbation as an indicator of ecosystem state. The current study uses the wide range of benthic environments in water depths between 500 and 3000 m of the Gulf of Maine, Scotian Shelf and adjacent slope and rise localities to study the spatial distribution of endobenthic bioturbation structures and biogenic sediment mixing rates, as well as the benthic environmental characteristics associated with them.

Interactions between benthic organisms and the sedimentary environment represent a fundamental subject that marine benthic ecology studies have explored in many ways (e.g. Aller, 1982; Rhoads and Boyer, 1982, for a review). Initially, studies investigating the relationships among biogenic sedimentary structures and environmental conditions in modern depositional settings were conducted in the 1960s and 1970s by German and Dutch researchers in the North Sea (e.g. Schäfer, 1956; Reineck et al., 1967, 1968) costal margin and researchers working along the Georgia coast, USA (e.g. Frey and Howard, 1972; Howard and Frey, 1973, 1975). These types of studies declined in the 1980s and early 1990s and only recently regained increasing interest (Gingras et al., 2011 and references therein).

The life processes of organisms produce biogenic structures in sediments (e.g. Bromley, 1996). Researchers categorize bioturbation structures as a sub-class of biogenic sedimentary structures, which comprises burrows, tracks, trails, and grazing patterns

produced by the activity of benthic organisms that reflect the disruption of physical and biogenic sedimentary stratification features (Frey and Pemberton, 1985). By transporting particles and solutes within the sediment, bioturbation controls chemical, biological, and physical processes (e.g. Aller, 1982; Rhoads and Boyer, 1982; Meadows et al., 1990; Mayer et al., 1995; Aller, 1994; Aller and Aller, 1998; Sun et al., 2002; Needham et al., 2004) and plays an important role in structuring microbial as well as meio- and macrofaunal communities (Widdicombe and Austen, 1999). Conversely, environmental conditions and abiotic and biotic parameters such as temperature, salinity, water depth, bottom currents, grain size, and organic matter supply strongly influence abundance and diversity of benthic organisms (Ramey and Snelgrove, 2003; and see Chapter 2). These variables also affect animal life traits (e.g. body form and size, feeding mode, activity level) and ultimately influence feeding behavior and morphology of bioturbation structures (e.g. Rosenberg, 2001; Kristensen and Kostka, 2005). Because of these connections, bioturbation structures offer potential good indicators of the environmental conditions of benthic habitats. Bioturbation structures in recent sediments, however, may be difficult to interpret, because burrows are often barely visible with the naked eye (Wetzel, 2010). X-radiography, a technique that allows the detection of structures and features that were not visible to the naked eye (Bouma, 1964), offers one approach to overcome this lack of visibility. First introduced and applied to the study of sedimentary rocks by Lehman (1939) (cited in Howard, 1968), this technique was soon found to be efficient for the study of structures and burrowing traces created by living animals within unconsolidated sediments (e.g. Calvert and Veevers, 1962; Bouma, 1964; Howard, 1968).

To understand bioturbation structure-environmental relationships in the sedimentological and geomorphological hetereogeneous benthic environment of the Gulf of Maine and adjacent Scotian shelf and slope, the specific objectives of this study were 1) to examine bioturbation intensity and type, as well as bioturbation structure characteristics, and 2) to evaluate the relationships of these bioturbation proxies and environmental variations across the study region, in particular with respect to environmental differences between the shallow basin sediments of the Gulf of Maine and the deep-sea sediments of the Northeast Channel and Fan.

Therefore, X-radiographs of multi-core slabs were used in conjunction with particle tracer depth distributions of the radioisotopes $^{210}Pb_{xs}$, $^{228}Th_{xs}$ and $^{234}Th_{xs}$ and the photopigment chlorophyll-a to study endobenthic bioturbation structures and biogenic sediment mixing rates. Abiotic and biotic environmental parameters, including sediment surface concentrations of total organic carbon and chlorophyll-a, organic matter qualities, as well as grain sizes and sedimentation rates were analyzed to further characterize the benthic environmental conditions of each sampling site.

3.2 Methods

3.2.1 Sediment sample collection

Seabed sediment from the Gulf of Maine, the Scotian Shelf and the North East Channel and Fan was collected on two cruises on board the Coast Guard Vessel *CCGS Hudson* in July/August 2009 and 2010 (Fig. 3.1). Specifically, sediment samples were recovered from Crowell Basin, Georges Basin, Jordan Basin, Roseway Basin, and the Northeast Channel and Fan using a multicorer (core tubes Ø 10 cm). In 2010, the remotely

operated vehicle ROPOS was used to collect sediment push cores (Ø 6.5 cm) at two locations in the Northeast Channel and Fan, labeled as NEF_1357A and NEC_1358. Especially in deep water, the sampling of seabed sediment is time consuming the advantage of this method is that the sample collection can be monitored limiting the risk of sampling failure.

Sediment cores were processed and prepared on board immediately after collection. Surface sediment core sections (0-10 cm) and most sections below 10 cm depth were sliced into one centimetre sections, and some core sections below 10 cm depth were sliced into two centimetre sections for subsequent analysis of radioisotopes (^{234}Th, ^{228}Th, ^{210}Pb), grain sizes, carbon isotopes (δ^{13}C), total organic carbon (TOC), total nitrogen TN), and chlorophyll-a. The sediment samples for chlorophyll-a, δ^{13}C, TOC and TN analyses were stored at -18 ˚C and kept frozen until laboratory analysis. X-radiography sediment slabs were prepared on board from collected multicores.

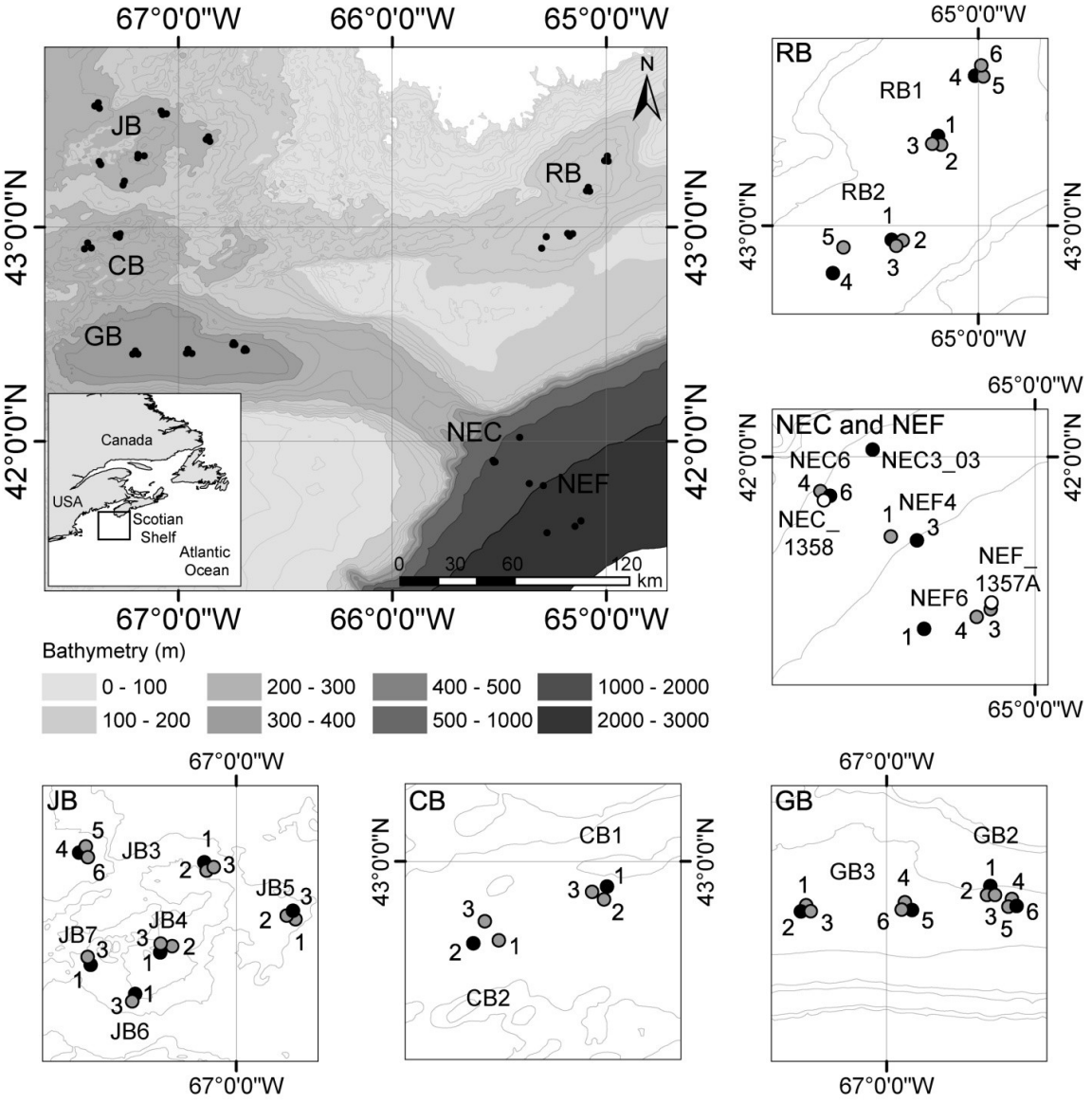

Figure 3.1: Regional setting of study area in the Gulf of Maine and Scotian Shelf, Slope and Rise localities. The map includes locations of sediment cores taken in Crowell Basin (CB), Georges Basin (GB), Jordan Basin (JB), Roseway Basin (RB), and in the Northeast Channel (NEC) and Fan (NEF) with white dots where only geochemical data, grey dots where only X-radiographs and back dots where both X-radiographs and geochemical data are available.

3.2.2 X-radiography

Two different approaches were used to prepare sediment slabs from collected multicores. In 2009, the sediment cores were extruded, sliced into rectangles and then transferred to Plexiglas trays (9.5 cm x 57 cm x 3 cm). Unfortunately, this technique created sampling artifacts that were visible on final X-radiographs. Therefore, in 2010, Plexiglas tray sizes were slightly modified to fit the inner diameter of multicore tubes and inserted directly into sediment cores. More precisely, a three-sided tray (Plexiglas tray with no front side) was initially inserted vertically into the sediment core to limit sediment compaction and disturbances. Subsequently, a front side was inserted into machined grooves to encase the sediment slab in the tray. The trays containing sediment slabs were then X-ray imaged using a Thales Flashscan 35 X-ray detector, illuminated with a Medison Acoma PX15HF electric X-ray generator, centered at 60 kV, 12 mA and with an exposure time of 2-4 seconds. X-radiographs were stored as 14-bit TIFF data files and analyzed with ImageJ (Schneider et al., 2012).

3.2.3 Sedimentological analyses

For particle size analysis, subsamples were disaggregated in a $NaPO_3$ (0.05 %) solution and sonicated for 1 h using an ultrasonic bath. After leaving the samples in the solution overnight, the analysis was performed with a HORIBA Partica LA-950 laser diffraction particle size analysis system. Relative percentages of clay (<3.9 µm), silt (3.9 - <62.5 µm) and sand (62.5 - <2000 µm), as well as the logarithmic graphic mean M_z, sorting coefficient or standard deviation σ_I, and skewness SK of grain size distributions (Folk and Ward, 1957) were then calculated from the particle size distribution report. Sediment

porosity Ø and water content of surface sediments were obtained using the wet-dry method after Bennett and Lambert (1971). Wet sediment samples were dried in an oven at 70°C and the sediment porosity was calculated using Eq. (1)

$$\phi = \frac{mw}{mw + \left(\frac{ms}{\rho s}\right)} \quad (1)$$

where mw is the water weight [g], ms is the sediment dry weight [g], and ρs is the grain density which was assumed to be 2.65 g cm^{-3} (e.g. Avnimelech et al., 2001).

3.2.4 Organic matter

Chlorophyll-a and phaeopigments

Sample aliquots of ~1 g thawed, wet sediment of the upper 0-10 cm (1 cm divisions) of the sediment cores collected in 2010 were transferred to high density polyethylene 15 ml centrifuge tubes and extracted in 10 ml 90 % acetone. Samples were sonicated for 5 minutes using an ultrasonic bath and stored horizontally overnight at -18 °C to ensure complete extraction. Acetone extracts were separated from sediments by centrifugation for ten minutes at 3000 rpm and the fluorescence of extracts were measured with a Turner Design 10 Fluorometer before and after acidification with ~2 drops 5 % HCl. Chlorophyll-a and phaeopigment concentrations were calculated after Riaux-Gobin and Klein (1993) and expressed in units of µg g^{-1} dry sediment.

Chlorophyll-a data for sediment sections 0-2 cm, 2-5 cm, and 5-10 cm collected in 2009 were provided by A. Robar and P. Snelgrove, Department of Ocean Sciences, Memorial University of Newfoundland, CA using the same analytical approach as used in 2010.

Standard deviations (1 σ) of chlorophyll-a concentrations were calculated from triplicate measurements of sample aliquots of ~17 % of the sediment samples collected in 2010.

TOC, TN and $\delta^{13}C$

Thawed, wet sediment samples (~1-2 mg) were transferred to high density polyethylene 45 ml centrifuge tubes, acidified overnight with 5 M hydrochloric acid, washed and centrifuged, and dried in a box oven at 40 °C until dry. Dried sediments were then finely powdered with mortar and pestle and transferred and stored in glass vials until analysis. Organic carbon (TOC) and total nitrogen (TN) contents were measured with a Carlo Erba NA1500 Series II Elemental Analyser, and stable carbon isotope signatures $\delta^{13}C$ were measured by interfacing the elemental analyser through a Confloll interface with a ThermoElectron DeltaVPlus Gas Source Isotope Ratio Mass Spectrometer. The data were normalized using the standards IAEA-N-1, IAEA-N-2, IAEA-CH-6, B2153 (low organic content soil standards), and two Memorial University laboratory standards (MUN-CO-2 ($CaCO_3$) and MUN Sulfanilamide). The average precision on these reference materials was ± 0.18 ‰ for $\delta^{13}C$, ± 1.40 wt.% for wt.% TOC and ± 1.51 wt.% for wt.% TN. The isotopic ratios are reported in units of per mil (‰) relative to VPDB and elemental data of TOC and TN are reported in weight %. Standard deviations (1 σ) of TOC, TN and $\delta^{13}C$ values of sediment samples were calculated from duplicate measurements of sample aliquots of ~10 % of all samples analyzed.

3.2.5 Radiochemistry

For analysis of the radioisotopes ^{210}Pb, ^{228}Th and ^{234}Th, sample aliquots of 5-15 g dried and finely ground sediment were measured for 24 h using Canberra germanium detectors (models: GL-3825R and GR-1518). Prior to the measurement the sediment samples were sealed airtight and left for 3 weeks to allow the ingrowth of the ^{210}Pb grandparent ^{222}Rn and the ^{228}Th and ^{228}Ra daughter nuclides ^{224}Ra and ^{228}Ac respectively. Sediment samples for the analysis of ^{234}Th (0-5 cm of sediment cores collected in 2010) were measured immediately after the cruise and were re-measured after a time period of approximately three months.

The obtained gamma-ray spectra were analyzed with the gamma acquisition and analysis software Genie 2000. The activities of radionuclides are reported in dpm g^{-1} (decays per minute per gram dry sediment), and were corrected for decay from sample collection to counting. Total activities of ^{210}Pb were measured by its gamma emission at 46.5 keV and activities of supported ^{210}Pb were determined by analyzing ^{226}Ra via its daughter isotopes ^{214}Pb (295 keV and 352 keV) and ^{214}Bi (609 keV). ^{228}Th and ^{228}Ra activities were obtained by measuring the gamma emissions of their daughter isotopes ^{212}Pb (238.6 keV) and ^{208}Tl (583.1 keV), and ^{228}Ac (338.4 keV, 911.1 keV and 968.9 keV) respectively. Excess activities of ^{210}Pb and ^{228}Th were then calculated by subtracting supported activities of ^{210}Pb from total activities of ^{210}Pb, and by subtracting the activities of total ^{228}Ra from total ^{228}Th activities. Excess activities of ^{234}Th were calculated by subtracting the activities obtained during the first measurement shortly after collecting the sediment samples from the activities obtained by re-measuring the samples after three months.

3.2.6 Principal component analysis

To better characterize benthic environments across the study region based on the variability of organic matter and substrate, a principal component analysis (PCA) was carried out with the sedimentological surrogates (percentages of sand, silt and clay, skewness and sorting of grain size distributions, water percentage and porosity, and sedimentation rates) and the organic matter surrogates (chlorophyll-a and total organic carbon concentrations, and chlorophyll-a to phaeopigment and total organic carbon ratios) using R 3.0.1 and the CRAN package FactoMineR (Husson et al., 2013). Sampling locations were grouped into four simplified environmental categories based on the PCA results and the variables that best explained differences among sampling sites across the study region, (Fig. 3.12 A and C).

3.3 Results

3.3.1 Sedimentary facies and bioturbation structures

Four distinct sedimentary facies (termed *Facies a-d*) were identified from X-radiographs and several of the sediment cores collected displayed clear facies boundaries (Fig. 3.2, Appendix 3.1 and 3.2). *Facies a* was found in 71 % of the sediment cores collected across the study region and was characterized by coarse-grained muds, often displaying distinct bioturbation structures. *Facies b* was characterized by compact, well-consolidated, fine-grained muds with varying degrees of mineralized bioturbation. Sedimentary *Facies b* was found in 66 % of the cores of which 76 % displayed distinct bioturbation structures. *Facies c* and *d* were similar to *Facies a* and *b*, respectively. *Facies c* consisted of coarse-grained mud matrices with varying numbers of embedded

ice-rafted debris clasts and was found in 27 % of the cores collected. *Facies c* generally exhibited low degrees of preserved bioturbation structures, while the fine-grained muds of *Facies d*, identified in only 7 % of the cores, displayed preserved sedimentary layering and/or distinct bioturbation structures.

In all sediment cores collected in Crowell Basin and Georges Basin either *Facies a* or *c* overlaid *Facies b* (Fig. 3.2 A-F, Appendix 3.1 and 3.2). In Jordan Basin, Roseway Basin and the Northeast Fan only some cores exhibited multiple sediment facies (Fig. 3.2 M-P and S-T). The sediment cores collected at JB5 stations in Jordan Basin also displayed interbedded coarser- and finer-grained sedimentary facies (*Facies a, b and c*) with a sequence, from surface to depth, of coarser-grained sediment at the surface (*Facies a and c*), compacted mud (*Facies b*), coarser-grained sediment (*Facies a*), and again compacted mud at depth (*Facies b*) (Fig. 3.2 J, Appendix 3.1 and 2.2).

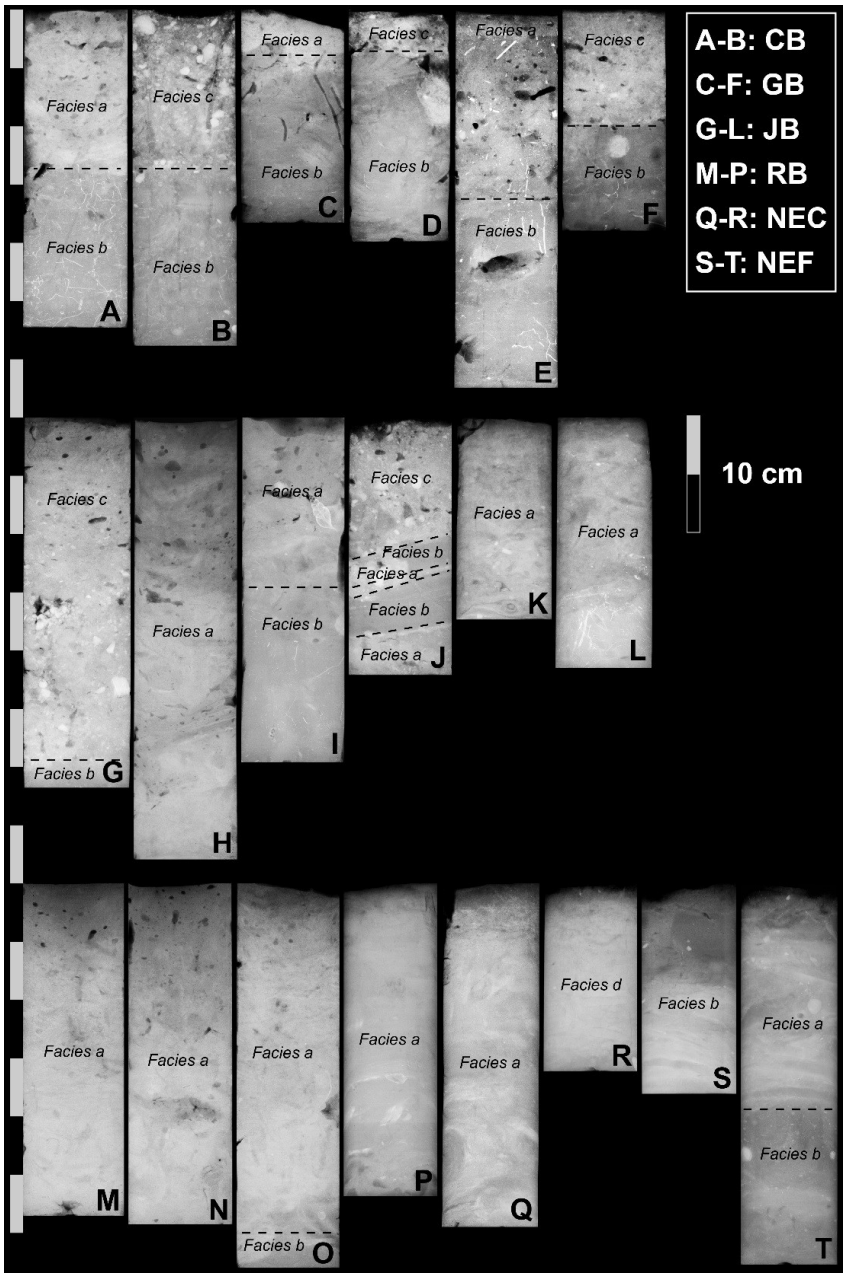

Figure 3.2: X-radiograph negatives from multi-cores showing sediment facies and characteristics of facies contacts. Lighter greys represent higher and darker greys lower bulk densities. Crowell Basin A-B: CB1_01 and CB2_02; Georges Basin C-F: GB2_01, GB2_06, GB3_02 and GB3_05; Jordan Basin G-L: JB3_01, JB3_04, JB4_01, JB5_03, JB6_01, and JB7_01; Roseway Basin M-P: RB1_01, RB1_04, RB2_01 and RB2_04; Northeast Channel Q-R: NEC_3_03 and NEC6_06; and Northeast Fan S-T: NEF4_03 and NEF6_04.

The thickness of overlying facies varied between 1 and 29 cm across the study area. Contacts between facies were either sharp, diffuse, or bioturbated. Most sediment cores collected in Crowell Basin and Northeast Fan NEF6 locations exhibited sharp contacts between upper and lower facies whereas X-radiographs of most cores from Georges Basin, Jordan Basin, and Roseway Basin (RB2 cores) showed bioturbated, indistinct contacts.

Bioturbation structures observed in X-radiographs were non-statistically grouped and informally named based on descriptive parameters such as, similar general geometry, burrow fill, and characteristics of the boundary to the surrounding sediment (termed *Group A-J*) (Fig. 3.3 and 3.4, Appendix 3.1, 3.2 and 3.3). Only bioturbation structures that occurred in more than one sediment core are further discussed in this chapter. Extensively mineralized bioturbation structures and concretions were generally found in compacted mud facies in Crowell Basin, Georges Basin, Jordan Basin, and Roseway Basin (Fig. 3.5). However, these structures presumably play an insignificant role in active bioturbation processes and are therefore not further discussed. For a discussion of bioturbation structure group distributions in relation to environmental patterns discovered with PCA, and an interpretation of potential feeding mechanisms see Appendix 3.4.

Group A

This group is characterized by simple, vertical to sometimes vertically inclined U- and J-shaped tubes (Fig. 3.3 A and B, Fig. 3.4 A). Bioturbation traces of this group were mostly open and unlined (*Sub-Group A1*) but with a few examples that exhibited a distinct lining

(*Sub-Group A2*). Most traces had one or two openings at the sediment-water interface and a few were located in deeper sediment segments (11-29 cm) with no obvious

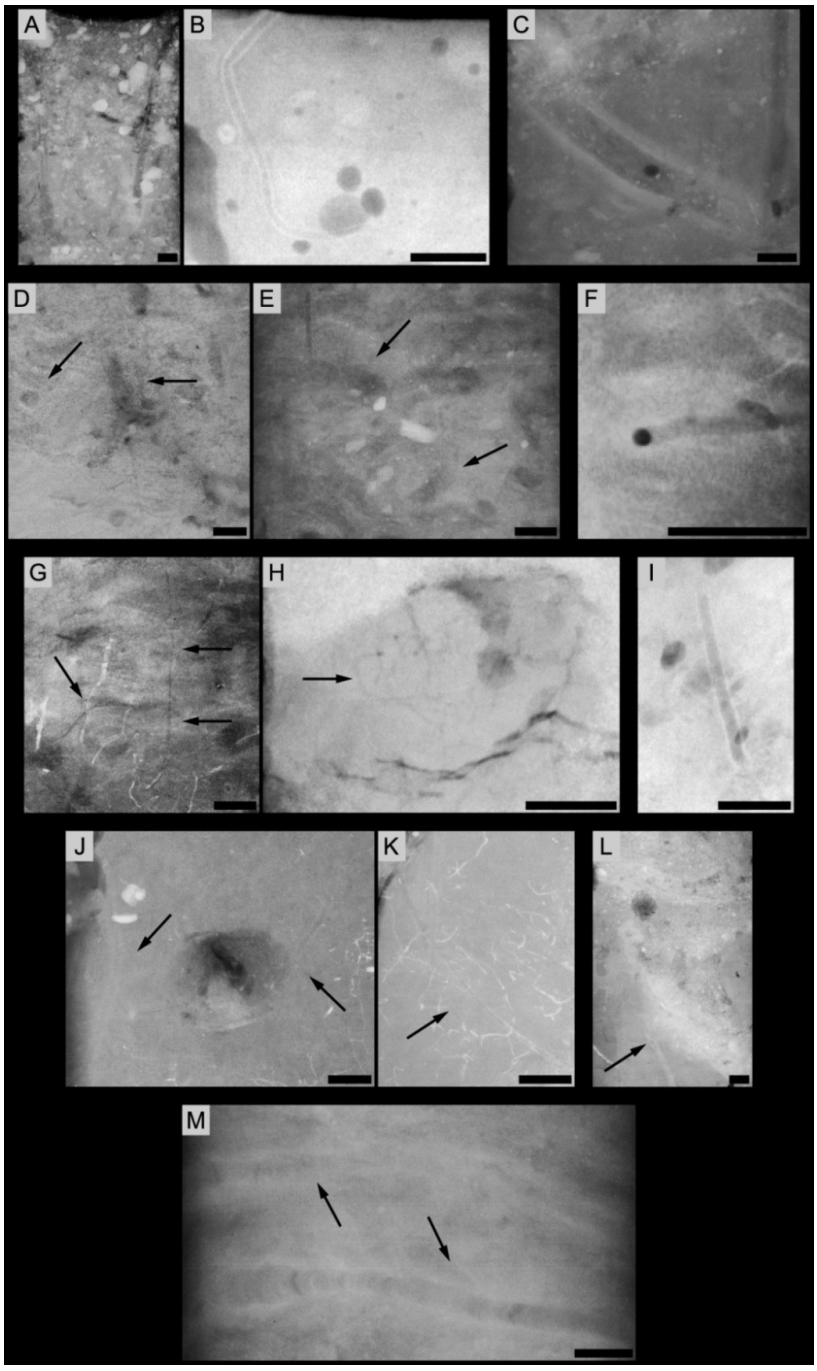

Figure 3.3: X-radiograph negatives showing bioturbation structure groups identified in collected multi-cores. Lighter greys represent higher and darker greys lower bulk densities. A-B: Group A, C: Group C, D-E: Group

B, F: Group D, G-H: Group G, I: Group F, J-K: Group E, L: Group H, and M: Group J. The scale bar represents 1 cm.

connection to the overlying water column (*Sub-Group A3*). Burrows of the latter type sometimes displayed mineralized tube walls (*Sub-Group A4*). Most tunnels of this group were open but some structureless infillings of tunnels also occurred. Maximum tube diameters varied between 0.02 and 0.7 cm.

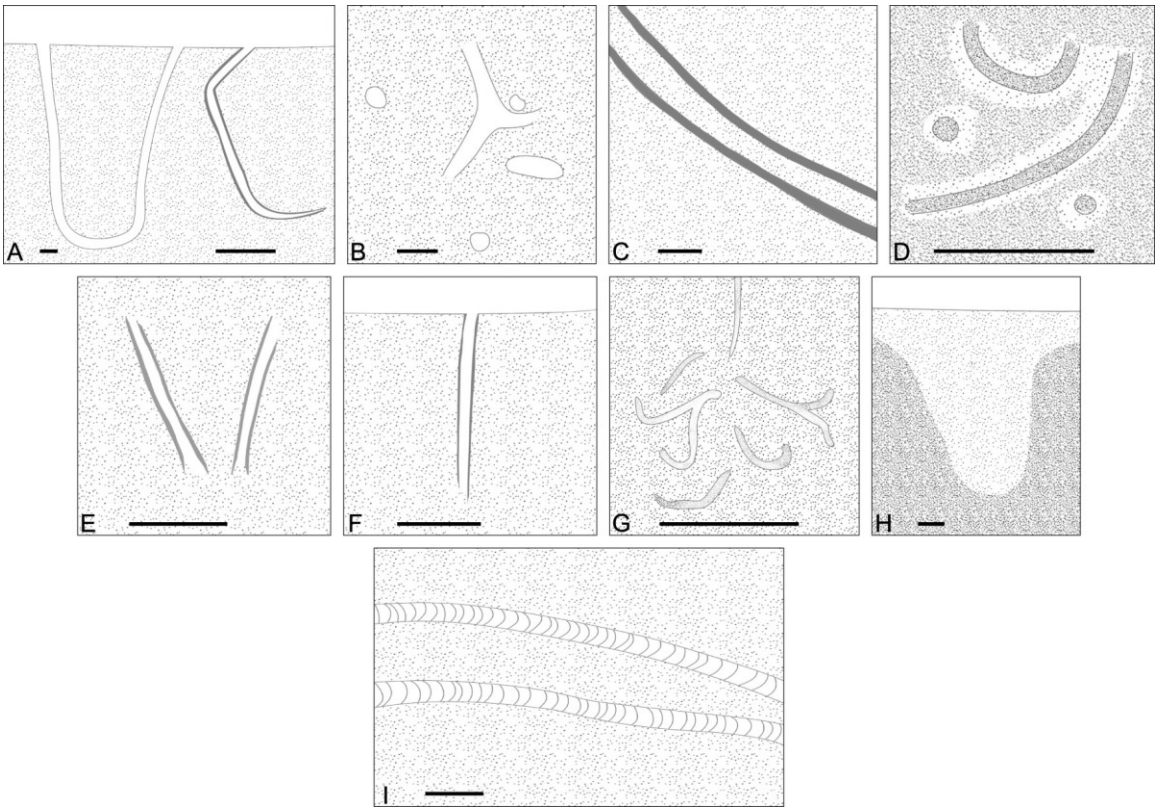

Figure 3.4: Schematic representation of bioturbation structure groups observed in sediment cores. A) Group A, B) Group B, C) Group C, D) Group D, E) Group E, F) Group F, G) Group G, H) Group H, and I) Group J. The scale bar represents 1 cm.

Group B

This group features horizontal and vertical, straight to locally slightly curving or sinuous, sometimes three-dimensional branching tunnel systems (Fig. 3.3 D and E, Fig. 3.4 B). Tubes were circular to elliptical in cross-section and mostly unlined with only a few burrows that exhibited thin to distinct wall linings. Intersections of branching tunnels were T- or Y-shaped. Most burrows of this group were open or exhibited a structureless fill that differed from the lithology of the host sediment. At stations GB3_05 in Georges

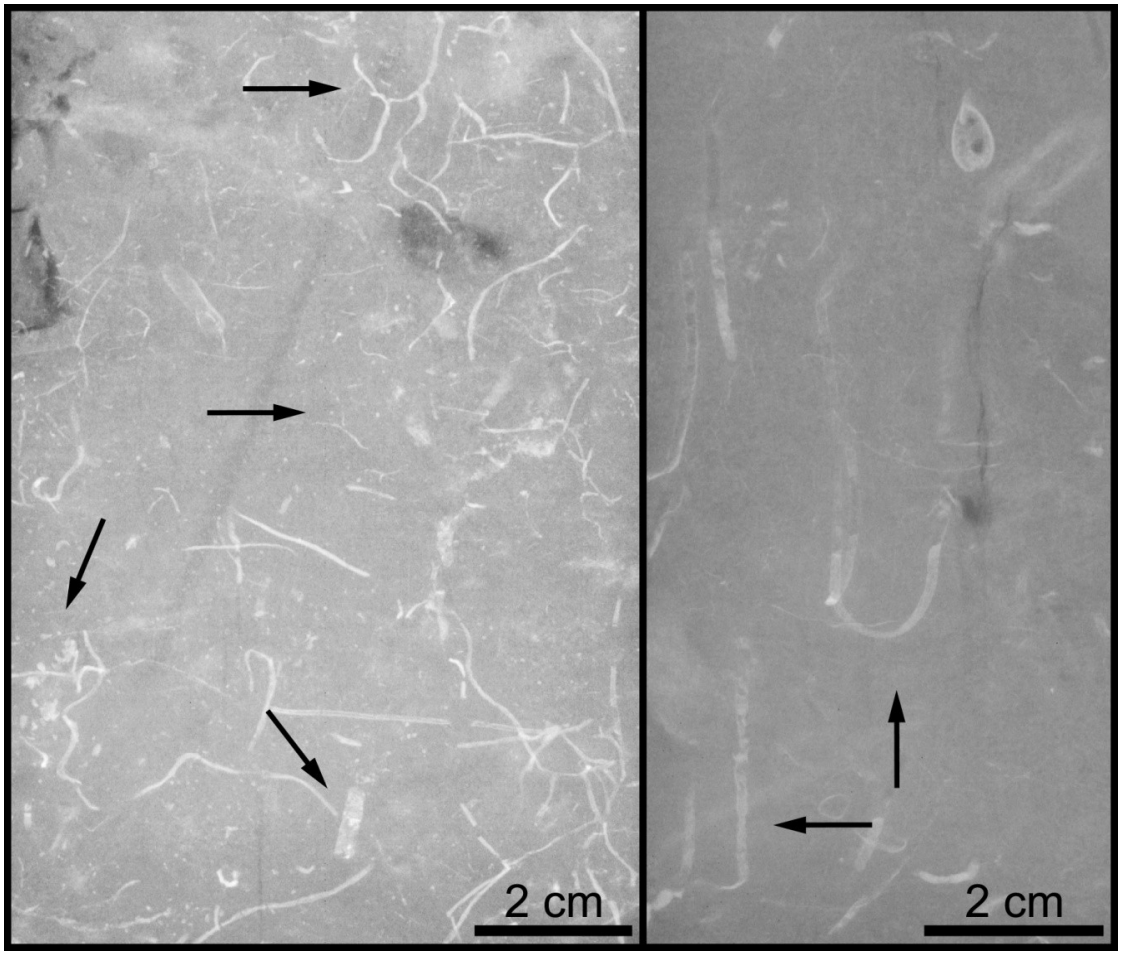

Figure 3.5: X-radiograph negatives displaying mineralized bioturbation structures and mineral concretions found in collected multi-cores. Lighter greys represent higher and darker greys lower bulk densities.

Basin, and RB2_03 and RB2_05 in Roseway Basin these structures penetrated into compacted mud and were infilled with material of an overlying surface layer of coarser-grained sediment (*Sub-Group B2*). In general, structures of this group occurred in deeper parts of collected sediment cores with average minimum and maximum penetration depths of 12 and 17 cm. However, traces of this type were also found in sediment layers located relatively close to the sediment-water interface (0-7 cm). Maximum diameters of tubes ranged from 0.08 to 1.7 cm.

Group C

Group C encompasses simple horizontal to horizontally inclined tubes with distinct lining (Fig. 3.3 C, Fig. 3.4 C). Tunnels were circular in cross-section and are open or have a structuresless fill with sediment of the same lithology as the host sediment. In collected cores, specimens of this group were located between 13 and 25 cm depth with maximum tube diameters of 0.3 to 0.9 cm.

Group D

This group is characterized by horizontal to sometimes vertical, straight to curving or sinuous tunnel segments (Fig. 3.3 F, Fig. 3.4 D). Tubes were found in depths of 8-20.5 cm and were surrounded by a thick mantle of coarser-grained substrate compared to the central tube. Maximum tube diameters varied between 0.06 and 0.2 cm.

Group E

Group E has vertical to vertically inclined, straight to locally curved tunnels (Fig. 3.3 J and K, Fig. 3.4 E). Often, tubes exhibited a distinct lining (*Sub-Group E1*) and were

sometimes partially mineralized (Sub-*Group E2*). Bioturbation structures of this type were found in deeper parts of collected cores in depths from 6.5 to 28 cm, with maximum tube diameters that ranged from 0.07 to 0.09 cm. Only one specimen of *Sub-Group E3*, a straight vertically inclined tube and oval in cross-section, occurred at station JB4_02. At two stations, JB3_03 and NEC3_03, specimens without distinct tube linings occurred, which constitute *Sub-Group E4*.

Group F

This group has vertical to vertically inclined, straight tunnels (Fig. 3.3 I, Fig. 3.4 F). Most structures were located in the upper layer and close to the sediment-water interface of sediment cores (0-9 cm) (*Sub-Group F1*). Especially in sediment cores collected in Georges Basin, specimens of this group penetrated into compacted mud and were filled with the coarser substrate of the overlying layer of sediment (*Sub-Group F2*) (Fig. 3.2 C-F). A few specimens were not filled and some tubes exhibited a distinct lining (*Sub-Group F3*), with maximum tube diameters of 0.04 to 0.6 cm.

Group G

Group G is characterized by multiple branching burrow systems with winding tunnels that are circular to elliptical in cross-sections (Fig. 3.3 G and H, Fig. 3.4 G). Intersections of branching tunnels were T- or Y-shaped and tunnels were open or sometimes filled with substrate of a different lithology as the host sediment. Only in a few cores, the multiple branching, dendritic tunnel networks were connected to a vertical master shaft. Most specimens of this group were located in deeper core segments with average penetration depths of 9-14 cm (*Sub-Group G1*). In three cores, collected in Georges

Basin (GB2_02), Jordan Basin (JB6_03), and the Northeast Fan (NEF4_03), tunnel systems of the same type were also found in surface layers (0-2 cm) (*Sub-Group G2*). Bioturbation structures of this group had maximum diameters ranging from 0.03 to 0.07 cm.

Group H

This group shows cylindrical- and cone-shaped, vertical structures (Fig. 3.3 L, Fig. 3.4 H) with maximum diameters of 2.8 to 4 cm. Specimens of this group occurred only in sediment cores collected in Georges Basin and all of them penetrated into compacted mud and are filled with essentially structureless infillings consisting of the coarser substrate of the overlying sediment layer.

Group J

Group J has horizontal, straight to slightly curving tunnels (Fig. 3.3 M, Fig. 3.4 I). Burrows of this group were generally located in deeper segments of sediment cores (~7-15 cm) and display either meniscate backfilling of tubes or potentially spreiten structures. Structure sizes ranged from 0.3 to 0.7 cm in maximum tube diameter.

The station averages of bioturbation structure diversity (measured as the number of bioturbation structure groups in one core) were generally higher in the Northeast Channel and Fan regions. Comparatively low diversities were observed in cores collected at most stations in Jordan Basin and in a few from Georges Basin (Fig. 3.6 A). The comparison of the average vertical extension (maximum depth-minimum depth) of all bioturbation structure groups per core showed that basin sediment values were

generally higher than in the Northeast Channel and Fan regions (Fig. 3.6 B). Average diameters of bioturbation structures observed in sediment cores collected in the Northeast Channel and Fan, as well as in Roseway Basin and Jordan Basin were small compared to those of structures in Crowell Basin and Georges Basin (Fig. 3.6 C).

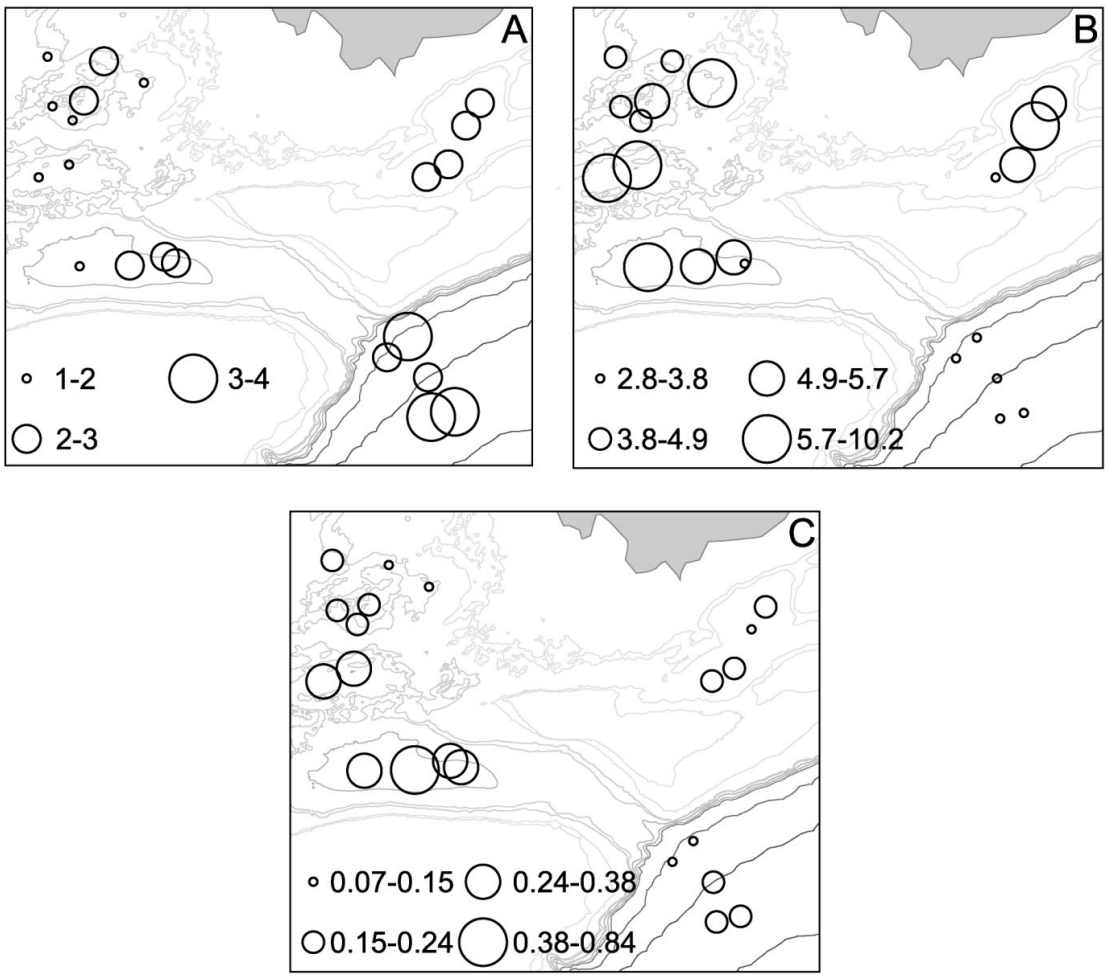

Figure 3.6: Spatial distribution of A) Bioturbation structure group diversity observed in X-radiographs of sediment cores collected. B) Vertical extension (cm) of bioturbation structures in cores. C) Diameter of bioturbation structures (mm) in cores. Graduated symbols represent averages of station triplets (e.g. RB1_01, _02 and _03); sediment cores with no bioturbation structures observed were excluded from calculations (CB1_02, GB3_02 and _03).

Bioturbation structure group diversities were comparatively high in sedimentary *Facies a* in Roseway Basin, and the Northeast Channel and Fan, in *Facies b* in Georges Basin and in *Facies d* in the Northeast Channel (Appendix 3.2). In Jordan Basin, bioturbation structure group diversities varied greatly in sedimentary facies and across the basin. In Georges Basin, sedimentary facies a contained almost no bioturbation structures, whereas relatively high structural diversities characterized *Facies b*. Sedimentary facies identified in Crowell Basin sedimentary cores showed low overall structure diversities and no structures in some cores.

3.3.2 Bioturbation and sedimentation rates

$^{210}Pb_{xs}$ activity profiles and biodiffusion coefficient D_b

Four different types of $^{210}Pb_{xs}$ profiles were observed in collected sediment cores (Fig. 3.7, Table 3.1). The degree of bioturbation in most cores and the lack of preserved physical sedimentary structures suggest that bioturbation was the dominant sediment mixing process influencing $^{210}Pb_{xs}$ profiles, rather than physical deposition and mixing processes (e.g. Bentley et al., 2006). Based on this broad assessment, a biodiffusion-decay model (references below) was fitted to the uppermost portions of $^{210}Pb_{xs}$ profiles, and biodiffusion coefficients (D_b) were calculated with Eq. 2 assuming that sediment particles were frequently and spatially randomly redistributed over small spatial scales by a diffusion-like process (e.g. Goldberg and Koide, 1962; Guinasso and Schink, 1975; Berner, 1980; Cochran, 1985; Boudreau, 1986). It is possible that styles of bioturbation other than biodiffusion are present which influence particle tracer depth distributions, such as bioadvection (Bentley and Nittrouer, 2012). However, given the lack of detailed

information on the abundance, functional group, and bioturbation style of benthic infauna, the application of a model incorporating bioadvection is impractical for the current study.

$$A = A_0 \exp\left(-z\left(\sqrt{\frac{\lambda}{D_b}}\right)\right) \quad (2)$$

Where A is the $^{210}Pb_{xs}$ activity [dpm g^{-1}], A_0 is the tracer activity at the sediment-water interface [dpm g^{-1}], λ is the decay constant of $^{210}Pb_{xs}$ (λ = 0.031 y^{-1}), and z is the depth in the sediment [cm].

Equation 2 was fitted to tracer distributions using a least square method and the Marquard-Levenberg algorithm (SigmaPlot 11.0). For a detailed description of the fitting process see Chapter 2. In case $^{210}Pb_{xs}$ activity depth distributions were comparatively steep and did not decrease exponentially with depth, Eq. 2 could not be fitted to the profile and biodiffusion coefficients were not computed.

Type I $^{210}Pb_{xs}$ profiles

Most sediment cores exhibited *Type I* $^{210}Pb_{xs}$ profiles, which were characterized by a nearly vertical segment of constant activities from the sediment surface to a depth of 2.5-9.5 cm and a distinct inflection point, below which the activity of $^{210}Pb_{xs}$ decreased exponentially with depth (Fig. 3.7 A and B). This $^{210}Pb_{xs}$ profile type occurred in cores collected in basin localities and the Northeast Fan. In general, sediment cores collected in basins had a deeper bioturbation depth than cores collected in the Northeast Fan.

Biodiffusion coefficients ranged from 0.5 to 31.7 cm^2 g^{-1} with higher values in basin sediments (Table 3.1).

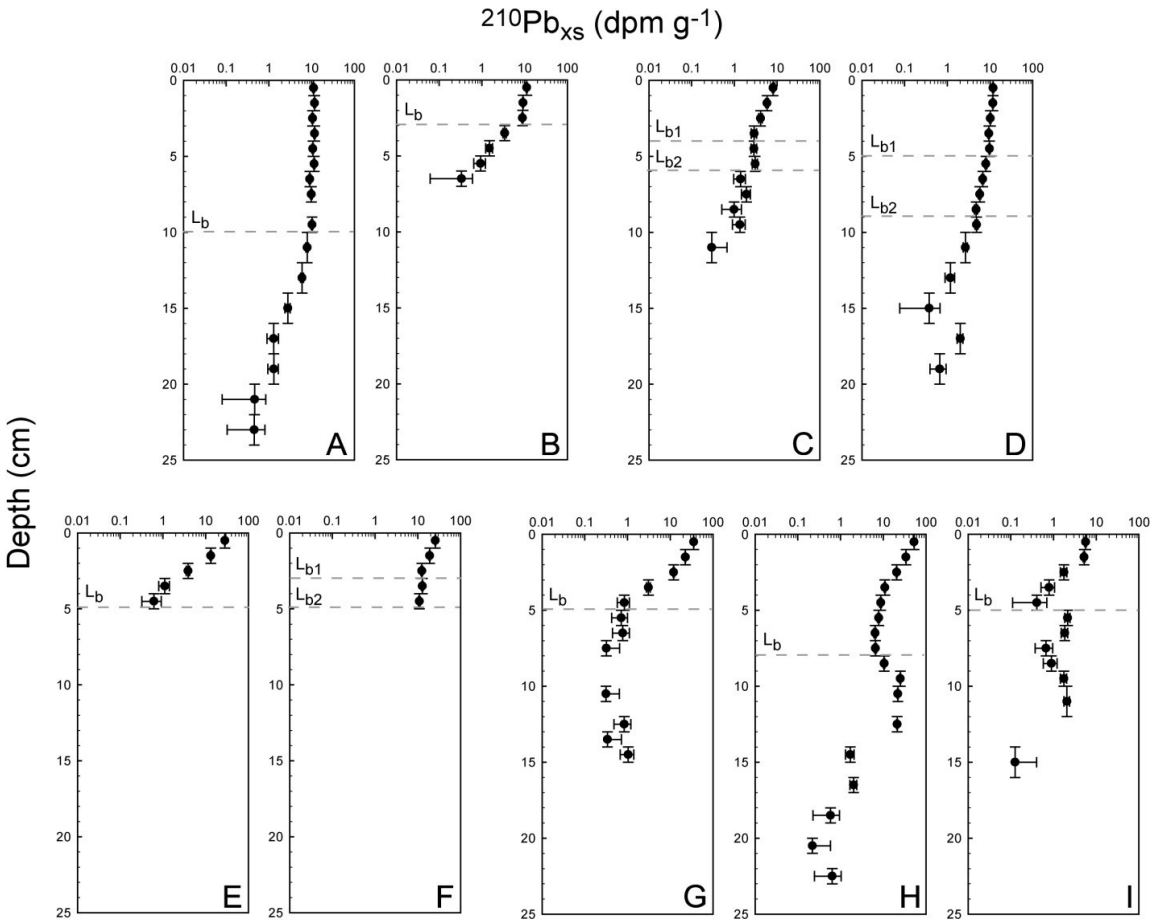

Figure 3.7: $^{210}Pb_{xs}$ activity profiles representing examples of four different profile types found in surface sediments of collected cores. (A) and (B) *Profile type I* (JB3_04 and NEF6_01), (C) and (D) *Profile type II* (GB2_06 and RB1_04), (E) and (F) *Profile type III* (NEC_1358 and NEF4_03), and (G), (H) and (I) *Profile type IV (*NEC6_06, NEC3_03 and JB5_03). Activity error bars are calculated from gamma acquisition net peak area uncertainties and vertical error bars represent the width of analyzed sediment segments in centimeters. Grey dashed lines are bioturbation depths (L_b).

Table 3.1: Biodiffusion coefficients (D_b), sediment mixing depths (L_b), excess activity penetration depths (z_p) and sedimentation rates (ω) as calculated from $^{210}Pb_{xs}$, $^{228}Th_{xs}$ and $^{234}Th_{xs}$ activity profiles.

	$^{210}Pb_{xs}$					$^{228}Th_{xs}$		$^{234}Th_{xs}$		Chl-a
	L_b (cm)	Profile Type	D_b (cm^2 yr^{-1})	ω (cm yr^{-1})	z_p (cm)	D_b (cm^2 yr^{-1})	z_p (cm)	D_b (cm^2 yr^{-1})	Profile Type
RB1_01	L_b 5.0	I	4.69 ± 2.63	0.20 ± 0.01	6.0 (24.0)	31.55 ± 1.75			II
RB1_04	L_{b1} 5.0	II	7.96 ± 4.03	0.11 ± 0.04	5.0 (26.0)	* 659.72 ± 1756.67			II
	L_{b2} 5.0 - 9.0		0.98 ± 0.04						
RB2_01	L_b 4.0	I		0.12 ± 0.01	4.0 (28.0)	68.12 ± 48.12			I
RB2_04	L_b 3.0	I		0.24 ± 0.05	3.0	56.60 ± 47.90	2.0	1.58 ± NA	I
JB3_01	L_b 7.0	I	31.67 ± 25.43	0.10 ± 0.01					III
JB3_04	L_b 10.0	I	* 99.85 ± 100.80	0.12 ± 0.01	5.0	5.31 ± 4.05			III
JB4_01	L_b 5.0	IV	0.27 ± 0.22	0.11 ± 0.03					II
JB5_03	L_b 5.0	IV	0.12 ± 0.07	0.30 ± 0.26	2.0				IV
JB6_01	L_{b1} 5.0	II		0.10 ± 0.02	6.0	* 18.85 ± 46.68	5.0	53.91 ± 39.88	IV
	L_{b2} 5.0 - 9.0		0.91 ± 0.12			±			
JB7_01	L_b 3.0	I		0.07 ± 0.01	7.0 (24.0)	31.06 ± 6.20	3.0	14.63 ± 11.34	I
CB1_01	L_b 4.0	I	15.54 ± 11.36	0.13 ± 0.02	5.0	3.19 ± 0.80			II
CB2_02	L_b 4.0	I	0.48 ± 0.05	0.06 ± 0.02	4.0	2.46 ± 1.57			II
GB2_01	L_b	NA							I
GB2_06	L_{b1} 4.0	II	0.27 ± 0.01	0.16 ± 0.11	2.0	0.64 ± NA			I
	L_{b2} 4.0 - 6.0								
GB3_02	L_b 7.0	I	1.40 ± 0.42	0.06 ± 0.01					II
GB3_05	L_b 5.0	I	0.85 ± 0.21	0.03 ± 0.00					II
NEC3_03	L_b 8.0	IV	0.16 ± 0.03	0.19 ± 0.10	1.0		4.0	22.63 ± NA	III
NEC6_06	L_b 5.0	IV	0.08 ± 0.02		2.0 (17.0)	0.67 ± NA	5.0	* 1.85 ± 3.43	III
NEC_1358	L_b 5.0	III	0.04 ± 0.01		4.0 (21.0)	17.60 ± NA	5.0	* 119.61 ± 202.92	III
NEF4_03	L_{b1} 3.0	III	0.25 ± 0.05		4.0 (23.0)	* 5.28 ± 10.94	2.0	3.21 ±	III
	L_{b2} 3.0 - 5.0		* 8.46 ± 15.37						
NEF6_01	L_b 3.0	I	2.04 ± 1.62	0.04 ± 0.00	(17.0)				III
NEF6_04	L_b 3.0	I	* 25.38 ± 71.31	0.12 ± 0.02	2.0		5.0	282.85 ± 240.84	III
NEF_1357A	L_b 3.0	I	4.22 ± 0.42	0.02 ± NA			4.0	45.62 ± NA	III

Uncertainties are standard errors (SE) for the best fit parameters of nonlinear regression calculations. Profile types correspond to $^{210}Pb_{xs}$ activity and chlorophyll-a concentration profiles defined in the text. Numbers in brackets represent $^{228}Th_{xs}$ activities in deeper sediment sections that were excluded from calculations.

Type II $^{210}Pb_{xs}$ profiles

Similar to *Type I* profiles, *Type II* $^{210}Pb_{xs}$ profiles exhibited a layer of enhanced sediment mixing at sediment core tops and distinct inflection points below which $^{210}Pb_{xs}$ activities decreased exponentially with depth (Fig. 3.7 C and D). The bioturbated surface layer, however, displayed two segments of different activity-depth gradients indicating a localized change in bioturbation intensity. Biodiffusion coefficients D_b were therefore calculated from both segments L_{b1} and L_{b2} using Eq. 2. *Type II* $^{210}Pb_{xs}$ profiles occurred in three sediment cores collected in Roseway Basin, Jordan Basin, and Georges Basin with L_{b1} and L_{b2} segments ranging from 4-5 cm, 4-6 cm, and 5-9 cm, respectively. Calculated biodiffusion coefficients varied between 0.3 and 8 $cm^2\ yr^{-1}$ (Table 3.1).

Type III $^{210}Pb_{xs}$ profiles

Type III $^{210}Pb_{xs}$ profiles consisted only of a surface layer of either nearly exponentially decreasing tracer activities or of a $^{210}Pb_{xs}$ profile similar to Type II, showing two segments of changing activity-depth gradients. Below this surface layer no $^{210}Pb_{xs}$ activities could be detected (Fig. 3.7 E and F). Bioturbation presumably dominated surface layer profiles, and biodiffusion coefficients were calculated by using Eq. 2. *Type III* $^{210}Pb_{xs}$ profiles were only found in two cores, NEC_1358 and NEF4_03, with total mixing depths of 5 cm and biodiffusion coefficients ranging from 0.04 to 0.3 $cm^2\ yr^{-1}$ (Table 3.1).

Type IV $^{210}Pb_{xs}$ profiles

$^{210}Pb_{xs}$ activities of *Type IV* tracer profiles tended to decrease nearly exponentially with depth in surface layers, which are presumably mixed by bioturbation. Profiles of $^{210}Pb_{xs}$

activities below surface layers were detected up to 15 to 23 cm depth and were characterized by either nearly constant activity-depth distributions or by fluctuating activity values with depth. In this layer, profiles showed no apparent trend over corresponding depth intervals (Fig. 3.7 G, H and I). $^{210}Pb_{xs}$ profiles of this type characterized cores from Jordan Basin and the Northeast Channel, and biodiffusion coefficients D_b were calculated from surface sediment profile segments extending from 0-5 cm and 0-8 cm depth and by using Eq. 2 (Table 3.1). Biodiffusion coefficients ranged from 0.1 to 0.3, with highest values in Jordan Basin 0.04 to 0.3 $cm^2\ yr^{-1}$.

Sedimentation rates ω

Sedimentation rates ω [cm y^{-1}] were calculated from $^{210}Pb_{xs}$ profiles below the bioturbated layer L_b and by using Eq. 3 (Bentley and Nittrouer, 2003).

$$A = A_0 \exp\left(-\frac{\lambda z}{\omega}\right) \quad (3)$$

Where A is the $^{210}Pb_{xs}$ activity [dpm g^{-1}], $A_{0\ is}$ the tracer activity at the sediment-water interface [dpm g^{-1}], λ is the decay constant of $^{210}Pb_{xs}$ (λ = 0.031 y^{-1}), and z is the depth in the sediment [cm].

Sedimentation rates ranged from 0.02 to 0.24 cm yr^{-1} across the study area and comparatively high sedimentation rates with values of >0.15 cm yr^{-1} characterized sediment cores from stations RB1_01, RB2_04, GB2_06 and NEC3_03 (Table 3.1). Sediment samples from stations GB3_05, NEF6_01 and NEF_1357A, on the other hand, were characterized by relatively low sedimentation rates of <0.05 cm yr^{-1}.

$^{228}Th_{xs}$ and $^{234}Th_{xs}$ activity profiles and biodiffusion coefficient D_b

Excess activities of ^{228}Th were detected in 17 of 23 sediment cores with penetration depths z_p of 1 to 27 cm (Table 3.1). Activity-depth profiles of $^{228}Th_{xs}$ showed a range of gradients throughout the study area and biodiffusion coefficients were calculated using Eq. 2 ($\lambda(^{228}Th) = 0.362$) and from near sediment surface profile segments ($z_p \leq 7$ cm) that displayed exponentially decreasing activity with depth (Fig. 3.8 A). Activity peaks below 7 cm depth were not used in these calculations and nor were $^{228}Th_{xs}$ profiles displaying high penetration depths and nearly vertical activity-depth distributions (Fig. 3.8 B and C). Calculated biodiffusion coefficients varied between 0.6 $cm^2\ yr^{-1}$and 68.1 $cm^2\ yr^{-1}$ across the study area (Table 3.1).

$^{234}Th_{xs}$ profiles in all sediment cores were characterized by exponential activity decreases with depth up to depths of 2 to 5 cm, from which biodiffusion coefficients were calculated using Eq. 2 (1.6 to 282.9 $cm^2\ yr^{-1}$) (Fig. 3.8 D and E, Table 3.2).

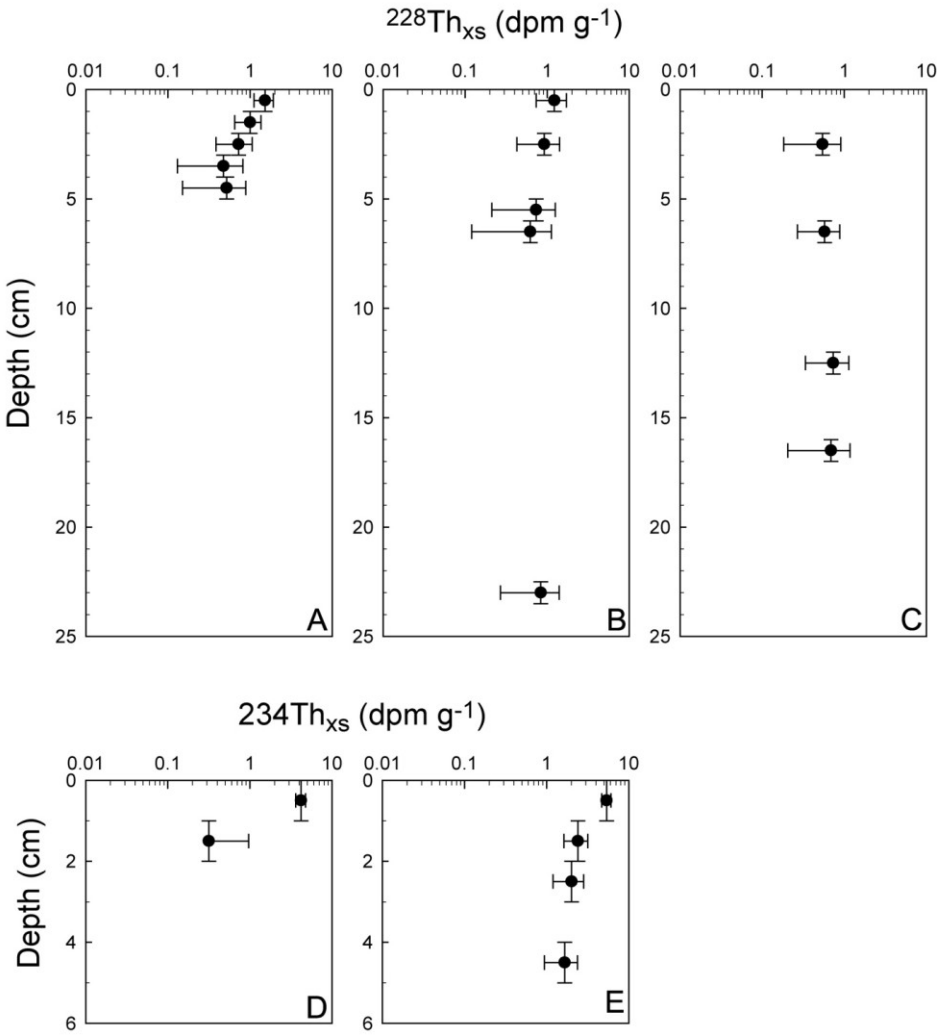

Figure 3.8: (A)-(C) $^{228}Th_{xs}$, and (D) and (E) $^{234}Th_{xs}$ activity profiles showing examples of profile gradients found in sediment cores throughout the study area. Activity error bars are calculated from gamma acquisition net peak area uncertainties and vertical error bars represent the width of analyzed sediment segments in centimeters.

Chlorophyll-a profiles (0-10 cm)

Four general chlorophyll-a profile types (0-10 cm) were observed in collected sediment cores (Fig. 3.9 A-D, Table 3.1).

Type I profiles had nearly vertical concentration-depth distributions, which were found in some cores collected in Georges Basin, Jordan Basin and Roseway Basin (Fig. 3.9 A): GB2_01, 06; JB7_01; and RB2_01, 04.

Type II profiles showed an approximately exponential decrease of chlorophyll-a concentrations with depth (Fig. 3.9 B). These profiles were observed in some cores collected in Crowell Basin, Georges Basin, Jordan Basin and Roseway Basin: CB1_01, CB2_02; GB3_02, 05; JB4_01; and RB1_01, 04.

Type III profiles generally showed a decreasing or nearly constant trend of chlorophyll-a concentrations within the upper 0-3.5 cm to 0-6.5 cm (Fig. 3.9 C). Below this surface layer chlorophyll-a concentrations gradually increased with depth. Chlorophyll-a profiles of this type were found in cores collected in Jordan Basin, and the Northeast Channel and Fan: JB3_01, 04; NEC3_03, NEC6_06, NEC_1358; and NEF4_03, NEF6_01, 04, NEF_1357A.

Type IV profiles were characterized by a subsurface concentration peak in about 2-5 cm depth (Fig. 3.9 D). Chlorophyll-a profiles of this type were only found in two cores collected in Jordan Basin: JB5_03 and JB6_01.

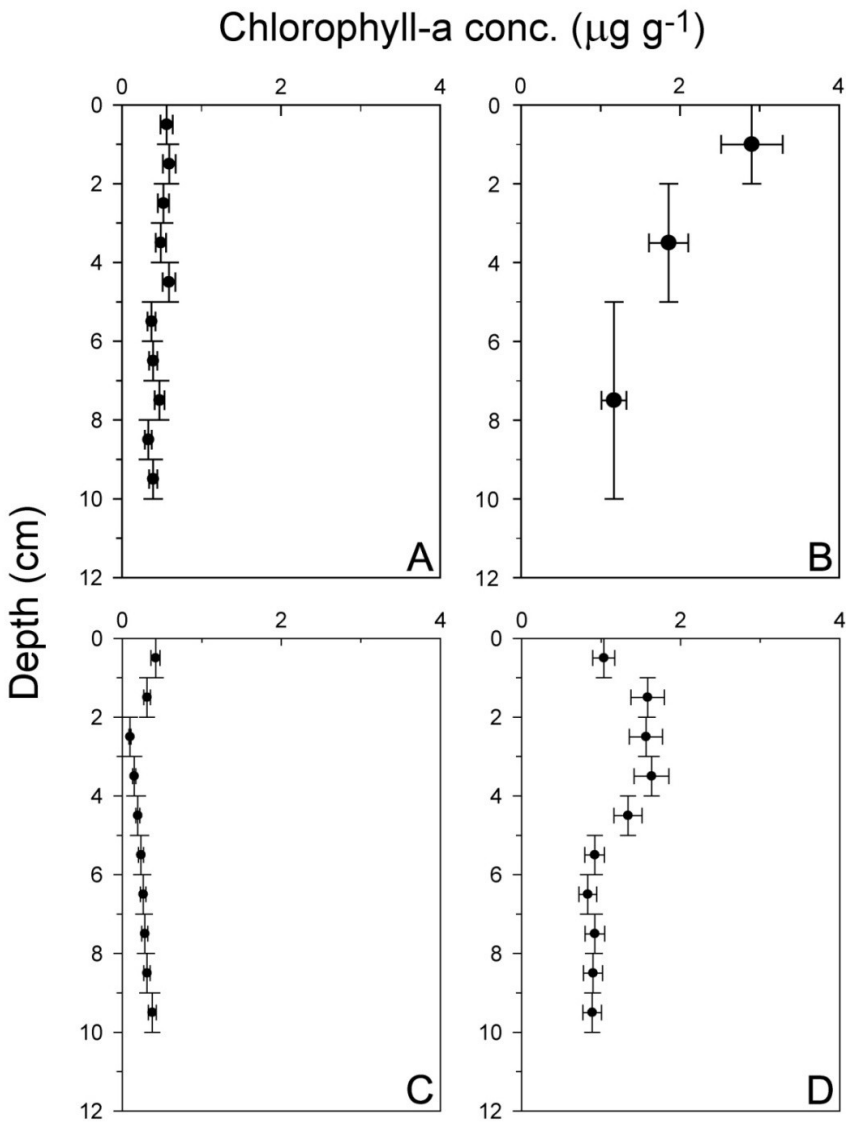

Figure 3.9: Chlorophyll-a concentration profiles showing examples of *profile types I-IV* found in surface sediments of collected cores. (A) *Profile type I* (RB2_04), (B) Profile type II (CB2_02) provided by A. Robar and P. Snelgrove, Department of Ocean Sciences, Memorial University of Newfoundland, CA, (C) *Profile type III* (NEC3_03), and (D) *Profile type IV* (JB6_01). Horizontal error bars are the averages of standard deviations calculated from replicate analyses (n=3) with 20 percent of the samples, and vertical error bars represent the width of analyzed sediment segments in centimeters.

3.3.3 Organic matter and substrate characterization of surface sediments

Grain sizes, sediment sorting, skewness, water content, and porosity (0-10 cm)

Surface sediments collected across the study area were poorly to very poorly sorted with lowest sorting coefficients in Georges Basin and Northeast Fan sediments and highest sorting coefficients in Roseway Basin sediments (Fig. 3.10 A). Mean Phi grain sizes ranged from 4.1 to 6.2 throughout the study area and sediments from most stations were characterized as silt, sandy silt and clayey and sandy silt (Fig. 3.10 A and B). The coarsest sediments occurred at station RB2_04 in Roseway Basin, station NEF6_01 in the Northeast Fan and station NEC6_06 in the Northeast Channel and were all characterized by silty sand and clayey sand and silt, respectively.

The skewness of grain size distributions varied from very coarse to very fine skewed (Fig. 3.10 B). On average, sediments collected in Jordan Basin and Crowell Basin were coarser skewed compared to other regions and the finest skewed sediments were observed in Roseway Basin and the Northeast Fan.

Average values for water content and porosity of surface sediments varied between 26.4 and 56.6 percent, and 0.5 and 0.8, respectively (Fig. 3.10 C). Sediments with generally low water content, low porosity, and high dry bulk density occurred at stations RB2_04 in Roseway Basin, JB5_03 in Jordan Basin, and CB2_02 in Crowell Basin. Sediment characterized by relatively high water content and high porosity was sampled at stations RB1_01 and RB1_04 in Roseway Basin, JB3_04 and JB7_01 in Jordan Basin, NEC3_03 in the Northeast Channel, and NEF4_03 in the Northeast Fan.

Surface sediments from all cores showed a polymodal grain size distribution trend with two or more grain size populations (Appendix 3.5). The most common grain size modes were fine sand and fine silt, with clay in fewer sediment cores.

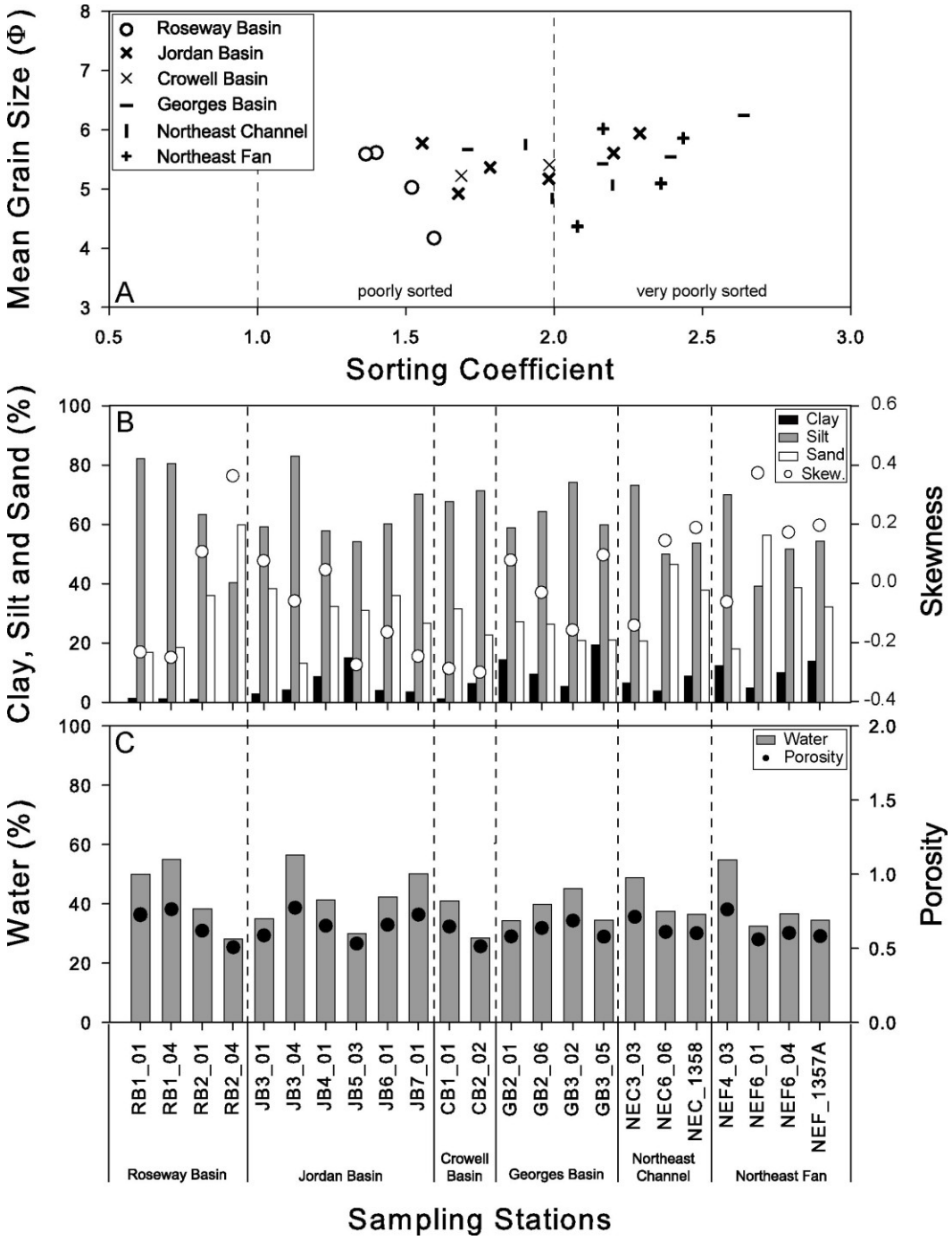

Figure 3.10: Substrate characteristics of surface sediments (0-10 cm) collected throughout the study area. Note that particles with diameters >3000 µm are not included in calculations. (A) Textural discrimination plot of surface sediments (0-10 cm), (B) Percentages of clay, silt and sand, and skewness of grain size distributions, and (C) Percent water and porosity of surface sediments.

Organic carbon concentration and provenance of surface sediments (0-2 cm)

C/N and $\delta^{13}C$ data throughout the study area indicate that organic carbon of surface sediments derived mainly from marine sources (Fig. 3.11 A). Chlorophyll-a content of surface sediments was generally higher in basin sediments, whereas sediments collected in greater depths of the Northeast Channel and Fan were characterized by relatively low chlorophyll-a concentrations. TOC values ranging from 0.25 to 1.77 wt. % varied less throughout the study area than chlorophyll-a concentrations (Fig. 3.11 B). Chlorophyll-a concentrations in basin sediments ranged from 0.58 to 2.90 µg g^{-1}, with highest values observed in Roseway Basin (station RB1_01 and RB1_04), Jordan Basin (station JB4_01) and Crowell Basin (station CB2_02). Surface sediments of the Northeast Channel had slightly higher chlorophyll-a concentrations than Northeast Fan sediments, and total chlorophyll-a concentrations varied between 0.04 µg g^{-1} at station NEF_1357A and 0.37 µg g^{-1} at station NEC3_03.

Normalized chlorophyll-a/phaeopigment and chlorophyll-a/TOC ratios, in general, showed higher organic matter qualities in basin sediments compared to the organic matter of fan and channel sediments (Fig. 3.11 C).

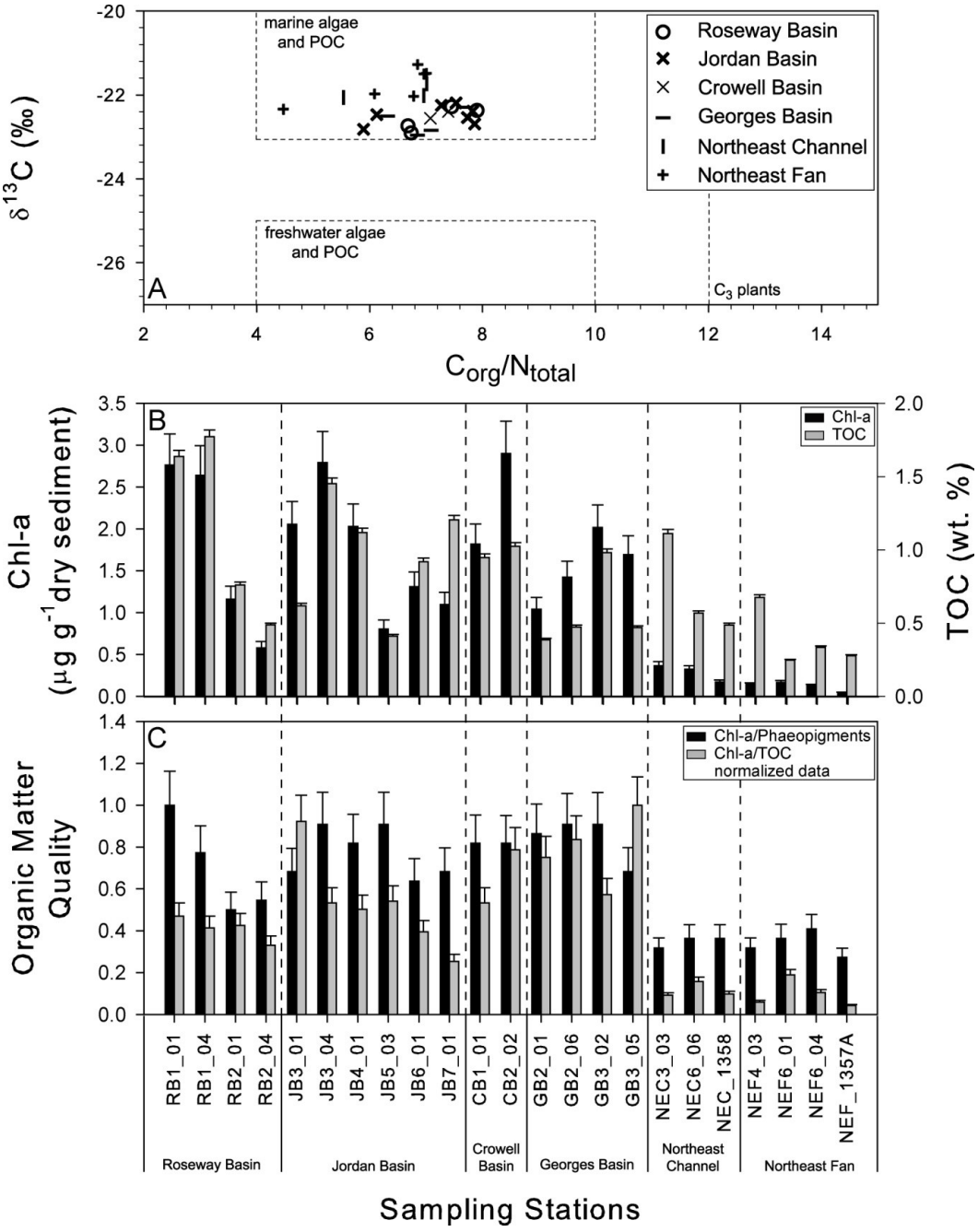

Figure 3.11: Organic carbon and chlorophyll-a of surface sediments (0-2 cm) collected throughout the study area. (A) Organic carbon provenance grouped according to sampling site localities, (B) Chlorophyll-a and total organic carbon (TOC) concentration of surface sediments, (C) Normalized chlorophyll-a/phaeopigment and chlorophyll-a/TOC ratios as indicators of organic matter quality. Error bars indicate standard deviations (1 σ) as calculated from triplicate measurements of ~10 % of all samples collected in 2010.

3.3.4 Environmental patterns of organic matter and substrate characteristics across the study region based on principal component analysis (PCA)

Sample site groupings based on PCA plot quadrants showed distinct spatial patterns of environmental variables across the study region (Fig. 3.12 A-C). Principal components 1 and 2 explained a total of 67.52 % of the variability of the environmental data with principal component 1 alone explaining 48.18 %. The variables total organic carbon, chlorophyll-a, silt and sand, skewness of grain size distributions, porosity, percent water, and the organic matter quality-related variable chlorophyll-a/total organic carbon weighed heavily (correlation coefficient ≥ 0.8) and reflected the predominant differences in benthic environmental conditions among sampling locations across the study region. Herein, with relatively high organic matter quality and input of chlorophyll-a, the regions Georges Basin, Crowell Basin, and some stations in Jordan Basin showed largely similar benthic environmental conditions (mainly categories 1 and 2) and could be clearly separated from the deep water Northeast Channel and Fan regions which are characterized by relatively coarse substrate and low organic matter input and quality (mainly category 3). The sampling stations of the Roseway Basin region varied widely in environmental variable composition. For instance, stations RB1_01 and RB1_04 showed similar characteristics to some stations in Jordan Basin; relatively porous substrates with high organic matter input but low quality (category 4). Stations RB2_01 and RB2_04 showed a similar trend to stations from the Northeast Channel and Fan regions (category 3).

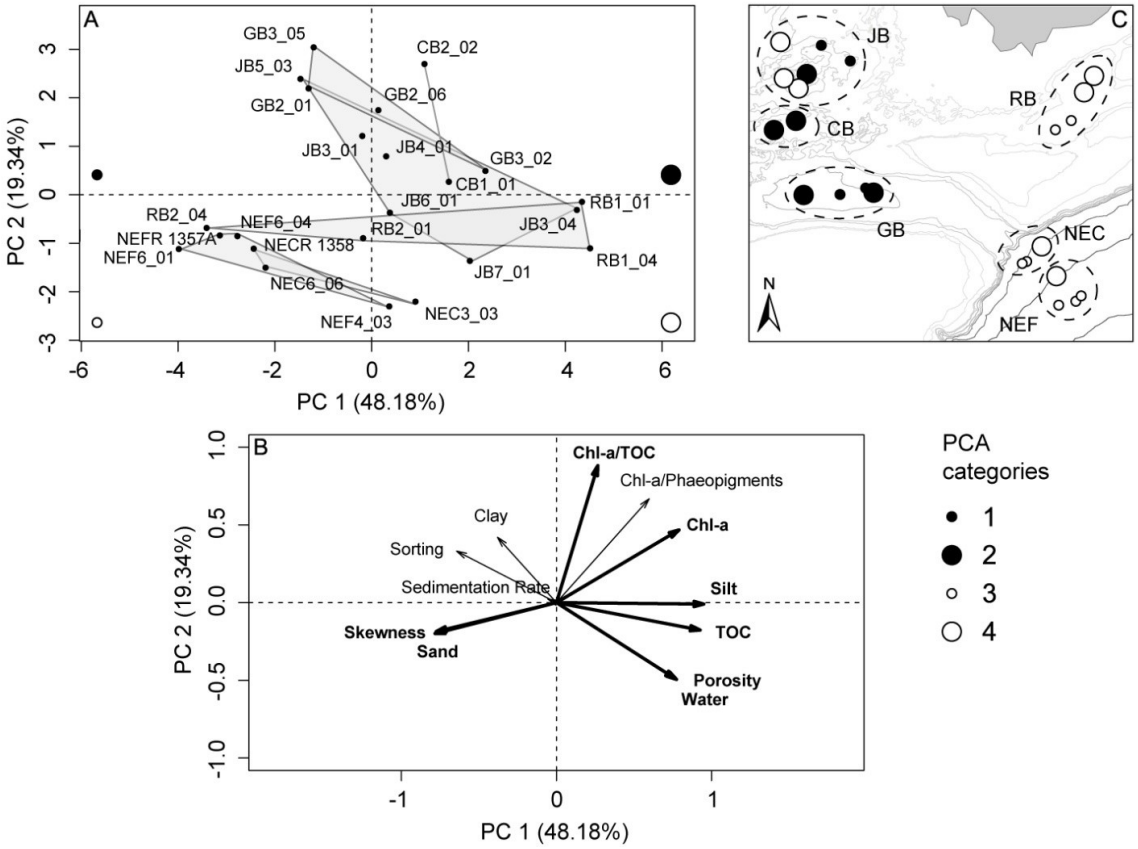

Figure 3.12: Results of principal component analysis with environmental variables analyzed in sediment cores collected from Crowell Basin (CB), Georges Basin (GB), Jordan Basin (JB), Roseway Basin (RB), the Northeast Channel (NEC) and Fan (NEF). Principal components 1 and 2 explain a total of 67. 52 % of the variability in environmental data collected across the study region. A) Scatter plot of principal components 1 (PC 1) and 2 (PC 2). Grey fields indicate the convex hulls of sampling stations within study regions. B) Vector plot of principal component loadings (PC 1 and PC 2). Heavily weighted loadings are indicated in bold. C) Component scores of PC 1 (graduated symbols) and PC 2 (graduated colors) as illustrated in A).

3.3.5 Spatial distribution of bioturbation structure diversity, vertical extent, and diameter of bioturbation structure groups in relation to environmental patterns

Correlations among bioturbation structure diversity, vertical extent, and diameter of bioturbation structure groups and environmental surrogates, including principal component 1 and 2, are shown in Figure 3.13 and Table 3.2.

The diversity of bioturbation structures in collected cores generally responded to the environmental patterns revealed by PCA and correlated negatively with both principal components 1 and 2 (Fig. 3.13, Table 3.2). Thus, higher bioturbation structure diversities were generally associated with category 3 sediments which predominantly occurred in the Northeast Channel and Fan, and in Roseway Basin. Similar trends were found for the average vertical extension of bioturbation structure groups in sediment cores which correlated significantly and positively with principal components 1 and 2 (Fig. 3.13, Table 3.2). Greater extensions therefore predominantly occurred in category 2 sediments as represented at several sampling locations in Jordan Basin, Crowell Basin, and Georges Basin. Diameters of bioturbation structures correlated weakly with principal component 2 and overall, showed only a few significant correlations with environmental surrogates.

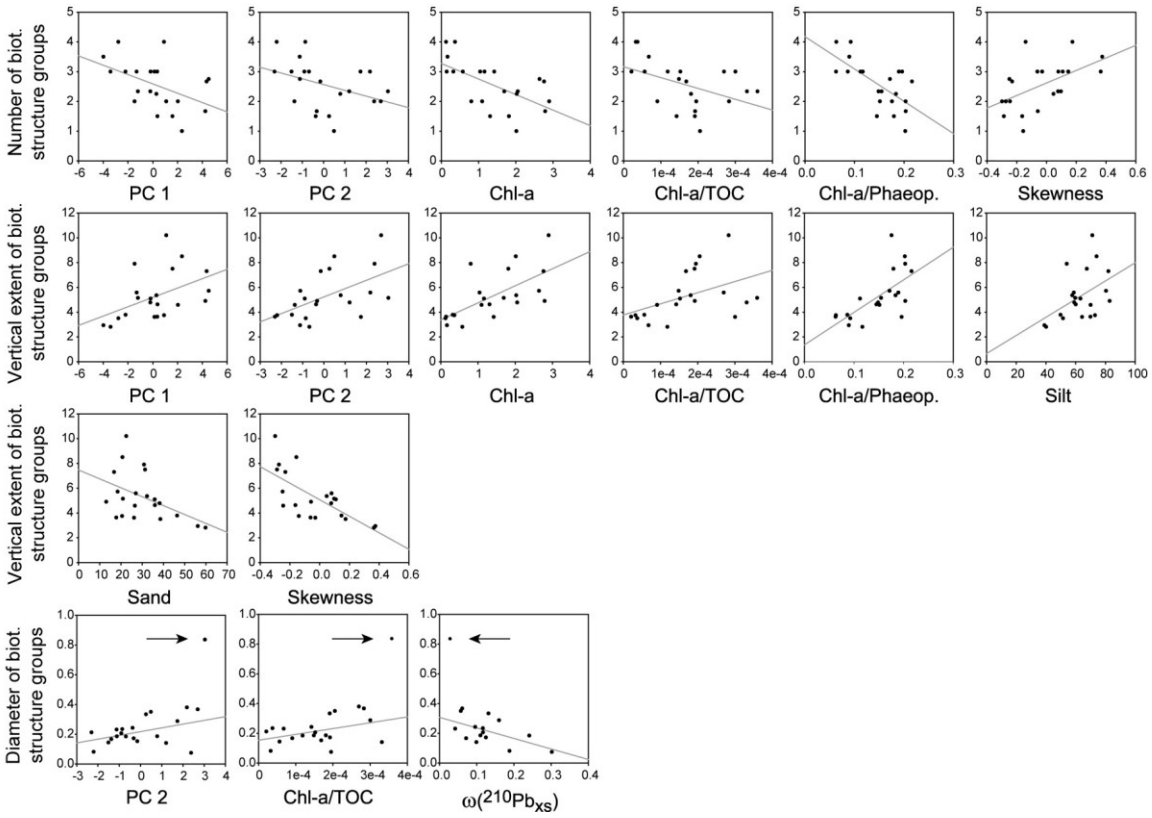

Figure 3.13: Scatterplots of significant Pearson product moment correlations among bioturbation structure group surrogates, number of structure groups per core, diameter, and vertical extent, and environmental variables, including principal components 1 and 2. Average values were calculated from station triplets (e.g. RB1_01, _02 and _03). Arrows indicate outlier data point (station GB3_05) that was not used in correlation calculation.

Table 3.2: Pearson product moment correlation coefficients of bioturbation structure and intensity surrogates and environmental variables, including principal components 1 and 2.

	No. of Biot. Struct. Groups	Diam. of Biot. Struct. Groups	Vertical Ext. of Biot. Struct. Groups
PC1	-0.47 **	0.00	0.46 **
PC2	-0.39 *	0.43 *	0.55 ***
Chl-a	-0.61 ***	0.22	0.65 ***
TOC	-0.34	-0.16	0.36
Chl-a/TOC	-0.45 **	0.41 *	0.46 **
Chl-a/Phaeo.	-0.67 ***	0.29	0.66 ***
Clay	0.13	0.07	0.01
Silt	-0.36	0.05	0.46 **
Sand	0.30	-0.09	-0.46 **
Water	-0.11	-0.22	-0.09
Porosity	-0.12	-0.20	-0.10
Sorting	0.22	0.19	-0.15
Skewness	0.54 ***	-0.06	-0.70 ***
Sed. Rate	0.18	-0.56 **	-0.09

	Biodiffusion Coefficient D_b			Bioturbation Depth		
	$^{210}Pb_{xs}$	$^{228}Th_{xs}$	$^{234}Th_{xs}$	$L_b(^{210}Pb_{xs})$	$z_p(^{228}Th_{xs})$	$z_p(^{234}Th_{xs})$
PC1	0.12	-0.22	-0.39	0.61 ***	0.61 ***	-0.20
PC2	0.13	-0.43	0.32	-0.01	-0.08	0.33
Chl-a	0.28	-0.27	-0.29	0.46 **	0.53 **	-0.03
TOC	0.02	-0.06	-0.45	0.55 ***	0.62 ***	-0.16
Chl-a/TOC	0.37	-0.31	-0.21	0.24	0.13	-0.08
Chl-a/Phaeo.	0.12	-0.33	-0.05	0.33	0.40	-0.01
Clay	-0.40	-0.60 *	0.26	-0.14	-0.53 **	0.11
Silt	0.03	-0.27	-0.30	0.57 ***	0.48 *	-0.15
Sand	0.16	0.40	0.15	-0.50 **	-0.30	0.09
Water	-0.09	-0.15	-0.28	0.57 ***	0.44 *	-0.25
Porosity	-0.08	-0.15	-0.24	0.57 ***	0.44 *	-0.18
Sorting	-0.40	-0.56 *	0.56	-0.35	-0.52 **	0.46
Skewness	0.00	0.43	0.26	-0.39 *	-0.41	0.02
Sed. Rate	-0.06	0.34	-0.16	0.09	-0.63 **	-0.47

	Biodiffusion Coefficient D_b			Bioturbation Depth		
	$^{210}Pb_{xs}$	$^{228}Th_{xs}$	$^{234}Th_{xs}$	$L_b(^{210}Pb_{xs})$	$z_p(^{228}Th_{xs})$	$z_p(^{234}Th_{xs})$
No. of Biot. Struct. Groups	-0.18	0.45	0.43	-0.29	-0.66 ***	0.05
Diam. of Biot. Struct. Groups	-0.05	-0.41	0.43	-0.16	0.23	0.05
Vertical Ext. of Biot. Struct. Groups	0.03	-0.30	-0.10	0.05	0.28	0.40

Levels of significance: *** if $p \leq 0.01$, ** if $p \leq 0.05$, and * if $p \leq 0.1$

3.3.6 Spatial distribution of bioturbation intensities and depths, and tracer profiles in relation to environmental patterns and bioturbation structures

Correlations among bioturbation intensities and environmental surrogates, including principal components 1 and 2, and bioturbation structures are shown Table 3.2.

Only few significant correlations were found among $^{228}Th_{xs}$ and $^{210}Pb_{xs}$ derived bioturbation depths (z_p, L_b) and several environmental parameters (Table 3.2). In particular, strong positive correlations existed between bioturbation depths and principal component 1. $^{210}Pb_{xs}$ bioturbation depths were also associated with chlorophyll-a and total organic carbon concentrations, silt and sand percentages, water content and sediment porosity, and the skewness of grain size distributions. This reflected a strong correlation with principal component 1. Not all $^{228}Th_{xs}$ derived bioturbation depths correlated with all principal component 1 constituents, but many showed associations with additional variables, particularly the percentage of clay, the sorting of grain size distributions, and the sedimentation rate. Only one strong correlation, however, was found between $^{228}Th_{xs}$ derived bioturbation depths and bioturbation structure diversity (Table 3.2).

3.4 Discussion

3.4.1 Influence of changing depositional benthic conditions and recent organic matter and substrate characteristics on bioturbation structure diversity

The benthos in the central and eastern part of Jordan Basin, Crowell Basin, and Georges Basin was potentially affected by depositional changes through time indicated by the presence of multiple sedimentary facies and the discontinuity contacts between

these facies. In particular, fine compacted mud overlain by coarser-grained substrate in these samples potentially indicated a change from low-energy hemipelagic deposition to bottom current winnowing as a result of increasing current strengths (Mullins et al., 1988). Compared to these regions, sedimentary facies of one type dominated sediments collected in the Northeast Channel and Fan, Roseway Basin, and the western part of Jordan Basin (associated with categories 3 and 4) suggesting that these sediments were deposited in relatively stable environmental and depositional conditions. Further, the dynamic depositional conditions in Crowell Basin, Georges Basin, and locally in Jordan Basin often linked to sediments with high organic matter input and quality. This is typical for the sampled shelf basin sediments, which also hosted relatively low bioturbation structure diversities.

The amount of chlorophyll-a and the quality of the organic matter may have exerted a strong influence on the spatial distribution of bioturbation structure group diversities and the vertical extent of bioturbation structures in the studied sediments. The trend of chlorophyll-a rich sediments, predominantly the shelf basin sediments, to show lower bioturbation structure diversities than sediments with low organic matter concentration may be a result of intensive mixing of surface sediments that also contain biodeformational structures. The number of benthic organisms, and consequently, the intensity of sediment mixing, depends on the availability of organic matter, which provides an indicator of the amount of food available for benthic organisms (Wetzel, 1991). Surface sediments with high organic matter input are therefore often completely bioturbated which makes it nearly impossible to recognize distinct structures in these mixed layers. In contrast to the organic matter-rich shelf basin sediments, the highest bioturbation structure diversities occurred in the Northeast Channel and Fan regions with

low organic matter input and quality. Surface sediments in these regions appeared less bioturbated, which allowed the preservation of a comparatively large number of bioturbation structures.

It is, however, debatable whether the low bioturbation structure diversities of surface sediments in these regions ultimately result from intense bioturbation or dynamic depositional conditions through environmental change. In fact, sedimentary facies underlying surface sediments generally exhibited higher structure diversities than overlying facies. However, because overlying sedimentary facies did not show any preserved primary sedimentary structures the more likely explanation for the low bioturbation structure diversities in these samples is intense mixing through benthic organisms.

In addition to the organic matter input and quality, the skewness of grain size distributions, the percentages of silt and sand, and the sedimentation rate appear to influence the spatial distribution of bioturbation structures. In this context, the skewness serves as an indicator of the proportions of the different grain size populations as described by Cronan (1972), in which negatively or coarse skewed sediments reflect a dominance of the finer mode over the coarser mode, and vice versa. In the current study, bioturbation structure diversities are low in sediments with predominantly fine modal grain size populations and high silt percentages. The organic matter in surface sediments, therefore, seems to associate strongly with finer sediment modes such as fine silt, which is consistent with studies conducted in other marine benthic environments (e.g. Secrieru and Oaie, 2009).

3.4.2 Bioturbation structure diversity in relation to particle tracer sediment mixing intensity

In bioturbated sediments the activity of benthic organisms controls the intensity at which the sediment is mixed. Previous studies describe high sediment mixing rates and mixing layer depths in sediments that received high amounts of organic matter (e.g. Legeleux et al., 1994; Trauth and Sarnthein, 1997; Teal et al., 2008; also see Chapter 2), and it seems therefore likely that high bioturbation intensities and depths correlate with bioturbation structure characteristics that also indicate intense biological mixing activities.

In the current study, only bioturbation depths obtained from $^{210}Pb_{xs}$ and $^{228}Th_{xs}$ sedimentary profiles relate to organic matter and substrate distributions across the study region. These roughly follow the same dependency patterns as the bioturbation structure diversity, however, only the $^{228}Th_{xs}$ derived bioturbation depth eventually correlated with bioturbation structure diversities. Because no correlations existed between the bioturbation depths derived from the other applied particle tracers ($^{210}Pb_{xs}$ and $^{234}Th_{xs}$), the interpretation of this relationship remains tentative. The lack of strong relationships between bioturbation intensities and bioturbation structure diversity may result from the fact that the mixed layer, as derived from radioisotope profiles (e.g. Fig. 3.8), predominantly captures tier one of the bioturbation structure assemblages (the sediment surface layer where organisms' abundance and biomass are highest, Wetzel, 2010). This neglects to account for deeper bioturbation activities that may contribute to the sediment mixing intensity in surface layers. Furthermore, bioturbation rates calculated using particle tracers with relatively long half-lives such as $^{210}Pb_{xs}$ represent mixing rates averaged over a longer period of time, with the time scale of a tracer approximately 5

times its half-life (see Chapter 2 and references therein). Consequently, not all bioturbation structures that contributed to the calculated sediment mixing rates were preserved or even visible in X-radiographs. This may have biased the interpretation towards the most recent structures.

3.4.3 Influence of organic matter input and quality on bioturbation structure extents and tracemaker behavior

Other than intensively mixed surface sediments, the low bioturbation structure diversities in organic-matter rich sediments (high food abundance) may be the result of missing specialized feeding behaviors of benthic organisms to search and access limited food sources, compared to very specialized feeding type traces in low organic matter sediments (low food abundance) such as in deep-sea regions. This argumentation is consistent with findings in Wetzel (1991) where deep-sea sediments with high organic carbon contents were dominated by biodeformational structures which lack any behavioral specialization. Wetzel (1991) further stated that sediments with low organic carbon concentration do not provide enough food for benthic organisms, generally resulting in a decreased bioturbated zone and vertical extension of tiers. This supports the presence of commonly small vertical extensions of bioturbation structure types in studied regions with low concentrations of chlorophyll-a and low organic matter qualities. Tiering refers to the vertical partitioning of the sediment and the endobenthic community (Bromley, 1996). In the current study, the cross-cutting relationships of open bioturbation structures in the majority of sediment cores indicated that sediments are tiered, and the average vertical extensions of bioturbation structures were used as an approximate

measure of tiering extensions. Greater vertical extensions of bioturbation structures were mainly linked to shelf basin sediments with high organic matter input and quality. In these environments the great extensions of bioturbation structures may have caused tiers to overlap and the vertical partitioning of those tiers is therefore less 'strict'. This indicates that food was abundant and easily accessible. Compared to basin sediments, the more stringent vertical partitioning of the sediment in low organic matter regions indicated that benthic organisms may have 'avoided' other organisms' niches and the resulting competition for food by acquiring unique feeding mechanisms. In this context, the vertical distribution of structures represented deposit feeding (bioturbation structure group G and J), as well as a combination of dwelling and deposit feeding (bioturbation structure group B) linked to noticeable increases in chlorophyll-a concentrations with depth in cores collected in the Northeast Channel and fan regions. This tracer-depth distribution may indicate food-caching, a unique feeding technique where organisms cache labile organic matter at depth to cope with episodic food inputs in otherwise low organic matter environments such as the deep sea (Wheatcroft et al., 1994). *Zoophycos*-like bioturbation structures (group J, in the current study) have previously been linked to food caching behavior (Wetzel et al., 2011) supporting the interpretation above.

3.4.4 Response of bioturbation structure diameters to patterns of organic matter quality and sedimentation rate

In the current study, bioturbation structure diameters responded somewhat to the distribution of organic matter quality. Burrow sizes may be attributed to the body size of an organism or individual body parts (Frey and Pemberton, 1985). With a significance level of ≤0.1 these relationships were marginal but nonetheless indicated a trend of

larger diameters, and therefore, larger body sizes associated with high quality organic matter, e.g. labile compounds such as chlorophyll-a that are more easily processed by benthic animals. Furthermore, organisms with larger body sizes can potentially move greater volumes of sediment, which supports the presence of intensely mixed surface layers in these sediments. In addition to organic matter quality, the bioturbation structure diameters responded to variations in sedimentation rate across the study region. Herein, the sedimentation rate exhibited a size-limiting factor in which smaller bioturbation structure diameters, and therefore potentially smaller organisms, were associated with slightly higher sedimentation rates. Variations in the calculated sedimentation rates, however, were very small and mostly lack strong environmental patterns compared to organic matter and substrate characteristics. Therefore, the interpretation of this relationship remains uncertain.

3.5 Summary

Sediment samples collected in the Gulf of Maine and Scotian Shelf, Slope, and Rise regions were categorized based on distributional patterns of the quality and quantity of the deposited organic matter, the percentages of silt and sand, and the proportions of dominant and subordinate sediment modes. In particular, sediment cores collected in the greater water depths of the Northeast Channel and Fan, with low inputs and low qualities of organic matter and relatively high percentages of sand, could be clearly distinguished from cores collected in shelf basins, except for Roseway Basin sediments that exhibited a broad range of environments.

The amount of fresh organic matter and the proportions of substrate modes strongly influenced the diversity of bioturbation structures and the vertical extensions of these

structures throughout the study region. Basin sediments, where abundant food, in particular phytodetritus, and fine silt or clay modes dominated, had sediment surfaces that are highly biomottled resulting in relatively low bioturbation structure diversities. These samples further exhibited comparatively wide vertical extents of bioturbation structure groups, which can be explained by a less 'strict' partitioning of tiers and a weak competition for food. Consequently, burrow diameters observed in sediment cores were instead controlled by sedimentation rates and were largely independent of organic matter abundances and qualities.

In general, bioturbation structure characteristics were unrelated to bioturbation intensity and depth computed from particle tracer distributions in sediments, except for mixing depths calculated based on $^{228}Th_{xs}$ profiles. However, because mixing depth and bioturbation structure diversity responded to similar distributional patterns of organic matter and substrate characteristics, both represented potential indicators for bioturbation intensity in the current study.

3.6 References

Aller, R.C. (1982). The effects of macrobenthos on chemical properties of marine sediment and overlying water. In: McCall, P.L., Tevesz, M.J.S. (Eds.). Animal-sediment relations -The biogenic alteration of sediments. Plenum Press, New York, 53-102.

Aller, R.C. (1994). Bioturbation and remineralization of sedimentary organic matter: Effects of redoxoscillation. Chemical Geology 114, 331-345.

Aller, R.C. and Aller, J.Y. (1998). The effect of biogenic irrigation intensity and solute exchange on diagenetic reaction rates in marine sediments. Journal of Marine Research 56, 905-936.

Avnimelech, Y., Ritvo, G., Meijer, L.E., Kochba, M. (2001). Water content, organic carbon and dry bulk density in flooded sediments. Aquacultural Engineering 25, 25-33.

Bennett, R.H. and Lambert. D.N. (1971). Rapid and reliable technique for determining unit weight and porosity of deep-sea sediments. Marine Geology 11, 201-207.

Bentley, S.J. and Nittrouer, C.A. (2003). Emplacement, modification, and preservation of event strata on a flood-dominated continental shelf: Eel shelf, Northern California. Continental Shelf Research 23, 1465-1493.

Bentley, S.J., Sheremet, A., Jaeger, J.M. (2006). Event sedimentation, bioturbation, and preserved sedimentary fabric: Field and model comparisons in three contrasting marine settings. Continental Shelf research 26, 2108-2124.

Bentley, S.J. and Nittrouer, C.A. (2012). Accumulation and intense bioturbation of bioclastic muds along a carbonate-platform margin: Dry Tortugas, Florida. Marine Geology 315-318, 44-57.

Berner, R.A. (1980). Early diagenesis – A theoretical approach. Princeton University Press.

Boudreau, B.P. (1986). Mathematics of tracer mixing in sediments: I. Spatially-dependent, diffusive mixing. American Journal of Science 286, 161-198.

Bouma, A.H. (1964). Notes on Xray interpretation of marine sediments. Marine Geology 2, 278-309.

Bromley, R.G. (1996). Trace Fossils: Biology, Taphonomy and Application. Second Edition. Chapman and Hall, London. 361 pp.

Calvert, S.E. and Veevers, J.J. (1962). Minor structures of unconsolidated marine sediments revealed by X-radiography. Sedimentology 1, 296-301.

Cochran, J.K. (1985). Particle mixing rates in sediments of the eastern equatorial Pacific: Evidence from ^{210}Pb, $^{239,240}Pu$ and ^{137}Cs distributions at MANOP sites. Geochimica et Cosmochimica Acta 49, 1195-1210.

Cronan, D.S. (1972). Skewness and kurtosis in polymodal sediments from the Irish Sea. Journal of Sedimentary Petrology 42, 102-106.

Folk, R.L. and Ward, W.C. (1957). Brazos river bar: A study in the significance of grain size parameters. Journal of Sedimentary Petrology 27, 3-26.

Frey, R.W. and Howard, J.D. (1972). Radiographic study of sedimentary structures made by beach and offshore animals in aquaria, Giorgia Coastal Region, Sapelo Island, U.S.A. Sedimentology and Biology, Vl. Senckenbergiana Maritima 4, 169-182.

Frey, R.W. and Pemberton, S.G. (1985). Biogenic structures in outcrops and cores. 1. Approaches to ichnology. Bulletin of Canadian Petroleum Geology 33, 72-115.

Gingras, M.K., MacEachern, J.A. and Dashtgard, S.E. (2011). Process ichnology and the elucidation of physic-chemical stress. Sedimentary Geology 237, 115-134.

Goldberg, E.D. and Koide, M. (1962). Geochronological studies of deep sea sediments by the ionium/thorium method. Geochimica et Cosmochimica Acta 26, 417-450.

Guinasso, N.L and Schink, D.R. (1975). Quantitative estimates of biological mixing rates in abyssal sediments. Journal of Geophysical Research-Oceans and Atmosphere 80, 3032-3043.

Howard, J.D. (1968). X-ray radiography for examanination of burrowing in sediments by marine invertebrate organisms. Sedimentology 11, 249-258.

Howard, J.D. and Frey, R.W. (1973). Characteristic physical and biogenic sedimentary structures in Georgia estuaries. The American Association of Petroleum Geologists Bulletin 57, 1169-1184.

Howard, J.D. and Frey, R.W. (1975). Regional animal-sediment characteristics of Georgia estuaries. Senckenbergiana Maritima 7, 33-103.

Husson, F., Josse, J., Le, S., Mazet, J. (2013). FactoMineR: Multivariate Exploratory Data Analysis and Data Mining with R. R package version 1.25. http://CRAN.R-project.org/package=FactoMineR.

Kristensen, E. and Kostka, J.E. (2005). Macrofaunal burrows and irrigation in marine sediment: Microbiological and biogeochemical interactions. In: Kristensen, E., Kostka, J.E., Haese, R. (Eds.). Interactions between macro- and microorganisms in marine sediments. American Geophysical Union, Washington, DC, 390 pp.

Legeleux, F., Reyss, J.-L., Schmidt, S. (1994). Particle mixing rates in sediments of the northeast tropical Atlantic: Evidence from 210Pbxs, 137Cs, 228Thxs and 234Thxs downcore distributions. Earth and Planetary Science Letters 128, 545-562.

Lehman, W.M. (1939). Neue Beobachtungen an Versteinerungen aus dem Hunsrück-Schiefer. Akademie der Wissenschaften zu Berlin (Preussen), Abbandl. 13, 17 pp.

Mayer, M.S., Schaffner, L., Kemp, W.M. (1995). Nitrification potentials of benthic macrofaunal tube and burrow walls: effects of sediment NH4+ and animal irrigation behaviour. Marine Ecology Progress Series 212, 157-169.

Meadows, P.S., Tait, J. and Hussain, S.A. (1990). Effects of estuarine infauna on sediment stability and particle sedimentation. Hydrobiologia 190, 263-266.

Mullins, H.T., Gardulski, A.F., Hine, A.C., Melillo, A.J., Wise, S.W., Applegate, J. (1988). Three-dimensional sedimentary framework of the carbonate ramp slope of central west Florida: A sequential seismic stratigraphic perspective. Geological Society of America Bulletin 100, 514-533.

Needham, S.J., Worden, R.H., McIlroy, D. (2004). Animal-sediment interactions: The effect of ingestion and excretion by worms on mineralogy. Biogeosciences 1, 113-121.

Ramey, P.A. and Snelgrove, P.V.R. (2003). Spatial patterns in sedimentary macrofaunal communities on the south coast of Newfoundland in relation to surface oceanography and sediment characteristics. Marine Ecology Progress Series 262, 215-227.

Reineck, H.E., Gutmann, W.F., Hertweck, G. (1968). Das Schlickgebiet südlich Helgoland als Beispiel rezenter Schelfablagerungen. Senckenbergiana Lethaea 48, 219-275.

Reineck, H.E., Dörjes, J., Gadow, S., Hertweck, G. (1968). Sedimentologie, Fauenzonierung und Faziesabfolge vor der Ostküste der inneren Deutschen Bucht. Senckenbergiana Lethea 49, 261-309.

Rhoads, D.C. and Boyer, L.F. (1982). The effects of marine benthos on physical properties of sediments-A successional perspective. In: McCall, P.L., Tevesz, M.J.S. (Eds.). Animal-sediment relations -The biogenic alteration of sediments. Plenum Press, New York, 3-52.

Riaux-Gobin, C. and Klein, B. (1993). Microphytobenthic biomass measurements using HPLC and conventional pigment analysis. In: Kemp, P.F., Cole, J.J., Sherr, B.F.,

Sherr, E.B. (Eds.). Handbook of methods in aquatic microbial ecology. Lewis Publishers, pp. 369-376.

Rosenberg, R. (2001). Marine benthic faunal successional stages and related sedimentary activity. Scientia Marina 65, 107-119.

Secrieru, D. and Oaie, G. (2009). The relation between the grain size composition of the sediments from the NW Black Sea and their total organic carbon (TOC) content. Geo-eco-marina 15, 5-11.

Schäfer, W. (1956). Wirkungen der Benthos-Organismen auf den jungen Schichtverband. Senckenbergiana Lethea 37, 183-263.

Schneider, C.A., Rasband, W.S., Eliceiri, K.W (2012). "NIH Image to ImageJ: 25 years of image analysis". Nature Methods 9, 671-675.

Sun, M.Y., Aller, R.C., Lee, C. and Wakeham, S.G. (2002). Effects of oxygen and redox oscillation on degradation of of cell-associated lipids in surficial marine sediments. Geochimica et Cosmochimica Acta 66, 2003-2012.

Teal, L.R., Bulling, M.T., Parker, E.R., Solan, M. (2008). Global patterns of bioturbation intensity and mixed depth of marine soft sediments. Aquatic Biology 2, 207-218.

Trauth, M.H. and Sarnthein, M. (1997). Bioturbational mixing depth and carbon flux at the seafloor. Paleoceanography 12, 517-526.

Uchupi, E. and Bolmer, S.T. (2008). Geologic evolution of the Gulf of Maine region. Earth-Science Reviews 91, 27-76.

Wetzel, A. (1991). Ecologic interpretation of deep-sea trace fossil communities. Palaeogeography, Palaeoclimatology, Palaeoecology 85, 47-69.

Wetzel, A. (2010). Deep-Sea ichnology: Observations in modern sediments to interpret fossil counterparts. Acta Geologica Polonica 60, 125-138.

Wetzel, A., Tjallingii, R., Wiesner, M.G. (2011). Bioturbational structures record environmental changes in the upwelling area off Vietnam (South China Sea) for the last 150,000 years. Palaeogeography, Palaeoclimatology, Palaeoecology 311, 256-267.

Wheatcroft, R.A., Olmez, I., Pink, F.X. (1994). Particle bioturbation in Massachusetts Bay: Preliminary results using a new deliberate tracer technique. Journal of Marine Research 52, 1129-1150.

Widdicombe, S. and Austen, M.C. (1999). Mesocosm investigation into the effects of bioturbation on the diversity and structure of a subtidal macrobenthic community. Marine Ecology Progress Series 189, 181-193.

CHAPTER 4 – Bioturbation in Arctic and Subarctic Canadian Fjords: Gibbs Fjord, Nunavut, and Nachvak, Saglek, Okak, and Anaktalak Fjords, Nunatsiavut

Lina M. Stolze[1]* and Samuel J. Bentley, Sr.[2]

*Corresponding author: Email: lmstolze@mun.ca

[1]Department of Earth Sciences, Memorial University of Newfoundland, St John's, Canada NL A1B 3X5

[2]Samuel J. Bentley, Sr., Department of Geology and Geophysics, Louisiana State University, Baton Rouge, Louisiana, USA 70803

In preparation for submission to: Canadian Journal of Earth Sciences.

Abstract

Fjords are morphologically, oceanographically and ecologically highly complex systems, and a wide range of environmental stresses (e.g. sedimentation rate, ice-rafted debris deposition, substrate consolidation, oxygen content, water turbidity, storm activity, and freshwater discharge) strongly influence the benthic biota. Few studies have investigated animal-sediment interactions in fjord environments, especially in modern Arctic and subarctic regions. The current study provides the first data of environmental influences on bioturbation in these environments. Sediment samples were collected at inner and outer locations of one Arctic (Gibbs Fjord, Baffin Island, Nunavut) and four subarctic fjords (Nachvak, Saglek, Okak, and Anaktalak Fjords, northern Labrador, Nunatsiavut) using a boxcorer on two ArcticNet/CHONe cruises in 2008 and 2009. Bioturbation rates were calculated from down-core depth distributions of excess ^{210}Pb and ^{228}Th, and bioturbation structures were described from X-radiographs of collected sediment cores. The organic matter concentration and quality as well as substrate conditions were described to characterize benthic conditions at each fjord location. Particle tracer distributions of fjord surface sediments indicated long-term diffusional mixing and short-term, potentially seasonal, non-local mixing processes. Outer fjord sediments received higher inputs of high quality organic matter, and appeared less influenced by varying depositional processes than inner fjord locations. Bioturbation structure diameters were relatively small and the sediment mixing depth was greater at inner fjord locations. Comparatively high organic matter concentrations may have inhibited the benthic fauna, which resulted in shallow bioturbation and low bioturbation structure diversity at outer fjord locations.

Keywords: Organic matter, biodiffusion, non-local mixing, bioturbation structure, bioturbation depth

4.1 Introduction

Fjords represent important habitats in high latitude coastal regions because of their oceanographic and morphologic complexity and estuarine ecological conditions (Syvitski et al., 1987). Modern fjords are long, narrow, deep, and steep-sided valleys often containing submarine sills, which causes poorly coupled ocean circulation and strong vertical hydrographic gradients in water properties. Further, the limited deep-water circulation in silled fjords may result in low currents, reduced oxygen, and low bioturbation activity (Bentley and Kahlmeyer, 2012).

In fjords, environmental stresses such as the sedimentation rate, ice-rafted debris deposition, substrate consolidation, oxygen content, water turbidity, storm activity, and freshwater discharge through seasonal glacial melting and increased precipitation and river runoff during summer, can all strongly affect the distribution of benthic biota (Buatois and Mángano, 2011). In many fjords, the oxygenated surface zone of sediments may be shallow as a result of a combination of high concentrations of organic matter and low physical and biological disturbances, limiting the niches available to the benthic infauna. However, this condition commonly occurs in temperate geographical regions whereas in high-latitude fjord basins, and especially in glacial fjords, the benthic fauna is carbon deprived (Syvitski et al., 1987). Carbon deposition in high latitude fjord sediments usually follows a seasonal pattern with spring to summer peaks of phytogenous detritus and riverine organic matter (Syvitski et al., 1987).

To date, only few studies have addressed animal-sediment interactions in fjord sediments and information is fragmentary, particularly in Arctic and subarctic fjords of Eastern Canada. This study provides the first data on relationships between bioturbation processes and environmental patterns that characterize benthic habitats in modern

Arctic and subarctic benthic fjord environments in Gibbs Fjord (Baffin Island, Nunavut) and Nachvak, Saglek, Okak, and Anaktalak Fjords (northern Labrador, Nunatsiavut) in Eastern Canada. The specific objectives of this study were 1) to determine bioturbation intensities and depths, as well as bioturbation structure characteristics revealed by X-radiography of sediment cores and 2) to evaluate bioturbation proxy-environmental relationships, particularly in terms of along-fjord, as well as latitudinal environmental variations.

4.2 Methods

4.2.1 Regional settings and sediment collection

For this study one Arctic and four subarctic fjords, namely Gibbs, Saglek, Nachvak, Okak and Anaktalak Fjords, were sampled during the collaborative ArcticNet (ArcticNet, 2015) and Canadian Healthy Oceans Network (Snelgrove et al., 2012) expedition on board the icebreaker *CCGS Amundsen* in September 2008 (leg 11a) and October 2009 (leg 4b) (Fig. 4.1). All of these fjords typify Arctic and/or subarctic fjords where sea ice strongly influences sedimentation, sediment transport, and sediment deposition at least semi-annually (Gilbert, 1983).

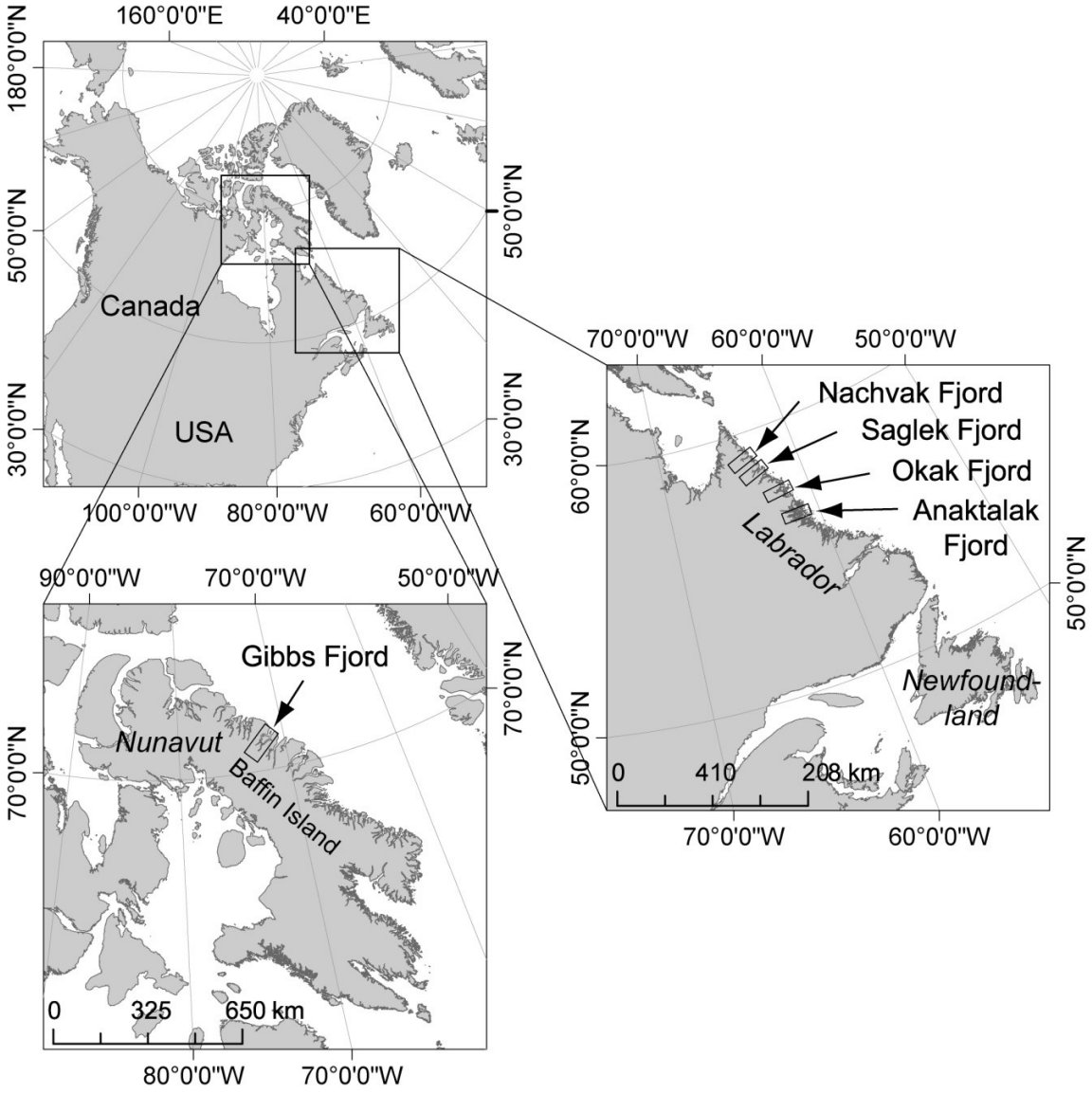

Figure 4.1: Regional settings of the fjords. Rectangles display arctic and subarctic locations, and the fjords: Gibbs Fjord (Baffin Island), and Nachvak, Saglek, Okak, and Anaktalak Fjords (Labrador).

Gibbs Fjord (GF) is situated on the eastern coast of Baffin Island in Baffin Bay, and until now, its benthic environment has not been explored. However, several studies have investigated sediment dynamics and modern environmental processes in a series of fjords located along the east coast of Baffin Island, in particular during the Geological

Survey of Canada's SAFE project (Sedimentology of Arctic Fjords Experiment) initiated in 1981 (Syvitski and Blakeney, 1983; Syvitski and Schafer, 1985). In general, benthic environments of the Baffin Island fjords are highly variable. They receive high rates of episodic sedimentation, most commonly from iceberg meltout and debris flows, sedimentation from fluvial discharge plumes, and turbidity currents (Hein and Syvitski, 1989). Fjords of Baffin Island are deep, high-energy environments with year-round well oxygenated water columns. Sea ice is present throughout most of the year with an average open water season of three months (Syvitski et al., 1990). Clark Fjord, one of the fjords studied during the SAFE project, is situated north of Gibbs Fjord and connected through an approximately 9 km long sidearm. Clark Fjord is multi-silled and free of sea ice for about 30 days per year (Syvitski and Schafer, 1985). Most of the sedimentation in these fjords occurs during the short fluvial discharge season in the summer months (Syvitski et al., 1987). The current study collected one sediment core at an inner location in Gibbs Fjord (GFII) and in a water depth of 452 m (Table 4.1 and Fig. 4.2).

Table 4.1: Sediment sampling locations, water depth, near seafloor salinity and temperature.

Fjord	Station	location	Year of collection	Latitude (DD)	Longitude (DD)	Depth (m)	Salinity (psu)[a]	Temperature (°C)[a]
Gibbs Fjord	GFII	inner	2008	70.7692	-72.2728	452	34	0.1
Nachvak Fjord	602	inner	2009	59.0542	-63.8697	151	33	-1.6
	600	outer	2009	59.0922	-63.4414	204	33	-1.8
Saglek Fjord	615	inner	2009	58.3281	-63.5450	138	32	-1.6
	617	outer	2009	57.5092	-62.6914	134	32	0.5
Okak Fjord	630	inner	2009	57.4753	-62.0583	50	32	1.0
	634	outer	2009	57.5714	-61.9458	101	33	-1.7
	633	outer	2009	57.6111	-61.9047	182	32	0.7
Anaktalak Fjord	624	inner	2009	56.4383	-61.9919	115	31	1.7

[a]Near bottom salinity and temperature data were provided by Y. Gratton and D. Boisvert (INRS-Eeau, terre et environment) and P. Guillot (Institut des Sciences de la mer de Rimouski (ISMER)).

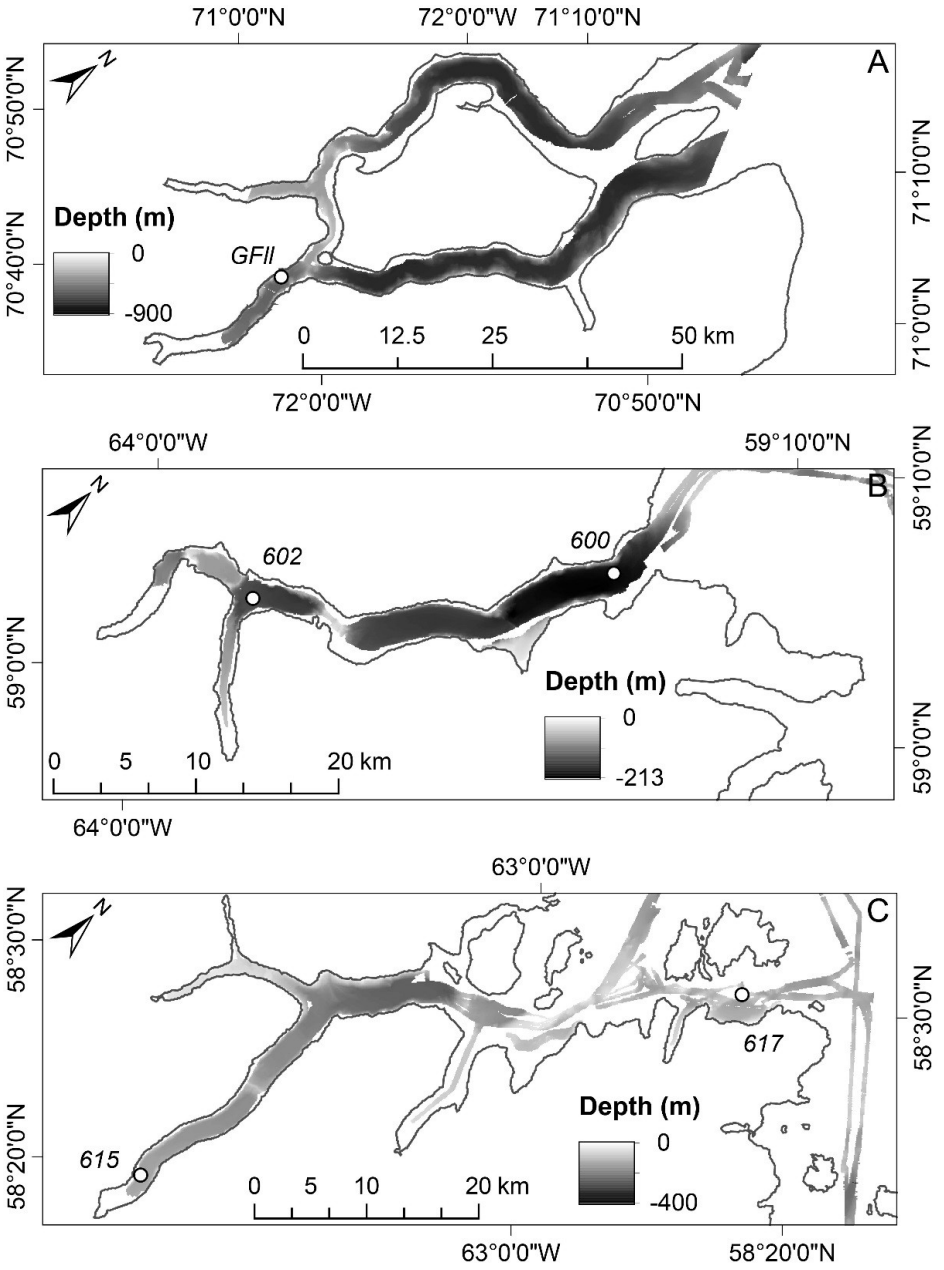

Figure 4.2: Location of sampling stations and bathymetries of A) Gibbs Fjord, B) Nachvak Fjord and C) Saglek Fjord. Bathymetry data were provided by the Ocean Mapping Group (OMG), 2003-2013 Multibeam Sonar Data collected from CCGS Amundsen and M/V Nuliajuk: Ocean Mapping Group, University of New Brunswick, Fredericton, New Brunswick, Canada. Shoreline data were retrieved from NOAA National Geophysical Data Center, GSHHG Coastline, September 19, 2014, http://www.ngdc.noaa.gov/mgg/shorelines/shorelines.html.

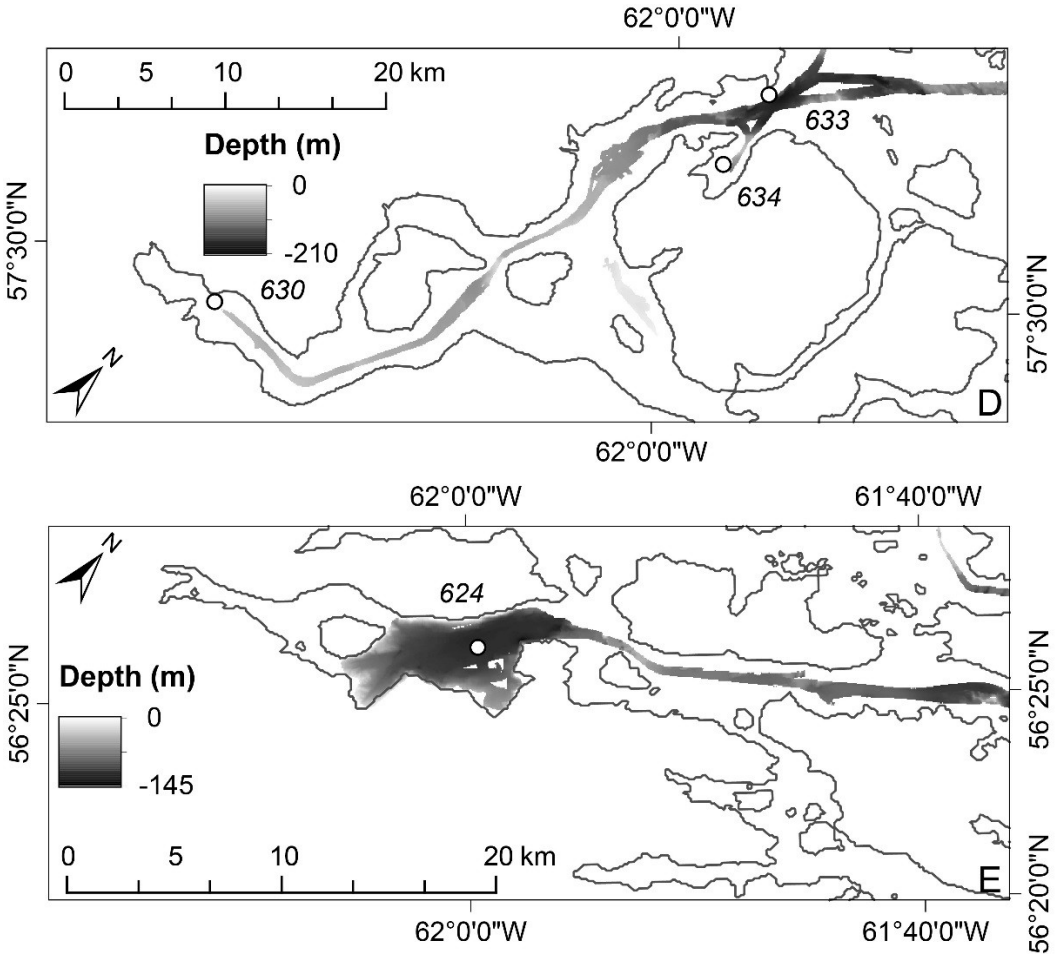

Figure 4.2 continued: Location of sampling stations and bathymetries of D) Okak Fjord and E) Anaktalak Fjord.

The Saglek (SF), Nachvak (NF), Okak (OF), and Anaktalak (AF) fjords are situated in Nunatsiavut (northern Labrador) in the Labrador Sea (Fig. 4.1) where the cold Labrador Current arrives from the north through Hudson Strait and Baffin Bay and significantly influences the coastal climate (Richerol et al., 2012). To the north, the fjords located in the Torngat Mountains are generally deeper than the southern Labrador fjords and glaciers may be present. Compared to the northern fjords, the fjords located further

south receive more precipitation (Syvitski et al., 1987). Whereas Saglek and Nachvak Fjord fall into the category of classic fjords with narrow inlets, tall and steep sidewalls and deep muddy basins separated by rock sills, Okak and Anaktalak Fjord, with their irregular shaped and shallow inlets, gently sloping sidewalls, and relatively large intertidal zones, are part of another category referred to as fjards (Brown et al., 2012; Carpenter, 2012). The land-fast sea ice, which covers the inner shelf and coastal embayments in spring and winter, and large numbers of icebergs, drifting southward along the shelf with the Labrador Current, are potential sources for ice-rafted debris deposited in fjords in Labrador (Bentley and Kahlmeyer, 2012). During the summer months snow and ice melt and increased river discharge stratify the water column and stabilize the pycnocline which is more pronounced in the northern fjords than in the southern fjords. In fall, the water column is generally non-stratified and homogenous. In general, the fjord waters are oxygen-rich and, therefore, water circulation presumably occurs at all depths (Richerol et al., 2012).

A total of 8 sediment cores were collected at inner and outer locations in the Labrador fjords and in water depths between 50 and 204 m (Fig. 4.2 and Table 4.1).

Nachvak, the northernmost subarctic fjord, is pristine and uninhabited and located in the Torngat Mountains National Park Reserve (Richerol et al., 2012). This multiple-silled fjord forms three main basins with water depths of about 180 m which receive most of their sediment load from river catchments such as the glaciated Ivitak Brook (Bentley and Kahlmeyer, 2012). In contrast, sediments in Saglek Fjord have been influenced by human activities and contaminated by polychlorinated biphenyl compounds (PCB) from a former military site (Brown et al., 2009). Saglek Fjord is a non-glacierized fjord that

receives most of its sediments from Nachvak Brook. Saglek Fjord consists of several basins separated by sills with water depths between 45 and 96 m (Richerol et al., 2012). Okak Fjord presently has no year-round settlements, although the historical record of human settlement (like the other Labrador fjords) spans thousands of years (Carpenter, 2012). Ikinet Brook and the North River are two main freshwater sources located close to the fjord head. A deep sill separates the fjord head from the central fjord, which consists of several relatively shallow basins and sills. The deepest regions of the fjord are found at its northern entrance, which is characterized by deep basins with an average depth of 200 m and sills with depths between 100 and 120 m (Richerol et al., 2012).

Anaktalak Fjord is the southernmost fjord in the current study. It is extensively used by the Inuit for harvesting and traveling, and since the establishment of the Vale's Voisey's Bay Ni-Cu mine between 1997 and 2002, its marine environment has received treated effluents from ongoing mining operations. Numerous islands of varying sizes block Anaktalak Fjord, which is characterized by a large basin of about 100-120 m depth forming the bay and an 85-m deep sill at the outer part of the bay (Richerol et al., 2012).

Sediment samples were collected with a 0.25 m^2 boxcorer. On board, boxcores were sub-sampled with PVC-core tubes (10 cm diameter) for geochemical analyses and with Plexiglas trays (57cm x 20cm x 2cm) for X-ray imaging. Plexiglas trays were sealed water-tight and PVC-cores were extruded and sliced into 1 cm and 2 cm intervals. Sediment samples for elemental (C_{org} and N_{total}), stable isotope ($\delta^{13}C$) and chlorophyll-a analyses were stored at -18 °C and kept frozen and in the dark until further analysis.

Sediment samples for granulometry and radioisotope analysis (^{228}Th, ^{210}Pb, and ^{137}Cs) were stored in watertight Whirl-PAK bags at 4 °C along with the Plexiglas trays.

4.2.2 Radiochemistry

For the analysis of the radioisotopes ^{210}Pb, ^{228}Th and ^{137}Cs, sample aliquots of 5-15 g dried and finely ground sediment were measured for 24 h using Canberra germanium detectors (models: GL-3825R and GR-1518). Prior to measurement, the sediment samples were kept in airtight containers for three weeks to allow the ingrowth of the ^{210}Pb grandparent ^{222}Rn and the ^{228}Th and ^{228}Ra daughter nuclides ^{224}Ra and ^{228}Ac, respectively.

Gamma-ray spectra were analyzed with the gamma acquisition and analysis software Genie 2000. The measured activities of radionuclides [dpm g^{-1}] were corrected for decay from sample collection to counting. Total activities of ^{210}Pb were measured by its gamma emission at 46.5 keV, and activities of supported ^{210}Pb were determined by analyzing ^{226}Ra via its daughter isotopes ^{214}Pb (295 keV and 352 keV) and ^{214}Bi (609 keV). ^{228}Th and ^{228}Ra activities were obtained by measuring the gamma emissions of their daughter isotopes ^{212}Pb (238.6 keV) and ^{208}Tl (583.1 keV), and ^{228}Ac (338.4 keV, 911.1 keV and 968.9 keV), respectively. Excess activities of ^{210}Pb and ^{228}Th were then calculated by subtracting the supported activities of ^{210}Pb from total activities of ^{210}Pb, and by subtracting the activities of total ^{228}Ra from total ^{228}Th activities. Activities of ^{137}Cs were determined directly by measuring its gamma emission at 661 keV.

4.2.3 Granulometry and X-radiography

Sediment subsamples were disaggregated in a $NaPO_3$ (0.05 %) solution and sonicated for 1 h using an ultrasonic bath. Sediment samples were left in the solution overnight before analysis with a HORIBA Partica LA-950 laser diffraction particle size analysis system. Relative percentages of clay (<3.9 µm), silt (3.9 - <62.5 µm) and sand (62.5 - <2000 µm), as well as the mean grain size, standard deviation (sorting), and skewness of grain size distributions within the upper 10 cm of the sediment (Folk and Ward, 1957) were calculated from the particle size distribution report.

Sediment porosity and water content of surface sediments were obtained using the wet-dry method after Bennett and Lambert (1971). Wet sediment samples were dried at 70 °C and sediment porosity was calculated using Eq. (1).

$$\phi = \frac{mw}{mw + \left(\frac{ms}{\rho s}\right)} \qquad (1)$$

where mw is the water weight [g], ms is the sediment dry weight [g], and ρs is the grain density which was assumed to be 2.65 g cm^{-3} (e.g. Avnimelech et al., 2001).

Sedimentary structures and burrow morphologies in sediment cores were analyzed by X-ray imaging of sediment slabs preserved in Plexiglas trays by using a Thales Flashscan 35 X-ray detector illuminated with an Acoma PX15HF X-ray generator. All images were stored as 14-bit TIFF data files and analyzed with ImageJ (Schneider et al., 2012). Burrow morphologies in X-radiographs were described with respect to burrow diameter (in cm), orientation and shape.

4.2.4 Chlorophyll-a, phaeopigments, total organic carbon, total nitrogen, and $\delta^{13}C$

Sample aliquots of ~1 g thawed, wet sediment of the upper 0-10 cm (1 cm divisions) of the sediment cores collected in 2009 were extracted with 10 ml of a 90 % acetone solution in high density polyethylene 15 ml centrifuge tubes. Samples were sonicated for 5 minutes using an ultrasonic bath and stored horizontally and overnight at -18 °C to ensure complete extraction. Acetone extracts were separated from sediments by centrifugation for 10 min at 3000 rpm. The fluorescence of extracts was measured with a Turner Design 10 Fluorometer before and after acidification with ~2 drops 5 % HCl. Chlorophyll-a and phaeopigment concentrations were calculated after Riaux-Gobin and Klein (1993) and expressed in µg g^{-1} dry sediment.

Chlorophyll-a data for sediments collected from station GFII (Gibbs Fjord) in 2008 were provided by H. Link and P. Archambault (ISMER-UQAR, Rimouski, CA).

Standard deviations (1 σ) of chlorophyll-a concentrations were calculated from triplicate measurements of ~13 % of the sediment samples collected in 2009 and of all samples that were provided by H. Link and P. Archambault. Triplicate measurements of the samples collected in 2009 were done on sample aliquots, whereas triplicate measurements of samples collected in Gibbs Fjord in 2008 (H. Link and P. Archambault), were done on three individual samples taken from the same location. Therefore, for samples collected in 2009 represent an assessment of measurement error, and standard deviations for samples from H. Link and P. Archambault represent a measure of environmental variability.

For the analysis of organic carbon (C_{org}), total nitrogen (N_{total}) and stable carbon isotope signatures $\delta^{13}C$, thawed wet sediment samples (~1-2 mg) were transferred to high density polyethylene 45 ml centrifuge tubes, acidified overnight with 5M HCl, washed,

centrifuged, and then dried at 40 °C. Dried sediments were finely powdered with mortar and pestle and stored in glass vials until analysis.

Organic carbon (C_{org}) and total nitrogen (N_{total}) were measured with a Carlo Erba NA1500 Series II Elemental Analyser, and stable carbon isotope signatures $\delta^{13}C$ were measured by interfacing the elemental analyser through a Confloll interface with a ThermoElectron DeltaVPlus Gas Source Isotope Ratio Mass Spectrometer. The data were normalized using the standards IAEA-N-1, IAEA-N-2, IAEA-CH-6, B2153 (low organic content soil standards), and two Memorial University laboratory standards (MUN-CO-2 ($CaCO_3$) and MUN Sulfanilamide). The average precision on these reference materials was ± 0.18 ‰ for $\delta^{13}C$, ± 1.40 wt.% for C_{org} and ± 1.51 wt.% for N_{total}. The isotopic ratios were reported in ‰ relative to VPDB and elemental data of C_{org} and N_{total} are reported in wt.%. Standard deviations (1 σ) of C_{org}, N_{total} and $\delta^{13}C$ values of sediment samples were calculated from duplicate measurements of sample aliquots of ~5 % of all samples analyzed.

4.3 Results

4.3.1 Bioturbation rates and depths, and particle tracer profiles

Chlorophyll-a concentration profiles

Chlorophyll-a concentrations from most stations generally decreased with depth, except for samples collected at stations 600 and 630 that showed no clear trend (Fig. 4.3). Although most cores showed a distinct decrease in surface concentrations of chlorophyll-a, a few cores (615, 633 and 634) exhibited chlorophyll-a profiles with nearly

constant concentrations in sediment surface zones (0-2 cm). Chlorophyll-a concentration peaks in surface zones occurred only in two cores collected from stations 617 and 630. Subsurface peaks or increases of chlorophyll-a concentrations were more abundant and occurred in sediments from all stations, except for station 634 in Okak Fjord.

$^{210}Pb_{xs}$ activity profiles and bioturbation depths

Except for station GFII in Gibbs Fjord, all $^{210}Pb_{xs}$ activity-depth profiles followed a general decreasing trend (Fig. 4.3). Most profiles, except for station 634, exhibited inflection points above which activities decreased with depth (e.g. 615) or were nearly constant (e.g. 617). Surface sediment $^{210}Pb_{xs}$ profiles at station 634 slightly increased up to 1.5 cm depth. The sediment segment above the inflection points is assumed to be influenced primarily by the mixing activities of benthic organisms and bioturbation depths (L_b) ranged from 1.5 cm at station 634 in Okak Fjord to 31 cm at station 600 in Nachvak Fjord (Table 4.2). Below the inflection points, the $^{210}Pb_{xs}$ activities in most cores decreased with depth nearly exponentially. Although generally decreasing, $^{210}Pb_{xs}$ activities at station 617 exhibited a subsurface activity peak at 19 cm. At station 600, activities below the inflection point and the surface sediment layer were nearly constant to a depth of 31 cm before decreasing again between 31 and 39 cm. $^{210}Pb_{xs}$ activity depth distributions at station GFII in Gibbs Fjord followed a different trend exhibiting a zone of reduced activities below the surface zone and between 4.5 and 10.5 cm. Below this zone activities decreased nearly exponentially to a depth of 21.5 cm.

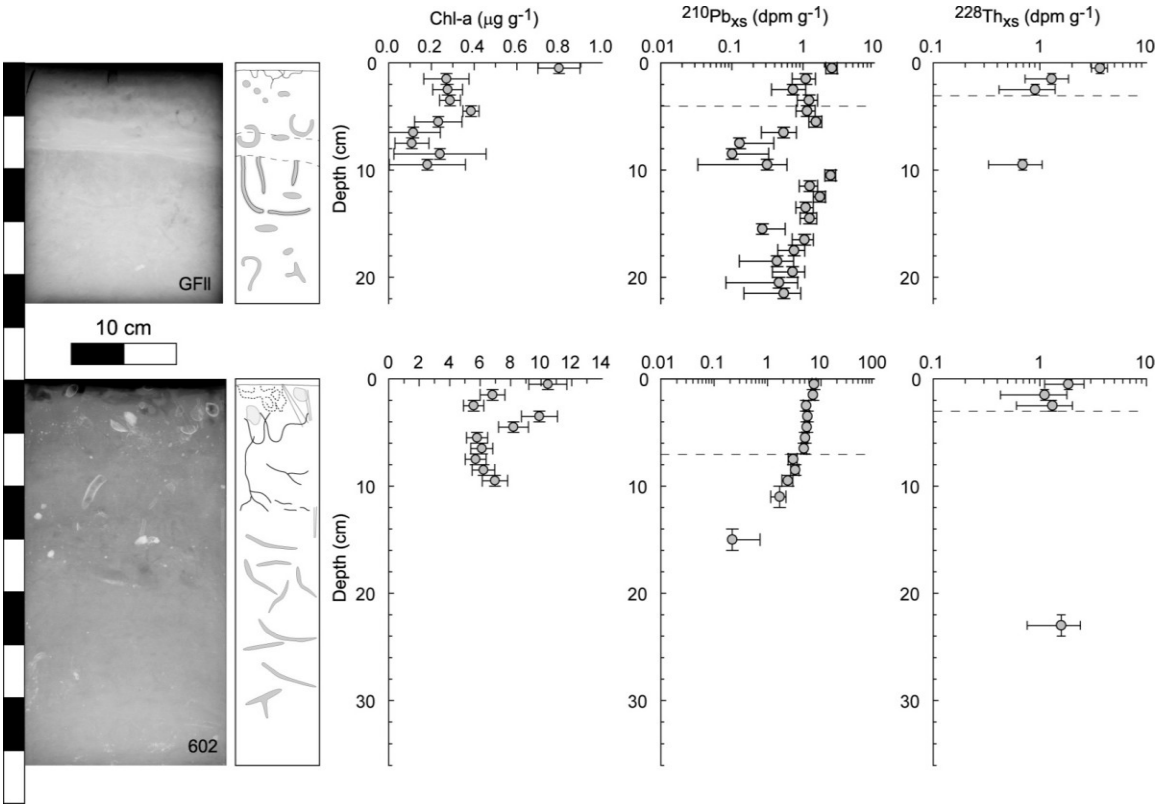

Figure 4.3: X-radiograph negatives from boxcores (lighter greys represent higher and darker greys lower bulk densities), schematic representations of bioturbation structure distributions within cores, and chlorophyll-a concentration, $^{210}Pb_{xs}$ and $^{228}Th_{xs}$ activity profiles found in surface sediments of collected cores. Vertical error bars represent the width of analyzed core segments in centimeters. Horizontal error bars of chlorophyll-a concentrations are averages of standard deviations calculated from replicate measurements. Horizontal error bars of $^{210}Pb_{xs}$ and $^{228}Th_{xs}$ activities are calculated from gamma acquisition net peak area uncertainties. Dashed lines indicate bioturbation depths L_b in $^{210}Pb_{xs}$ profiles and z_p in $^{228}Th_{xs}$ profiles. Sites GFII: inner Gibbs Fjord and 602: inner Nachvak Fjord.

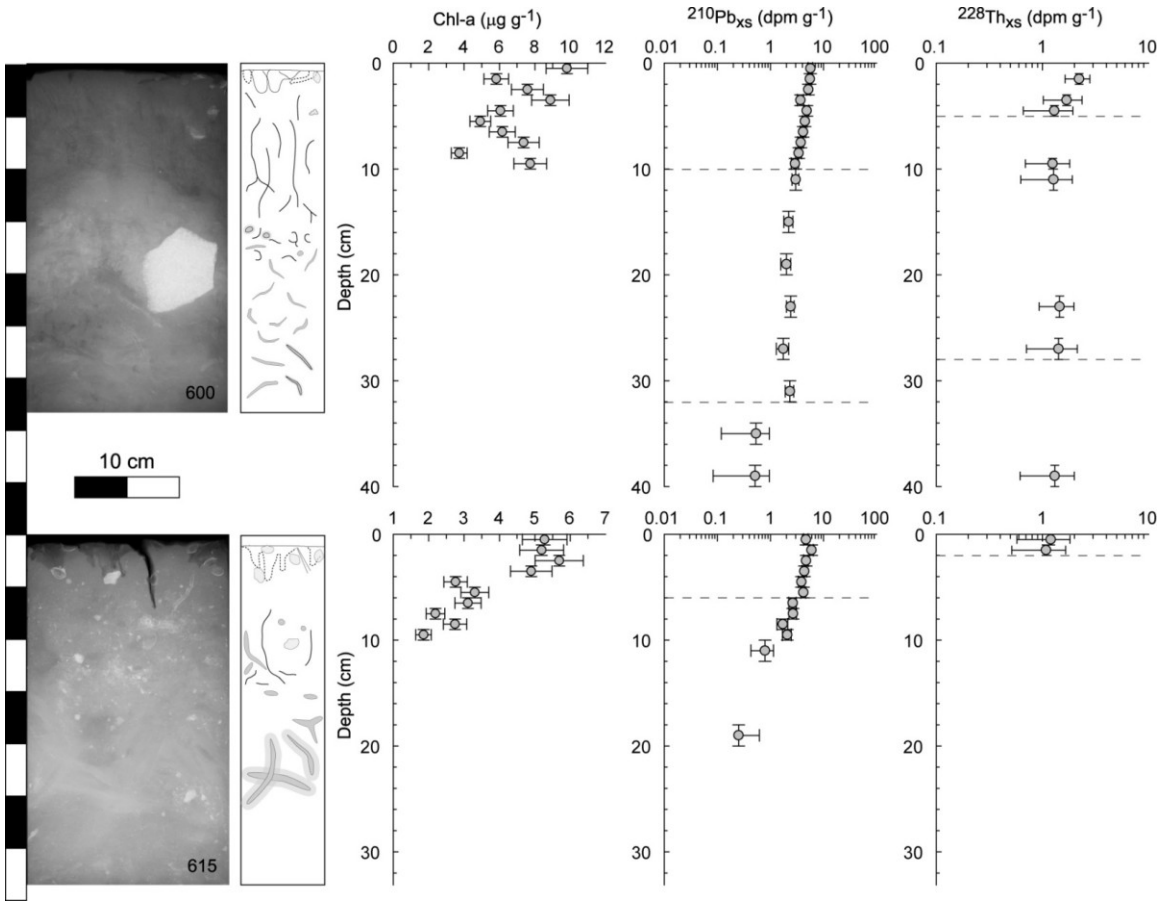

Figure 4.3 continued. Sites 600: outer Nachvak Fjord and 615: inner Saglek Fjord.

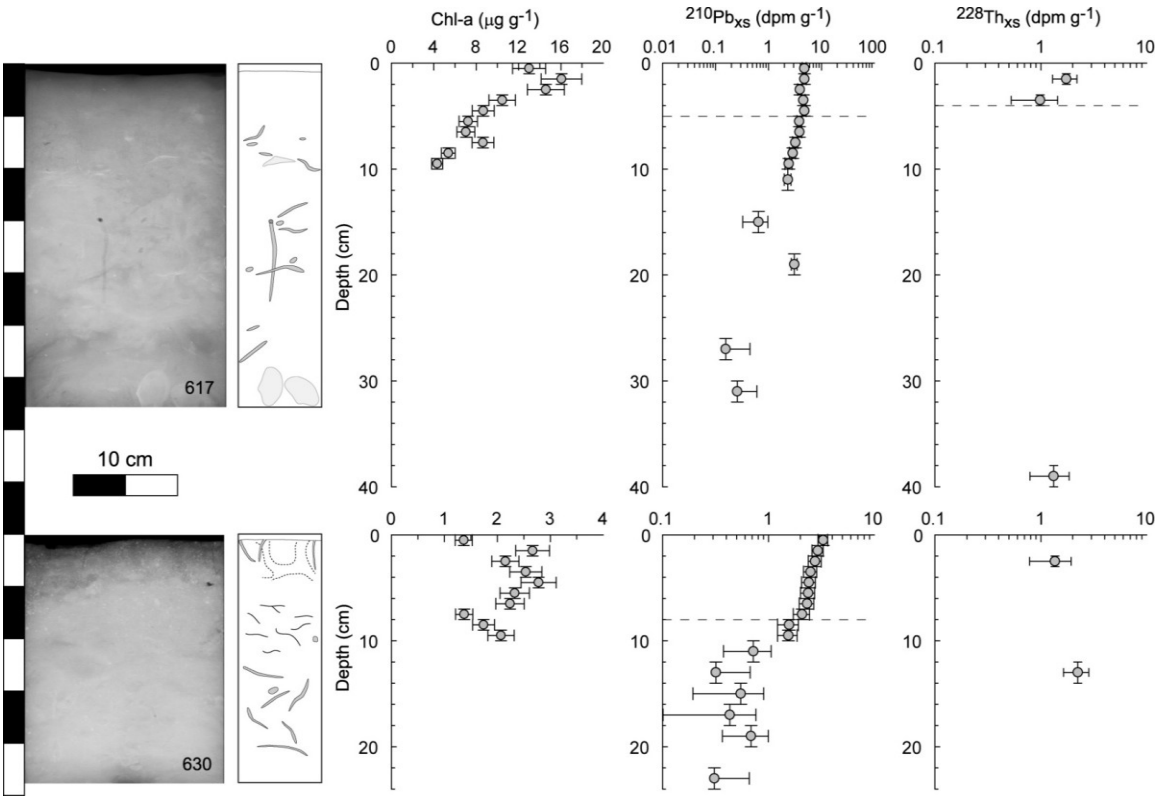

Figure 4.3 continued. Sites 617: outer Saglek Fjord and 630: inner Okak Fjord.

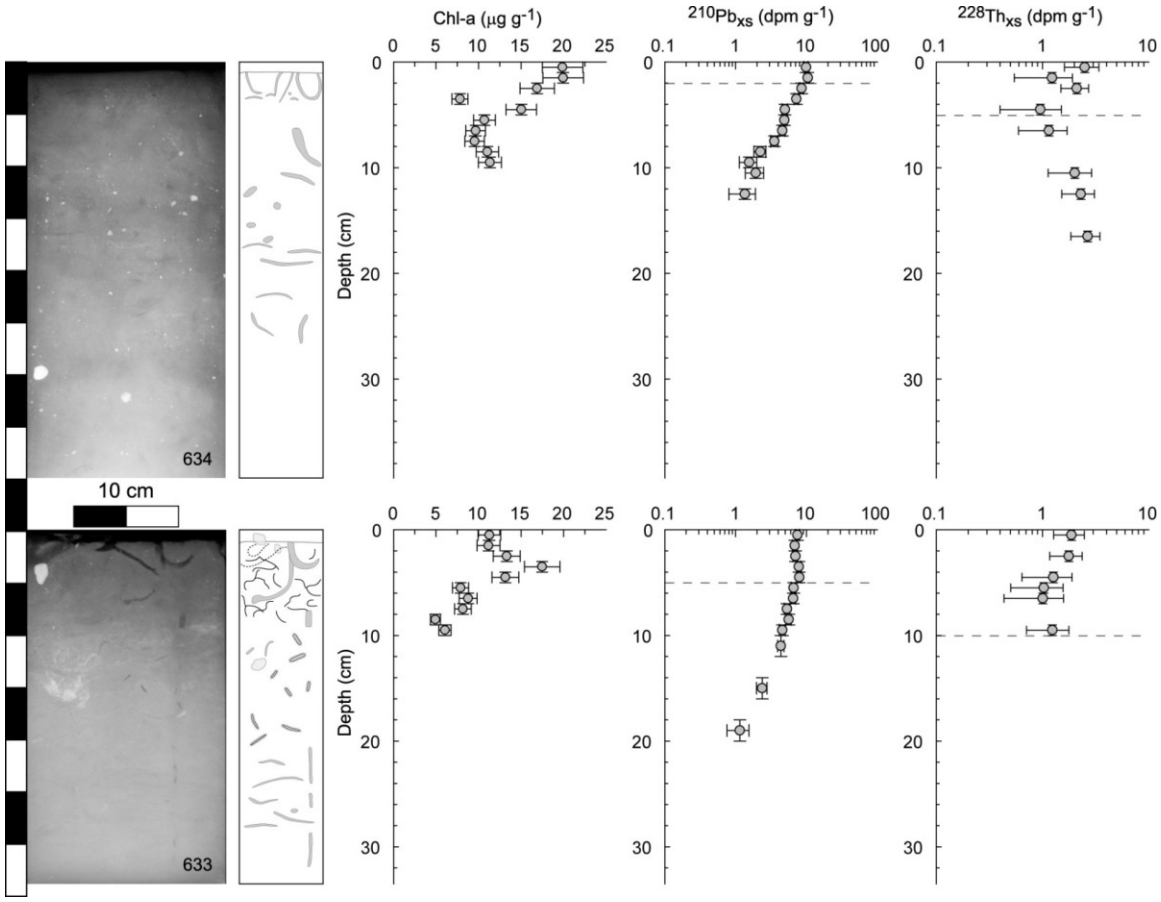

Figure 4.3 continued. Sites 634: outer Okak Fjord and 633: outer Okak Fjord.

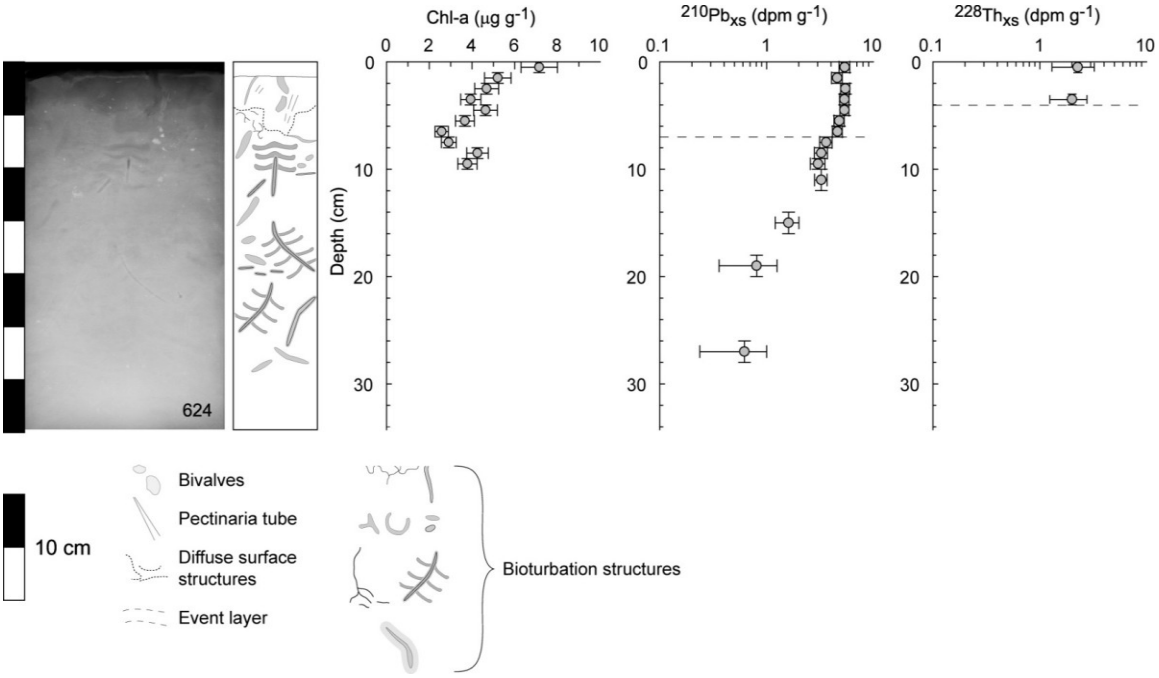

Figure 4.3 continued. Site 624: inner Anaktalak Fjord.

Table 4.2: Biodiffusion coefficients (D_b), sediment mixing depths (L_b), excess activity penetration depths (z_p) and sedimentation rates (ω) as calculated from $^{210}Pb_{xs}$, $^{228}Th_{xs}$ and ^{137}Cs activity profiles.

		$^{210}Pb_{xs}$			$^{228}Th_{xs}$		^{137}Cs
Fjord	**Station**	**L_b (cm)**	**D_b (cm^2 y^{-1})[a]**	**ω (cm y^{-1})**	**z_p (cm)[b]**	**D_b (cm^2 y^{-1})[a]**	**ω (cm y-1)**
Gibbs Fjord	GFII	3.50	0.16 ± 0.16	0.26 ± 0.08	9.50 2.50	0.48 ± 0.21	0.30
Nachvak	602	6.50	5.46 ± 2.26	0.14 ± 0.04	23.00 2.50	* 8.01 ± 14.01	0.30
	600	L_{b1} 9.50	7.66 ± 2.74	0.11 ± 0.04	39.00 4.50	13.31 ± 4.62	0.39
		L_{b2} 31.00	* 139.97 ± 192.02		39.00	NA ± NA	
Saglek	615	5.50	* 10.40 ± 12.07	0.16 ± 0.05	1.50 1.50	35.73 ± NA	0.07
	617	4.50	NA ± NA	0.37 ± 0.13	39.00 3.50	4.48 ± NA	0.26
Okak	630	7.50	8.50 ± 1.69	0.19 ± 0.06	13.00 13.00	NA ± NA	0.14
	634	1.50	NA ± NA	0.16 ± 0.01	16.50 4.50	* 18.09 ± 21.97	0.16
	633	4.50	NA ± NA	0.29 ± 0.03	9.50 9.50	62.16 ± 41.26	0.19
Anaktalak	624	6.50	* 167.82 ± 370.12	0.30 ± 0.05	3.50 3.50	220.75 ± NA	0.45

Uncertainties are standard errors (SE) for the best fit parameters of nonlinear regression calculations.

[a]Data values marked with a star exhibit high standard errors and are excluded from the discussion. NAs indicate cores in which profile segments were too steep and the biodiffusion model could not be fitted, as well as when the profile consisted of only two data points and no errors could be calculated.

[b]Biodiffusion coefficients were calculated from $^{228}Th_{xs}$ profile segments indicated in the right column. The left column of z_p values represent total penetration depth.

$^{228}Th_{xs}$ activity profiles, bioturbation and penetration depths

Except for sediments at station 630 in the Okak Fjord, all sediment cores collected showed decreasing $^{228}Th_{xs}$ activities within surface zones ranging from zero to ten centimeters depth (Fig. 4.3). This zone is thought to be mostly influenced by biogenic sediment mixing. Several $^{228}Th_{xs}$ profiles further exhibited two segments with surface zones of decreasing activities and subsurface zones of either nearly constant, increasing or decreasing activities. In cores collected from stations GFII, 602 and 617 subsurface segments consisted of only one data point showing no clear trend between surface and subsurface profile segments.

The greatest penetration depths of $^{228}Th_{xs}$ activities were observed in sediment cores collected at stations 600 and 617 in Nachvak and Saglek Fjord, respectively (Table 4.2).

Bioturbation and sedimentation rates (D_b and ω)

Biodiffusion coefficients (D_b) were calculated from $^{210}Pb_{xs}$ and $^{228}Th_{xs}$ activity profiles above inflection points within the bioturbated zone (L_b) and in surface profile segments, respectively using Eq. 2. This analysis assumed a diffusion-like process, where sediment particles are randomly and frequently redistributed over small spatial scales (e.g. Goldberg and Koide, 1962; Guinasso and Schink, 1975; Berner, 1980; Cochran, 1985; Boudreau, 1986).

$$A = A_0 \exp\left(-z\left(\sqrt{\frac{\lambda}{D_b}}\right)\right) \qquad (2)$$

where A is the $^{210}Pb_{xs}$ activity [dpm g^{-1}], A_0 is the tracer activity at the sediment-water interface [dpm g^{-1}], λ is the decay constant of $^{210}Pb_{xs}$ (λ = 0.031 y^{-1}), and z is the depth in the sediment [cm].

Below bioturbated zones sedimentation accumulation rates (ω) were calculated from activity-depth distributions of the particle tracer $^{210}Pb_{xs}$ and ^{137}Cs, which was first introduced to the atmosphere in 1954 from nuclear weapon tests, and by using Eq. 3 (Bentley and Nittrouer, 2003),

$$A = A_0 \exp\left(-\frac{\lambda z}{\omega}\right) \quad (3)$$

where A is the $^{210}Pb_{xs}$ activity [dpm g^{-1}], A_0 is the the$^{210}Pb_{xs}$ activity at the sediment-water interface [dpm g^{-1}], λ is the decay constant of ^{210}Pb (λ = 0.031 y^{-1}), z is the depth in sediment [cm], and ω is the sediment accumulation rate [cm y^{-1}], and Eq. 4 (Krishnaswami et al., 1980),

$$\omega\,(^{137}Cs) = \frac{(z_p - L_b)}{(T - 1954)} \quad (4)$$

where ω (^{137}Cs) is the sediment accumulation rate obtained from ^{137}Cs activity-depth distributions [cm y^{-1}], z_p is the maximum penetration depth of ^{137}Cs in sediment cores [cm], L_b($^{210}Pb_{xs}$) is the mixing layer depth [cm] obtained from excess ^{210}Pb profiles, and T is the year of sample collection [y] (Krishnaswami et al., 1980). Equation 2 and 3 were

then fitted to tracer distributions with a least square method and the Marquard-Levenberg algorithm using SigmaPlot 11.0 (Systat Software, San Jose, CA, USA).

$^{210}Pb_{xs}$ and $^{228}Th_{xs}$ derived biodiffusion coefficients ranged from 0.16 $cm^2\ y^{-1}$ in Gibbs Fjord to 8.50 $cm^2\ y^{-1}$ in Okak Fjord, and from 0.48 $cm^2\ y^{-1}$ in Gibbs Fjord to 220.75 $cm^2\ y^{-1}$ in Anaktalak Fjord, respectively (Table 4.2). The latter biodiffusion coefficient was calculated from only two data points, as were the $^{228}Th_{xs}$ derived coefficients from sediments collected at stations 615 and 617 in Saglek Fjord. Therefore, these data must be interpreted carefully because they may not reflect actual sediment mixing rates. Biodiffusion coefficients with standard errors larger than the actual value were excluded and not further interpreted. Both, the $^{210}Pb_{xs}$ and $^{228}Th_{xs}$ profiles of sediment core 600 displayed two bioturbated zones, a surface zone with biodiffusion coefficients of 7.66 and 13.31 $cm^2\ y^{-1}$ and one zone between 10 and 31 and 39 cm, respectively. Given the steepness of these profile sections, the biodiffusion coefficient calculated using $^{210}Pb_{xs}$ is inaccurate with a relatively large error. Similarly, fitting the biodiffusion model to the $^{228}Th_{xs}$ profile of core 600 produced unrealistically high values and biodiffusion coefficients for this profile section are therefore unavailable.

Although there are no along-fjord trends visible, a general north-to-south trend of increasing $^{210}Pb_{xs}$ and $^{228}Th_{xs}$ derived biodiffusion coefficients can be observed.

4.3.2 Bioturbation structures

Bioturbation traces observed in X-radiographs are described in terms of general morphological characteristics, such as dominant orientation, burrow fill, boundary with

the surrounding sediment, location in core, and diameter. The diameter and location of structures in the sediment core are given in Table 4.3.

Generally, surface sediments of all cores, except for core 617, which was collected in Saglek Fjord and showed a potentially biomottled core top, contained a high proportion of vertically oriented bioturbation structures (Fig. 4.3). In most cores, the dominance of vertical structures in surface zones changed to dominance of horizontally oriented structures at greater depths.

Table 4.3: Sediment core averages of bioturbation structure diversity, diameter and vertical extent.

Fjord	Station	Location	Number of bioturbation structures in core	Diameter (cm)	Vertical extent (cm)
Gibbs Fjord	GFII	inner	4	0.17	10.3
Nachvak Fjord	602	inner	4	0.13	11.3
	600	outer	5	0.16	9.4
Saglek Fjord	615	inner	3	0.27	8.3
	617	outer	1	0.40	11.0
Okak Fjord	630	inner	4	0.28	6.5
	634	outer	3	0.16	10.8
	633	outer	6	0.33	12.5
Anaktalak Fjord	624	inner	6	0.22	11.3

Gibbs Fjord (core: GFII)

The X-radiograph of the core GFII collected in Gibbs Fjord showed that sediments were completely bioturbated (Fig. 4.3). Bioturbation traces in surface sediments (0-8 cm) comprised small, vertical, U- and Y-shaped, sometimes branching structures connected to the sediment-water interface, and larger, relatively smooth, unlined, horizontal to oblique, open, rarely branched tubes. The latter also penetrated into a coarser grained sediment layer at 5 to 7.5 cm depth and also occurred at greater core depths between

11 and 22 cm. Below the coarser grained sediment layer, these traces were slightly smaller than in surface sediment layers, exhibiting a vertical to sometimes curving component and were locally thinly lined.

Nachvak Fjord (cores: 600 and 602)

The X-radiograph of sediment core 600 showed a few small bivalves (~0.7-0.8 cm in diameter) and one gastropod shell close to the sediment-water interface (Fig. 4.3). The surface layer (0-3 cm) also contained some shallow, horizontally to vertically oriented and, diffuse structures, as well as small U- to Y-shaped, open and surface-connected burrows. A few vertical, straight tunnels with locally branched, Y-shaped ends were found between 0 and 15 cm depths. In 13 to 20 cm depth, a few small, branching, sometimes winding tunnels, as well as smooth, unlined, horizontal to oblique and open tunnels were visible. The latter sometimes exhibit a halo in depths between 13 and 15 cm and also occur in deeper sediment sections at the bottom of the core.

A few bivalve shells (~0.9-1.7 cm in diameter), shell fragments and potential Pectinaria sp. tubes (~3-5 cm long) with thick walls occurred in the surface layer (0-5 cm) of sediment core 602 (Fig. 4.3). The upper half of the core also contained a few small ice-rafted debris clasts. In 0 to 3 cm shallow, slightly diffuse, trough-like to horizontally oriented tunnel-like structures that were connected to the sediment-water interface were visible. Multiple branching, locally winding, and predominantly horizontally to obliquely oriented tunnel structures were found at 11 cm depth. The tunnels were open or were filled with substrate that differed from the lithology of the surrounding sediment. At about 7 cm depth, the branching structures were sometimes connected to predominantly

vertical shafts, which appeared to be connected to the sediment-water interface. The bottom half of the sediment core contained relatively large, smooth, unlined, horizontal to oblique and open tunnels, which were most abundant between 11 and 35 cm depth.

Saglek Fjord (cores: 615 and 617)

Sediment core 615 contained few fragments of mineralized tubes and some ice-rafted debris clasts with a greater number of clasts within the upper half of the core. Several bivalve shells (~1.2-1.5 cm in diameter) and a Pectinaria sp. tube were found close to the sediment-water interface in 0-5 cm depth of core 615 (Fig. 4.3). Also within the surface layer, trough-like, slightly diffuse structures were present at the sediment-water interface. Between 7 and 13 cm depth, a few horizontal to vertical, sometimes branching, very fine, and in this core, slightly visible structures were observed. The bottom half of the core, at depths between 15 and 30 cm, some larger, smooth tunnels, which were either open or filled with substrate that differed from the lithology of the host sediment occurred. The straight to curved tunnels were horizontally, obliquely to vertically oriented and surrounded by a relatively wide halo.

Sediment core 617 exhibited two relatively large bivalve shells at the bottom of the core with a length of ~4 cm and at 30 cm depth with a length of ~3 cm (Fig. 4.3). Only a few traces were found between 5 and 32 cm depth. These structures consisted of smooth, vertical to oblique and horizontal, sometimes curving, open tunnels that were locally thinly lined. These tunnels were most abundant at 8-19 cm depth.

Okak Fjord (cores: 630, 633 and 634)

Ice-rafted debris clasts occurred throughout sediment core 630, with a greater number of clasts within the upper 9 cm of the sediment (Fig. 4.3). Two types of bioturbation structures that were connected to the sediment-water interface were also found in surface layers of this core. Diffuse, vertical to horizontal, sometimes curved, open and unlined traces, as well as a few simple, open, vertical to slightly oblique structures were located at 0-6 cm and 0-3 cm, respectively. In greater depths, between 6 and 23 cm, the core exhibited horizontal, oblique to vertical smooth tubes that were locally surrounded by a thin halo. At 6-12 cm depth these traces were relatively small (0.03-0.07 cm in diameter) and predominantly horizontally oriented, and slightly larger (0.1-0.4 cm in diameter) and without dominant orientation at 12-23 cm depth.

Core 633 exhibited two bivalve shells, one at the sediment-water interface and one at about 11 cm depth, and very few ice-rafted debris clasts at 0-3 cm depth or in deeper sediment layers (Fig. 4.3). The X-radiograph also showed vertical to oblique, curved, sometimes U- or J-shaped, open, unlined structures that opened at the sediment-water interface at 0-4 cm depth, as well as branched (sometimes multiply branched), open, straight to curved and sometimes sinuous, unlined structures at 0-12 cm depth. Between 4 and 20 cm depth, the core showed vertical, oblique and horizontal, straight and rarely curving, thinly lined, open or filled burrows with finer substrate than the surrounding sediment structures with diameters of 0.2 to 0.3 cm. Predominantly horizontal, smooth, straight tunnels that were open or filled with substrate of a different lithology than the host sediment were located near the bottom of the core at 20-32 cm depth. One

relatively long, vertical, unlined and open shaft extended from near the surface at about 6 cm depth to the bottom of the core at 32 cm depth.

Sediment core 634, collected in the small basin inlet in Okak Fjord, was generally lightly bioturbated and with some ice-rafted debris clasts found throughout the core (Fig. 4.3). The surface layer (0-4 cm) of the core was biomottled, with a few vertical, simple straight to U-and J-shaped, open traces with one or two openings at the sediment-water interfaced, as well as horizontally oriented, open, straight to slightly curved structures visible in the X-radiograph of the core.

Some dominantly horizontal to sometimes oblique, smooth tunnels were located at greater depths between 8 and 39 cm of the core.

Anaktalak Fjord (core: 624)

The X-radiograph of core 624 showed that the sediment was strongly bioturbated (Fig. 4.3). The surface layer contained a few shell and tube fragments and there were generally only very few ice-rafted debris clasts throughout the core. At 0-7 cm depth a few small, curved and winding, branched, probably open tunnel systems were found. Vertical, horizontal and oblique, smooth, straight to curving tunnels, open or filled with finer material than the surrounding substrate were located between 4 and 34 cm depth. Also present in this depth range, in 4-26 cm depth, were structures that consisted of vertically oriented, curved, open, lined central shafts that were surrounded or connected to unlined, horizontally oriented, slightly bent downwards lobes with up-ward bent ends. A few relatively small (0.07-0.1 cm in diameter), horizontal, short, straight to slightly

curved structures, open or filled with substrate that was finer than the host sediment and surrounded by a light halo were visible between 17 and 21 cm depth.

The number of bioturbation structures found in sediment cores ranged from 1 to 6 with the highest numbers observed in cores 633 (Okak Fjord) and 624 (Anaktalak Fjord) (Table 4.3). Average diameters of bioturbation structures in each sediment core varied between 0.1 cm in Nachvak Fjord and 0.4 cm in Saglek Fjord. Sediment core depth ranges of bioturbation structures were lowest in core 630 collected in Okak Fjord, whereas the largest ranges were observed in sediment core 633.

4.3.3 Environmental parameters

Substrate (in 0-10 cm sediment depth)

Grain sizes of fjord sediments varied from 5 to 7 Phi and were moderately well to poorly sorted (Fig. 4.4 A and Table 4.4). Silt was the dominant grain size in all sediment cores collected, with percentages varying between 69 and 99 % (Fig. 4.4 B). The skewness of grain size distributions varied between very coarse skewed at station 617 in Saglek Fjord to symmetrical at stations 602, 624, 630, and GFII in Nachvak, Anaktalak, Okak, and Gibbs Fjord, respectively (Fig. 4.4 B and Table 4.4). Among the sub-sampled sediment sections within the first 0-10 cm of each core, the magnitudes of sorting, skewness and mean grain size varied most in sediment cores GFII, 615, 624, and 630 as indicated by comparatively high standard deviations (Table 4.4).

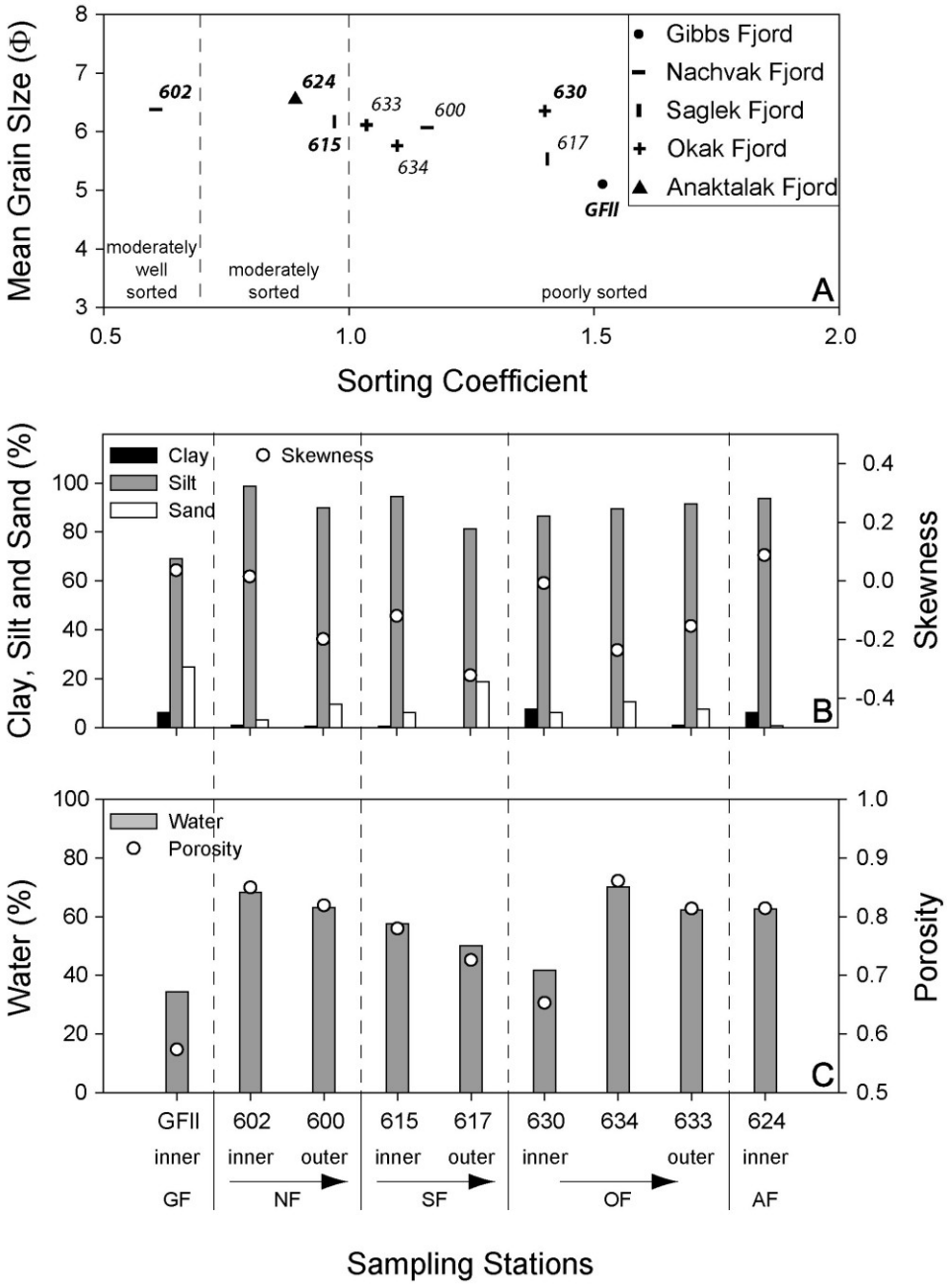

Figure 4.4: Substrate characteristics of fjord surface sediments (0-10 cm). Note that particles with diameters >3000 μm are not included in calculations. (A) Plot of mean grain size versus grain size sorting, (B) Percentages of clay, silt and sand, and skewness of grain size distributions, and (C) Percent water and porosity of surface sediments. Abbreviations for fjord names are: GF=Gibbs Fjord, NF=Nachvak Fjord, SF=Saglek Fjord, OF=Okak Fjord, and AF=Anaktalak Fjord.

Table 4.4: Mean, minimum, maximum, and standard deviation of the substrate characteristics grain size, sorting, skewness, and clay, silt and sand percentages for surface sediment sections (0-10 cm) of each core.

		Mean Phi (0-10 cm)				Sorting (0-10cm)				Skewness (0-10 cm)				STDEV		
Fjord	**Station**	**Mean**	**Min**	**Max**	**STDEV**	**Mean**	**Min**	**Max**	**STDEV**	**Mean**	**Min**	**Max**	**STDEV**	**% Clay**	**% Silt**	**% Sand**
Gibbs Fjord	GFII	5.10	3.00	6.15	1.31	1.52	1.14	1.77	0.25	0.04	-0.15	0.14	0.13	4.65	22.37	26.16
Nachvak Fjord	602	6.38	6.23	6.68	0.18	0.59	0.49	0.73	0.10	0.01	-0.03	0.05	0.03	1.58	1.72	NA
	600	6.07	5.94	6.28	0.13	1.15	0.93	1.30	0.16	-0.20	-0.27	-0.10	0.07	0.49	2.85	2.89
Saglek Fjord	615	6.08	5.25	6.33	0.46	0.97	0.56	2.15	0.67	-0.12	-0.57	0.01	0.25	0.56	8.23	8.60
	617	5.44	5.27	5.76	0.19	1.40	1.18	1.50	0.13	-0.32	-0.35	-0.27	0.03	0.00	4.21	4.21
Okak Fjord	630	6.35	6.08	6.61	0.21	1.40	1.06	1.76	0.29	-0.01	-0.25	0.14	0.17	6.65	5.30	3.07
	634	5.76	5.55	5.97	0.16	1.10	1.04	1.21	0.08	-0.24	-0.29	-0.21	0.03	0.00	1.53	1.53
	633	6.11	5.95	6.46	0.21	1.04	0.97	1.12	0.06	-0.15	-0.24	-0.04	0.08	1.89	1.43	2.44
Anaktalak Fjord	624	6.66	6.34	7.22	0.36	0.88	0.60	1.55	0.40	0.09	0.01	0.28	0.11	8.43	8.32	NA

In the majority of sediment cores sampled, the strongest variations among grain size distributions of sub-sampled sediment sections occurred mostly between 6 and 7 Phi (fine silt), with the exception of grain size distributions of cores 630 and 624 that showed relatively high variation around 11 Phi (clay) (Appendix 4.1). Other relatively strong deviations were identifiable in fine silt to clay, as well as in medium to fine sand grain size fractions.

Water percentages of surface sediments ranged from 34 to 70 % among cores collected in fjords (Fig. 4.4 C). Sediment porosities followed a similar pattern with lowest values in Gibbs Fjord and generally higher values in the Labrador fjords, peaking at station 634 in Okak Fjord.

Average cumulative weight percentages showed three to four grain size subpopulations in sediment cores collected in the Labrador fjords with comparatively well sorted coarse to medium sand, less well sorted medium sand to medium silt, well sorted coarse silt to clay, and less well or better sorted clay fractions (Fig. 4.5). Grain size distributions of sediments collected in Gibbs Fjord showed less distinctive subpopulations with better sorted finer clay and coarse sand fractions. Average cumulative weight percentage grain size curves of outer fjord sediments were similar in progression with slight variations in the clay fractions. The graphs of inner fjord sediments were less similar in their progression and varied, in particular, in sand and clay fractions.

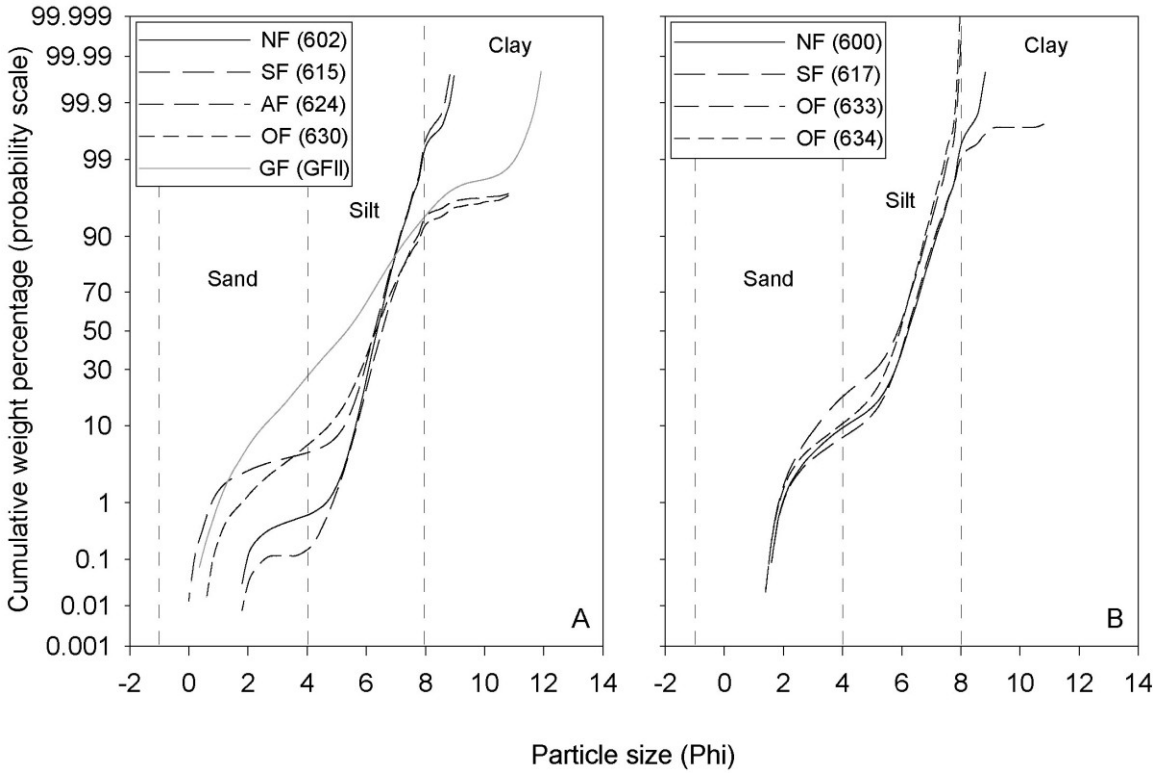

Figure 4.5: Cumulative weight percentages of grain size distributions on probability scale of A) inner fjord sediments and B) outer fjord sediments. Abbreviations for fjord names are: GF=Gibbs Fjord, NF=Nachvak Fjord, SF=Saglek Fjord, OF=Okak Fjord, and AF=Anaktalak Fjord.

Appendix 4.2 shows average cumulative weight percentages of fjord sediment grain size distributions and variations in sorting and number of subpopulations among sediment sections sub-sampled from each core within 0-10 cm depth. The outer fjord locations in Nachvak, Saglek and Okak Fjord varied little in the number of subpopulations and sorting, with largest spreads in the medium sand to medium silt ranges. Grain size distributions of sediment core 633 in Okak Fjord also showed larger spreading in the fine silt to clay range, with very little variation in the medium silt to fine silt ranges. As compared to outer fjord locations, grain size distributions of sediment cores collected at

inner fjord locations of the Labrador fjords varied to greater extents and the largest spreads occurred in the sand to medium silt and fine silt to clay fractions. Similar to the sediment cores of outer locations, the grain size distributions with the least spread in proximal fjord sediments were observed within medium to fine silt ranges. The least amount of spreading of cumulative weight percentages of grain size distributions was observed in sediment cores 617 in Saglek Fjord and 634 in Okak Fjord. Particularly at inner locations, the number of subpopulations varied between two and four, with the exception of sediment core 630. Herein, the greatest variation was identifiable in sand fractions of sediments. Cumulative weight percentages of grain size distributions of sediments collected in Gibbs Fjord showed relatively strong variation throughout all grain size fractions observed (Appendix 4.2).

Organic matter (in 0-2 cm sediment depth)

Organic carbon in surface sediments collected from the Labrador fjords derived mainly from marine sources as suggested by $\delta^{13}C$ values and C/N ratios (Fig. 4.6 A). Sedimentary organic carbon from Gibbs Fjord, however, was apparently partly derived from terrestrial organic matter sources with a slightly lighter carbon isotope signature of -24 ‰.

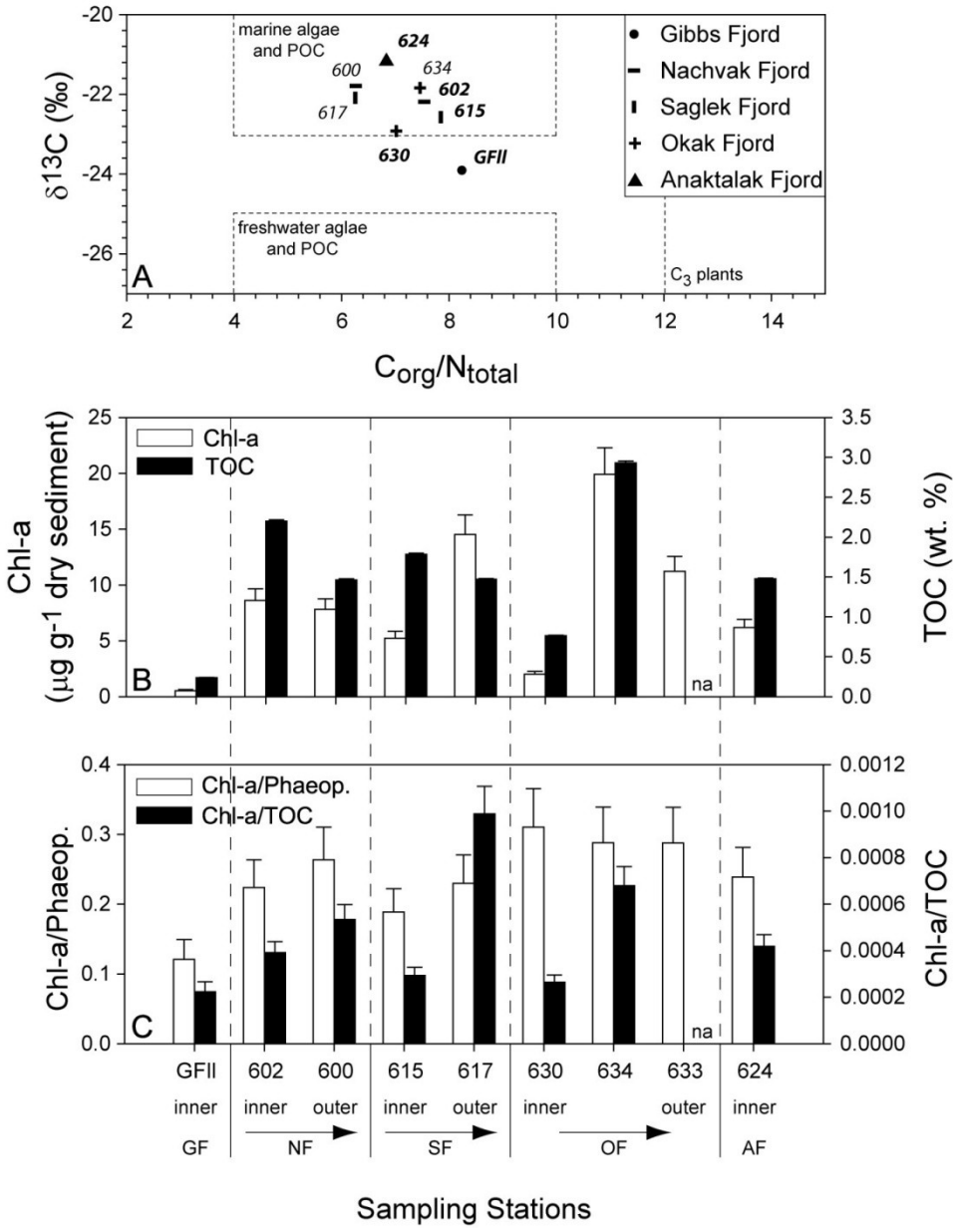

Figure 4.6: Organic carbon and chlorophyll-a of surface sediments (0-2 cm) collected throughout the study area. (A) Organic carbon provenance grouped according to sampling site localities. (B) Chlorophyll-a and total organic carbon (TOC) concentration of surface sediments. (C) Organic matter quality derived from chlorophyll-a/phaeopigment and chlorophyll-a/TOC ratios. Error bars indicate standard deviations (1 σ). Abbreviations for fjord names are: GF=Gibbs Fjord, NF=Nachvak Fjord, SF=Saglek Fjord, OF=Okak Fjord, and AF=Anaktalak Fjord.

Overall, chlorophyll-a and total organic carbon concentrations varied greatly among all sampling stations and were higher in Labrador fjords sediments (Fig. 4.6 B). With 0.5 µg g^{-1} chlorophyll-a and 0.2 wt. % TOC, sediments collected at station GFII in Gibbs Fjord exhibited the lowest organic matter concentrations. The highest values were observed at station 634 in Okak Fjord with 20 µg g^{-1} chlorophyll-a and 3 wt. % TOC.

The highest chlorophyll-a/phaeopigment and chlorophyll-a/TOC ratios were found at all stations in Okak Fjord and at station 617 in Saglek Fjord. Sediments collected in Gibbs Fjord exhibit the lowest organic matter qualities as indicated by comparatively small chlorophyll-a/phaeopigment and chlorophyll-a/TOC ratios (Fig. 4.6 C).

4.4 Discussion

4.4.1 Application of short- and long-lived particle tracers to identify long-term and seasonal sediment mixing processes in fjord environments

The simultaneous application of the particle tracers $^{210}Pb_{xs}$, $^{228}Th_{xs}$ and chlorophyll-a allowed to interpret mixing processes over short- and long-term time scales in marine fjord sediments. The photopigment chlorophyll-a has a half-life of approximately 50 days (calculated after Sun et al., 1993) and in the current study provided information on short-term processes that occurred over the summer months prior to sediment collections in September 2008 and October 2009.

By studying particle mixing in North Sea sediments, Boon and Duineveld (1998) determined that a diffusion model could best describe chlorophyll-a profiles with exponential depth decreases. Chlorophyll-a profiles exhibiting subsurface concentration maxima, however, were best described by a non-local mixing model. In the current

study, all sediment cores showed subsurface chlorophyll-a concentration peaks and/or increasing concentrations towards the bottom of the profile, and thus, demonstrated non-local mixing processes where surface material was moved to deeper layers. Therefore, the biodiffusion model was inappropriate for describing chlorophyll-a profiles in the current study. Compared to other chlorophyll-a profiles, the profiles of sediment cores 602 and 600 (Nachvak Fjord), and 630 and 633 (Okak Fjord) most clearly indicated non-local mixing trends through relatively clear subsurface concentration peaks and increases towards the bottom of profiles.

The radiotracers $^{210}Pb_{xs}$ and $^{228}Th_{xs}$ have half-lives of 22.36 y and 1.91 y, respectively, and can be used to interpret long-term sediment mixing processes at up to approximately five times their specific timescales (Smith et al., 1993; Lecroart et al., 2007; Teal et al., 2008; Lecroart et al., 2010).

Mostly due to sparse data, $^{228}Th_{xs}$ profiles displayed ambiguous mixing trends. On one hand, the profile shapes of all cores, except for core 630, indicated diffusive-like particle mixing in surface layers. On the other hand, $^{228}Th_{xs}$ activities were observed in deeper layers than expected based on its half-life of 1.91 y at stations 602, 600, 617, 630, and 634. Non-local particle transport to greater depths in these sediments was therefore assumed. Wetzel (2010) noted that burrows that contain particle tracers, such as short-lived radioisotopes, were probably produced recently within the sediment. The deep activities of $^{228}Th_{xs}$ in some of the sampled cores may consequently suggest that the structures in these depths are still active and that sediment and food particles are moved vertically over larger distances by benthic organisms. This observation supports the assumption of non-local sediment mixing interpreted from profiles of the short-lived chlorophyll-a. X-radiographs of all sediment cores showed traces of deep burrowing

endobenthos, however, not all $^{228}Th_{xs}$ particle tracer profiles were apparently affected by the deep-burrowing organisms. The majority of cores sampled at outer fjord locations displayed $^{228}Th_{xs}$ activities in greater depths. In samples that lacked deep penetrating $^{228}Th_{xs}$ activities, which is true for most of the cores collected at inner fjord locations, the deep burrowing endofauna was likely low in abundance as discussed by Wetzel (2010), or was ineffective with respect to particle transport. For instance, the X-radiograph of sediment core 624 collected in Anaktalak Fjord exhibited abundant bioturbation structures throughout the core. However, the depth-activity profile of the short-lived radioisotope $^{228}Th_{xs}$ indicated no particle mixing activities in greater depths of the core, and the trace-producing endofauna potentially used feeding mechanisms that caused little or no vertical particle transport through the sediment.

Except for station GFII in Gibbs Fjord and 633 in Okak Fjord, all activity-depth profiles of the long-lived particle tracer $^{210}Pb_{xs}$ implied diffusion-like particle mixing in sediment surface layers, which was inconsistent with non-local mixing profiles for chlorophyll-a, and in some cases for $^{228}Th_{xs}$, in similar sediment depth layers. This inconsistency may have been a result of longer-term (multi-year) biodiffusion-like processes overprinting seasonal non-local mixing activities that coincided with summer phytoplankton blooms.

In sediment core GFII collected in Gibbs Fjord, surface $^{210}Pb_{xs}$ activity-depth distributions paralleled chlorophyll-a concentration profiles. In this case, short-term bioturbation probably coincided with sedimentation to produce similar profiles for both tracers. The grain size distribution profile and the presence of an event sedimentation layer with a base at about eight centimeter depth, identified in the X-radiograph of core GFII, supported this interpretation (Appendix 4.3). Large-scale episodic deposition events, such as slumping from the steep fjord margin sides, are common phenomena in fjords

(Syvitski et al., 1987; Buatois and Mángano, 2011). In this case, the mass sedimentation event probably eroded some of the original fjord bottom surface and cut through and buried surface bioturbation structures. Subsequently, benthic organisms re-colonized the sediment surface and, at the time of the core collection, the top part of the event layer had been partially destroyed. The bioturbation structures above the event layer therefore represented a relatively early successional stage, potentially comprising opportunistic, surface feeding benthic organisms. Compared to the other sampled Labrador fjords, both $^{210}Pb_{xs}$ and $^{228}Th_{xs}$ derived biodiffusion coefficients within the upper four and three centimeters in Gibbs Fjord were low (with 0.16 and 0.48 $cm^2\ y^{-1}$), supporting the assumption of relatively recent bioturbation above the event sedimentation layer. Similarly, but to a lesser degree, the $^{210}Pb_{xs}$ activity-depth distribution of sediment core 633 in Okak Fjord displayed a subsurface peak at 5 cm depth that coincided with a concentration peak of chlorophyll-a. The X-radiograph of this core exhibited no evidence for a mass sedimentation event and a possible explanation for the matching profiles of the long-lived and short-lived particle tracers may have been an overall dominance of non-local mixing in these sediments.

4.4.2 Influence of inner-outer fjord and latitudinal organic matter and substrate trends on bioturbation processes

For the Labrador fjords, a general north to south trend of increasing bioturbation intensities may be associated with decreasing salinities, increasing fjord floor temperatures, and decreasing sedimentation rates along this latitudinal gradient (Fig. 4.7). Salinity, temperature, and sedimentation rate are known to influence bioturbation in marine sediments (e.g. Boudreau, 1994, Middleburg et al., 1997, Wetzel, 2010, Buatois

and Mángano, 2011). However, given the sparse bioturbation intensity data, interpretations of the observed trend are largely speculative and thus, these relationships will not be discussed in detail.

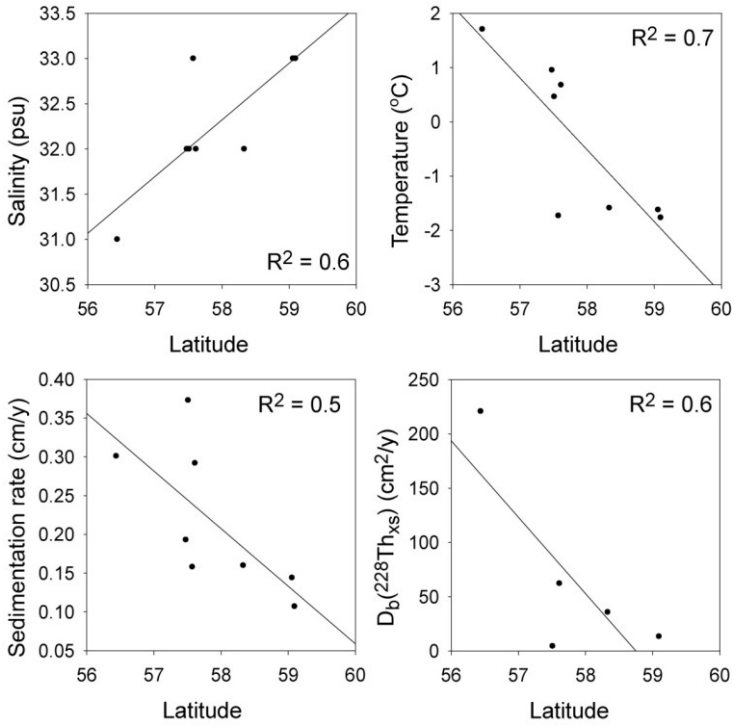

Figure 4.7: Scatterplots of Latitude and Longitude versus salinity, temperature, sedimentation rate, and $^{228}Th_{xs}$ bioturbation rate. Solid lines are regression lines and R^2 values are indicated for each plot.

Inner-outer fjord organic matter and substrate trends

Inner-outer fjord location trends in benthic environmental characteristics were detected in the Nachvak, Saglek, and Okak fjords. Only the sampled fjords where data from both inner and outer locations are available can be compared with respect to environmental trends.

As expected and revealed by $\delta^{13}C$ values of surface sediments, the marine origin of organic carbon increased towards the outer locations of all three fjords, distal from river catchments and the potential input of terrigenous organic matter. Except for Nachvak Fjord, where sedimentary chlorophyll-a concentrations are similar throughout the fjord, chlorophyll-a concentrations in Saglek and Okak fjords increased toward outer fjord locations. Fjords often receive biological material such as plankton from currents from shelf waters resulting in plankton blooms and increased transport of organic material to the seafloor (Syvitski and Shaw, 1995). This delivery of material, coupled with potentially minor grazing activities on phytoplankton by zooplankton in the water column, may have further enhanced the quality of organic matter reaching the benthos, as reflected in higher chlorophyll-a to total organic carbon and phaeopigment ratios. For instance, Parsons et al. (1983) found high primary productivity close to a frontal zone at the mouth of the Saanich Inlet fjord on the west coast of British Columbia, Canada along with lower zooplankton and heterotrophic activities than in more stable waters within the inlet.

In contrast to outer fjord locations, particularly in summer, a stable water column that inhibits phytoplankton production often characterizes inner locations of fjords. However, increased phytoplankton production associated with decreased water column stability and enhanced vertical turbulence can also occur in proximity to frontal zones such as fjord sills (Syvitski et al., 1987). In Nachvak Fjord, the slightly higher chlorophyll-a concentrations at station 602 (inner) than at station 600 (outer), are therefore likely explained by the fact that this sediment core was collected close to a steep sill, as seen in the fjord bathymetry (Fig. 4.2).

Similar to the organic matter trends, inner and outer fjord locations differed in substrate characteristics. Outer fjord locations of the Labrador fjords Nachvak, Saglek and Okak showed a trend of increased sand and coarse silt as inferred from coarsely skewed frequency distributions and generally poor sorting of the substrate. The skewness of grain size distributions is environmentally sensitive and can be used to distinguish among depositional environments (Duane, 1964, Martins, 1965). Symmetrical to slightly coarse skewed grain size distributions and slightly higher clay contents at inner fjord locations suggest a depositional environment where neither low energy nor high energy processes, such as deposition in sheltered areas or wave or current action, dominate for any length of time. Further, fjord basins are excellent traps for fine-grained particles and fjord sills prevent outward transport of finer particles, which is reflected in the higher percentages of clay observed in the sampled inner fjord sediments.

However, all sediment cores collected at inner locations of each fjord, except for core 602, displayed strong deviations in substrate sorting, mean grain size and skewness, suggesting more variable benthic environments through time with respect to depositional processes. Although grain size distributions of sediments collected at outer fjord locations exhibited similar cumulative weight percentage curve progressions that indicated analogous depositional processes, grain size distributions of sediments from inner fjord locations varied, not only from one fjord to the other, but also within the surface layers of each core. The relatively high variability of substrate characteristics in these cores therefore suggests that these locations represented highly variable and changing environments that reflect the action of various physical and post-depositional mixing processes. As discussed earlier, the sediment core GFII collected in Gibbs Fjord

represented an event sedimentation facies and differences in substrate characteristics among sub-sampled sediment sections are therefore not surprising.

Except for sediments collected at stations 630 in Okak Fjord and GFII in Gibbs Fjord, sediments collected at inner fjord locations were generally better sorted than sediments from outer locations, resulting in higher substrate porosities. Because poorly sorted sediments offer a greater diversity of potential habitable niches than homogenous sediments, these conditions may also support a higher diversity of benthic organisms (Syvitski et al., 1987). However, in the marine benthic environment high biodiversity does not necessarily ensure high diversity of bioturbation structures because structures result from the specific feeding strategies used by the animals (e.g. Bromley, 1996). This was also reflected in the findings of the current study with no obvious correlation between bioturbation structure diversity and sediment sorting and substrate porosity.

Bioturbation structure diameter and bioturbation depth in relation to inner-outer fjord environmental trends

Environmental conditions of outer fjord benthic habitats appeared more stable with less variability in depositional processes compared to inner fjord locations. Further, potential food sources appeared to be of a higher quality and quantity in outer fjord sediments. Consequently, outer fjord locations apparently offer more favorable environmental conditions for benthic organisms, which bioturbation surrogates should then reflect. Interestingly, of the bioturbation proxies studied only the bioturbation structure diameters and bioturbation depths (L_b) responded to the expected inner to outer fjord environmental trends. The lack of significant relationships between environmental patterns and bioturbation proxies may have resulted from sparse data that limited

definitive interpretations. This constraint is especially true for data on bioturbation rates. Alternatively, the environmental parameters or parameter assemblages that actually control bioturbation processes in fjord sediments may not have been characterized in the current study.

In each fjord, a higher proportion of smaller-sized bioturbation structures occurred in inner fjord sediments. In brackish fjord environments, smaller sizes and lower abundances typically characterize biogenic traces (Schatz, 2012; Schatz et al., 2013). As a result of seasonal increased freshwater discharges, inner fjord locations commonly experience stronger seasonal salinity fluctuations (Buatois and Mángano, 2011) than outer fjord locations, exerting environmental stress on the benthic fauna. Although seasonal salinity fluctuations were not characterized in the current study, they may explain the relatively small bioturbation structure diameters in fjord heads and in inner fjord locations compared to structures at outer locations.

In the Labrador fjords, $^{210}Pb_{xs}$ bioturbation depth profiles generally mimic benthic chlorophyll-a concentration trends and greater bioturbation depths apparently coincided with lower chlorophyll-a concentrations typical of inner fjord sediments. Intuitively, bioturbation depths are expected to correlate positively with organic matter input because, assuming oxygen concentration and deposition rate are not limiting factors, the latter link to higher benthic population density resulting in higher particle mixing rates (Wetzel, 1991). Further, bioturbation studies conducted in Arctic and temperate geographical regions contradict the findings of the current study, in that bioturbation depths correlated positively with benthic chlorophyll-a concentrations (see Chapter 2 and 3). On average, sedimentary chlorophyll-a concentrations in Arctic and temperate sediments were lower than those of the fjord sediments studied here, which suggests

that relatively high organic matter input may have inhibited the activity of benthic organisms and, therefore, bioturbation rather than increasing the mixing activities of benthic organisms. High concentrations of organic matter and a relatively shallow redox front characterize many fjord sediments that are largely undisturbed by physical and biological processes. These sediments are typically dominated by surface-feeding organisms and low bioturbation (Syvitski et al., 1987). By studying bioturbation structures in upwelling environments off Vietnam, Wetzel et al. (2011) inferred that increased delivery of organic matter to the seafloor during time periods when the overlying water column is oxygen-deficient, promotes shallow bioturbation and a tendency to low structure diversity, small structure diameters, and shallow burrowing depth. Among all fjord locations studied here, station 634 in Okak Fjord was distinctive as a result of high benthic organic matter concentrations and sediments with high porosities and water content associated with low $^{210}Pb_{xs}$ mixing depths and relatively low levels of bioturbation structure diversity. This site lies within a small, relatively sheltered basin separated from the main fjord body by a shallow sill. Physical stresses through bottom currents, for instance, may be limited in this basin. Furthermore, by studying dinoflagellate cyst assemblages in surface sediments at the same locations of stations 634 in Okak Fjord and 624 in Anaktalak Fjord, Richerol et al. (2012) argued that anoxia within the sediment or human-related pollution may have recently influenced both fjords. In the current study, the X-radiograph of sediment core 624 exhibited a bioturbation structure that resembled the trace fossil *Spirophyton* and was present only in this particular core. *Spirophyton* has been described as an opportunistic ichnotaxon associated with extremely variable and unpredictable environmental conditions (Ekdale, 1985). In this context, sediments collected at station 624 in Anaktalak Fjord varied

greatly with respect to depositional processes, as demonstrated by wide ranges in grain sizes, grain size sorting and skewness, which supports the assumption that this is a highly variable and unpredictable environment.

4.5 Summary

Surface sediments of all collected cores were potentially characterized by seasonally occurring non-local mixing processes as indicated by chlorophyll-a concentration profiles. Non-local mixing processes, where particles were transported vertically over greater distances were especially obvious in sediments collected in the Nachvak Fjord and in inner Okak Fjord. Long-term mixing processes as interpreted from mainly $^{210}Pb_{xs}$ activity-depth distributions, however, implied diffusion-like mixing processes, except for sediments collected in Gibbs Fjord and at station 633 in outer Okak Fjord. In Gibbs Fjord, grain sizes and X-radiography indicated the occurrence of a mass sedimentation event, such as slumping from the margin sides. Particle tracer profiles in this core suggested relatively recent bioturbational mixing of surface sediment.

A trend of deep penetrating $^{228}Th_{xs}$ activities in only a few inner fjord sediment cores likely implied that the endofauna are either low in abundance or inefficient in particle mixing at these locations. However, except for sediment core 600, which exhibited significant $^{228}Th_{xs}$ activities in deeper sediment zones, deep tracer activities of outer fjord sediments comprised only a few data points and interpretations towards active, deep occurring bioturbation activities in these sediments are tentative.

Because the collected data set was relatively small, especially the ratio of observations to variables measured, statistical approaches to interpret the data were mostly omitted. However, several trends from inner to outer fjord environments were observed,

suggesting that outer fjord sediments received higher inputs of high quality organic matter, and appeared less influenced by varying depositional processes compared to inner fjord locations. Even though substrate surrogates indicated relatively sheltered conditions at inner fjord locations, they also showed that depositional processes must have varied substantially over time. The only bioturbation surrogates that followed the inner-outer environmental trend were bioturbation structure diameter and mixing depth. Comparatively small bioturbation structure diameters characterized inner fjord locations, probably as a result of salinity fluctuations. Bioturbation depths appeared to correlate with sedimentary organic matter concentrations and deeper mixing occurred at inner fjord locations. In the latter case, high organic matter inputs presumably inhibited the benthic infauna, resulting in shallow bioturbation and low structure diversity. Despite a weak trend of decreasing salinity and increasing temperature associated with increasing bioturbation intensities along a latitudinal gradient, the lack of statistical significance made this interpretation highly uncertain.

This study offered insights into the largely unexplored interrelations between bioturbation processes and environmental patterns in recent sediments of Arctic and subarctic fjords of Eastern Canada. Additional sampling campaigns would help to further substantiate the observed environmental and bioturbation trends and complement the data collected presented here.

4.6 References

ArcticNet (2015). http://www.arcticnet.ulaval.ca/index.php.

Avnimelech, Y., Ritvo, G., Meijer, L.E., Kochba, M. (2001). Water content, organic carbon and dry bulk density in flooded sediments. Aquacultural Engineering 25, 25-33.

Bennet, H.R. and Lambert, D.N. (1971). Rapid and reliable technique for determining unit weight and porosity of deep-sea sediments. Marine Geology 11, 201-207.

Bentley, S.J. and Nittrouer, C.A. (2003). Emplacement, modification, and preservation of event strata on a flood-dominated continental shelf: Eel shelf, Northern California. Continental Shelf Research 23, 1465-1493.

Bentley, S.J. and Kahlmeyer, E. (2012). Patterns and mechanisms of fluvial sediment flux and accumulation in two subarctic fjords: Nachvak and Saglek Fjords, Nunatsiavut, Canada. Canadian Journal of Earth Sciences 49, 1200-1215.

Berner, R.A. (1980). Early diagenesis – A theoretical approach. Princeton University Press.

Boon, A.R. and Duineveld, G.C.A. (1998). Chlorophyll a as a marker for bioturbation and carbon flux in southern and central North Sea sediments. Marine Ecology Progress Series 162, 33-43.

Boudreau, B.P. (1986). Mathematics of tracer mixing in sediments: I. Spatially-dependent, diffusive mixing. American Journal of Science 286, 161-198.

Boudreau, B.P. (1994). Is burial velocity a master parameter for bioturbation? Geochimica et Cosmochimica Acta 58, 1243-1249.

Bromley, R.G. (1996). Trace Fossils: Biology, Taphonomy and Application. Second Edition.Chapman and Hall, London. 361 pp.

Brown, Y.M., Sheldon, T.A., Burgess, N.M., Reimer, K.J. (2009). Reduction of PCB contamination in an Arctic coastal environment: a first step in assessing ecosystem recovery after removal of a point source. Environmental Science & Technology 43, 7635-7642.

Brown, T., Reimer, K., Sheldon, T., Bell, T., Bentley, S., Pienitz, R., Gosselin, M., Blais, M., Carpenter, M., Estrada, E., Richerol, T., Kahlmeyer, E., Luque, S., Sjare, B., Fisk, A., Iverson, S. (2012). A first look at Nunatsiavut Kangidualuk ('fjord') ecosystems. Nunavik and Nunatsiavut: From science to policy. An integrated Regional Impact Study (IRIS) of climate change and modernization, 271-301.

Buatois, L.A. and Mángano, M.G. (2011). Ichnology. Organisms-substrate interactions in space and time. Cambridge University Press, Cambridge, 358 pp.

Carpenter, M. (2011). Benthic habitats of a sub-arctic fjard – The case study of Okak Bay, Labrador. Geography Master of Science thesis, Memorial University of Newfoundland, St. John's, Canada.

Cochran, J.K. (1985). Particle mixing rates in sediments of the eastern equatorial Pacific: Evidence from ^{210}Pb, $^{239,240}Pu$ and ^{137}Cs distributions at MANOP sites. Geochimica et Cosmochimica Acta 49, 1195-1210.

Duane, D.B. (1964). Significance of skewness in recent sediments, Western Pamlico Sound, North Carolina. Journal of Sedimentary Petrology 34, 864-874.

Ekdale, A.A. (1985). Paleoecology of the marine endobenthos. Paleogeography, Paleoclimatology, Paleoecology 50, 63-81.

Folk, R.L. and Ward, W.C. (1957). Brazos river bar: A study in the significance of grain size parameters. Journal of Sedimentary Petrology 27, 3-26.

Gilbert, R. (1983). Sedimentary processes of Canadian arctic fjords. Sedimentary Geology 36, 147-175.

Goldberg, E.D. and Koide, M. (1962). Geochronological studies of deep sea sediments by the ionium/thorium method. Geochimica et Cosmochimica Acta 26, 417-450.

Guinasso, N.L and Schink, D.R. (1975). Quantitative estimates of biological mixing rates in abyssal sediments. Journal of Geophysical Research-Oceans and Atmosphere 80, 3032-3043.

Hein, F.J. and Syvitski, J.P.M. (1989). Sea floor gouges and pits in deep fjords, Baffin Island: Possible mammalian feeding traces. Geo-Marine Letters 9, 91-94.

Krishnaswami, S., Benninger, L.K., Aller, R.C., Von Damm, K.L. (1980). Atmospherically-derived radionuclides as tracers of sediment mixing and accumulation in near-shore marine and lake sediments: Evidence from ^{7}Be, ^{210}Pb, and ^{239,240}Pu. Earth and Planetary Science Letters 47, 307-318.

Lecroart, P., Schmidt, S., Jouanneau, J.-M. (2007). Numerical estimation of the error of the biodiffusion coefficient in coastal sediments. Estuarine, Coastal and Shelf Science 72, 543-552.

Lecroart, P., Maire, O., Schmidt, S., Grémare, A., Anschutz, P., Meysman, F.J.R. (2010). Bioturbation, short-lived radioisotopes, and the tracer-dependence of biodiffusion coefficients. Geochimica et Cosmochimica Acta 74, 6049-6063.

Martins, L.R. (1965). Significance of skewness and kurtosis in environmental interpretation. Journal of Sedimentary Petrology 35, 768-770.

Middelburg, J.J., Soetaert, K., Herman, P.M. (1997). Empirical relationships for use in global diagenetic models. Deep-Sea Research 44, 327-344.

Parsons, T.R., Perry, R.I., Nutbrown, E.D., Hsieh, W., Lalli, C.M. (1983). Frontal zone analysis at the mouth of Saanich Inlet, British Columbia, Canada. Marine Biology 73, 1-5.

Richerol, T., Pienitz, R., Rochon, A. (2012). Modern dinoflagellate cyst assemblages in surface sediments of Nunatsiavut fjords (Labrador, Canada). Marine Micropaleontology 88-89, 54-64.

Riaux-Gobin, C. and Klein, B. (1993). Microphytobenthic biomass measurement using HPLC and conventional pigment analysis. In: Kemp, P., Sherr, B., Sherr, E., Cole, J. (Eds.). Handbook of methods in aquatic microbial ecology. Lewis Publishers, Boca Raton, pp. 369-376.

Schatz, E. (2012). Ichnology of Holocene glaciomarine sediments: Maktak, Coronation, and North Pangnirtung Fjords, Baffin Island, Canada. Earth Sciences Master of Science thesis, Department of Geological Sciences, University of Saskatchewan, Saskatoon, Canada, pp. 103.

Schatz, E.R., Mángano, M.G., Aitken, A.E., Buatois, L.A. (2013). Response of benthos to stress factors in Holocene Arctic fjord settings: Maktak, Coronation, and North Pangnirtung Fjords, Baffin Island, Canada. Paleogeography, Paleoclimatology, Paleoecology 386, 652-668.

Schneider, C.A., Rasband, W.S., Eliceiri, K.W (2012). "NIH Image to ImageJ: 25 years of image analysis". Nature Methods 9, 671-675.

Smith, C.R., Pope, R.H., DeMaster, D.J., Magaard, L. (1993). Age-dependent mixing of deep-sea sediments. Geochimica et Cosmochimica Acta 57, 1473-1488.

Snelgrove P.V.R., Archambault, P., Juniper, K., Lawton, P., and others (2012). Canadian Healthy Oceans Network (CHONe): An academic–government partnership to

develop scientific guidelines for conservation and sustainable usage of marine biodiversity. Fisheries 37, 296-304.

Sun, M.-Y., Lee, C., Aller, R.C. (1993). Laboratory studies of oxic and anoxic degradation of chlorophyll-a in Long Island Sound sediments. Geochimica et Cosmochimica Acta 57, 147-157.

Syvitski, J.P.M. and Blakeney, C.P. (Compilers) (1983). Sedimentology of Arctic Fjords Experiment: HU82-031 data report, Volume 1, Canadian Data Report of Hydrography and Ocean Sciences 12, 935 pp..

Syvitski, J.P.M. and Schafer, C.T. (1985). Sedimentology of Arctic fjords experiment (SAFE): Project introduction. Arctic 38, 264-270.

Syvitski, J.P.M., Burrell, D.C., Skei, J.M. (Eds.) (1987). Fjords - Processes and products. Springer-Verlag, New York, 379 pp..

Syvitski, J.P.M., LeBlanc, K.W.G., Cranston, R.E. (1990). The flux and preservation of organic carbon in Baffin Island fjords. Geological Society of London Special Publication 53, 177-200.

Syvitski, J.P.M. and Shaw, J. (1995). Sedimentology and geomorphology of fjords. In: Perillo, G.M.E. (Ed.). Geomorphology and Sedimentology of Estuaries. Developments in Sedimentology 53. Elsevier Science, Amsterdam, 471 pp.

Teal, L.R., Bulling, M.T., Parker, E.R., Solan, M. (2008). Global patterns of bioturbation intensity and mixed depth of marine soft sediments. Aquatic Biology 2, 207-218.

Wetzel, A. (1991). Ecologic interpretation of deep-sea trace fossil communities. Palaeogeography, Palaeoclimatology, Palaeoecology 85, 47-69.

Wetzel, A. (2010). Deep-sea ichnology: Observations in modern sediments to interpret fossil counterparts. Acta Geologica Polonica 60, 125-138.

Wetzel, A., Tjallingii, R., Wiesner, M.G. (2011). Bioturbational structures record environmental changes in the upwelling area off Vietnam (South China Sea) for the last 150,000 years. Palaeogeography, Palaeoclimatology, Palaeoecology 311, 256-267.

CHAPTER 5 – Summary and Conclusions

The goal of this Ph.D. thesis was to gain an understanding of first-order environmental controls on bioturbation intensity, structures and depth in marine benthic habitats on regional and across-climatic scales. This investigation involved field studies in three contrasting climatic regions along Canada's East Coast and Arctic margins, and has produced comprehensive baseline data on benthic conditions and bioturbation processes for each of these settings. Specifically, bioturbation intensity, depth and structures were used as bioturbation proxies and tested for linkages with organic matter, substrate, and sedimentation rate in each of the three study regions.

5.1 Overarching conclusions

5.1.1 Summary of key results

Chapter 2 - Canadian Arctic Archipelago

All sediment cores collected from benthic habitats across the Arctic Archipelago were bioturbated to varying degrees, potentially by the action of benthic macrofauna. Particle tracer depth distributions in most sediment cores indicated diffusion-like mixing processes; however, strong evidence for seasonal non-local sediment mixing was found in some cores collected in Baffin Bay. Of the bioturbation proxies studied, the bioturbation rate and depth were correlated to environmental patterns identified across the Arctic Archipelago in which bioturbation rates and depths seemed to be mainly controlled by correlated combinations of organic matter and substrate characteristics. In particular, relatively high bioturbation rates and deep mixing depths were found in close

proximity to polynyas where increased input of high quality organic matter and silty substrate provide optimal conditions for sediment mixing activities of macrofaunal organisms. On the contrary, low bioturbation rates and shallow mixing were observed where sediments received increased inputs of clay and terrestrial organic carbon, and less labile and reactive organic substances, such as those produced by marine phytoplankton. The proxies bioturbation structure diameter and diversity appeared to be independent of organic matter input, origin, and quality. However, temperature and percentages of sand were identified as potentially limiting controls for bioturbation structure diameters.

Chapter 3 - Gulf of Maine and Scotian Shelf and Slope

The deep-sea Northeast Channel and Fan benthic habitats differed from basin benthic habitats of the Gulf of Maine and Scotian Shelf through strong variations in organic matter concentration, organic matter quality, and proportions of sand. Most bioturbation structure groups identified from X-radiographs occurred in a variety of benthic settings, and tracemakers appeared to be broadly adapted to a variety of benthic environmental conditions. Of the bioturbation proxies analyzed, the bioturbation structure diversity and the vertical extent of structures were controlled by variations in correlated combinations of organic matter input and substrate characteristics across the study region. Low bioturbation diversities, supposedly a result of highly biomottled surface sediments, and large vertical extents of structures into sediments were found in basin sediments where the benthic habitats are silt-mode dominated and characterized by increased inputs of high quality organic matter. Larger vertical extents of bioturbation structures in shallower basin sediments may indicate less strict partitioning of vertical space by benthic

macrofauna, resulting from little or no competition for food. In contrast, relatively narrow vertical extents of structures indicated competition for food and space, and specialized feeding behaviors were predominantly observed in sediment cores collected in deep-sea channel and fan environments. Further evidence of potential food caching behavior was observed, supporting the assumption of specialized feeding behaviors in these regions. Bioturbation structure diameters predominantly responded to variation in sedimentation rate across the study region and were independent of organic matter input and quality. Regions with relatively small structure diameters were characterized by comparatively high sedimentation rates. As with bioturbation structure diversities and vertical extents of structures, correlated with combinations of substrate and organic matter characteristics seemed to strongly influence bioturbation depths. In this case, greater bioturbation depths occurred in regions with increased input of organic matter and silty sediments with high water content. Bioturbation rates were independent of environmental variation across the study region.

Chapter 4 - Arctic and Subarctic Fjords

Particle tracer distributions indicated seasonal, summertime, non-local mixing processes in fjord sediments. Inner to outer fjord environmental trends were discovered where sediments collected at outer fjord locations received elevated, high quality organic matter. Substrate surrogates indicated relatively sheltered but highly variable depositional processes through time at inner fjord locations. Distributions of bioturbation structure diameter and bioturbation depth corresponded to environmental trends with comparably small diameter and deeper mixing depth in cores from inner fjord locations. The increased input of organic matter at outer fjord locations apparently inhibited

bioturbation processes that consequently resulted in shallow mixing depths. Further, in the Labrador Fjords, a weak southward latitudinal trend was observed with increasing bioturbation rates, which correlated with decreasing salinity and sedimentation rate, and increasing fjord bottom temperature.

Bioturbation-environmental relationships on regional and across-climatic scales

Correlated combinations of environmental variables, characteristic for each geographic region, influenced bioturbation processes in all samples in the current study.

The proxy bioturbation depth responded to environmental variation in benthic habitat conditions on regional scales, in all three studied regions, where organic matter concentrations and grain size distributions represented a major environmental control. Similarly, bioturbation structure diameters corresponded to regional environmental patterns characteristic for each studied region. Because these bioturbation proxies correlated with certain environmental factors in each region, they are potential predictors of environmental conditions and change in these environments and spatial scales, but also in environments elsewhere with similar environmental conditions and spatial scales. The proxies bioturbation intensity, and bioturbation structure diversity and vertical extent within the sediment also represent potential regional predictors for the Canadian Arctic Archipelago and the Gulf of Maine and Scotian Shelf region, respectively.

On a larger, across-climatic scale, the three regions studied in chapters 2, 3 and 4 can be distinguished from each other through variations in environmental characteristics of their benthic habitats, as illustrated by principal component analysis (PCA) (Fig. 5.1). Except for a few stations with similar environmental categories, variations of correlated

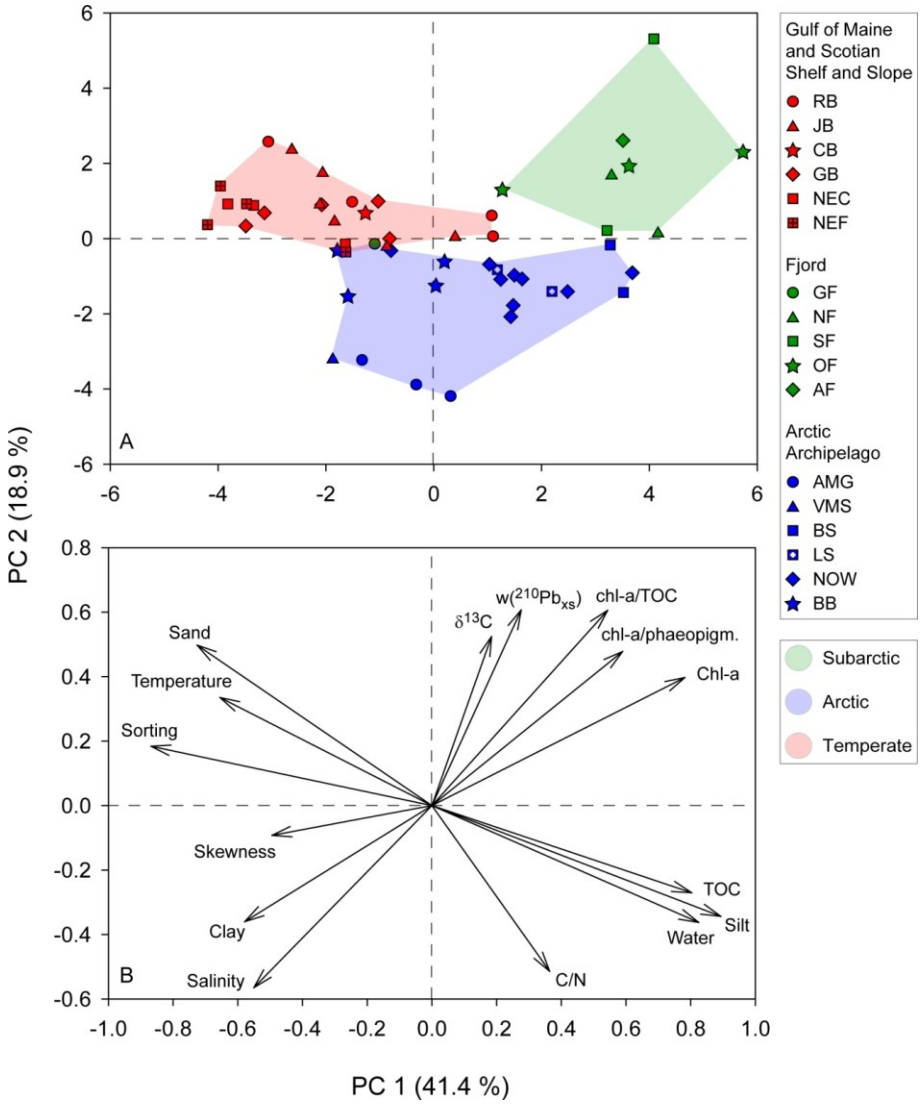

Figure 5.1: Scatter and vector plot of principal component analysis results with environmental variables analyzed in sediment cores collected in the Canadian Arctic Archipelago (chapter 2), the Gulf of Maine and Scotian Shelf region (chapter 3) and Baffin Island and Labrador Fjords (chapter 4). Salinity and temperature data for the Gulf of Maine and Scotian Shelf basins, and the Northeast Channel and Fan were extracted in ArcMap from georeferenced data layers provided by Greenlaw, M., Sameoto, J.A., Lawton, P., Wolff, N.H., Incze, L.S., Pitcher, C.R., Smith, S.J., Drozdowski, A. (2010). A geodatabase of historical and contemporary oceanographic datasets for investigating the role of the physical environment in shaping patterns of seabed biodiversity in the Gulf of Maine. Canadian Technical Report of Fisheries and Aquatic Sciences 2895, Fisheries and Oceans Canada, Science Branch, Maritimes Region, Dartmouth, Nova Scotia, Canada.

combinations of substrate characteristics (primarily: percent clay, silt, sand and water, and sediment sorting), organic matter quality and bottom temperature mainly differentiate the fjords from the Gulf of Maine and Scotian Shelf and Slope study sites (Fig. 5.1). Combinations of quality and source of organic matter, sedimentation rate, sand percentages, and bottom salinity separate study sites of the Arctic Archipelago from subarctic fjords and temperate study regions (Fig. 5.1).

On an across-climatic scale, the vertical bioturbation structure extents in sediments, bioturbation depths, and bioturbation intensities also respond to environmental trends and vary strongly among climatic regions (Fig. 5.2). Specifically, vertical extents of bioturbation structures correlate strongly with the environmental parameters that comprise principal components 1 and 2 and, therefore vary most strongly across the studied climatic regions (Table 5.1). Bioturbation rates and depths correlate primarily with environmental parameters comprising principal component 2. Of these three bioturbation proxies, the vertical extent of bioturbation structures in sediments responds most strongly to variations in environmental conditions of benthic habitats and, consequently, represents a potential predictor of environmental conditions and change across all three climatic regions studied in this Ph.D. thesis.

Consequently, the environmental differences between the three studied regions should not be treated as an environmental gradient following a latitudinal trend, but rather as three distinct geographic regions, each with its own characteristic environmental patterns and bioturbation-environmental relationships. The character of the bioturation-environmental relationships therefore depends not only on the spatial scale studied, but also on the environmental heterogeneity across each study area.

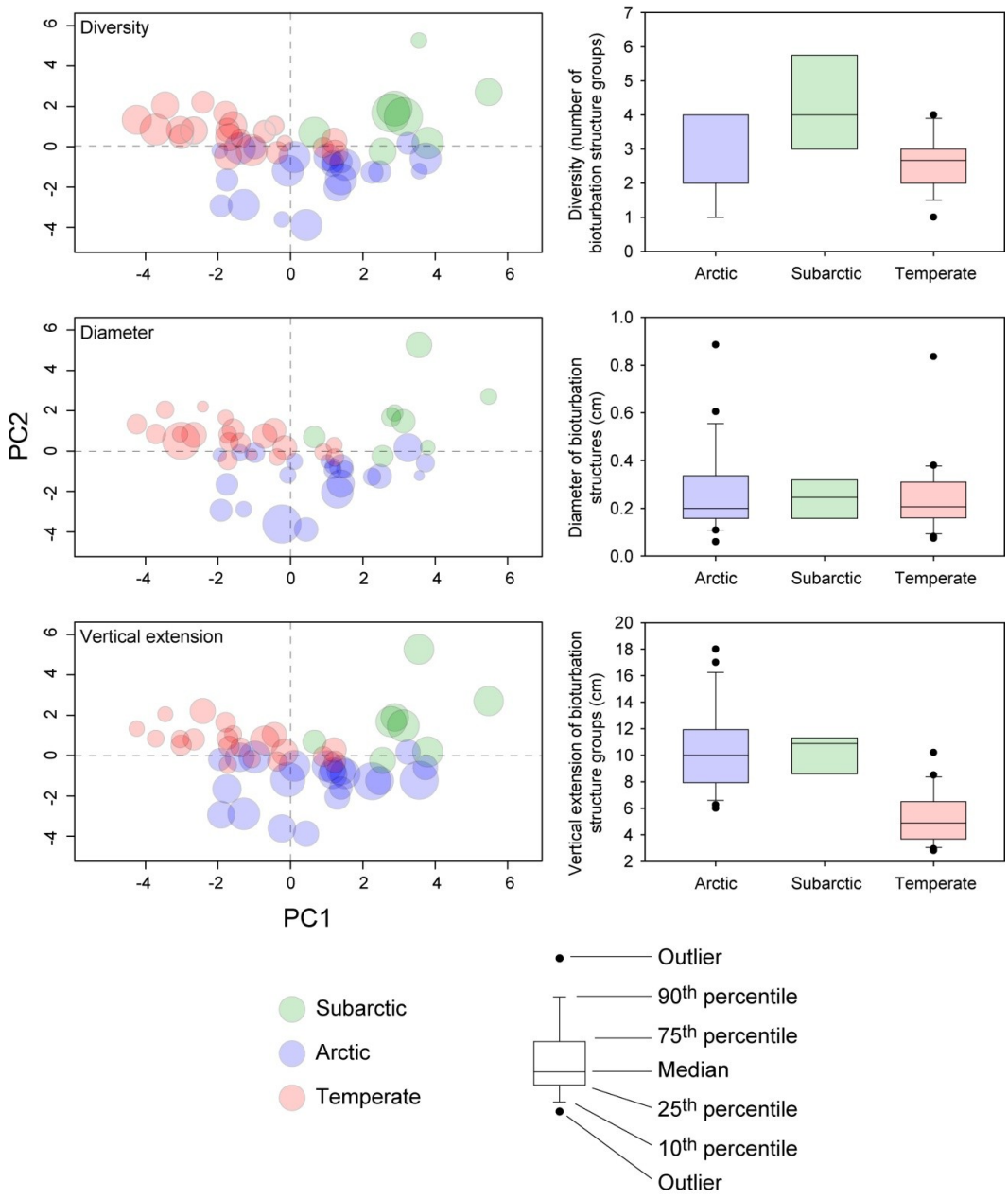

Figure 5.2: Left-hand side: Scatter-bubble plots of principal components 1 and 2 and bioturbation proxies. Graduated symbols represent bioturbation proxy magnitudes that can be found in data tables of chapter 2, 3 and 4. Right-hand side: Boxplots of bioturbation proxies grouped according to climatic region. Note that at least nine data points are required to calculate the 5th, 10th, 90th and 95th percentile in Sigmaplot 11. For subarctic regions only eight data points were available.

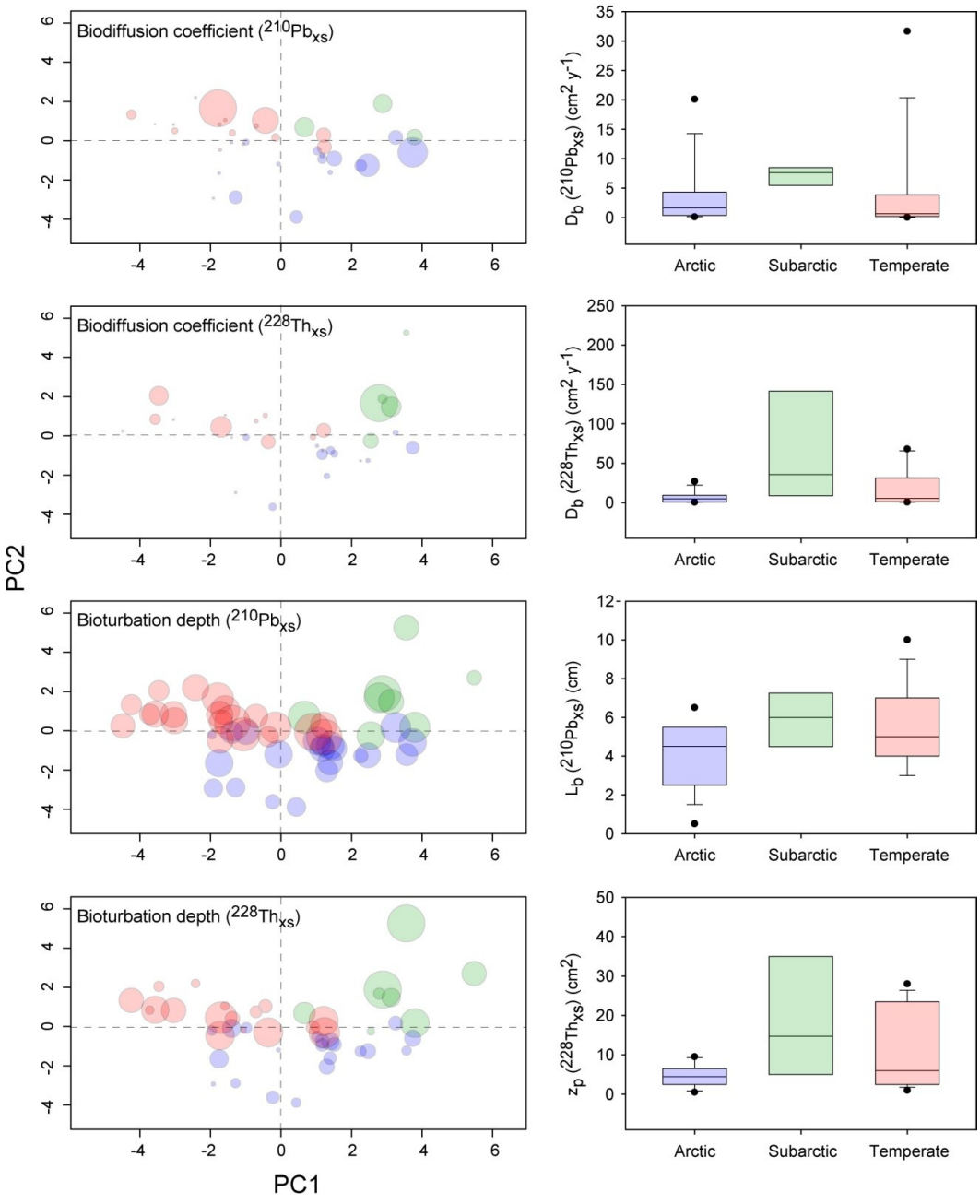

Figure 5.2 continued.

Table 5.1: Pearson product moment correlation coefficients of bioturbation proxies and environmental variables collected across arctic, subarctic and temperate regions, including principal components 1 and 2 from principal component analysis (Fig. 5.1).

	Biot. structure diversity	Biot. structure diameter	Vert. extent of biot. structures	Biot. rate $^{210}Pb_{xs}$	Biot. rate $^{228}Th_{xs}$	Biot. depth $L_b(^{210}Pb_{xs})$	Biot. depth $L_b(^{228}Th_{xs})$
Salinity	-0.421 **	0.201	-0.179	-0.216	-0.711 ***	-0.173	-0.381 *
Temperature	-0.288 *	-0.027	-0.616 ***	-0.023	-0.005	0.323 *	0.029
Chl-a	0.139	-0.014	0.350 *	0.307 *	0.183	0.035	0.333 *
TOC	0.032	-0.068	0.564 ***	0.291	0.022	-0.011	0.016
C/N	-0.138	-0.083	0.389 **	-0.135	-0.088	-0.254 *	-0.358
$\delta^{13}C$	0.112	-0.296 *	-0.054	0.048	0.412 *	0.306 *	0.309
Chl-a/TOC	0.029	0.022	0.241	0.346 *	0.163	0.160	0.460 **
% Clay	-0.017	0.344 *	-0.142	-0.427 *	-0.123	-0.225	-0.384 **
% Silt	0.169	0.080	0.615 ***	0.154	0.123	0.124	-0.022
% Sand	-0.164	-0.215	-0.592 ***	0.003	-0.087	-0.041	0.151
Sorting coeff.	-0.185	-0.022	-0.475 ***	-0.346 *	-0.293	-0.064	-0.081
Skewness	0.252 *	0.152	-0.327 *	-0.083	0.238	-0.204	-0.132
% Water	0.210	0.038	0.508 ***	0.123	0.068	0.069	0.020
Chl-a/Phaeop.	0.149	-0.029	0.154	0.283	0.270	0.323 *	0.261 *
ω ($^{210}Pb_{xs}$)	0.278 *	-0.182	0.057	-0.015	0.440 *	0.121	0.223
PC 1	0.196	-0.048	0.585 ***	0.278	0.234	0.108	0.184
PC 2	0.099	-0.217	-0.254 *	0.177	0.376 *	0.290 *	0.477 ***

Levels of significance: *** if $p \leq 0.001$, ** if $p \leq 0.01$, and * if $p \leq 0.1$.

5.2 Recommendations for future studies and outlook

In the current study, most activity-depth distributions of the long-lived particle tracer $^{210}Pb_{xs}$ indicated diffusion-like sediment mixing processes and thus the validity of applying a biodiffusion model. However, the short-lived particle tracers $^{228}Th_{xs}$ and specifically chlorophyll-a, often indicated mixing processes that transport sediment particles over larger distances non-randomly. As a consequence, it is recommended that future studies apply a non-local mixing model in addition to the biodiffusion model based on the data from this Ph.D. thesis.

Interrelations between bioturbation processes and benthic environmental conditions identified in this Ph.D. study provide valuable, comprehensive information that may be beneficial in interpreting and predicting the effects of natural and anthropogenic

environmental alterations on biological activities, macrofaunal feeding mechanisms, and sediment transport types in benthic habitats along Canada's East Coast and Arctic margins. The findings of the current study further may be transferable to and used in other geographical regions with similar environmental conditions.

Integrating the data from this Ph.D. thesis with biological data sets produced by fellow CHONe scientists will provide valuable information about functional roles of certain macrofaunal species and community traits in marine benthic ecosystems along the extent of Canada's East Coast and Arctic margins. In relatively pristine geographical regions, such as the Canadian Arctic and Subarctic, where climate change has already altered ecosystems but where little is known about marine benthic habitats, studies linking changing ecosystem functions to alterations of benthic habitat conditions are particularly helpful in establishing guidelines regarding conservation and sustainable use of marine biodiversity resources. The data set produced and presented here, in combination with data produced concurrently within the framework of CHONe, can be applied on regional to inter-regional scales. When implemented into ecosystem prediction models concerning the effects of benthic habitat alterations through environmental, namely anthropogenic, stresses, these data may also be applied on a global scale.

APPENDICES

Appendix Chapter 2

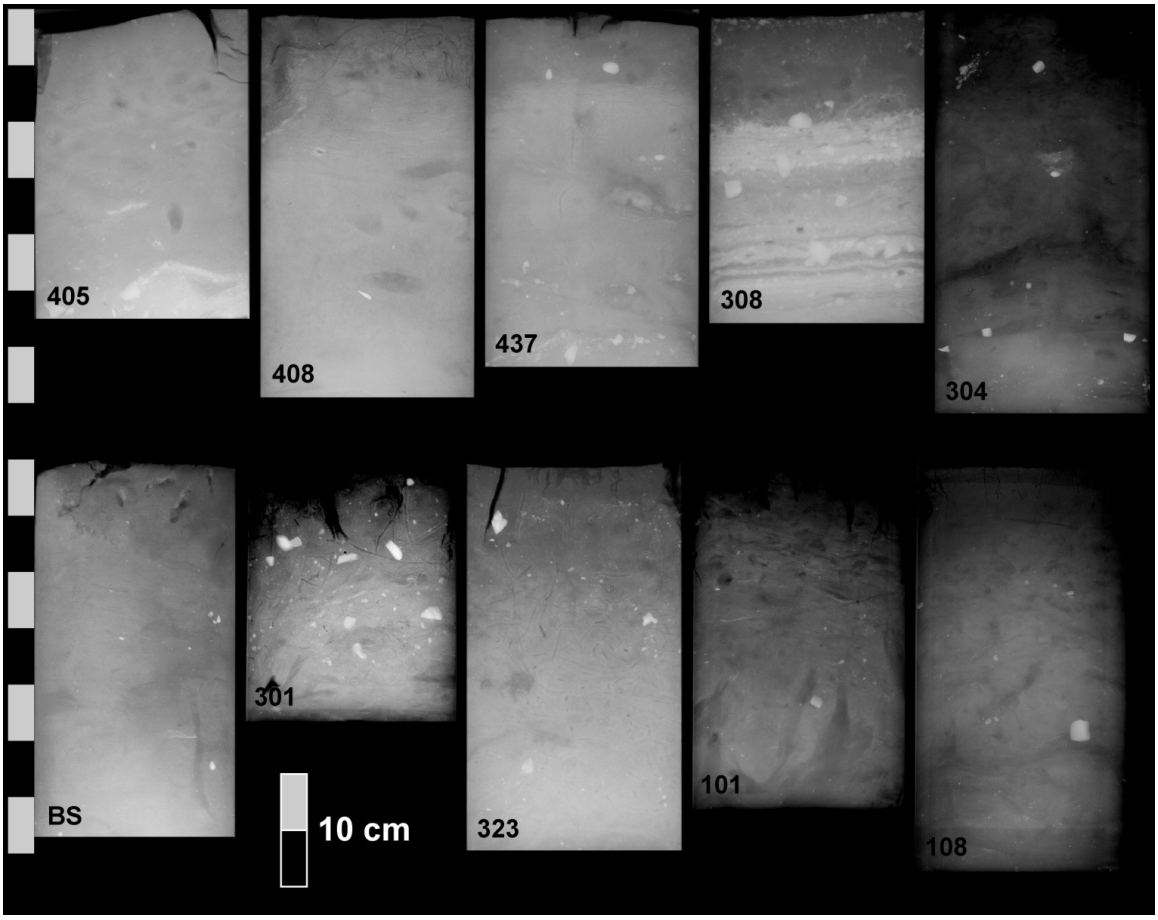

Appendix 2.1: X-radiographs of sediment cores collected (stations 405 to 108).

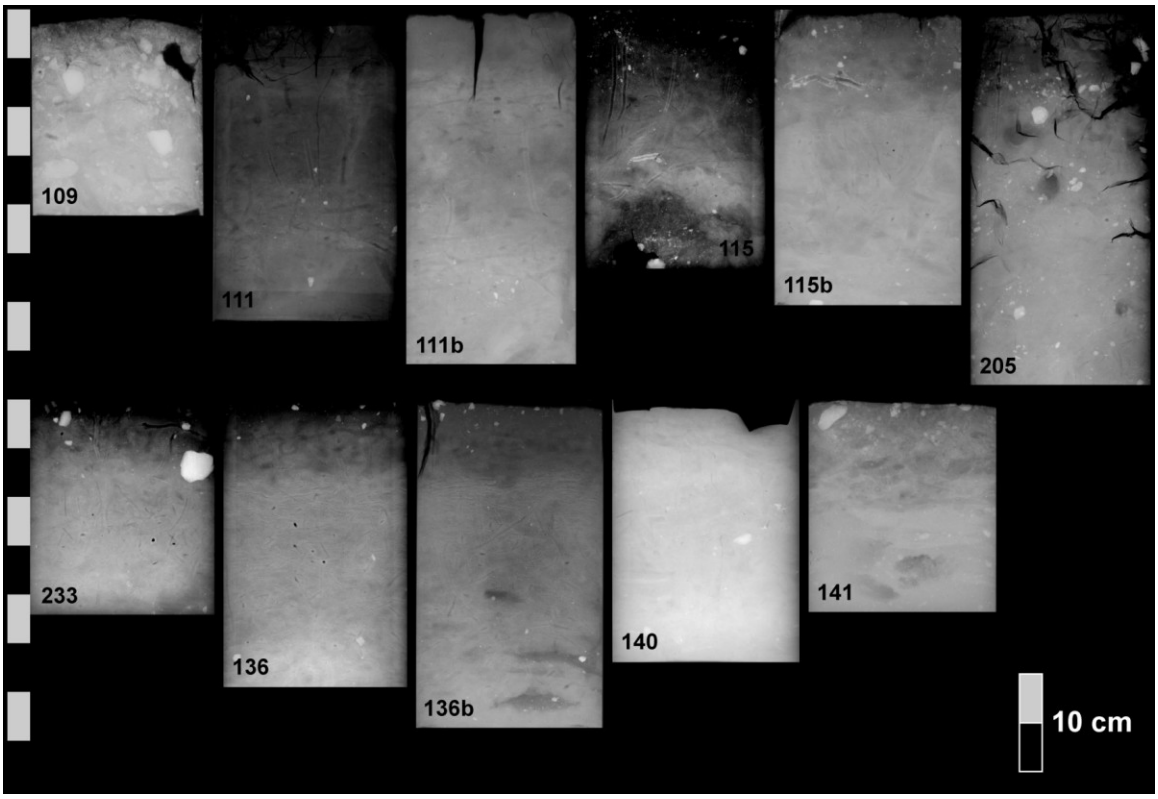

Appendix 2.1 continued (stations 109 to 141).

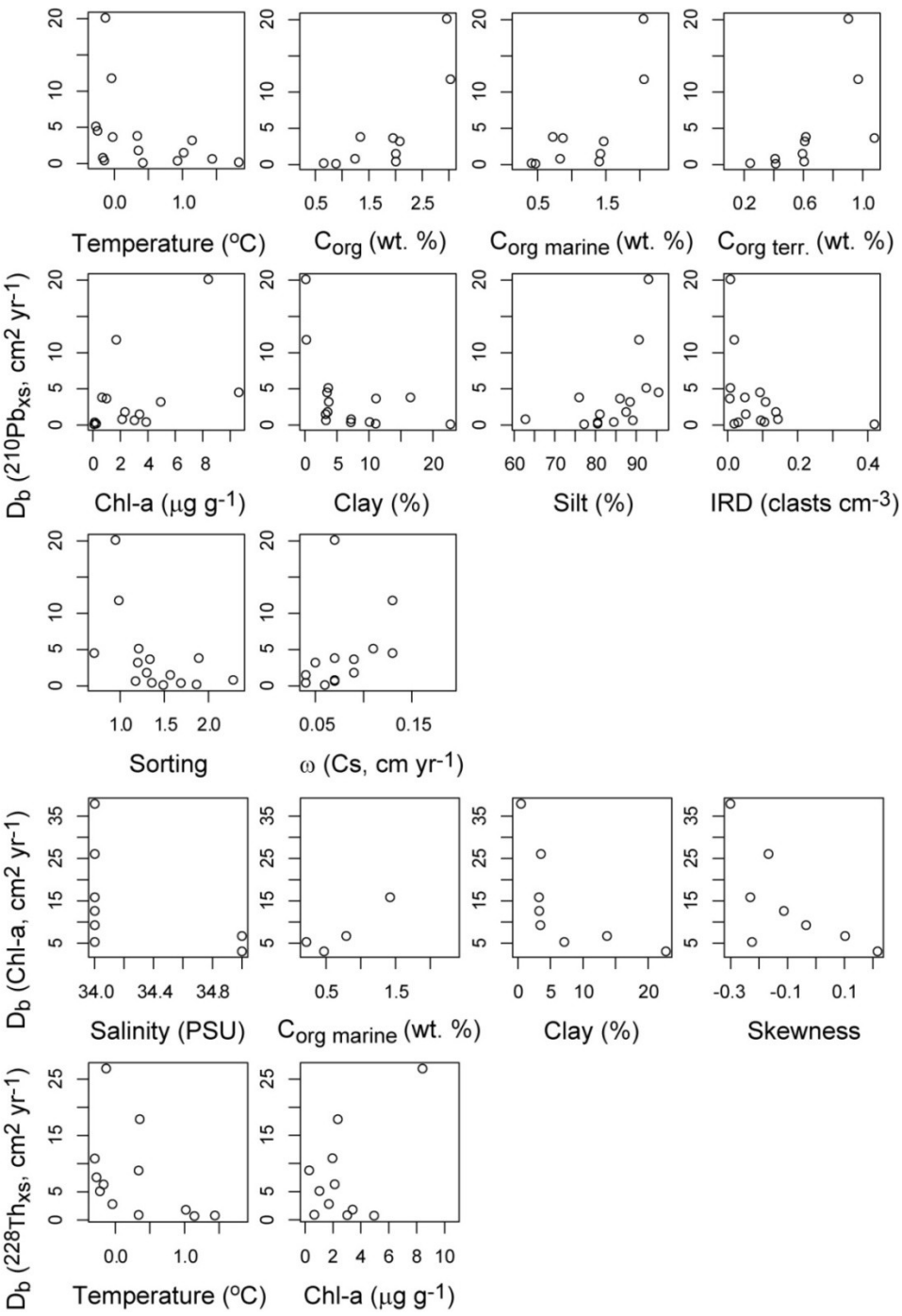

Appendix 2.2: Scatter plots showing relationships between bioturbation proxies and environmental variables where significant correlations were ($p \leq 0.1$) found.

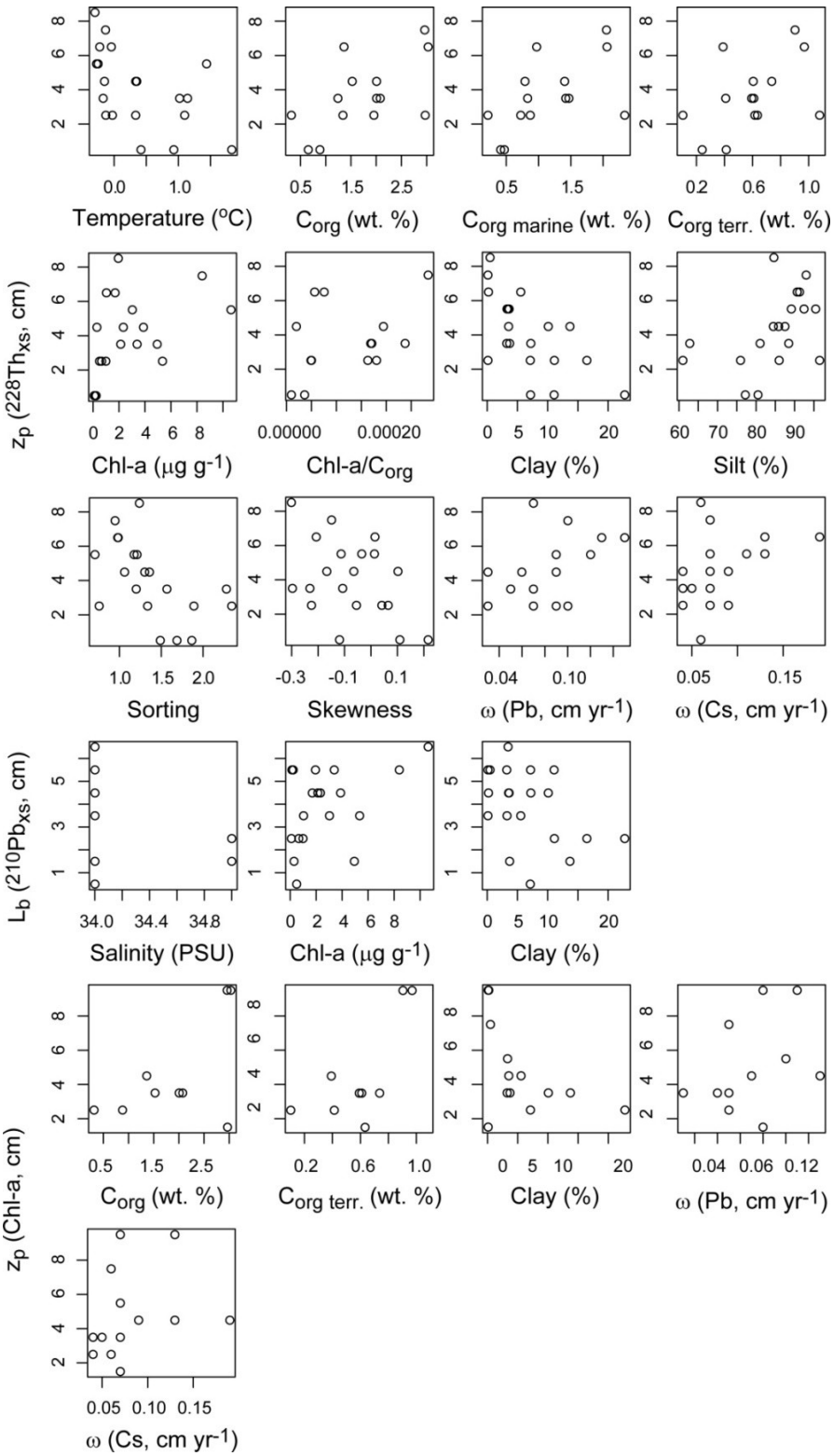

Appendix 2.2 continued.

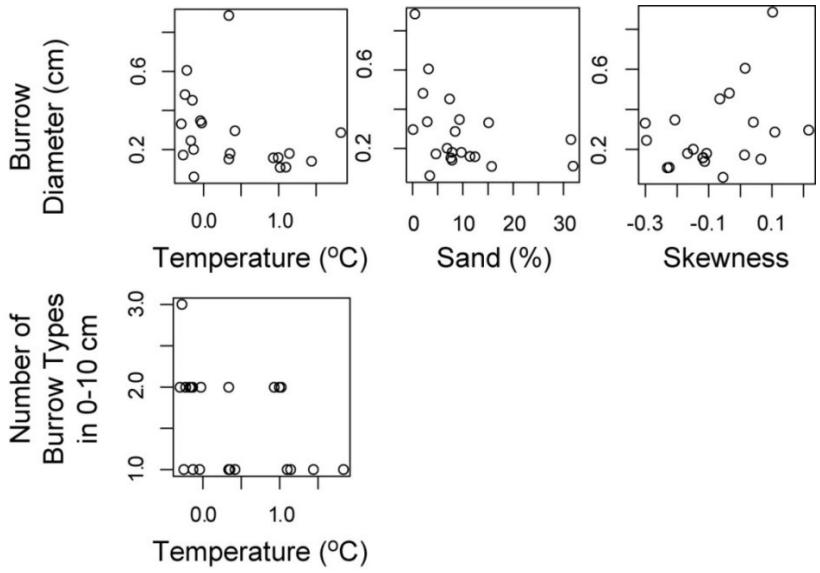

Appendix 2.2 continued.

Appendix 2.3: Principal component analysis results. Scores and loadings of principal components 1 (PC 1) and 2 (PC 2), and eigenvalues and variance of principal components.

Scores				Loadings					Eigenvalues and Variance			
Region	Station	PC1	PC2		PC1	p<0.05	PC2	p<0.05		Eigenvalue	Percentage of Variance	Cumulative Percentage of Variance
AMG	405	-0.784	-2.206	Depth	0.009	No	0.239	No	PC1	5.848	38.989	38.989
AMG	408	0.671	-2.138	Temperature	-0.509	Yes	0.127	No	PC2	3.188	21.253	60.242
AMG	437	-2.388	-1.249	C_{org}	0.907	Yes	0.154	No	PC3	1.570	10.469	70.710
VMS	308	-3.536	-3.584	Chl-a	0.671	Yes	0.250	No	PC4	1.429	9.527	80.237
BS	BS	2.595	-1.166	C_{org} mar	0.888	Yes	0.264	No	PC5	1.025	6.832	87.070
BS	304	3.898	0.331	C_{org} terr	0.694	Yes	-0.151	No	PC6	0.758	5.053	92.123
LS	301	0.474	0.215	Chl-a/C_{org}	0.386	No	0.766	Yes	PC7	0.452	3.017	95.139
LS	323	0.980	1.530	Clay	-0.688	Yes	-0.569	Yes	PC8	0.264	1.757	96.897
NOW	101	3.469	-0.281	Silt	0.880	Yes	-0.355	No	PC9	0.225	1.499	98.395
NOW	108	0.531	1.552	Sand	-0.487	Yes	0.791	Yes	PC10	0.153	1.017	99.412
NOW	109	-2.906	3.057	IRD	-0.472	Yes	-0.237	No	PC11	0.054	0.363	99.775
NOW	111	1.474	-0.976	Skewness	-0.154	No	-0.887	Yes	PC12	0.021	0.143	99.918
NOW	111b	4.271	1.802	Sorting	-0.875	Yes	0.353	No	PC13	0.011	0.076	99.994
NOW	115	0.343	0.299	ω($^{210}Pb_{xs}$)	0.509	Yes	-0.222	No	PC14	0.001	0.006	100.000
NOW	115b	0.380	0.714	ω(^{137}Cs)	0.377	No	-0.507	Yes	PC15	0.000	0.000	100.000
NOW	205	1.090	-2.521									
NOW	233	-0.017	2.337									
BB	136	-0.784	0.696									
BB	136b	-1.693	0.147									
BB	140	-3.100	-1.430									
BB	141	-4.971	2.871									

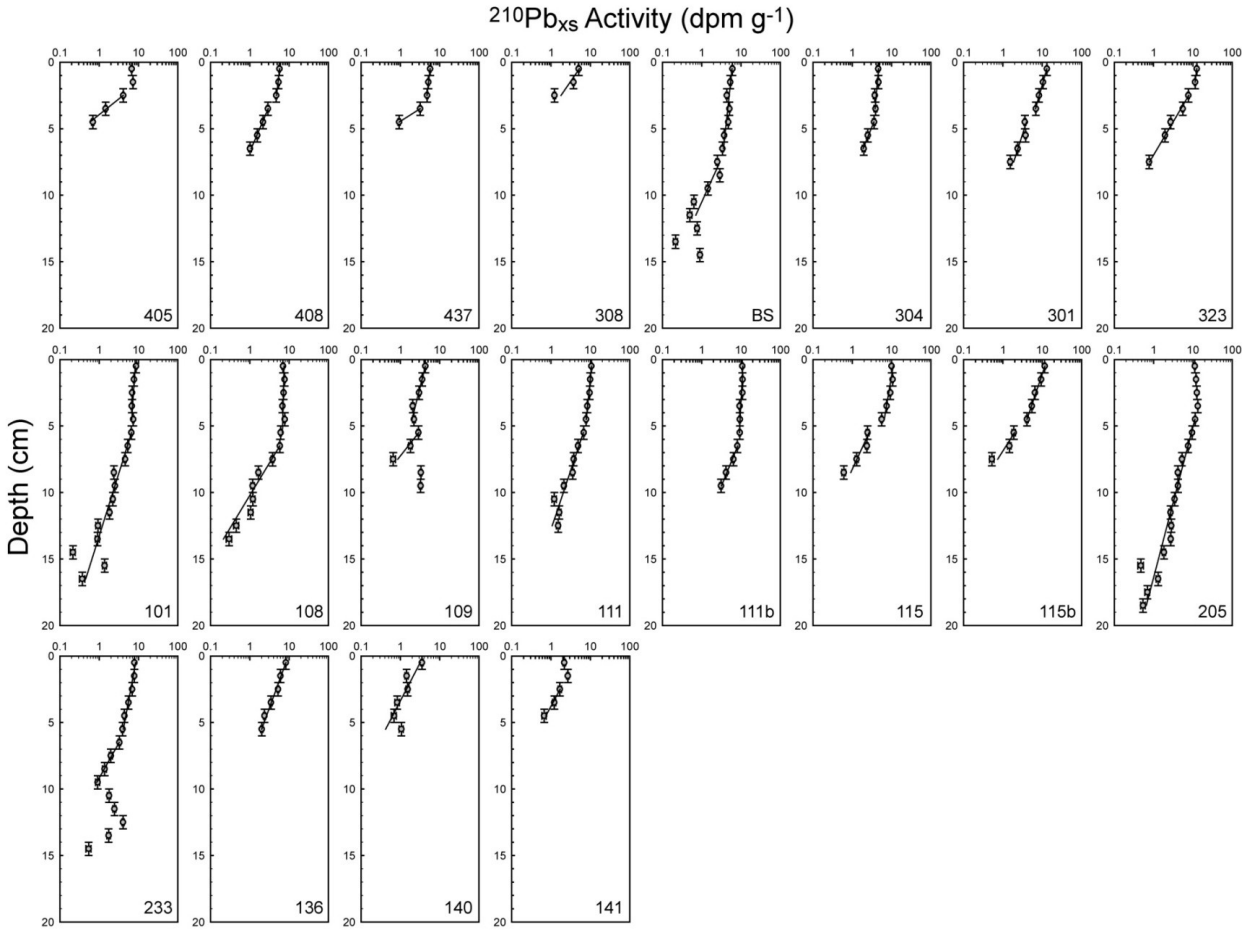

Appendix 2.4: $^{210}Pb_{xs}$ activity-depth distributions. Horizontal error bars represent standard deviations of net peak areas (1 σ) from gamma counting of radionuclides. Vertical error bars represent the thickness of analyzed sediment sections. Solid lines indicate regression results of fitting Eq. 5 and/or 8 to $^{210}Pb_{xs}$ activity-depth distributions.

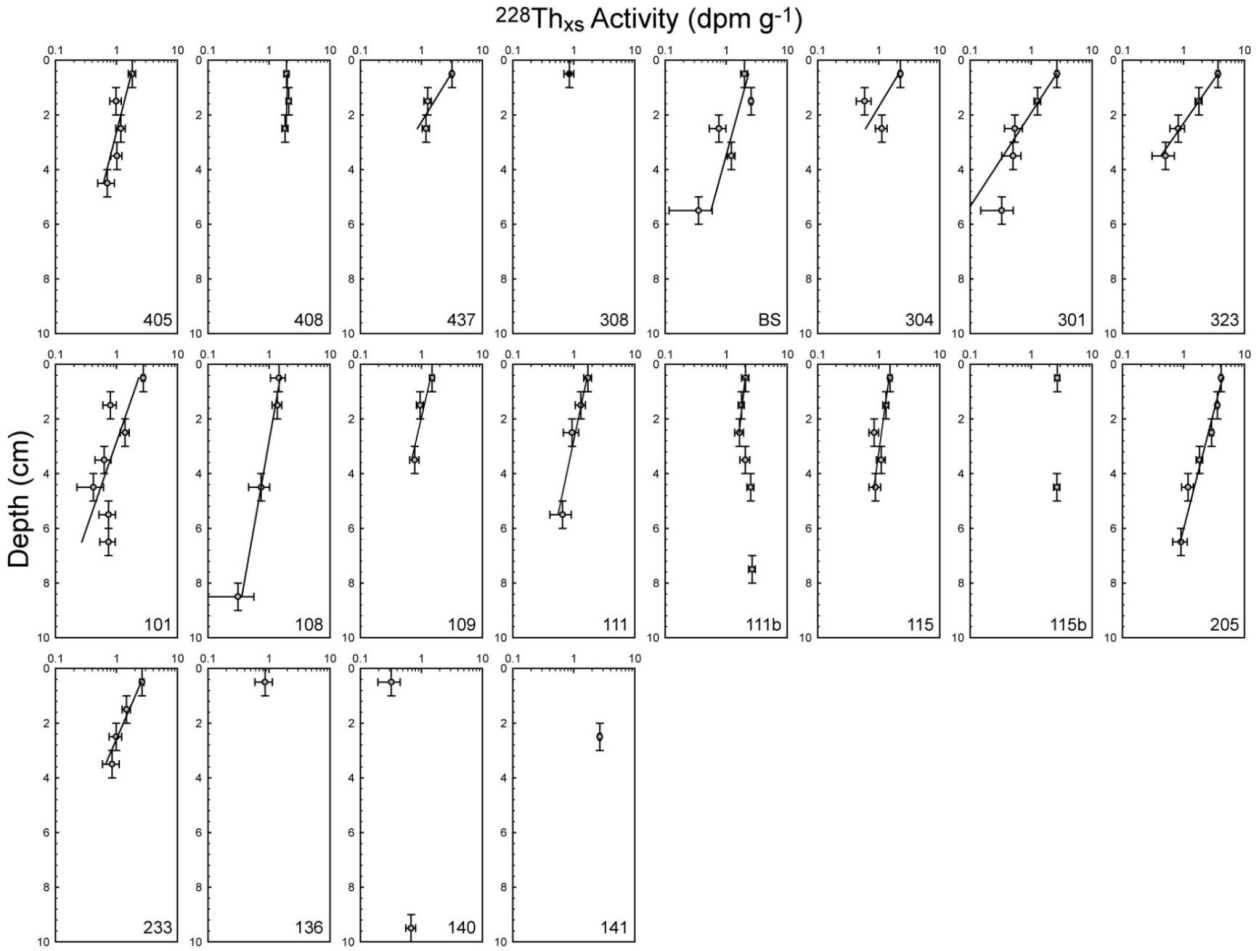

Appendix 2.5: $^{228}Th_{xs}$ activity-depth distributions. Horizontal error bars represent standard deviations of net peak areas (1 σ) from gamma counting of radionuclides. Vertical error bars represent the thickness of analyzed sediment sections. Solid lines indicate regression results of fitting Eq. 5 to $^{228}Th_{xs}$ activity-depth distributions.

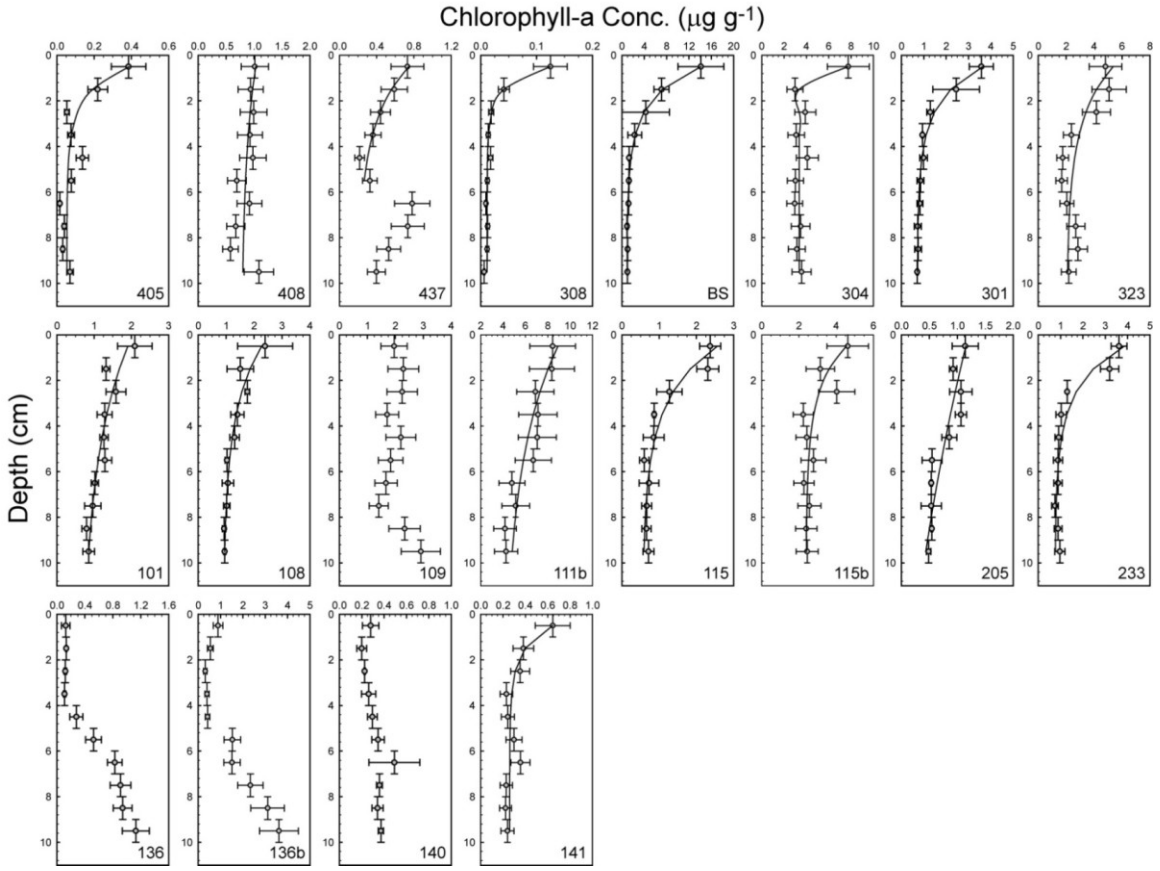

Appendix 2.6: Chlorophyll-a concentration-depth distributions. Horizontal error bars represent standard deviations (1 σ) of triplicate measurements of all sediment samples provided by H. Link and P. Archambault (ISMER-UQAR, Rimouski, CA) and approximately 40 % of the sediment samples collected in 2009. Vertical error bars represent the thickness of analyzed sediment sections. Solid lines indicate regression results of fitting Eq. 6 to chlorophyll-a concentration-depth distributions.

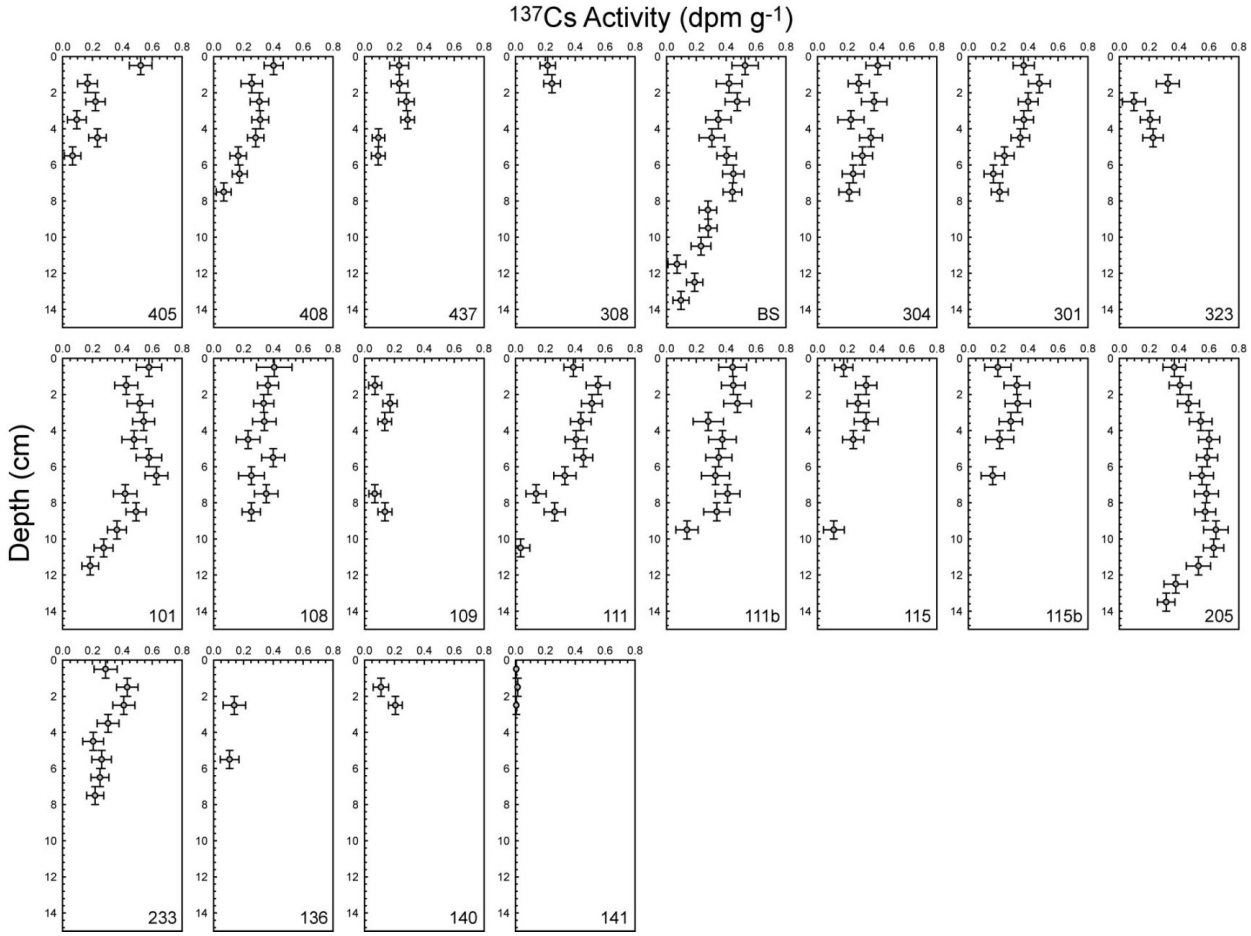

Appendix 2.7: ^{137}Cs activity-depth distributions. Horizontal error bars represent standard deviations of net peak areas (1 σ) from gamma counting of radionuclides. Vertical error bar represent the thickness of analyzed sediment sections.

Appendix 2.8: Pearson and Spearman correlation coefficients (r_p, r_s) of relationships between bioturbation proxies and environmental variables. Significant correlations with $p \leq 0.1$ are highlighted in gray.

	Db_Pb				Db_Th				Db_Chl-a			
Environmental	Pearson		Spearman		Pearson		Spearman		Pearson		Spearman	
Variable	r_p	p	r_s	p	r_p	p	r_s	p	r_p	p	r_s	p
depth	-0.147	0.600	-0.304	0.271	-0.01	0.98	-0.29	0.35	0.066	0.877	0.262	0.531
salinity	-0.129	0.646	-0.077	0.785	-0.16	0.62	-0.06	0.84	-0.503	0.204	-0.630	0.094
temperature	-0.429	0.110	-0.557	0.031	-0.46	0.13	-0.59	0.045	-0.398	0.329	-0.333	0.420
TOC	0.785	0.007	0.745	0.013	0.44	0.28	0.00	1.00	0.793	0.207	0.800	0.200
chl	0.492	0.074	0.530	0.051	0.54	0.090	-0.04	0.92	0.020	0.963	0.524	0.183
TOC_mar	0.755	0.012	0.697	0.025	0.41	0.31	0.02	0.96	0.913	0.087	0.800	0.200
TOC_terr	0.647	0.043	0.830	0.003	0.42	0.30	0.19	0.65	0.410	0.590	0.600	0.400
chlTOC_ratio	0.402	0.250	0.430	0.214	0.49	0.22	0.07	0.87	0.616	0.384	0.800	0.200
clay	-0.484	0.068	-0.539	0.038	-0.31	0.32	-0.28	0.38	-0.656	0.078	-0.833	0.010
silt	0.488	0.065	0.668	0.007	0.26	0.41	0.20	0.53	0.299	0.472	0.381	0.352
sand	-0.165	0.558	-0.225	0.420	-0.07	0.82	-0.08	0.80	0.176	0.677	0.429	0.289
IRD	-0.380	0.163	-0.515	0.049	-0.19	0.55	-0.32	0.31	-0.481	0.228	-0.476	0.233
skewness	-0.231	0.407	-0.218	0.435	-0.15	0.63	-0.20	0.53	-0.675	0.066	-0.714	0.047
sorting	-0.524	0.045	-0.600	0.018	-0.29	0.36	-0.17	0.60	-0.191	0.651	-0.143	0.736
w_Pb	0.400	0.198	0.481	0.114	0.06	0.85	0.01	0.97	0.131	0.780	0.243	0.599
w_Cs	0.333	0.266	0.649	0.016	-0.03	0.94	0.24	0.45	0.013	0.975	0.158	0.709

	Lb_Pb				zp_Th				zp_Chl-a			
Environmental	Pearson		Spearman		Pearson		Spearman		Pearson		Spearman	
Variable	r_p	p	r_s	p	r_p	p	r_s	p	r_p	p	r_s	p
depth	0.057	0.811	0.056	0.815	0.115	0.628	0.154	0.516	-0.100	0.733	0.031	0.915
salinity	-0.518	0.019	-0.541	0.014	-0.348	0.132	-0.372	0.106	-0.292	0.311	-0.361	0.205
temperature	-0.207	0.382	-0.313	0.179	-0.538	0.014	-0.603	0.005	-0.323	0.260	-0.333	0.244
TOC	0.380	0.180	0.281	0.330	0.592	0.026	0.571	0.033	0.558	0.094	0.378	0.282
chl	0.428	0.068	0.326	0.173	0.430	0.066	0.539	0.017	0.194	0.506	0.172	0.556
TOC_mar	0.424	0.130	0.359	0.207	0.575	0.032	0.585	0.028	0.473	0.168	0.302	0.396
TOC_terr	0.161	0.582	-0.007	0.982	0.462	0.096	0.345	0.227	0.702	0.024	0.472	0.168
chlTOC_ratio	0.216	0.457	0.272	0.346	0.380	0.180	0.475	0.086	0.140	0.699	0.157	0.664
clay	-0.435	0.055	-0.460	0.041	-0.627	0.003	-0.615	0.004	-0.495	0.072	-0.517	0.058
silt	0.335	0.149	0.209	0.376	0.465	0.039	0.593	0.006	0.334	0.243	0.378	0.183
sand	-0.045	0.850	0.243	0.302	-0.064	0.788	-0.040	0.866	0.011	0.969	0.183	0.530
IRD	-0.298	0.203	-0.302	0.196	-0.326	0.161	-0.188	0.427	-0.436	0.119	-0.430	0.125
skewness	-0.283	0.227	-0.331	0.154	-0.437	0.054	-0.370	0.108	-0.451	0.106	-0.371	0.191
sorting	-0.236	0.317	-0.130	0.584	-0.543	0.013	-0.634	0.003	-0.321	0.264	-0.374	0.188
w_Pb	0.278	0.279	0.213	0.413	0.450	0.070	0.482	0.050	0.382	0.198	0.501	0.081
w_Cs	0.251	0.316	0.208	0.408	0.404	0.097	0.403	0.098	0.289	0.316	0.506	0.065

	Diameter top				Diameter entire core				Type top			
Environmental	Pearson		Spearman		Pearson		Spearman		Pearson		Spearman	
Variable	r_p	p	r_s	p	r_p	p	r_s	p	r_p	p	r_s	p
depth	0.193	0.402	0.339	0.133	-0.102	0.661	-0.218	0.342	0.152	0.511	0.192	0.405
salinity	0.204	0.375	0.220	0.337	0.348	0.123	0.240	0.294	-0.059	0.798	-0.045	0.846
temperature	-0.300	0.186	-0.214	0.352	-0.339	0.133	-0.485	0.026	-0.378	0.091	-0.453	0.039
TOC	0.153	0.586	0.082	0.771	-0.075	0.789	0.004	0.990	0.076	0.788	0.031	0.913
chl	-0.255	0.278	-0.263	0.264	-0.060	0.802	-0.078	0.743	-0.105	0.660	0.000	1.000
TOC_mar	0.064	0.821	-0.034	0.904	-0.177	0.527	-0.082	0.771	0.027	0.924	0.124	0.660
TOC_terr	0.322	0.242	0.234	0.401	0.188	0.502	0.211	0.451	0.171	0.542	0.031	0.913
chlTOC_ratio	-0.322	0.242	-0.220	0.431	-0.422	0.117	-0.350	0.201	0.184	0.511	0.278	0.315
clay	0.111	0.631	0.203	0.377	0.265	0.245	0.247	0.281	-0.068	0.771	0.057	0.806
silt	0.184	0.424	-0.092	0.693	0.203	0.377	0.198	0.389	-0.028	0.903	-0.105	0.651
sand	-0.264	0.247	-0.081	0.726	-0.393	0.078	-0.487	0.025	0.090	0.697	0.144	0.535
IRD	-0.079	0.733	0.041	0.861	0.019	0.936	0.012	0.960	-0.316	0.163	-0.332	0.141
skewness	0.199	0.386	0.027	0.909	0.369	0.100	0.312	0.168	-0.122	0.598	-0.158	0.493
sorting	-0.214	0.351	0.008	0.973	-0.349	0.121	-0.348	0.123	0.145	0.532	0.233	0.310
w_Pb	-0.047	0.859	-0.177	0.497	-0.101	0.698	-0.025	0.923	0.039	0.882	-0.054	0.838
w_Cs	0.076	0.765	-0.037	0.884	0.395	0.105	0.393	0.106	0.110	0.664	0.039	0.879

Appendix 2.8 continued.

	Type entire				Tiers			
Environmental	Pearson		Spearman		Pearson		Spearman	
Variable	r_p	p	r_s	p	r_p	p	r_s	p
depth	0.217	0.345	0.279	0.221	0.089	0.700	0.074	0.751
salinity	0.058	0.802	0.043	0.854	-0.020	0.933	0.033	0.886
temperature	-0.152	0.511	-0.165	0.474	-0.396	0.075	-0.393	0.078
TOC	0.157	0.576	0.093	0.741	0.264	0.341	0.180	0.520
chl	-0.017	0.943	-0.006	0.979	0.234	0.321	0.188	0.429
TOC_mar	0.069	0.806	0.149	0.596	0.191	0.496	0.199	0.476
TOC_terr	0.321	0.244	0.169	0.546	0.363	0.183	0.237	0.394
chlTOC_ratio	0.070	0.804	0.145	0.606	0.256	0.358	0.228	0.414
clay	0.095	0.683	0.162	0.484	-0.006	0.978	0.067	0.772
silt	0.111	0.632	-0.026	0.910	0.271	0.235	0.187	0.418
sand	-0.179	0.438	-0.035	0.882	-0.268	0.241	-0.245	0.284
IRD	-0.236	0.303	-0.306	0.178	-0.151	0.513	-0.241	0.293
skewness	0.099	0.669	0.077	0.741	0.144	0.532	0.178	0.440
sorting	0.059	0.799	0.176	0.445	-0.150	0.516	-0.056	0.808
w_Pb	0.095	0.716	0.097	0.711	0.228	0.380	0.206	0.428
w_Cs	0.118	0.641	0.142	0.575	0.199	0.428	0.232	0.355

Appendix 2.9: Pearson and Spearman correlation coefficients (rp, rs) of relationships environmental variables. Significant correlations with p ≤ 0.1 are highlighted in gray.

	depth				salinity				temperature			
Environmental	Pearson		Spearman		Pearson		Spearman		Pearson		Spearman	
Variable	r_p	p	r_s	p	r_p	p	r_s	p	r_p	p	r_s	p
depth					-0.358	0.112	-0.360	0.108	0.278	0.222	0.260	0.256
salinity	-0.358	0.112	-0.360	0.108					-0.095	0.684	0.060	0.796
temperature	0.278	0.222	0.260	0.256	-0.095	0.684	0.060	0.796				
TOC	0.023	0.936	0.079	0.781	-0.206	0.462	-0.209	0.454	-0.532	0.041	-0.368	0.177
chl	-0.021	0.931	0.071	0.767	-0.380	0.099	-0.499	0.025	-0.341	0.141	-0.364	0.115
TOC_mar	0.123	0.663	0.229	0.413	-0.398	0.141	-0.419	0.120	-0.464	0.081	-0.414	0.125
TOC_terr	-0.221	0.428	-0.289	0.296	0.311	0.260	0.384	0.158	-0.543	0.036	-0.336	0.221
chlTOC_ratio	0.327	0.234	0.386	0.156	-0.611	0.015	-0.698	0.004	-0.129	0.646	-0.296	0.283
clay	-0.133	0.565	-0.091	0.695	0.788	0.000	0.681	0.001	0.182	0.431	0.249	0.276
silt	0.074	0.750	-0.032	0.889	-0.151	0.515	-0.280	0.218	-0.323	0.154	-0.421	0.058
sand	0.015	0.947	0.244	0.286	-0.393	0.078	-0.541	0.011	0.201	0.381	0.297	0.190
IRD	0.226	0.324	0.365	0.104	0.261	0.253	-0.060	0.796	0.082	0.723	0.253	0.269
skewness	-0.201	0.382	-0.281	0.218	0.658	0.001	0.621	0.003	0.063	0.788	0.077	0.741
sorting	-0.040	0.862	0.040	0.862	0.067	0.772	0.140	0.544	0.447	0.042	0.432	0.050
w_Pb	0.114	0.663	0.074	0.777	-0.493	0.044	-0.446	0.073	-0.161	0.538	-0.172	0.509
w_Cs	-0.153	0.543	-0.314	0.204	-0.115	0.650	0.000	1.000	-0.484	0.042	-0.443	0.065

	TOC				chl				TOC_mar			
Environmental	Pearson		Spearman		Pearson		Spearman		Pearson		Spearman	
Variable	r_p	p	r_s	p	r_p	p	r_s	p	r_p	p	r_s	p
depth	0.023	0.936	0.079	0.781	-0.021	0.931	0.071	0.767	0.123	0.663	0.229	0.413
salinity	-0.206	0.462	-0.209	0.454	-0.380	0.099	-0.499	0.025	-0.398	0.141	-0.419	0.120
temperature	-0.532	0.041	-0.368	0.177	-0.341	0.141	-0.364	0.115	-0.464	0.081	-0.414	0.125
TOC					0.737	0.002	0.789	0.000	0.967	0.000	0.946	0.000
chl	0.737	0.002	0.789	0.000					0.796	0.000	0.871	0.000
TOC_mar	0.967	0.000	0.946	0.000	0.796	0.000	0.871	0.000				
TOC_terr	0.794	0.000	0.775	0.001	0.386	0.155	0.393	0.147	0.612	0.015	0.589	0.021
chlTOC_ratio	0.439	0.102	0.511	0.052	0.881	0.000	0.911	0.000	0.541	0.037	0.636	0.011
clay	-0.646	0.009	-0.650	0.009	-0.536	0.015	-0.702	0.001	-0.741	0.002	-0.768	0.001
silt	0.757	0.001	0.793	0.000	0.546	0.013	0.663	0.001	0.728	0.002	0.825	0.000
sand	-0.361	0.187	-0.182	0.516	-0.200	0.398	-0.063	0.791	-0.266	0.337	-0.086	0.761
IRD	-0.472	0.076	-0.531	0.042	-0.167	0.481	-0.065	0.784	-0.429	0.110	-0.422	0.117
skewness	-0.277	0.318	-0.261	0.348	-0.201	0.396	-0.328	0.158	-0.365	0.181	-0.368	0.177
sorting	-0.767	0.001	-0.771	0.001	-0.573	0.008	-0.589	0.006	-0.732	0.002	-0.764	0.001
w_Pb	0.423	0.171	0.527	0.079	0.183	0.498	0.295	0.268	0.464	0.129	0.640	0.025
w_Cs	0.140	0.649	0.199	0.515	0.068	0.797	0.006	0.981	0.111	0.718	0.216	0.478

	TOC_terr				chlTOC_ratio				clay			
Environmental	Pearson		Spearman		Pearson		Spearman		Pearson		Spearman	
Variable	r_p	p	r_s	p	r_p	p	r_s	p	r_p	p	r_s	p
depth	-0.221	0.428	-0.289	0.296	0.327	0.234	0.386	0.156	-0.133	0.565	-0.091	0.695
salinity	0.311	0.260	0.384	0.158	-0.611	0.015	-0.698	0.004	0.788	0.000	0.681	0.001
temperature	-0.543	0.036	-0.336	0.221	-0.129	0.646	-0.296	0.283	0.182	0.431	0.249	0.276
TOC	0.794	0.000	0.775	0.001	0.439	0.102	0.511	0.052	-0.646	0.009	-0.650	0.009
chl	0.386	0.155	0.393	0.147	0.881	0.000	0.911	0.000	-0.536	0.015	-0.702	0.001
TOC_mar	0.612	0.015	0.589	0.021	0.541	0.037	0.636	0.011	-0.741	0.002	-0.768	0.001
TOC_terr					0.071	0.802	0.068	0.810	-0.236	0.396	-0.157	0.576
chlTOC_ratio	0.071	0.802	0.068	0.810					-0.650	0.009	-0.754	0.001
clay	-0.236	0.396	-0.157	0.576	-0.650	0.009	-0.754	0.001				
silt	0.610	0.016	0.593	0.020	0.100	0.722	0.368	0.177	-0.454	0.039	-0.642	0.002
sand	-0.482	0.069	-0.475	0.074	0.342	0.212	0.321	0.243	-0.193	0.403	-0.236	0.302
IRD	-0.438	0.103	-0.676	0.006	-0.197	0.481	0.002	0.995	0.565	0.008	0.285	0.211
skewness	0.011	0.968	0.093	0.742	-0.637	0.011	-0.661	0.007	0.713	0.000	0.608	0.003
sorting	-0.634	0.011	-0.629	0.012	-0.101	0.719	-0.264	0.341	0.417	0.060	0.583	0.006
w_Pb	0.172	0.593	0.170	0.598	0.033	0.918	0.233	0.466	-0.629	0.007	-0.597	0.011
w_Cs	0.164	0.593	0.432	0.140	-0.389	0.189	-0.307	0.308	-0.200	0.427	-0.149	0.556

Appendix 2.9 continued.

Environmental Variable	silt Pearson r_p	silt Pearson p	silt Spearman r_s	silt Spearman p	sand Pearson r_p	sand Pearson p	sand Spearman r_s	sand Spearman p	IRD Pearson r_p	IRD Pearson p	IRD Spearman r_s	IRD Spearman p
depth	0.074	0.750	-0.032	0.889	0.015	0.947	0.244	0.286	0.226	0.324	0.365	0.104
salinity	-0.151	0.515	-0.280	0.218	-0.393	0.078	-0.541	0.011	0.261	0.253	-0.060	0.796
temperature	-0.323	0.154	-0.421	0.058	0.201	0.381	0.297	0.190	0.082	0.723	0.253	0.269
TOC	0.757	0.001	0.793	0.000	-0.361	0.187	-0.182	0.516	-0.472	0.076	-0.531	0.042
chl	0.546	0.013	0.663	0.001	-0.200	0.398	-0.063	0.791	-0.167	0.481	-0.065	0.784
TOC_mar	0.728	0.002	0.825	0.000	-0.266	0.337	-0.086	0.761	-0.429	0.110	-0.422	0.117
TOC_terr	0.610	0.016	0.593	0.020	-0.482	0.069	-0.475	0.074	-0.438	0.103	-0.676	0.006
chlTOC_ratio	0.100	0.722	0.368	0.177	0.342	0.212	0.321	0.243	-0.197	0.481	0.002	0.995
clay	-0.454	0.039	-0.642	0.002	-0.193	0.403	-0.236	0.302	0.565	0.008	0.285	0.211
silt					-0.785	0.000	-0.505	0.019	-0.355	0.115	-0.389	0.081
sand	-0.785	0.000	-0.505	0.019					0.009	0.970	0.156	0.500
IRD	-0.355	0.115	-0.389	0.081	0.009	0.970	0.156	0.500				
skewness	0.212	0.357	0.103	0.658	-0.733	0.000	-0.812	0.000	0.278	0.222	-0.084	0.718
sorting	-0.950	0.000	-0.942	0.000	0.754	0.000	0.590	0.005	0.215	0.350	0.287	0.208
w_Pb	0.561	0.019	0.758	0.000	-0.293	0.253	-0.202	0.437	-0.118	0.652	-0.237	0.360
w_Cs	0.462	0.054	0.618	0.006	-0.369	0.132	-0.384	0.116	-0.125	0.622	-0.246	0.324

Environmental Variable	skewness Pearson r_p	skewness Pearson p	skewness Spearman r_s	skewness Spearman p	sorting Pearson r_p	sorting Pearson p	sorting Spearman r_s	sorting Spearman p	w_Pb Pearson r_p	w_Pb Pearson p	w_Pb Spearman r_s	w_Pb Spearman p
depth	-0.201	0.382	-0.281	0.218	-0.040	0.862	0.040	0.862	0.114	0.663	0.074	0.777
salinity	0.658	0.001	0.621	0.003	0.067	0.772	0.140	0.544	-0.493	0.044	-0.446	0.073
temperature	0.063	0.788	0.077	0.741	0.447	0.042	0.432	0.050	-0.161	0.538	-0.172	0.509
TOC	-0.277	0.318	-0.261	0.348	-0.767	0.001	-0.771	0.001	0.423	0.171	0.527	0.079
chl	-0.201	0.396	-0.328	0.158	-0.573	0.008	-0.589	0.006	0.183	0.498	0.295	0.268
TOC_mar	-0.365	0.181	-0.368	0.177	-0.732	0.002	-0.764	0.001	0.464	0.129	0.640	0.025
TOC_terr	0.011	0.968	0.093	0.742	-0.634	0.011	-0.629	0.012	0.172	0.593	0.170	0.598
chlTOC_ratio	-0.637	0.011	-0.661	0.007	-0.101	0.719	-0.264	0.341	0.033	0.918	0.233	0.466
clay	0.713	0.000	0.608	0.003	0.417	0.060	0.583	0.006	-0.629	0.007	-0.597	0.011
silt	0.212	0.357	0.103	0.658	-0.950	0.000	-0.942	0.000	0.561	0.019	0.758	0.000
sand	-0.733	0.000	-0.812	0.000	0.754	0.000	0.590	0.005	-0.293	0.253	-0.202	0.437
IRD	0.278	0.222	-0.084	0.718	0.215	0.350	0.287	0.208	-0.118	0.652	-0.237	0.360
skewness					-0.177	0.442	-0.134	0.563	-0.007	0.978	0.016	0.951
sorting	-0.177	0.442	-0.134	0.563					-0.519	0.033	-0.606	0.010
w_Pb	-0.007	0.978	0.016	0.951	-0.519	0.033	-0.606	0.010				
w_Cs	0.211	0.400	0.296	0.232	-0.469	0.050	-0.564	0.015	0.688	0.002	0.628	0.007

Environmental Variable	w_Cs Pearson r_p	w_Cs Pearson p	w_Cs Spearman r_s	w_Cs Spearman p
depth	-0.153	0.543	-0.314	0.204
salinity	-0.115	0.650	0.000	1.000
temperature	-0.484	0.042	-0.443	0.065
TOC	0.140	0.649	0.199	0.515
chl	0.068	0.797	0.006	0.981
TOC_mar	0.111	0.718	0.216	0.478
TOC_terr	0.164	0.593	0.432	0.140
chlTOC_ratio	-0.389	0.189	-0.307	0.308
clay	-0.200	0.427	-0.149	0.556
silt	0.462	0.054	0.618	0.006
sand	-0.369	0.132	-0.384	0.116
IRD	-0.125	0.622	-0.246	0.324
skewness	0.211	0.400	0.296	0.232
sorting	-0.469	0.050	-0.564	0.015
w_Pb	0.688	0.002	0.628	0.007
w_Cs				

Appendix Chapter 3

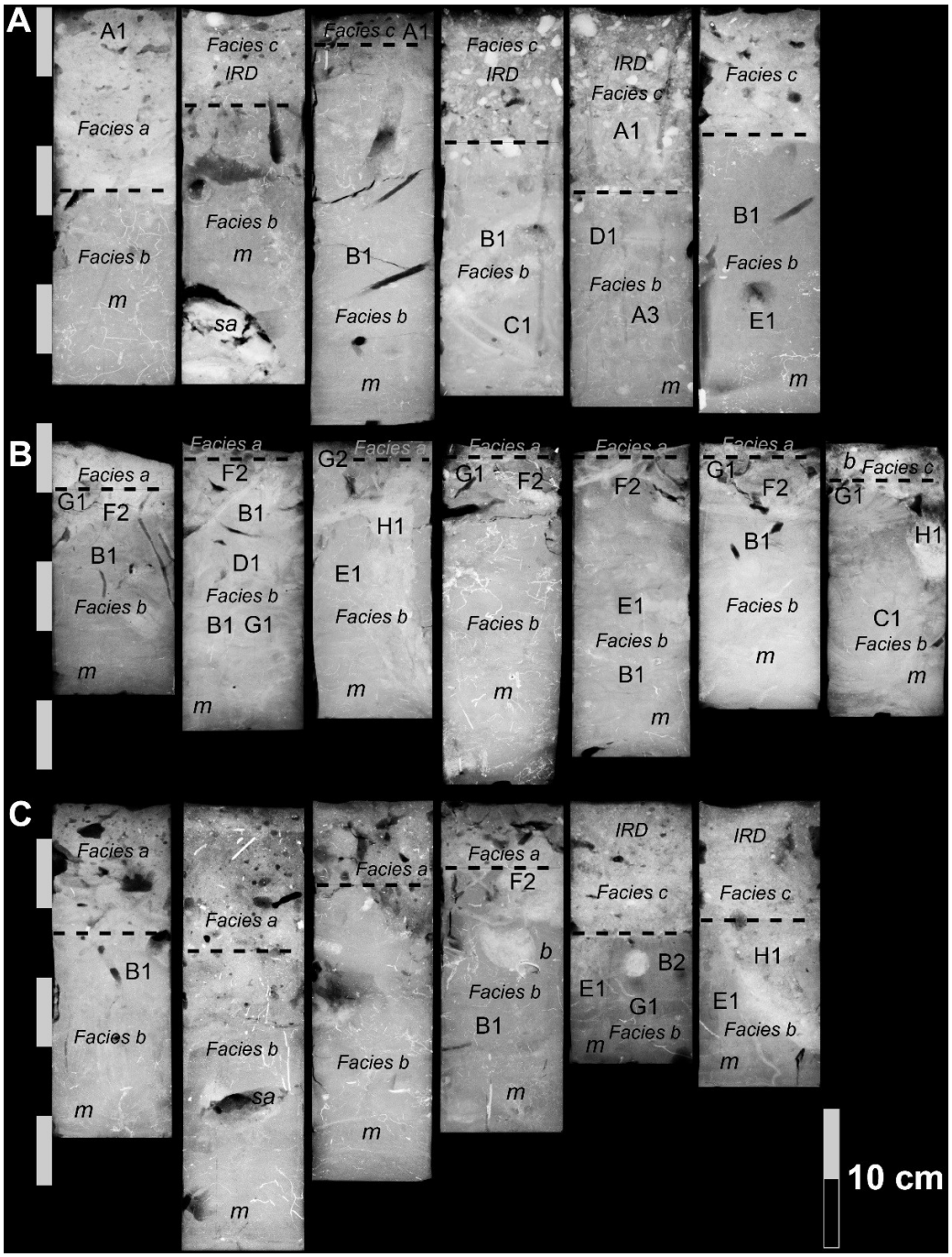

Appendix 3.1: X-radiograph negatives collected in Gulf of Maine basins and shelf, slope and rise localities of the Scotian Shelf region. A: CB1_01, 02, 03 and CB2_01, 02, 03; B: GB2_01, 01_d, 02, 03, 04, 05, 06; C:

GB3_01, 02, 03, 04, 05, 06. Abbreviations: Capital letters and numbers correspond to bioturbation structure groups, IRD=ice-rafted debris clast, m=mineralized structures, sa=sampling artifact, b=bivalve/shell, g=gastropod/shell, l=sedimentary layering. Dashed vertical lines indicate discontinuity contacts of sedimentary facies.

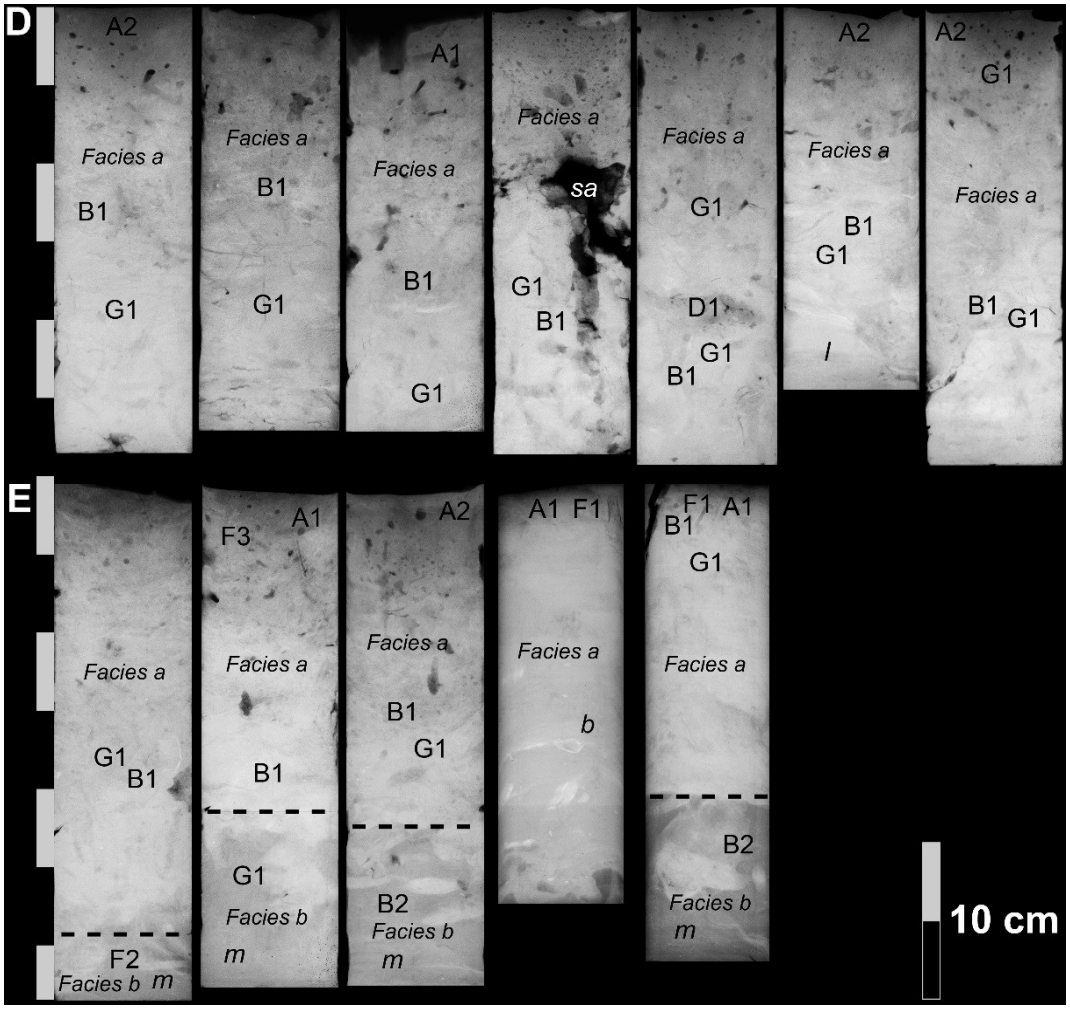

Appendix 3.1 continued: D: RB1_01, 02, 03, 04, 04_d, 05, 06; E: RB2_01, 02, 03, 04, 05.

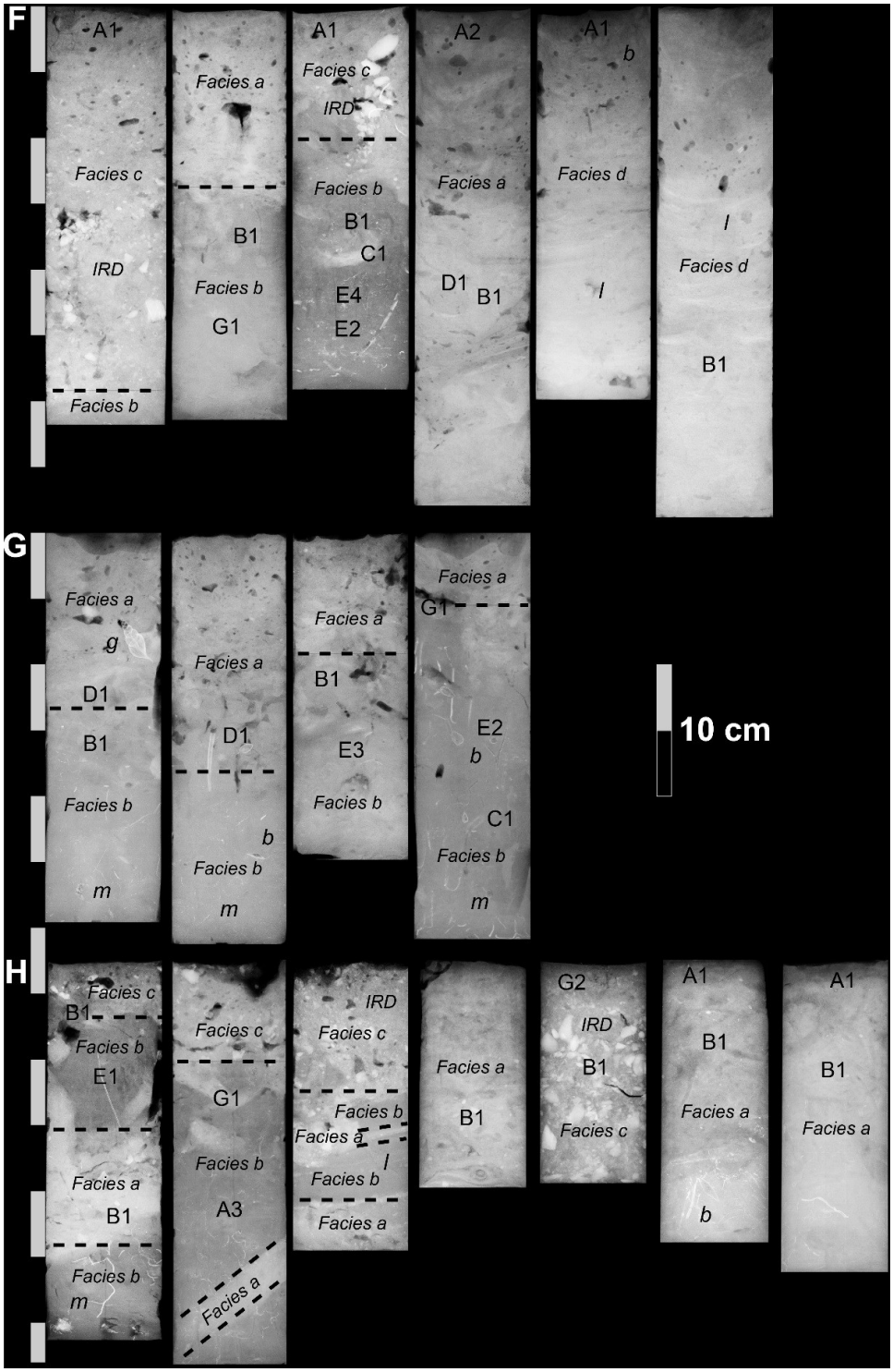

Appendix 3.1 continued: F: JB3_01, 02, 03, 04, 05, 06; G: JB4_01, 01_d, 02, 03; H: JB5_01, 02, 03, JB6_01, 03 and JB7_01, 03.

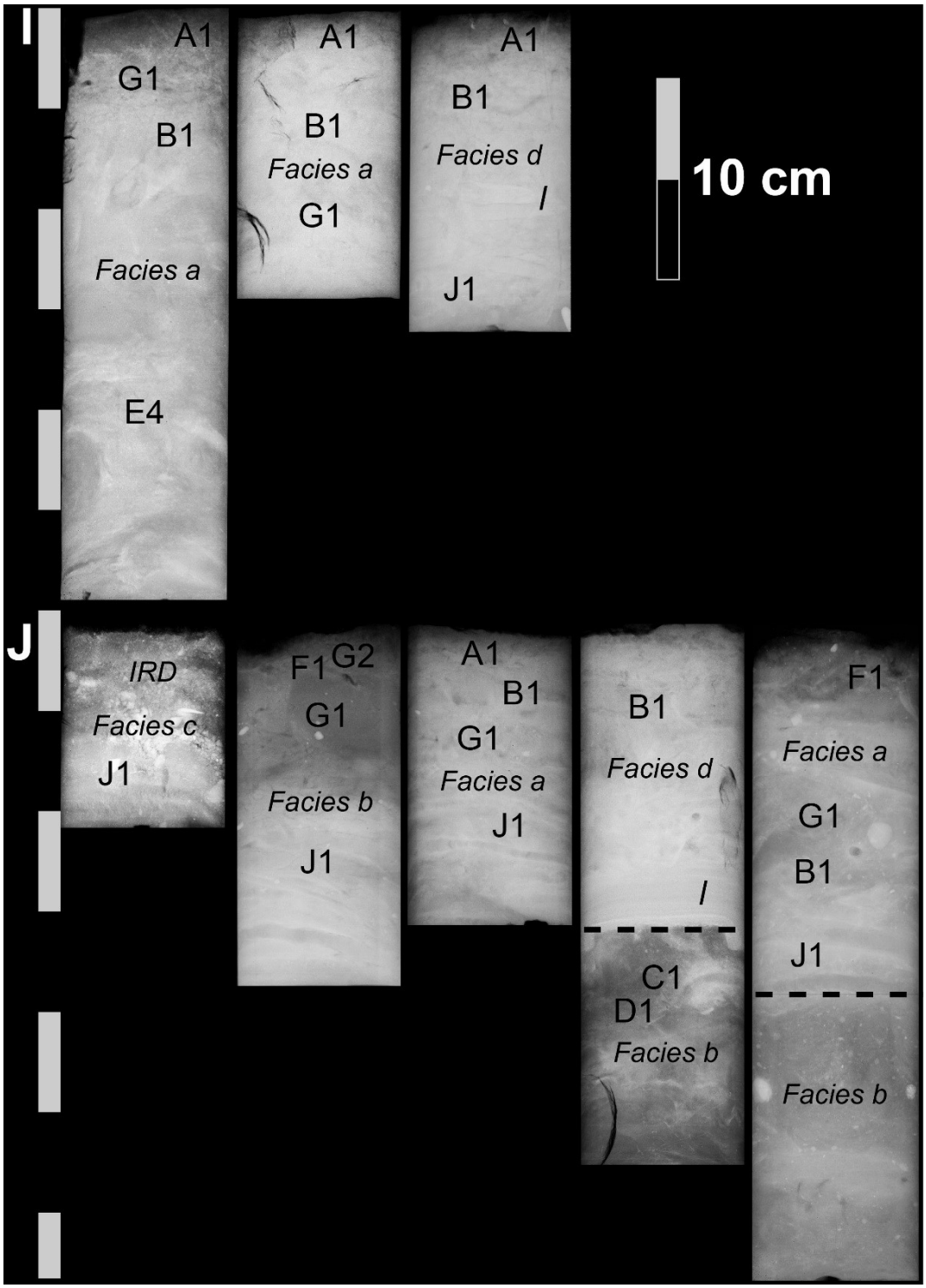

Appendix 3.1 continued: I: NEC3_03, NEC6_04, 06; J: NEF4_01, 03, NEF6_01, 03, 04

Appendix 3.2: Sedimentary facies and bioturbation structure groups identified in X-radiographs collected in Gulf of Maine basins and shelf, slope and rise localities of the Scotian Shelf region. Fields highlighted in grey with the number 1 indicate the occurrence of a bioturbation structure or biogenic component. Fields with the number 0 indicate the absence of a bioturbation structure or biogenic component.

		Sedimentary facies			Bioturbation structure group									Other biogenic components		
Region	Station	Facies	Facies contact description	Depth of contact (cm)	A	B	C	D	E	F	G	H	J	mb	b	g
Crowell Basin	CB1_01	a	sharp	13	1	0	0	0	0	0	0	0	0	0	0	0
		b			0	0	0	0	0	0	0	0	0	1	0	0
	CB1_02	c	sharp	6	0	0	0	0	0	0	0	0	0	0	0	0
		b			0	0	0	0	0	0	0	0	0	1	0	0
	CB1_03	c	sharp	3	1	0	0	0	0	0	0	0	0	0	0	0
		b			0	1	0	0	0	0	0	0	0	1	0	0
	CB2_01	c	sharp	10	0	0	0	0	0	0	0	0	0	0	0	0
		b			0	1	1	0	0	0	0	0	0	0	0	0
	CB2_02	c	sharp	14	1	0	0	0	0	0	0	0	0	0	0	0
		b			1	0	0	1	0	0	0	0	0	1	0	0
	CB2_03	c	sharp	9	0	0	0	0	0	0	0	0	0	0	0	0
		b			0	1	0	0	1	0	0	0	0	1	0	0
Georges Basin	GB2_01	a	bioturbated	4	0	0	0	0	0	0	0	0	0	0	0	0
		b			0	1	0	0	0	1	1	0	0	1	0	0
	GB2_01_d	a	bioturbated	1	0	0	0	0	0	0	0	0	0	0	0	0
		b			0	1	0	1	0	1	1	0	0	1	0	0
	GB2_02	a	bioturbated	2	0	0	0	0	0	0	1	0	0	0	0	0
		b			0	0	0	0	1	0	1	1	0	1	0	0
	GB2_03	a	bioturbated	1	0	0	0	0	0	0	0	0	0	0	0	0
		b			0	0	0	0	0	1	1	0	0	1	0	0
	GB2_04	a	bioturbated	1	0	0	0	0	0	0	0	0	0	0	0	0
		b			0	1	0	0	1	1	0	0	0	1	0	0
	GB2_05	a	bioturbated	1	0	0	0	0	0	0	0	0	0	0	0	0
		b			0	1	0	0	0	1	1	0	0	1	0	0
	GB2_06	c	bioturbated	3	0	0	0	0	0	0	0	0	0	0	0	0
		b			0	0	1	0	0	0	1	1	0	1	1	0
	GB3_01	a	sharp	9	0	0	0	0	0	0	0	0	0	0	0	0
		b			0	1	0	0	0	0	0	0	0	1	0	0
	GB3_02	a	sharp	10	0	0	0	0	0	0	0	0	0	0	0	0
		b			0	0	0	0	0	0	0	0	0	1	0	0
	GB3_03	a	sharp	6	0	0	0	0	0	0	0	0	0	0	0	0
		b			0	0	0	0	0	0	0	0	0	1	0	0
	GB3_04	a	bioturbated	5	0	0	0	0	0	0	0	0	0	0	0	0
		b			0	1	0	0	0	1	0	0	0	1	1	0
	GB3_05	c	bioturbated	9	0	0	0	0	0	0	0	0	0	0	0	0
		b			0	1	0	0	1	0	1	0	0	1	0	0
	GB3_06	c	bioturbated	8	0	0	0	0	0	0	0	0	0	0	0	0
		b			0	0	0	0	1	0	0	1	0	1	0	0
Jordan Basin	JB3_01	c	sharp	29	1	0	0	0	0	0	0	0	0	0	0	0
		b			0	0	0	0	0	0	0	0	0	0	0	0
	JB3_02	a	diffuse	14	0	0	0	0	0	0	0	0	0	0	0	0
		b			0	1	0	0	0	0	1	0	0	0	0	0
	JB3_03	c	diffuse	10	1	0	0	0	0	0	0	0	0	0	0	0
		b			0	1	1	0	1	0	0	0	0	0	0	0
	JB3_04	a			1	1	0	1	0	0	0	0	0	0	0	0
	JB3_05	d			1	0	0	0	0	0	0	0	0	0	1	0
	JB3_06	d			0	1	0	0	0	0	0	0	0	0	0	0
	JB4_01	a	diffuse	14	0	0	0	1	0	0	0	0	0	0	0	1
		b			0	1	0	0	0	0	0	0	0	1	0	0
	JB4_01_d	a	sharp	19	0	0	0	1	0	0	0	0	0	0	0	0
		b			0	0	0	0	0	0	0	0	0	1	1	0
	JB4_02	a	diffuse	9	0	0	0	0	0	0	0	0	0	0	0	0
		b			0	1	0	0	1	0	0	0	0	0	0	0
	JB4_03	a	diffuse	6	0	0	0	0	0	0	1	0	0	0	0	0
		b			0	0	1	0	1	0	1	0	0	1	1	0

Appendix 3.2 continued.

		Sedimentary facies			Bioturbation structure group									Other biogenic components		
Region	Station	Facies	Facies contact description	Depth of contact (cm)	A	B	C	D	E	F	G	H	J	mb	b	g
	JB5_01	c			0	1	0	0	0	0	0	0	0	0	0	0
		b	bioturbated, diffuse, sharp	5, 7, 28	0	1	0	0	1	0	0	0	0	0	0	0
		a			0	1	0	0	0	0	0	0	0	0	0	0
		b			0	0	0	0	0	0	0	0	0	1	0	0
	JB5_02	c			0	0	0	0	0	0	0	0	0	0	0	0
		b	bioturbated, sharp/oblique	7, 20-25	1	0	0	0	0	0	1	0	0	0	0	0
		a			0	0	0	0	0	0	0	0	0	0	0	0
	JB5_03	c			0	0	0	0	0	0	0	0	0	0	0	0
		b			0	0	0	0	0	0	0	0	0	0	0	0
		a	all sharp	10, 13, 15, 20	0	0	0	0	0	0	0	0	0	0	0	0
		b			0	0	0	0	0	0	0	0	0	0	0	0
		a			0	0	0	0	0	0	0	0	0	0	0	0
	JB6_01	a			0	1	0	0	0	0	0	0	0	0	0	0
	JB6_03	c			0	1	0	0	0	0	1	0	0	0	0	0
	JB7_01	a			1	1	0	0	0	0	0	0	0	0	1	0
	JB7_03	a			1	1	0	0	0	0	0	0	0	0	0	0
Roseway Basin	RB1_01	a			1	1	0	0	0	0	1	0	0	0	0	0
	RB1_02	a			0	1	0	0	0	0	1	0	0	0	0	0
	RB1_03	a			1	1	0	0	0	0	1	0	0	0	0	0
	RB1_04	a			0	1	0	0	0	0	1	0	0	0	0	0
	RB1_04d	a			0	1	0	1	0	0	1	0	0	0	0	0
	RB1_05	a			1	1	0	0	0	0	1	0	0	0	0	0
	RB1_06	a			1	1	0	0	0	0	1	0	0	0	0	0
	RB2_01	a	diffuse	30	0	1	0	0	0	0	1	0	0	0	0	0
		b			0	0	0	0	0	1	0	0	0	1	0	0
	RB2_02	a	diffuse	21	1	1	0	0	0	1	0	0	0	0	0	0
		b			0	0	0	0	0	0	1	0	0	1	0	0
	RB2_03	a	bioturbated	22	1	1	0	0	0	0	1	0	0	0	0	0
		b			0	1	0	0	0	0	0	0	0	1	0	0
	RB2_04	a			1	0	0	0	0	1	0	0	0	1	1	0
	RB2_05	a	bioturbated	19	1	1	0	0	0	1	1	0	0	0	0	0
		b			0	1	0	0	0	0	0	0	0	1	0	0
Northeast Channel	NEC3_03	a			1	1	0	0	1	0	1	0	0	0	0	0
	NEC6_04	a			1	1	0	0	0	0	1	0	0	0	0	0
	NEC6_06	d			1	1	0	0	0	0	0	0	1	0	0	0
Northeast Fan	NEF4_01	c			0	0	0	0	0	0	0	0	1	0	0	0
	NEF4_03	b			0	0	0	0	0	1	1	0	1	0	0	0
	NEF6_01	a			1	1	0	0	0	0	1	0	1	0	0	0
	NEF6_03	d	sharp	15	0	1	0	0	0	0	0	0	0	0	0	0
		b			0	0	1	1	0	0	0	0	0	0	0	0
	NEF6_04	a	sharp	17	0	1	0	0	0	1	1	1	0	0	0	0
		b			0	0	0	0	0	0	0	0	0	0	0	0

Appendix 3.3: Bioturbation structure groups identified in X-radiographs collected in Gulf of Maine basins and shelf, slope and rise localities of the Scotian Shelf region.

Location	Sediment core	Location in core (cm)		Group	Sub-group	Diameter (cm)	
		Min depth	Max depth			Min	Max
Crowell Basin	CB1_01	0	4.5	A	A1	0.40	0.70
	CB1_03	2	6	A	A1	0.20	0.30
		11	25	B	B1	0.10	0.30
	CB2_01	12	25	B	B1	0.30	0.40
		20	25	C	C1	0.80	0.90
	CB2_02	0	14	A	A1	0.30	0.60
			16	D	D1	0.10	0.20
		16	28	A	A3	0.10	0.20
	CB2_03		14	B	B1	0.40	0.50
		17	24	E	E1		0.10
Georges Basin	GB2_01	3	5	G	G1	0.03	0.04
		3	7	F	F2	0.30	0.50
		2.5	12	B	B1	0.20	
	GB2_01_d	5	7	B	B1	0.10	0.20
		1	7	F	F2	0.40	0.50
		8	11	D	D1		0.10
		13	18	B	B1		0.10
		11	18	G	G1	0.04	0.06
	GB2_02	0	2	G	G2	0.03	0.05
		7	12	E	E1	0.06	0.09
		0	20	H	H1	2.40	2.80
	GB2_03	1	4	G	G1	0.02	0.03
		1	5	F	F2	0.40	0.50
	GB2_04	0.5	4	F	F2	0.20	0.50
		11	16	E	E1	0.06	0.10
		16	19	B	B1	0.90	0.10
	GB2_05	1	3.5	G	G1	0.02	0.05
		1	6.5	F	F2	0.50	0.60
		7	8.5	B	B1		0.40
	GB2_06	3	6.5	G	G1	0.03	0.04
		3	9	H	H1	NA	
		13	15	C	C1	0.30	0.40
	GB3_01	9	17.5	B	B1	0.20	0.50
	GB3_04	4	9	F	F2	0.20	0.30
		16	18.5	B	B1		0.20
	GB3_05	10.5	12	B	B2		1.70
		10	14.5	E	E1		0.10
		13	17	G	G1	0.02	0.04
	GB3_06	7.5	17	H	H1	3.00	4.00
			19	E	E1		0.07
		11	20	E	E1	0.06	0.07

Appendix 3.3 continued.

Location	Sediment core	Location in core (cm)		Group	Sub-group	Diameter (cm)	
		Min depth	Max depth			Min	Max
Jordan Basin	JB3_01	0	3.5	A	A1	0.06	0.10
	JB3_02	15	20	B	B1	0.09	0.10
		17	20	B	B1	0.06	0.08
		20	28	G	G1	0.03	0.05
	JB3_03	0	2.5	A	A1	0.03	0.09
			18	C	C1		0.30
		15	19	B	B1	0.20	0.30
		15	19	B	B1	0.10	0.40
		19.5	26	E	E4	0.08	0.10
		21.5	28	E	E2	0.20	0.30
	JB3_04	0	4	A	A2	0.08	0.10
			21	D	D1		0.07
		17.5	23	B	B1	0.10	0.20
		17.5	25	B	B1	0.30	0.40
	JB3_05	0	3	A	A1	0.10	
	JB3_06	26	30.5	B	B1	0.30	0.40
	JB4_01	10	18	D	D1	0.08	0.10
			18	B	B1	0.40	0.10
	JB4_01_d		14	D	D1		0.09
	JB4_02	11	14.5	B	B1		0.50
		14.5	21.5	E	E3		0.20
	JB4_03	4.5	7.5	G	G1	0.03	0.05
		13.5	19.5	E	E2		0.10
		21	22	C	C1		0.30
		20	29	A	A4		0.10
	JB5_01	2.5	6	B	B1	0.09	0.10
		6.5	14.5	E	E1	0.07	0.08
		15.5	21.5	B	B1	0.08	0.10
	JB5_02	9	13	G	G1	0.03	0.04
		11	29	A	A3	0.09	0.10
	JB6_01	8	13.5	B	B1	0.40	0.50
		13.5	17	B	B1		0.50
	JB6_03	0	2	G	G2	0.05	0.07
		6	13.5	B	B1		0.20
	JB7_01	0	0.5	A	A1		0.04
		0	2	A	A1	0.06	0.07
		3.5	13	B	B1	0.20	0.40
	JB7_03	0	2.5	A	A1	0.04	0.07
		0	4	A	A1	0.05	0.07
		8	17	B	B1	0.20	0.30

Appendix 3.3 continued.

Location	Sediment core	Location in core (cm)		Group	Sub-group	Diameter (cm)	
		Min depth	Max depth			Min	Max
Northeast Channel	NEC3_03	0	1.5	A	A1	0.03	0.04
		3	5	G	G1	0.04	0.06
		5	10	B	B1	0.08	0.20
		17.5	24	E	E4		0.10
	NEC6_04	0	1.5	A	A1	0.05	0.10
		3	10.5	B	B1		0.20
		10.5	13.5	G	G1		0.03
	NEC6_06	0	2	A	A1		0.09
		3	5.5	B	B1	0.10	0.30
		5.5	8.5	B	B1		0.10
		8.5	15.5	J	J1		0.30
Northeast Fan	NEF4_01	7.5	10	J	J1		0.50
	NEF4_03	0	1.5	G	G2	0.03	0.04
		0	3	F	F1	0.10	0.20
		5	10	G	G1	0.03	0.04
		11.5	16.5	J	J1	0.20	0.70
	NEF6_01	0	1	A	A1		0.02
		3	4	B	B1		0.20
		4	6.5	B	B1	0.10	0.20
		6.5	8	G	G1	0.03	0.05
		8	13.5	J	J1	0.30	0.50
	NEF6_03	4	7.5	B	B1		0.30
		7.5	12	B	B1	0.30	0.40
			18	C	C1		0.60
		16.5	20.5	D	D1	0.05	0.06
	NEF6_04	0	3.5	F	F1		0.10
		6.5	8.5	G	G1	0.03	0.04
		10	14.5	B	B1		0.30
		14.5	18.5	J	J1	0.40	0.60

Appendix 3.3 continued.

Location	Sediment core	Location in core (cm)		Group	Sub-group	Diameter (cm)	
		Min depth	Max depth			Min	Max
Roseway Basin	RB1_01	0	4	A	A2		0.10
		5	16.5	B	B1	0.30	0.40
		5	16.5	B	B1	0.30	0.40
		15	26	G	G1	0.03	0.04
	RB1_02	8	13	B	B1	0.10	0.30
		13	21	B	B1		0.10
		17.5	21	G	G1	0.02	0.04
	RB1_03	0	7	A	A1		0.10
		17.5	25	B	B1	0.30	0.50
		21	25	G	G1	0.03	0.04
	RB1_04	12	21	G	G1	0.02	0.04
		15.5	28	B	B1	0.50	0.70
	RB1_04_d	9	16	G	G1	0.04	0.06
		17.5	20.5	D	D1		0.06
		20	22	G	G1	0.03	0.04
		19.5	28	B	B1	0.40	0.50
	RB1_05	0	3	A	A2	0.06	0.08
		11.5	16.5	B	B1		0.20
		16.5	21	B	B1	0.20	0.30
		16.5	21	G	G1	0.03	0.04
	RB1_06	0	3	A	A2	0.07	0.10
		3	5.5	G	G1	0.02	0.04
		18	23	G	G1	0.03	0.04
		13.5	24	B	B1		0.40
	RB2_01	19	22.5	G	G1	0.03	0.04
		15	26	B	B1	0.20	0.40
		26	31	F	F2	0.30	0.50
	RB2_02	2.5	6	F	F3	0.10	0.20
		0	6.5	A	A1		0.05
		13	18.5	B	B1	0.08	0.10
			20.5	B	B1		0.40
			24	B	B1	0.40	0.50
		26.5	29	G	G1		0.04
	RB2_03	0	1.5	A	A2		0.10
		14.5	21	B	B1	0.30	0.60
		19.5	25	G	G1		0.03
		24	29	B	B2	0.40	0.80
	RB2_04	0	2	A	A1		0.03
		0	2	F	F1		0.04
	RB2_05	0	1	A	A1		0.04
		1	3	B	B1		0.30
		0	3	F	F1	0.05	0.07
		4	7.5	G	G1		0.04
		7.5	13.5	G	G1		0.03
		24	27	B	B2		1.50

Appendix 3.4: Bioturbation structure classification and distribution of bioturbation structure types in relation to environmental patterns observed in the current study

Bioturbation structure classification

The morphologies of bioturbation structure groups A, F, C and H emphasize a stationary dwelling function and therefore can be placed within the ethological classification of dwelling traces (Bromley, 1996). The distinct linings or mantles and the occasional passive filling of some of these structures support the assumption that these structures are permanent and maintained domiciles of benthic organisms. The funnel-shaped structures of group H may further represent a combination of dwelling and resting traces of, i.e. anemones and sponges (Gingras et al., 2008).

The morphologies and active fill characteristics of bioturbation structure groups B and E and the occasionally observed branching of tunnels in group B indicate a combination of dwelling and deposit-feeding structures where animals exploit the substrate for food (e.g. Frey and Pemberton, 1985).

Bioturbation structure groups D, G and J may belong to the ethological group of feeding traces of deposit feeding organisms ingesting subsurface sediment as described in Rindsberg (2012) and Bromley (1996). The wide halo around structures of group D may indicate selective feeding where the animal preferably ingests finer grains resulting in a coarser grained substrate matrix surrounding the burrow. Structure group J further may represent systematic feeding structures similar to the trace fossil *Zoophycos* described in Wetzel et al. (2011).

Abundance of bioturbation structure types across the study region

Bioturbation structures of Group A, B and G showed high abundances and were observed in cores from 22, 39 and 27 stations, respectively. Group C, D, H, and J showed relatively low abundances with occurrences at 5, 7, 3, and 4 stations. With respect to regional occurrences only Group H and J showed low abundances and occurred in 1 and 2 out of 6 regions (Appendix 3.4.1 and Fig. 3.4.2 A-I). Bioturbation structure groups A, B and J occurred in all four sedimentary facies identified. However, while structure groups A and B predominantly occurred in facies a and a and b, respectively, structure group J occurred in all four facies equally. Bioturbation structure groups D, E, F, and H were found in facies a and b where structure groups E, F and H predominantly occurred in sedimentary facies b, and structure group D predominantly occurred in facies a. Bioturbation structure group G was found in sedimentary facies a, b and c (mostly in facies a and b), while structure group C was only found in facies b (see also Appendix 3.2).

Appendix 3.4.1: Bioturbation structures, burrow diameter, location in core (depth range), max depth in core, and number of stations/regions where present.

	Burrow Diameter (cm)		Depth Range (cm)		Max Depth (cm)		Stations where present	Regions where present
Group	Average	STDEV	Average	STDEV	Average	STDEV	(out of 56)	(out of 6)
A	0.12	0.14	4.5	4.3	6.4	8.6	22	5
B	0.24	0.17	5.9	3.3	17.1	7.0	38	6
C	0.55	0.35	2.7	2.1	19.6	3.9	5	4
D	0.08	0.03	4.5	2.4	17.3	3.8	7	5
E	0.09	0.06	6.5	1.3	19.9	5.0	10	4
F	0.26	0.15	4.0	1.2	7.3	7.8	12	3
G	0.03	0.01	4.4	2.9	13.9	8.8	27	5
H	2.70	0.42	11.8	7.3	15.3	5.7	3	1
J	0.30	0.10	4.8	1.7	14.8	3.2	5	2

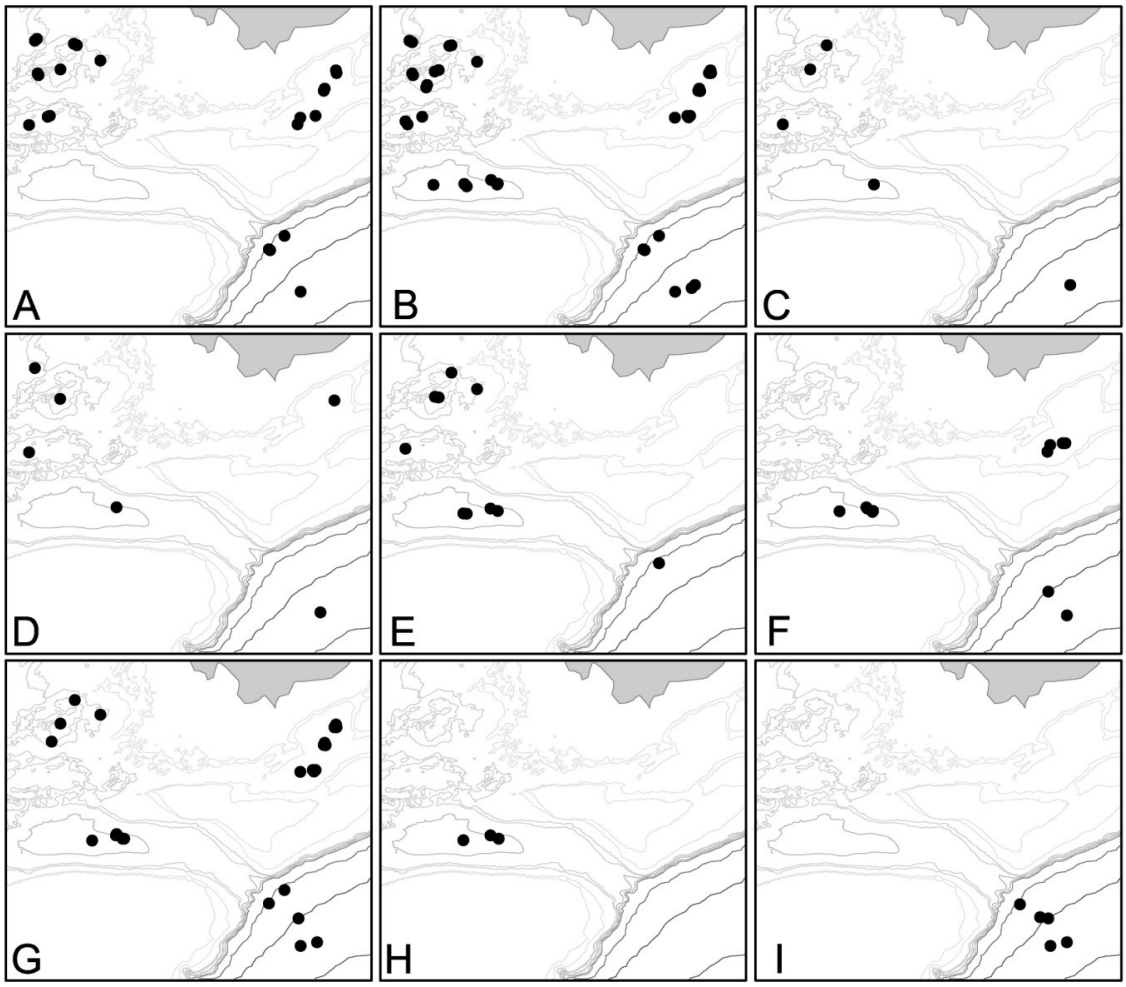

Appendix 3.4.2: Spatial distribution of bioturbation structure groups across study region: A) Group A, B) Group B, C) Group C, D) Group D, E) Group E, F) Group F, G) Group G, H) Group H, and I) Group J.

Spatial distribution of bioturbation structure groups in relation to environmental patterns

Slight distributional trends of bioturbation structure groups with respect to PCA derived environmental categories (for an explanation of environmental categories see main chapter and Fig. 3.12) were observed (Appendix 3.4.3 and 3.4.4). While the bioturbation

structures composing group A, B, D, F, and G occurred in all environmental categories, structure groups C, E, H, and J were present in just a few environments.

Structures of group A occur predominantly in PCA category 4 and 3 sediments; most of the simple vertical structures of group F occurred in category 3 and 1 sediments. Few specimens of structure group H were observed exclusively in category 1 and 2 sediments collected in Georges Basin. Bioturbation structures belonging to group C were mostly in sediment cores of category 2 sediments. Bioturbation structures of group B associated predominantly with category 4 sediments, and structure group E specimens were observed predominantly in category 1 and 2 sediments. Whereas bioturbation structure groups D and G associated with all environmental categories, structure group J occurred exclusively in categories 3 and 4 in greater water depths of the Northeast Channel and Fan.

Appendix 3.4.3: Numbers of cores corresponding to PCA categories 1-4 in which bioturbation structure groups A-J and subgroups A1-J1 are present.

	Bioturbation structure group								
PCA category	**A**	**B**	**C**	**D**	**E**	**F**	**G**	**H**	**J**
1	3	7	1	1	5	4	7	2	0
2	4	8	3	3	4	2	3	1	0
3	6	9	1	1	0	5	7	0	3
4	9	14	0	2	1	1	10	0	2

	Bioturbation structure subgroup																		
PCA category	**A1**	**A2**	**A3**	**A4**	**B1**	**B2**	**C1**	**D1**	**E1**	**E2**	**E3**	**E4**	**F1**	**F2**	**F3**	**G1**	**G2**	**H1**	**J1**
1	2	0	1	0	6	1	1	1	4	1	0	1	0	4	0	6	1	2	0
2	3	0	1	1	8	0	3	3	2	1	1	0	0	2	0	3	0	1	0
3	6	1	0	0	9	2	1	1	0	0	0	0	3	0	1	7	0	0	3
4	5	4	0	0	14	0	0	2	0	0	0	1	1	1	0	9	2	0	2

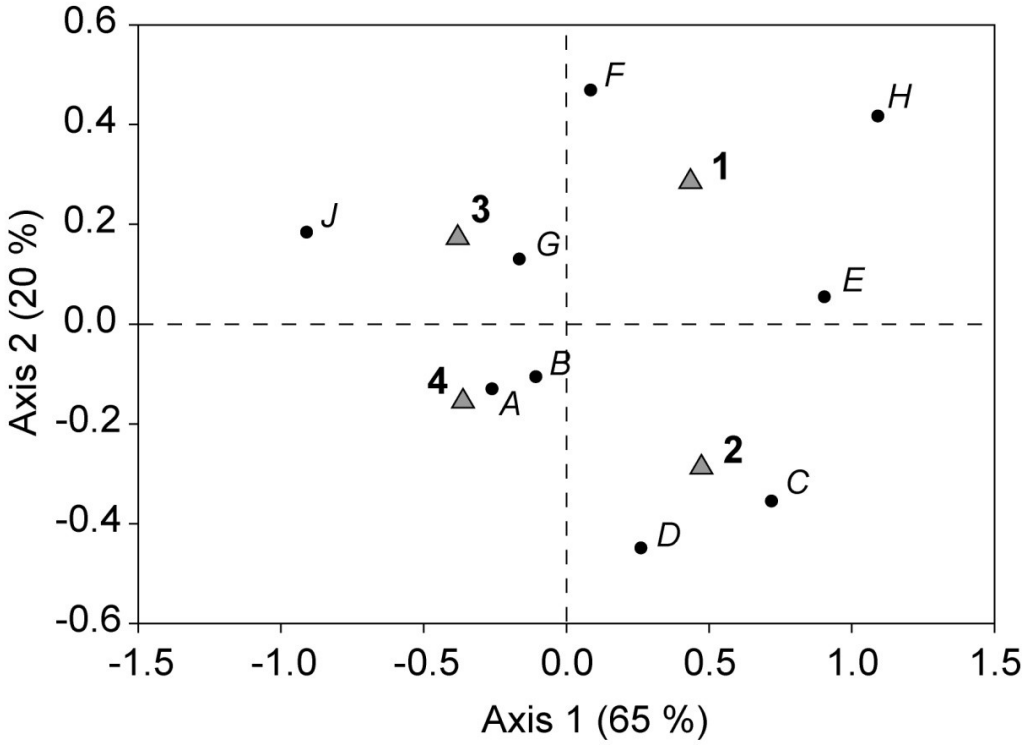

Appendix 3.4.4: Correspondence Analysis scatter plot showing associations among PCA environmental categories 1-4 (grey triangles) and bioturbation structure groups A-J (black dots).

Bioturbation traces as indicator for environmental conditions

The morphology of bioturbation structures (e.g. burrows and tubes) results primarily from organism feeding modes, activity levels and body forms, as well as environmental conditions and substrate characteristics which, in turn, control animal behavior (Kristensen and Kostka, 2005). Consequently, the spatial distribution of bioturbation structure groups observed in the current study potentially indicates the adaption of the tracemakers behavior to the environmental conditions of its benthic habitat. In general, most bioturbation structure groups seemed to be adapted to a wide range of benthic environmental conditions characterized through PCA, and based on the correspondence

analysis conducted, only slight distributional trends in relation to environmental patterns of organic matter and substrate were observed in the current study.

Collectively, dwelling traces related to a variety of environments and benthic conditions. The U- and J-shaped dwelling structures (group A) appeared particularly well adapted to the low organic matter qualities and relatively high sediment porosities. Because simple vertical dwelling structures of group F linked to high as well as to low organic matter qualities, but occurred only in sediments with comparatively high sand content, substrate seemed to be the most influencing factor on the distributions of these structures. The latter is consistent with the findings of Hauck et al. (2009) who observed high numbers of biogenic structures with vertical morphologies and increased suspension-feeding behaviors in sandy sediments. The funnel-shaped dwelling and resting traces (group H) occurred only in sediments with high organic matter quality collected in Georges Basin. The funnel-shaped dwelling and resting traces potentially represent a stationary life-style and the trace-producing animal may depend on the mobility and availability of food sources, as well as weak food competition between benthic and pelagic organisms. High grazing activities of the pelagic zooplankton in the water column, for example, can decrease the quality of the organic matter that reaches the seafloor (Morata et al., 2008). However, the bioturbation structures of this group were passively filled with coarse substrate of surface sediment layers and it is unclear whether these structures were still active and contributed to recent bioturbation processes in this region. Specimens of bioturbation structure group C appear to reflect a more specialized behavior and depend on high benthic organic matter quantities and qualities typical for the shelf basin sediments in the eastern part of the study region.

Dwelling and feeding traces (groups B and E) dominate most benthic settings in the current study, except for regions with higher proportions of sand and low organic matter input and quality. On one hand, these structures appeared to be adapted to high organic matter input and relatively porous sediments (group B). On the other hand, the distribution of some of these feeding types (group E) only linked to environments characterized by high quality organic matter. Thus, substrate seems to be the environmental variable that mainly controls the distribution of these bioturbation structures in the currents study.

Deposit feeding traces (groups D, G, and J) linked to environments with relatively porous substrate with high organic matter input. The branching and winding burrow systems of group G were more abundant in benthic environments with relatively high organic matter input but low organic matter quality. These traces therefore may indicate a specialized feeding behavior where the animal successively probed the sediment in search for food in order to cope with the strong competition for high quality food sources among benthic organisms in these regions. In contrast, the Zoophycos-like systematic feeding traces (group J) in the deep water environments of the Northeast Channel and Fan, characterized by low organic matter input and quality, may indicate seasonally pulsed organic matter inputs to the benthos in otherwise organic matter poor environments (e.g. Wetzel et al., 2011).

Conclusion

In general most bioturbation structure groups appeared to be adapted to a wide range of benthic environmental conditions observed in the current study, and only few slight and rather tentative distributional trends of bioturbation structures in relation the benthic

environments characterized through PCA were observed. Strongest relationships included U- and J-shaped, and simple horizontal to horizontally inclined dwelling traces associating with environments characterized through high organic matter input, and in particular high organic matter qualities. The dwelling structures indicating sedentary life-styles of the benthic organisms related to environments that receive high quality organic matter potentially indicating low competition for food in these regions. The more specialized branching and the Zoophycos-like deposit-feeding structures particularly associated with organic matter poor sediments in deep sea regions.

However, because of the relatively weak relationships between environmental patterns and feeding modes, the latter should not be used as indicator of environmental conditions in the current study.

References

Gingras, M.K., Dashtgard, S.E., McEachern, J.A., Pemberton, S.G. (2008). Biology of shallow marine ichnology: a modern perspective. Aquatic Biology 2, 255-268.

Hauck, T.E., Dashtgard, S.E., Pemberton, S.G., Gingras, M.K. (2009). Brackish-water ichnological trends in a microtidal barrier island-embayment system, Kouchibouguac National Park, New Brunswick, Canada. Palaios 24, 478-496.

Morata, N., Renaud, P.E., Brugel, S., Hobson, K.A., Johnson, B.J. (2008). Spatial and seasonal variations in the pelagic-benthic coupling of the southeastern Beaufort Sea revealed by sedimentary biomarkers. Marine Ecology Progress Series 371, 47-63.

Rindsberg, A.K. (2012). Ichnotaxonomy: Finding patterns in a welter of information. I: Knaust, D. and Bromley, R.G. (Eds.). Trace fossils as indicators of sedimentary environments. Elsevier, 924 pp.

Smith, J.N., Boudreau, B.P., Noshkin, V. (1986). Plutonium and 210Pbxs distributions in northeast Atlantic sediments: subsurface anomalies caused by non-local mixing. Earth and Planetrary Science Letters 81, 15-28.

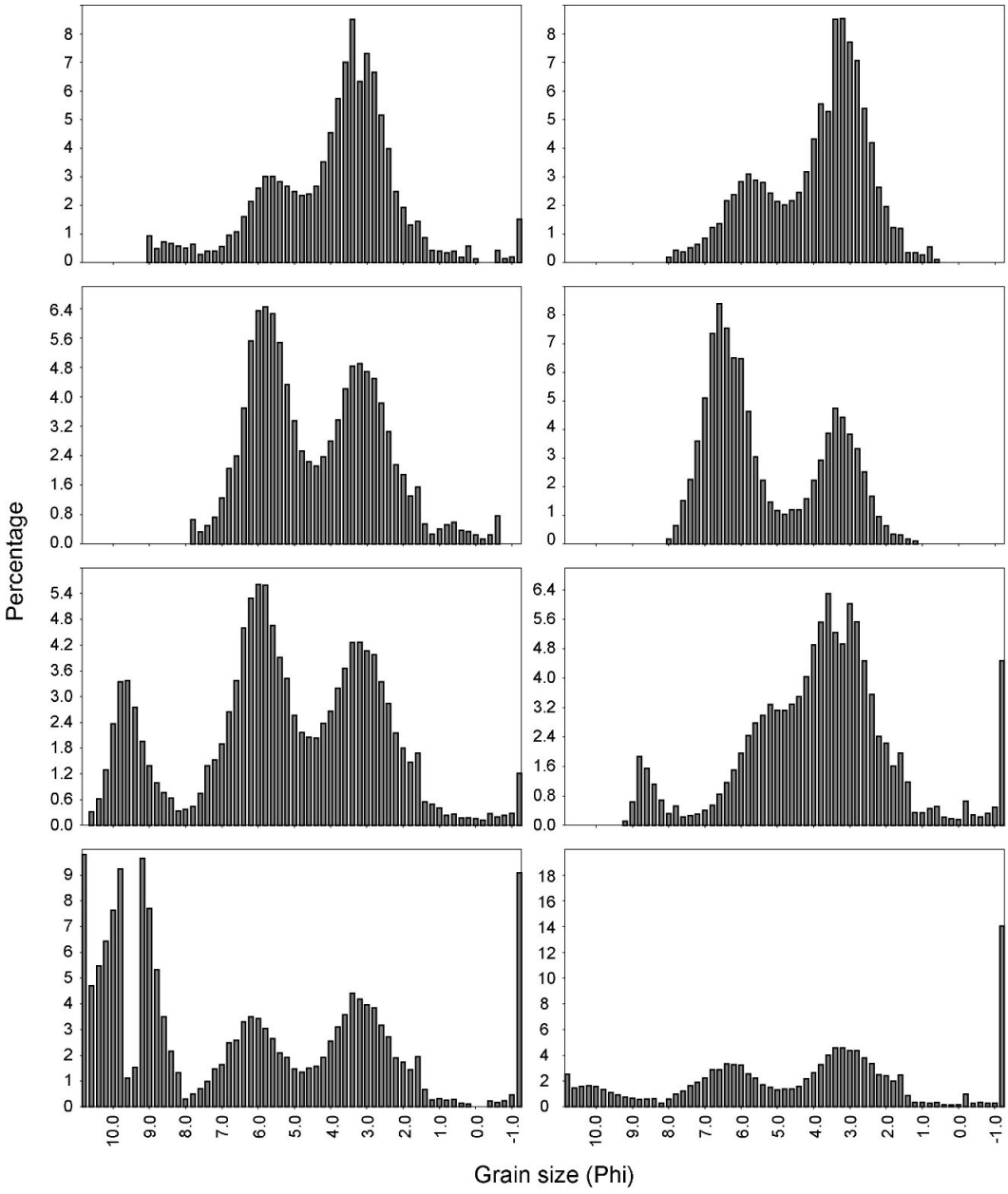

Appendix 3.5: Grain size distributions of surface sediments. Plots represent grain size distribution averages within 0-10 cm depth. Upper left to lower right: RB1_01, RB2_02, RB2_01, RB2_04, JB3_01, JB3_04, JB4_01, and JB5_03.

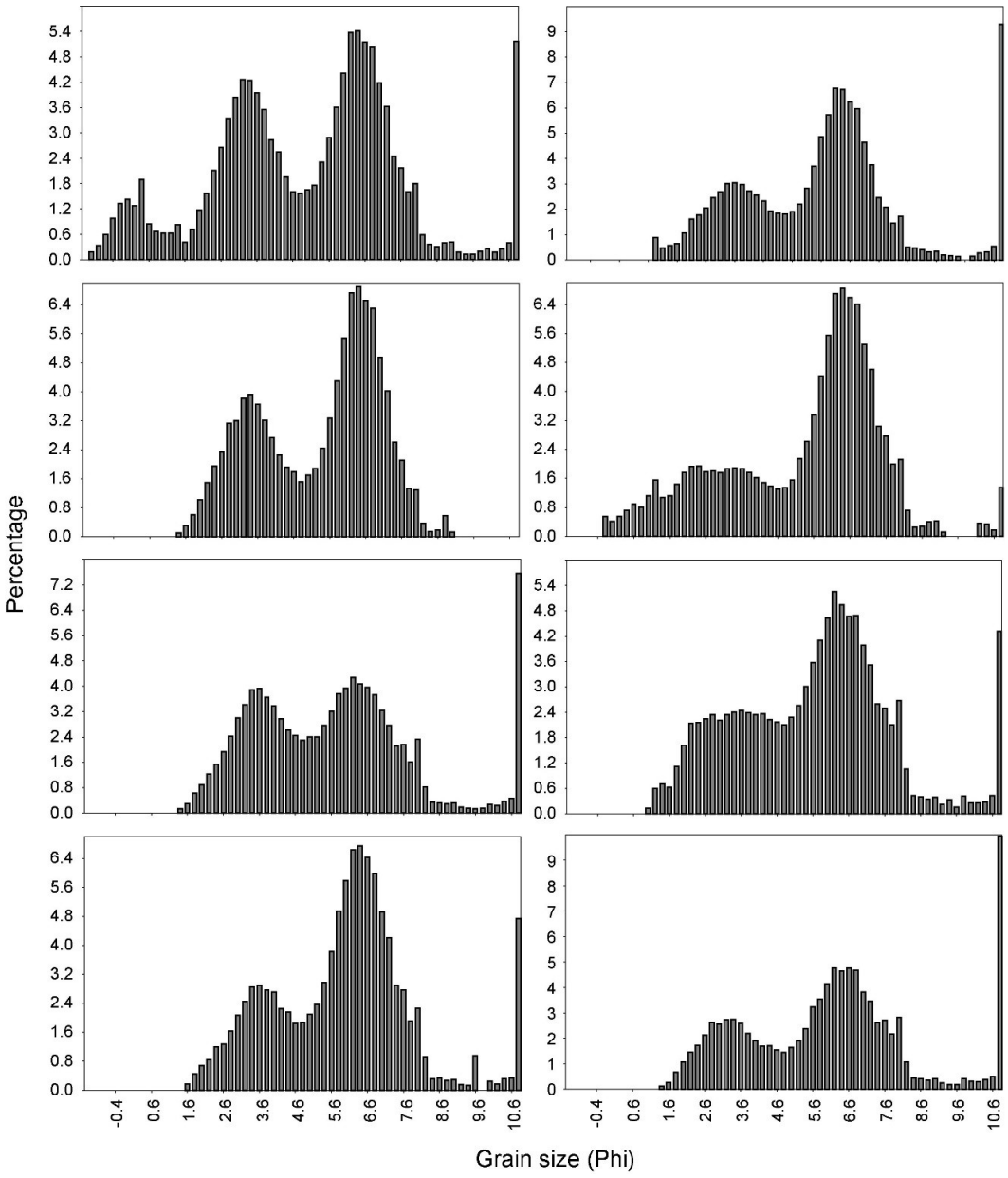

Appendix 3.5 continued. Upper left to lower right: JB6_01, JB7_01, CB1_01, CB2_02, GB2_01, GB2_06, GB3_02, and GB3_05.

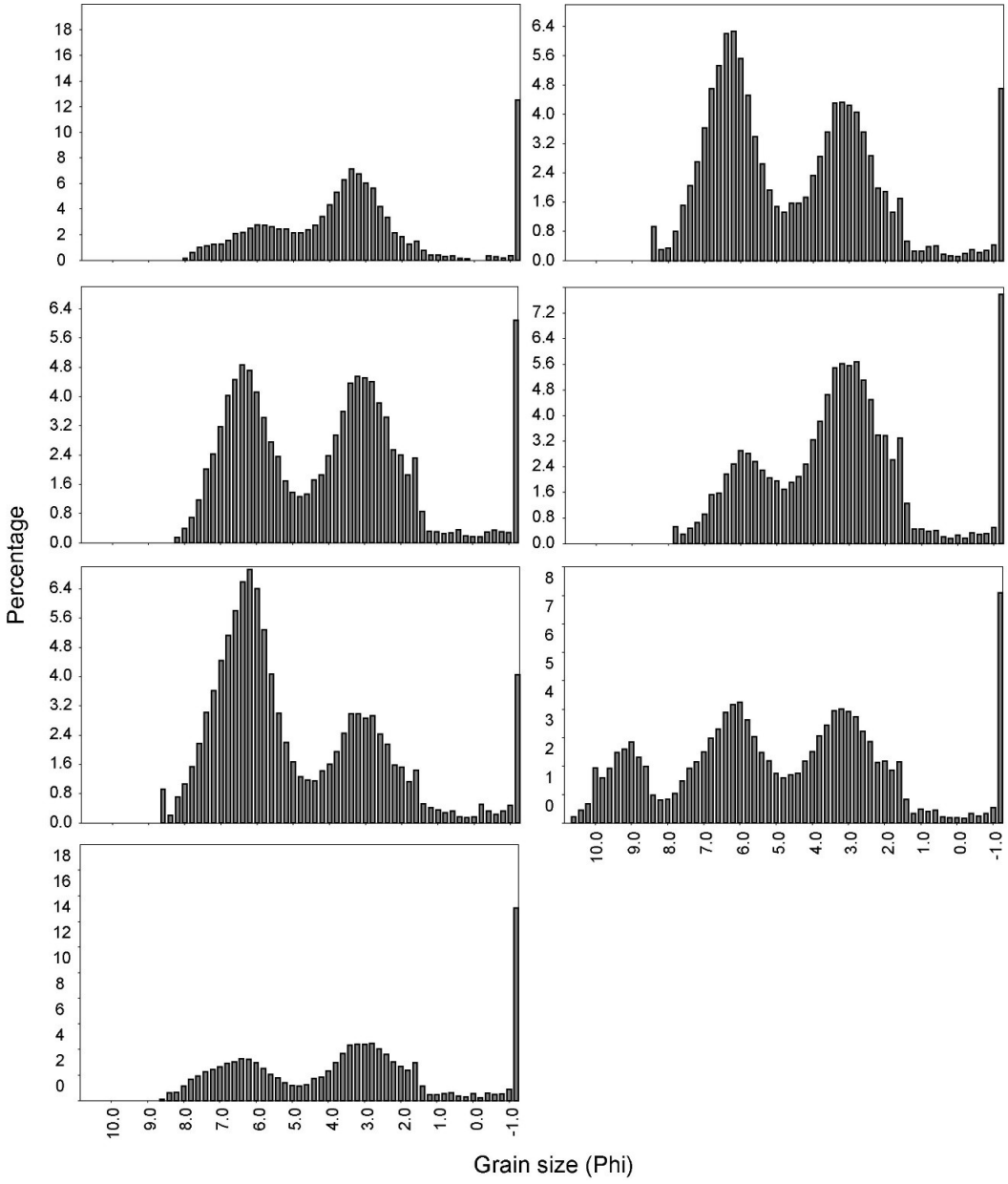

Appendix 3.5 continued. Upper left to lower right: NEC3_03, NEC6_06, NEC_1358, NEF4_03, NEF6_01, NEF6_04, NEF_1357A.

Appendix Chapter 4

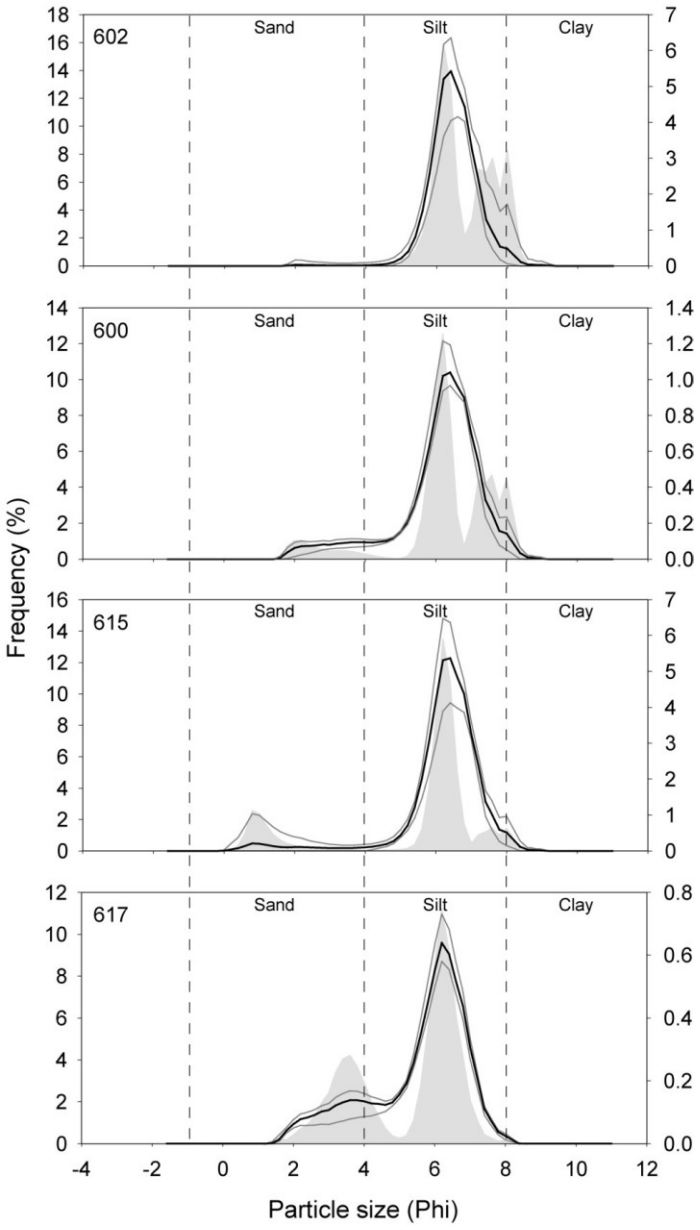

Appendix 4.1: Particle size frequency curves of particle size distributions in surface sediments of fjords studied. Black lines represent mean particle size frequencies of the sediment segments measured within each core. Grey lines are minimum and maximum values of particle size frequencies and show the variations of particle size distributions within the upper 10 cm of each sediment core collected. Grey filled areas represent the variance of particle size frequencies.

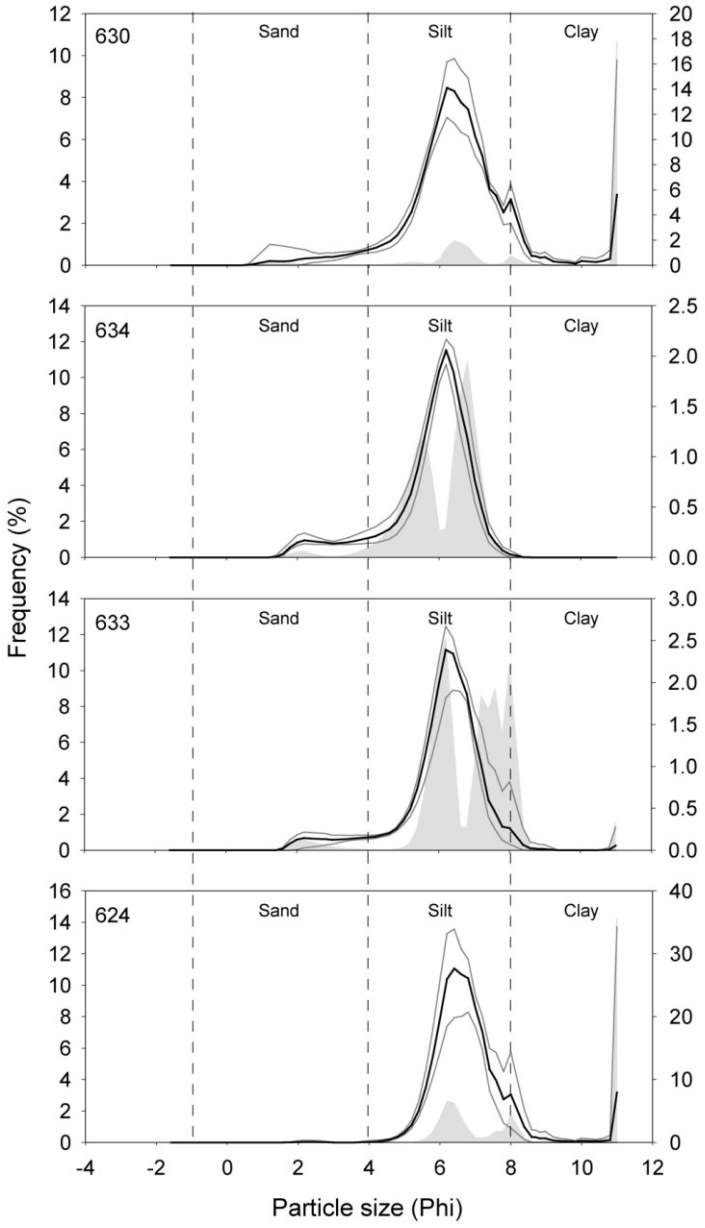

Appendix 4.1 continued.

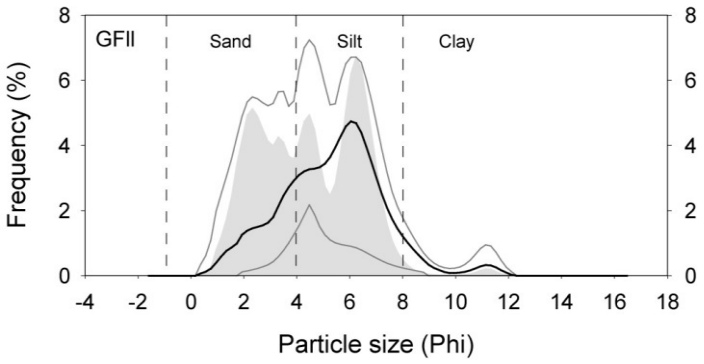

Appendix 4.1 continued.

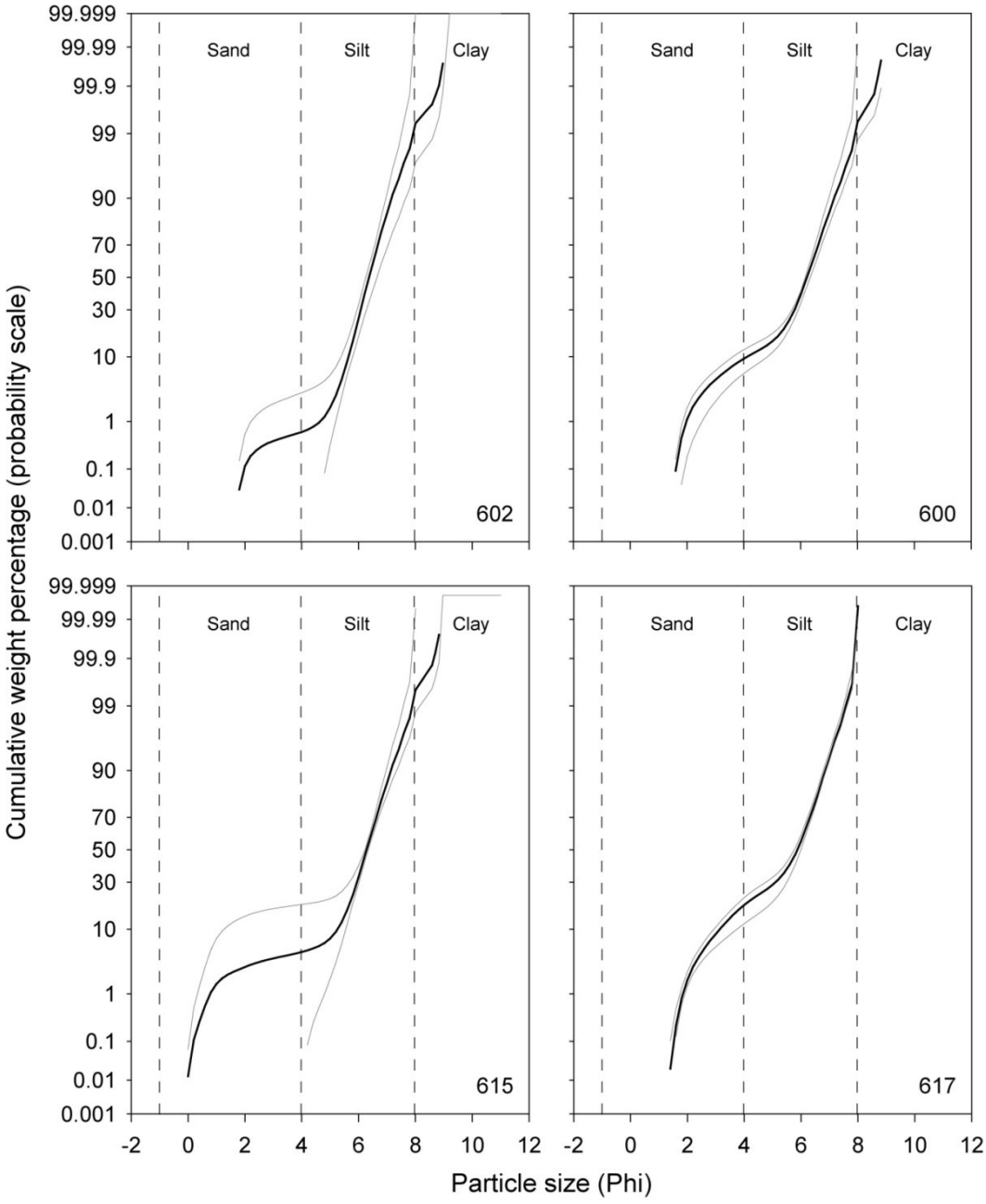

Appendix 4.2: Cumulative weight percentages of grain size distributions on probability scale of fjord sediments collected. Black lines represent mean particle size weight percentages of the sediment segments measured within each core. Grey lines are minimum and maximum values of particle size weight percentages and show the variations of particle size distributions within the upper 10 cm of each sediment core collected.

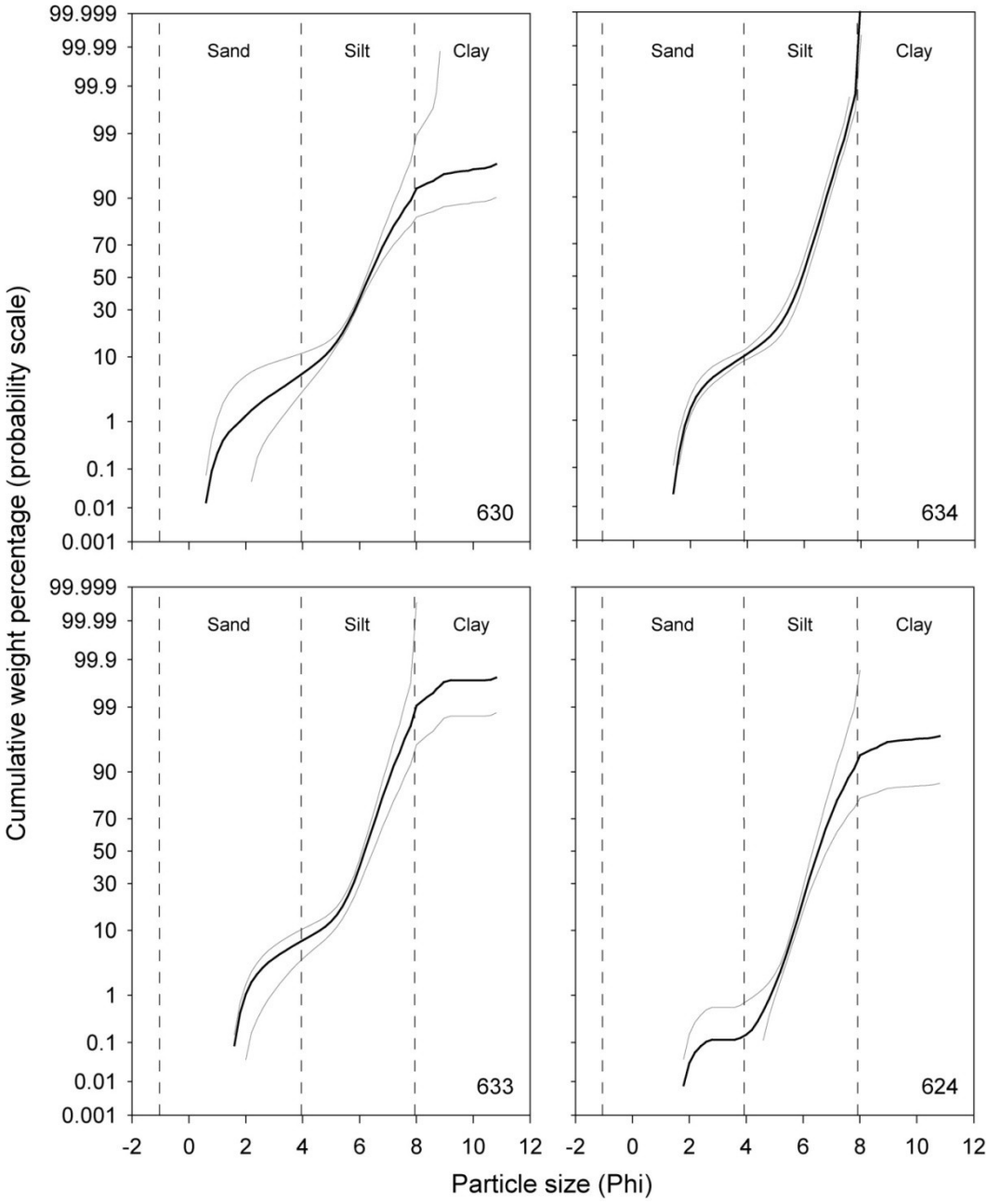

Appendix 4.2 continued.

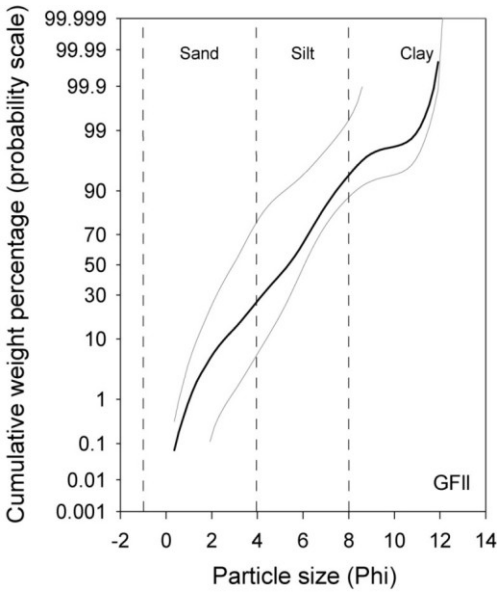

Appendix 4.2 continued.

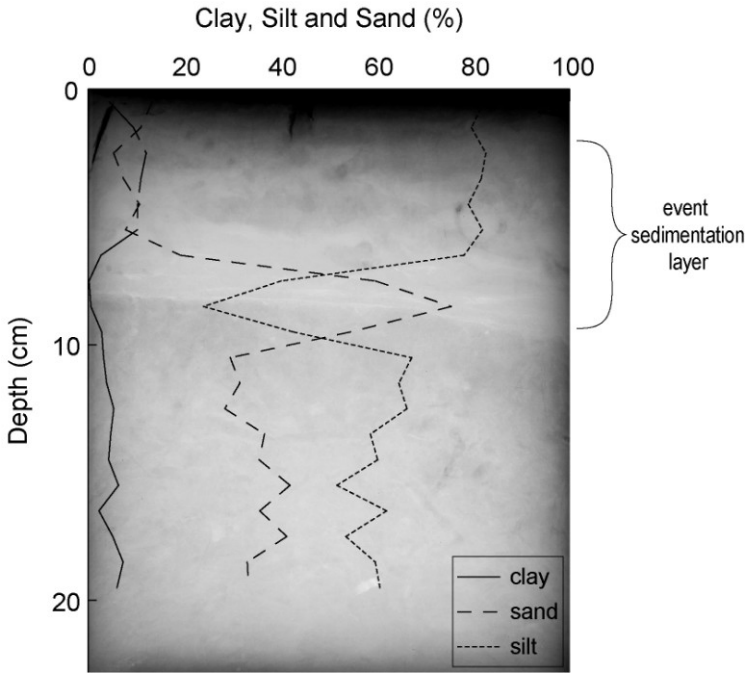

Appendix 4.3: Percentage profiles of clay, silt and sand in sediment core GFII collected in Gibbs Fjord, Baffin Island indicating an event sedimentation layer within the upper 10 cm of the core.